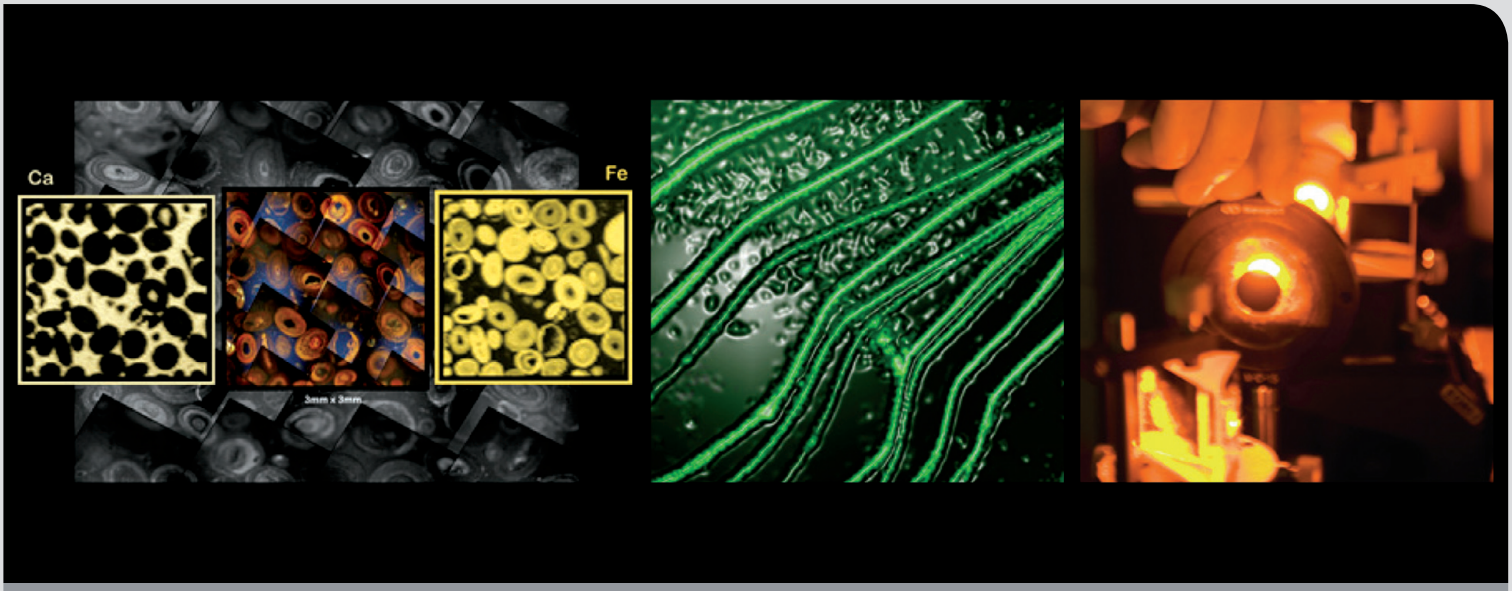

KIT SCIENTIFIC REPORTS 7559

Annual Report 2009

Institute for Nuclear Waste Disposal
Institut für Nukleare Entsorgung

H. Geckeis, T. Stumpf (eds.)

KIT Scientific Publishing

H. Geckeis, T. Stumpf (eds.)

Annual Report 2009

Institute for Nuclear Waste Disposal
Institut für Nukleare Entsorgung

Karlsruhe Institute of Technology

KIT SCIENTIFIC REPORTS 7559

Cover illustration (from left to right):
Ca and Fe distributions and microscopic images of a sample from the Konrad repository for low- and intermediate-level radioactive waste from μ-XRF measurements at the INE-Beamline at ANKA; Fluorescence-optical image of sorbed colloids concentrated on crystal steps of muscovite, but also distributed over basal planes, in the presence of 10-5 M Eu3+ (from the doctoral Thesis of A. Filby); OPO Laser in operation (from the doctoral Thesis of M. Schmidt).

Annual Report 2009

Institute for Nuclear Waste Disposal
Institut für Nukleare Entsorgung

H. Geckeis
T. Stumpf
(eds.)

KIT Scientific Publishing

Report-Nr. KIT-SR 7559

Impressum

Karlsruher Institut für Technologie (KIT)
KIT Scientific Publishing
Straße am Forum 2
D-76131 Karlsruhe
www.ksp.kit.edu

KIT – Universität des Landes Baden-Württemberg und nationales
Forschungszentrum in der Helmholtz-Gemeinschaft

Diese Veröffentlichung ist im Internet unter folgender Creative Commons-Lizenz
publiziert: http://creativecommons.org/licenses/by-nc-nd/3.0/de/

KIT Scientific Publishing 2010
Print on Demand

ISSN 1869-9669

Table of contents

1 Introduction to the Institut für Nukleare Entsorgung

R&D at the Institut für Nukleare Entsorgung, INE, (Institute for Nuclear Waste Disposal) deals with the long-term safety assessment for final disposal of nuclear waste, the separation of minor actinides from high-level waste (partitioning) and the immobilization of high-level liquid waste by vitrification. All activities are integrated into the programme Nuclear Safety Research within the Energy Center of the Karlsruhe Institute of Technology (KIT). INE contributes to the German provident research for the safety of nuclear waste disposal, for which the federal government is responsible.

Based on the present operation road map for nuclear power plants in Germany, about 17000 tons of spent fuel will be generated. More than 6200 t of this has been shipped to France and UK for reprocessing to recover plutonium and uranium. Therefore, two types of high level, heat producing radioactive waste, i.e. spent fuel and vitrified high level waste, have to be disposed of safely.

There is an international consensus that storage in deep geological formations is the safest way to dispose of high level heat producing radioactive waste. It ensures the effective protection of the population and the biosphere against radiation exposure over very long periods of time. The isolation and immobilization of nuclear waste in a repository is accomplished by the appropriate combination of redundant barriers (multi-barrier system). INE research focuses on the geochemical aspects of nuclear waste disposal. Special emphasis is given to actinides and long-lived fission products because of their significant contribution to the radiotoxicity for long periods of time.

Relevant scenarios for the geological long-term behaviour of nuclear waste disposal have to take into account possible radionuclide transport via the groundwater pathway. Thermo-mechanical studies are performed at INE in order to describe the evolution of the repository after closure. The possible groundwater access to emplacement gallery rooms is assumed to cause waste form corrosion. Radionuclide mobility is then determined by the various geochemical reactions in the complex aquatic systems: i.e. dissolution of the nuclear waste form (high-level waste glass, spent fuel), interaction with corroded container material, radiolysis phenomena, redox reactions, complexation with inorganic and organic ligands, colloid formation, surface sorption reactions at mineral surfaces, precipitation of pure solid phases and solid solutions. Prediction and quantification of all these processes require the availability of thermodynamic data and a comprehensive understanding of the reactions at a molecular scale.

Relevant radionuclide concentrations in natural groundwater are in the nano-molar range, which is small in relation to the main groundwater components. Quantification of chemical reactions occurring in these systems calls for the application and development of state-of-the-art sophisticated methods and experimental approaches, which provide insight into the chemical speciation of radionuclides at very low concentrations. Innovative laser and X-ray spectroscopic techniques are continuously developed and applied. A theoretical group performs quantum chemical calculations on actinide complexes as an additional tool to support experimental results.

The methods for long term safety of a repository for nuclear waste has to be demonstrated by application of modeling tools on real natural systems over geological time scales. The experimental research program at INE aims to acquire fundamental knowledge on model subsystems and to derive model parameters. Geochemical models and thermodynamic databases are developed as a basis for the description of geochemical behaviour of radionuclides in complex natural aquatic systems. The prediction of radionuclide migration in the geosphere necessitates a coupled modelling of geochemistry and transport. Transferability and applicability of model predictions are examined by designing dedicated laboratory experiments, field studies in underground laboratories and by studying natural analogue systems. This strategy allows to identify and to analyse key uncertainties related to the accuracy and the relevance of the developed models.

The partitioning & transmutation (P&T) strategy is pursued in many international research programmes. The objective is to reduce the time horizon for safe disposal of high level waste from some hundred thousand to less than thousand years by significant reduction of the radiotoxicity and heat inventory. The aim of R&D at INE is to separate long-lived minor actinides from high active nuclear waste for subsequent transmutation into short-lived or stable fission products. INE develops highly selective extracting agents and performs experiments to derive kinetic and thermodynamic data for the extraction reaction. R&D spans theoretical and experimental work dedicated to a mechanistic understanding of extraction ligand selectivity on a molecular scale, in order to optimize extraction processes.

With the third R&D topic at INE, the vitrification of high level waste, INE contributes to the decommissioning of nuclear facilities. The core process technology for the Vitrification Pilot Plant (VEK) at the Karlsruhe Reprocessing Plant (WAK) site located at the KIT Campus North has been developed at INE. This work comprises design of process components, including the glass melting furnace and the off-gas cleaning installation. After completion of the cold commissioning phase the hot operation of the VEK facility started in September 2009. INE has been involved in functional testing of major process systems, the preparation of qualification records and certification of product quality, as well as in the performance of the recent cold test operation. At present, INE plays a substantial role in operation of the VEK plant.

INE laboratories are equipped with the infrastructure necessary to perform radionuclide/actinide research, including hot cells, alpha glove boxes, inert gas alpha glove boxes and radionuclide laboratories. State-of-the-art analytical instrumentation and methods are applied for analysis and speciation of radionuclides and radioactive materials. α–, β–, γ–spectroscopy instruments exist for the sensitive detection and analysis of radionuclides. Trace element and isotope analysis is made by instrumental analytical techniques such as X-ray fluorescence spectrometry (XRF), atomic absorption spectrometry (AAS), ICP-atomic emission spectrometry (ICP-AES) and ICP-mass spectrometry (ICP-MS). Surface sensitive analysis and characterisation of solid samples is done by X-ray diffraction (XRD), scanning electron microscopy (SEM), photoelectron spectroscopy (XPS), atomic force microscopy (AFM) and laser-ablation coupled with ICP-MS. Laser spectroscopic techniques are developed and applied for sensitive actinide and fission product speciation such as time-resolved laser fluorescence spectroscopy (TRLFS), laser photoacoustic spectroscopy (LPAS), sum frequency infrared spectroscopy, laser-induced breakdown detection (LIBD) and Raman spectroscopy. Recently a tunable optical parametric oscillator (OPO) laser system with TRLFS-detection was installed for high resolution spectroscopy at liquid helium temperature. Investigation of actinide-ion complexation and polymerization in solution is facilitated by nano-electrospray time-of-flight mass spectrometry (ESI-TOF-MS). Structural insight into actinide species is obtained by extended X-ray fine structure (EXAFS) spectroscopy at the INE-Beamline at the Karlsruhe synchrotron source ANKA. The INE-Beamline, in the direct vicinity of INE hot laboratories and in combination with the other analytic methods, represents a world-wide unique experimental and analytic infrastructure, which both profits from and contributes to INE's expertise in the field of chemistry and spectroscopy of the actinides.

Additional facilities at INE include a non-radioactive vitrification test facility (1:1 mock-up of the VEK plant) used to investigate and to simulate vitrification processes for hot plants. The INE CAD workstations enable construction and planning of hardware components, process layout and flowsheets. The institute workshop is equipped with modern machine tools to manufacture components for specific experimental and analytical devices in hot laboratories.

2 Highlights

Contributions collected in this report provide a representative overview of the scientific outcome of INE research activities in 2009. The structure of the report follows widely the organization of the institute according to research topics: Basic research towards understanding geochemical reactions of radionuclides on a molecular scale (1) and applied studies on radionuclide retention in multi-barrier system under 'real' repository conditions (2). Both topics are strongly linked together and cover a broad range of chemical aspects for long term safety assessment of a repository for nuclear waste. In order to obtain detailed chemical information on radionuclide speciation and structures, speciation methods and analytical techniques are consequently developed at INE (3). Beside spectroscopic methods, quantum chemical calculations are increasingly implemented as an additional tool to gain insight into the molecular and electronic structure of radionuclide species. These experimental and theoretical tools are applied to geochemical studies and also to achieve mechanistic understanding of solvent extraction processes developed for separation of minor actinides from fission lanthanides, which is indispensible for partitioning & transmutation.
Research and development dedicated to the immobilization of high-level radioactive liquid waste is much more technically oriented. In this field, a vitrification plant on the WAK site using INE technology started hot operation of nuclear waste in Sept. 2009. In parallel the Vitrification Project China based on KIT-INE's technology was launched between Chinese organizations and a German consortium in August 2009. Important achievements of the research activities in 2009 are listed below.

Fundamental data to describe the hydration of actinides in aqueous solution are lacking for transuranic ions for the common coordination number nine. Therefore, we **synthesized a series of trivalent hydrated actinide triflates** ($CF_3SO_3^-$: Tf) of the type $[An(H_2O)_9]Tf_3$ starting **from uranium to curium and including californium**. The synthesis of the U and Np compounds was challenging because of their redox instability in water and that of Cf because of the small amounts available and its strong radiolysis. All of the synthesized compounds are isostructural among each other and with the homologous lanthanides showing nine coordinated H_2O molecules in a tricapped trigonal prismatic coordination geometry. The An-OH_2 distances from XRD structure analysis were well reproduced by quantum chemical calculations. These results are important to deduce ionic actinide radii, especially with donors such as water, and to understand better the stabilisation of actinides in aqueous solution (Chapt. 5.1).

For prominent radiotoxic elements the safety analysis of nuclear waste disposal relies on the solubility control by solid phases. Frequently, these elements are present as minor components in the waste forms. For example, the concentration of **uranium in cemented wastes** is in the range of 15 µmol g^{-1}. In this case, the relevant solid phase which retains U(VI) could be identified. A combination of the different analytical techniques, as well as comparison with reference samples and with U-free cement material, was applied. Consistent results from XRD, XANES/EXAFS, and TRLFS suggest the **existence of a uranophane-like phase $Ca(UO_2)_2(SiO_3OH)_2{\cdot}5H_2O$ in cement** samples corroded both in $MgCl_2$-rich brine and in NaCl-rich brine. Other solid U(VI) phases such as becquerelite, meta-schoepite or di-uranates were not found or may exist at low concentrations only (Chapt. 6.2).

A 2009 highlight at INE in actinide speciation method development is **surface diffraction crystal truncation rod measurements (CTR) on the calcite (104) surface**, the results of which were used as input parameters in surface complexation modelling (Chapt. 9.1). This type of hyphenated technique will certainly be a driving force in **accurate model development of water-mineral interface processes**. The result of these investigations are part of the doctoral thesis of Frank Heberling and was awarded two prestigious prizes: the Bernd Rendel Prize of the Deutsche Forschungsgemeinschaft (DFG) and the Rudolf Rohrbach Prize from the Fakultät für Bau-, Geo- und Umweltwissenschaften of KIT Campus South.

Fluorescence spectroscopy at cryogenic temperature on actinides such as Cm(III) in crystalline hosts often provides highly resolved spectra, yielding structural information at trace level concentrations. In inhomogeneous matrices such as glass however, only broad bands are observed. Resonant excitation of the lowest emitting state will induce sharp emission bands from nearly identical sub-sites. Scanning the excitation wavelength can provide information on the various sites. Such **fluorescence line narrowing (FLN)** has been observed at INE for an unusual environment: **Cm(III) sorbed onto γ-Al_2O_3 or clay**, where Cm(III) is observed to form a ternary carbonate complex with displacement of nearly all hydration water molecules. Whereas FLN experiments are performed usually at mM concentration, we observed this effect in 10^{-7} M Cm solution. FLN may be very helpful to

elucidate incorporation of actinide in glass or disordered structures by radiation damage (Chapt. 9.2).

In quantum chemical calculations polarizable continuum models are frequently used for an approximate description of metal ion interaction with solvents (e.g., water). However, since there is no canonical way in defining the parameters, ambiguous data are obtained. **Molecular dynamics** provides a useful key to describe solvation effects. Therefore, we derived **force field parameters for actinides**, water and counterions **based on highly accurate large-scale, state-of-the-art quantum chemical calculations**. The resulting coordination numbers, resident times for competing exchange mechanisms, as well as thermodynamical data, can be compared directly to experimental data. This project is a European collaboration with CEA / Saclay und Université Lille (Chapt. 9.5).

The complexation of Cm(III) and Eu(III) with BTP and BTBP ligands was studied by TRLFS in both organic and aqueous solution. It was shown for the first time that the **selectivity of BTP and BTBP is due to different enthalpies of complexation for An(III) and Ln(III).** Furthermore, it was shown that selectivity is not confined to the organic phase (in which extracting agents work), but is also observed in aqueous solution. This is the scientific background for developing innovative separations processes based on the selective masking of americium and curium using hydrophilic BTP- and BTBP-type complexing agents (Chapt. 7).

Also, **a new BTP-type extracting agent, CA-BTP,** was synthesized, successfully tested for the selective extraction of americium, and patented. CA-BTP maintains the good selectivity and stability of $CyMe_4$-BTBP (which is the current reference extracting agent) while addressing $CyMe_4$-BTBP's weak points: CA-BTP has much better solubility in the organic phase plus improved mass transfer kinetics. In this way, CA-BTP is an important step towards an industrial applicability (Chapt. 7).

Based on **KIT-INE's vitrification technology** the VEK vitrification plant was constructed with the aim to immobilize about 60 m^3 of HLLW with a total activity of $7.7 \cdot 10^{17}$ Bq stored on site of the former WAK pilot reprocessing plant. In February 2009 the second operational license was granted thereby clearing the way for final preparation of VEK for hot operation. Preceding the start-up of the routine vitrification operation a one week hot test operation with a reduced level of radioactivity (mix of HLLW simulate and genuine HLLW) was conducted in early September 2009. Start-up of routine processing of the stored HLLW immediately followed the radioactive test by mid September. As of December 31, 2009, **VEK immobilized 24 m^3 of radioactive waste** in 19.2 metric tons of glass, which was poured into 48 canisters. The process performance proved to be excellent. The operation could be maintained at a time availability of almost 100 %. As a most important result, no impact of noble metals on the melting operation could be observed so far (Chapt. 8).

By end of July 2009 the contract of the **Vitrification Project China** (VPC) between the Chinese organizations involved and the German industry consortium about construction of a vitrification plant was signed. After a three months period, the contract became effective on October 30, 2009. The final composition of the Chinese HLLW was delivered shortly after signing. The vitrification technology of the Chinese plant will be based on the technology of KIT-INE. The application of the technology in this project by the German consortium is regulated in the scope of a licence agreement. The delivery of the licence documentation according to this agreement took place in November 2009 (Chapt. 8).

3 Education and Training

Teaching

Teaching of students and promotion of young scientists is of fundamental importance to ensure high level competence and to maintain a leading international position in the field of nuclear and radiochemistry. INE scientists are strongly involved in teaching at KIT-Campus South and the Universities of Heidelberg, Berlin, Jena and Mainz.

Dr. Andreas Bauer is lecturing Clay Mineralogy at the University of Jena. His lecture is dealing with mineralogical characterization of these materials and the importance of quantifying surface reactions. In the second part of the lectures generally sound, practical advice on powder X-ray diffraction is provided, as well as a useful set of step-by-step instructions for the novice.

The lecture of Dr. Mathias Flörsheimer at the University of Heidelberg deals with radionuclide adsorption/desorption processes and chemical reactions at the natural mineral/electrolyte interfaces. Applying nonlinear optical techniques, interface selective chemical analytical information can be obtained, which allows us to understand the macroscopic immobilization processes at the molecular level.

Prof. Dr. Horst Geckeis, director of INE, holds a chair of radiochemistry at KIT Campus South. He teaches fundamental and applied radiochemistry for chemistry students in diploma courses. A radiochemistry module consisting of basic and advanced lectures on nuclear chemistry topics and laboratory courses has been set up for master students in Karlsruhe.

Prof. Dr. Petra Panak, heading a working group on actinide speciation at INE, holds a professorship of radiochemistry at the University of Heidelberg. A basic course in radiochemistry is offered for bachelor and/or master students. The basic course comprises two lectures (Radiochemistry I and II), providing fundamental knowledge on radioactive decay processes, chemistry of radionuclides and their applications. Furthermore, an advanced course on radiochemistry has been established recently for master students. In the context of this advanced course two lectures on the chemistry of f-elements and medical applications of radionuclides are obligatory. The advanced radiochemistry lectures are supplemented by a scientific internship at the INE hot laboratories.

About 50 students from Karlsruhe and Heidelberg participated in two three week radiochemistry laboratory courses in 2009 held at KIT-Campus North (KIT-CN) in FTU radiochemistry and INE hot laboratories. Students are interested in nuclear chemistry topics and appreciate the various semester courses. This is reflected in the increasing numbers of students in 2009 fulfilling scientific internships at INE.

Lectures and practical training courses given by Dr. Thorsten Schäfer at the Freie Universität Berlin, Institute of Geological Sciences, Department of Earth Sciences focused in 2009 on a master degree course on laboratory and field methods in hydrogeology including performance and analysis of tracer tests, pumping tests and permeability determination (Applied Hydrogeology III), as well as a special topic course on “Environmental radioactivity”.

Dr. Thorsten Stumpf gave lectures at the University of Heidelberg in the field of chemistry of f-elements and radioanalytical methods. He changed his habilitation from the University of Heidelberg to KIT. In summer 2009 he was awarded permission to teach and the right for examinations at the Department of Chemistry and Bioscience at KIT.

The lecture of Dr. Clemens Walther at the University of Mainz deals in 2009 with electric power generation. All currently applied major techniques for electricity generation are presented with a focus on nuclear energy and the scientific basics of nuclear fission. Advantages and drawbacks of each technique are compared. Present resources, sustainability and technical development are also discussed.

Through these close cooperations with universities, students are educated in the field of nuclear and actinide chemistry, which most universities can no longer offer. Hence, INE makes a vital contribution to the intermediate and long-perspective of maintaining nuclear science competence.

PhD-students

In 2009 thirteen PhD students were working at INE on their dissertations. Three of them were awarded a doctoral degree. These topics include:

- Interaction of aquatic colloids with mineral surfaces (completed).
- Study on the incorporation mechanism of actinide and lanthanides of Ca-containing secondary phases (completed).
- Structural study on Cm(III) and Eu(III) complexes with ligands relevant to partitioning (completed).
- Co-precipitation of actinides with calcite -

interfacial reactions and kinetics.

- Influence of colloids on radionuclide mobility.
- Influence of humic substances on the geochemical behaviour in groundwater: The role of the large colloid fraction.
- Sorption study of actinides onto natural clay.
- Spectroscopic and thermodynamic study on selected chemical reactions of actinides in aqueous solution.
- Sorption of Eu(III)/Cm(III) onto aluminum oxide/hydroxide.
- Development and application of coupled quantum chemical and molecular dynamic solvation models.
- Study on the complexation behaviour of actinides by ESI-MS.
- Separation of trivalent actinide from lanthanide ions by N-donor ligands.
- Study on the speciation of Cm(III)/Eu(III) complexes relevant for partitioning.
- The effect of nano- to microscale heterogeneity and redox reaction kinetics on radionuclide mobility.

The German Federal Ministry appropriated special funds in 2009 for establishing networks between German and Russian synchrotron communities. INE was successful in an application to this fond to host a PhD student from Rostov-on-Don for a stay for just over three months. She was involved in theoretical calculations to support RIXS and high resolution X-ray emission spectroscopy developments at the INE-Beamline, in N 1s NEXAFS experiments at the BESSYII and in 4f RIXS studies at HASYLAB.

4 National and international cooperation

INE R&D involves a number of national and international cooperations and projects. These are described in the following.

The EURATOM FP7 Collaborative Project (CP) “Redox Controlling Systems” (ReCosy) started in April 2008. Main objectives of ReCosy are the sound understanding of redox phenomena controlling the long-term release/retention of radionuclides in nuclear waste disposal and providing tools to apply the results to Performance Assessment/Safety Case. The project is coordinated by INE, with Amphos 21 as the coordination secretariat and 32 institutions from 13 European countries contributing to the four year CP. The international interest in the project is large and organizations from the Finland, Japan, Korea, UK and USA have signed associated group agreements. A key event in 2009 was an inter-comparison exercise on redox determination methods. There were 19 organizations participating the exercise, hosted by INE. The outcome will be an important basis for defining state-of-the-art, identifying pending issues and defining future activities in this field.

INE was one of the core members of the European "Network of Excellence for Actinide Sciences” (ACTINET-6) within the 6th FP of the EC, which ended 2008. The negotiations for the follow up project ACTINET-I3 extended on over the entire year 2009. The contract for the three year project was finally signed by the Commission in January 2010. ACTINET-I3 is an Integrated Infrastructure Initiative (I3). In contrast to the former ACTINET the consortium has only eight members. These are the leading European actinide laboratories CEA, JRC-ITU and KIT-INE, as well as FZD, PSI, CNRS, KTH and UNIMAN. The objectives of ACTINET-I3 are: (i) to establish and strengthen a network of actinide facilities across the EU and to foster their joint development in terms of capacity and performance; (ii) to support and manage jointly a programme of access to appropriate infrastructures for training and associated research projects making use of the proposed facilities; (iii) to conduct on a limited scale a set of Joint Research Activities (JRA) involving consortium member organisations, with an objective to improve the performance of infrastructures by developing new relevant instrumentations and/or data of common interest. Further, these activities will be complemented by a virtual infrastructure, the Theoretical User Lab, providing a limited support in theory and modeling, with a focus on the combing theory and experiments. The opening of the actinide laboratories and the integrated beam lines for external scientists to perform experimental work within well-defined joint research projects was very successful in ACTINET-6. This instrument will be continued in ACTINET-I3. The first call for proposals was launched in February 2010.

With funding from the EU 7th Framework EURATOM Programme, the project “Towards a European Competence Center for Nuclear Magnetic Resonance (NMR) on Actinides” began in autumn 2009. This project spans nine months and entails establishment of a round table of experts in NMR applications to investigations of radioactive materials and organization of a workshop on this subject. The project partners are KIT, University of Cambridge, Université Liège, Royal Institute of Technology, CEA Marcoule and the JRC-ITU.

Two international projects focus on the stability of the bentonite buffer/backfill in contact with water conducting features and the influence of colloids on radionuclide migration in crystalline host rock: the Colloid Formation and Migration (CFM) experiment, coordinated by NAGRA (National Cooperative for the Disposal of Radioactive Waste, Switzerland), and the Colloid Project, initiated by SKB (Swedish Nuclear Fuel and Waste Management Co., Sweden). Both projects are currently jointly working together using the experimental set-up at the Grimsel Test Site (Switzerland). Additional partners involved are from Japan (JAEA, AIST, CRIEPI), South Korea (KAERI), Finland (POSIVA Oy), Switzerland (NAGRA, PSI-LES), and Spain (CIEMAT). INE plays a decisive role in the laboratory program of both projects and is also mainly carrying out the field activities.

INE is involved in various bi- and multilateral cooperations with national universities on different topics. Scientific cooperation with various German universities, research institutions and industrial partners is partly supported by the German Federal Ministry for Economics and Technology (BMWi), the geoscientific research and development program GEOTECHNOLOGIEN funded by the Federal Ministry for Education and Research (BMBF) and the German Research Foundation (DFG) and the Federal Ministry for the Environment, Nature Conservation and Nuclear Safety (BMU). These research programs are dedicated to actinide and long-lived fission product geochemistry and, specifically, the impact of reactive surfaces, colloidal and natural organic matter. The BMWi funded collaborative projects THEREDA, HATT, KOLLORADO-2 and the BMBF/DFG funded project RECAWA should be specifically mentioned here.

Within the THEREDA project INE generates a centrally managed and administered database of evaluated thermodynamic parameters in cooperation with Gesellschaft für Anlagen- und Reaktorsicherheit (GRS) mbH, Braunschweig, Forschungszentrum Dresden-Rossendorf, Institut für Radiochemie (FZD-IRC), Technische Universität Bergakademie Freiberg, Institut für Anorganische Chemie (TU-BAF) and AF-Colenco AG, Baden (Schweiz). Thermodynamic data are required for environmental applications in general and radiochemical issues in particular. This database is to be developed to a national (reference) standard and will be the basis for performance assessment calculations for a national nuclear waste repository.

The HATT project focus on the migration of radionuclides in natural clay formations and in bentonite considered as technical barrier. Within this project not only the mechanism of sorption of radionuclides on clay, but also the influence of organic matter naturally occurring in the clay stone on the radionuclide migration are studied. Parallel to the characterization of clay organic compounds, the interaction of actinides with humic substances, kerogen-like compounds and small organic molecules are examined. Beside INE, the members of this collaborative project are GRS, FZD-IRC, University of Mainz, University of Potsdam, University of Munich and University of Saarland.

The bilateral GRS- INE project KOLLORADO-2 started mid 2009 as the successor of the project KOLLORADO focusing on the erosion stability of the compacted bentonite barrier as a function of the contact water chemistry/hydraulics and the formation of near-field colloids/nanoparticles as potential carriers for actinides/radionuclides. The outline of this project comprises both a detailed experimental program on the influence of surface roughness/charge heterogeneity on nanoparticle mobility and actinide bentonite nanoparticle sorption reversibility, as well as approaches to implement the obtained process understanding in reactive transport modeling codes.

In the BMBF/DFG funded joint research project RECAWA with partners from KIT (Institute of Reinforced Concrete Structure and Building Materials; KIT-IfMB, Institut of Mineralogy and Geochemistry; KIT-IMG), the University Frankfurt (Institute of Geoscience, UniFaM-IfG) and industrial partners (Rheinkalk Akdolit, Lafarge Cement and Schäfer Kalk), basic understanding of processes with regard to the reactivity and dynamics of calcite mineral surfaces during crystal growth in aquatic systems will be developed. INE focuses on the immobilization of environmentally relevant anionic trace elements (Se, U) on calcite surfaces using an integrated approach on the basis of batch sorption and co-precipitation experiments with molecular calculations and spectro-microscopic information.

In 2009 a memorandum of understanding (MoU) was negotiated between the USDOE / LANL Carlsbad Area Field Office and INE on actinide chemistry research in support of the Safety Case for the Waste Isolation Pilot Plant (WIPP) and the German disposal concepts. A workshop was held in Carlsbad, NM. Topics discussed covered actinide complexation / solubilities in brines, redox systems, Pitzer approach, as well as microbial effects and reactions of Mg based backfill / buffer materials.

A new project funded by the Bundesministerium für Bildung und Forschung in the framework of the funding concept ‘Basic research Energy 2020+’ entitled "Grundlegende Untersuchungen zur Entwicklung und Optimierung von Prozessen zur Abtrennung langlebiger Radionuklide (Partitioning)“ started in 2009. This is a cooperative project between the KIT (both Campus North and South), Forschungszentrum Jülich and the Universities of Erlangen and Heidelberg The aim is to establish an understanding the differing reactivity between 4f and 5f elements with the ultimate goal of using this information to optimize their separation in partitioning.

In 2009 activities in the Helmholtz – Russia Joint Research Group (HRJRG) entitled “Actinide Nano-Particles: Formation, Stability, and Properties Relevant to the Safety of Nuclear Waste Disposal” continued for their second year. This HRJRG is a cooperative effort between KIT-INE and the Chemistry Department of Lomonosov Moscow State University, with the goal of developing a molecular-level understanding of the formation, stability, and properties of nano-sized actinide containing colloids relevant to safe spent nuclear fuel (SNF) and high level radioactive waste (HLW) disposal, thereby filling conceptual gaps in the source term and transport models used in long-term assessment for deep geological repositories.

The Helmholtz University Young Scientist Group (HHNG) “Elucidation of Geochemical Reaction Mechanisms at the Water/Mineral Phases Interface” is supported by HGF and FZK since 2006. The partner of the HHNG is the Faculty of Chemistry and Geosciences of the University of Heidelberg. The project runs for five years with funds totaling 1.25 million Euro, including funding of the positions for the working group leader and for scientific or technical staff members, as well as non-personnel items. The leader of the working group has teaching functions at the Heidelberg University. In 2009

the group was evaluated successfully and will be funded until end of 2010.

The Virtual Institute (VI) “Advanced Solid-Aqueous Radio-Geochemistry“ supported by HGF and coordinated by INE began in March 2008. The work is focused on the elucidation of reaction mechanisms, which are responsible for the migration and/or retardation of radionuclides. The investigations range over a broad scale of complexity, from a thorough study of a model system for the formation of solid solutions (calcite, powellite), up to monitoring the complex interaction of cations and anions with cementious material under repository conditions. Experimental work, modern spectroscopy and Monte Carlo simulations, as well as quantum mechanical calculations are performed to achieve a process understanding on a molecular level. Members of the VI are KIT, the universities of Frankfurt (Germany) and Oviedo (Spain) and the Paul Scherrer Institut (PSI) in Switzerland. In February 2009 the workshop „From Atomistic Calculations to Thermodynamic Modeling“ was organized by the VI during the annual meeting of the German Association for Crystallography in Frankfurt. Furthermore, session 19h at the Goldschmidt 2009 Conference in Davos „Computational Geochemistry and the Geologic Disposal of Radionuclides“ was presented by VI members.

5 Fundamental Studies: Process understanding on a molecular scale

In the following section recent achievements are presented on basic actinide chemistry in aqueous solution which are relevant to the migration of actinides and long-lived fission products in the near- and far-field of a nuclear repository in deep geological formations. This includes provision of reliable thermodynamic data and models but also fundamental understanding of relevant processes. The reported studies deal with the chemistry of actinides in aqueous solution, their interaction with mineral/water interfaces and the formation of actinide containing solid solution phases. Whereas the first topic is oriented to derive realistic solubility data, both last topics are aimed at the elucidation of retention/ retardation mechanism and their thermodynamic quantification. These fundamental studies are strongly linked to applied studies on natural systems relevant for safety assessment. Finally, we have included in 5.4 recent basic studies on actinide chemistry by diploma and PhD students, which are not directly related to the INE research program, but will illustrate nicely the diversity of actinide chemistry.

5.1 Chemistry and thermodynamic of actinides in aqueous solution

M. Altmaier, N.L. Banik, B. Brendebach, M.A. Denecke, R. Götz, W. Hauser, R. Klenze, P. Lindqvist-Reiss, J. Lützenkirchen, C.M. Marquardt, V. Neck, P.J. Panak, J. Rothe, B. Schimmelpfennig, A. Skerencak, C. Walther.

In co-operation with:

C. Apostolidis[a)], F. Bruchertseifer[a)], R. Caciuffo[a)], E. Colineau[a)], Th. Fanghänel[a)], D. Fellhauer[a)], R.G. Haire[b)], N. Magnani[a)], A. Morgenstern[a)], J. Rebizant[a)], R. Sykora[b)], O. Walter[c)].

[a] *Joint Research Centre, Institute for Transuranium Elements, Karlsruhe* [b] *Transuranium Research Laboratory, Oak Ridge National Laboratory, USA* [c] *Institut für Technische Chemie, Karlsruhe Institute of Technology*

Introduction

KIT-INE research activities on the chemistry and thermodynamics of actinides are targeted to provide a reliable quantitative description of aqueous systems within accurate chemical models. Studies have focused on the determination of thermodynamic data, e.g. for An(IV) solubility and speciation in alkaline $CaCl_2$ solutions at high ionic strength, or Cm(III) complexation with sulphate at elevated temperatures. More fundamental studies have investigated the possibility of using advanced spectroscopic techniques to explore the chemistry of tetravalent Protactinium or examined the hydration of trivalent Actinides, again using a broad set of complementary experimental techniques.

Solubility of tetravalent actinides in alkaline $CaCl_2$ solution

Corrosion of an excess of cementitious waste in $MgCl_2$ brine leads to highly concentrated $CaCl_2$ systems at $pH_c \leq 12$. Recent solubility studies on Th(IV) [1] have shown that the solubility of $ThO_2 \cdot xH_2O$(am) in alkaline $CaCl_2$ solutions is enhanced orders of magnitude relative to comparable Ca-free solutions. A reliable model of actinide solubility and speciation is required. Supported by EXAFS investigations [2], a comprehensive thermodynamic model based on the hitherto unknown ternary complex, $Ca_4[Th(OH)_8]^{4+}$ has been derived. Extending our work on Th(IV), experiments have been performed to assess the analogous Np(IV), Pu(IV) and U(IV) systems.

Solubility batch experiments were conducted in an Ar glove box at 22 ± 2°C by addition of solid $AnO_2 \cdot xH_2O$ (with An = Np, Pu) to pre-equilibrated 0.25 - 4.5 M $CaCl_2$ solutions at pH_c = 10 - 12. Reducing redox conditions were adjusted either with 2 mM $Na_2S_2O_4$ or addition of iron powder. The pH, pe and [Np] was monitored up to 180 d until stable conditions indicated that equilibrium had been achieved.

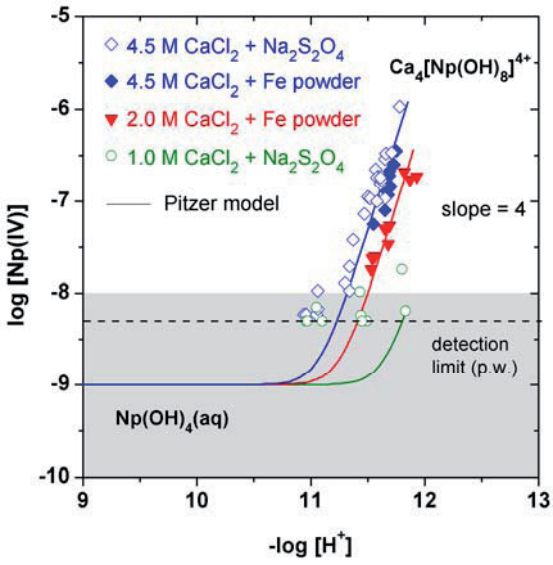

***Fig. 1**: Solubility of Np(IV) hydrous oxide in alkaline $CaCl_2$ solution in the presence of Fe powder or$Na_2S_2O_4$. Solid lines represent the An(IV) concentration calculated with the Pitzer model.*

Studies with $NpO_2 \cdot xH_2O$ (see Fig. 1) show that in 2.0 and 4.5 M $CaCl_2$, the Np concentration increases with a slope of +4 (log [Np] vs. pH_c) at $pH_c > 11$ as expected for the formation of the ternary complex $Ca_4[Np(OH)_8]^{4+}$:

$$Np(OH)_4(am) + 4\ H_2O + 4\ Ca^{2+} \Leftrightarrow Ca_4[Np(OH)_8]^{4+} + 4\ H^+$$

At $CaCl_2$ concentrations ≤ 1.0 M this effect is negligible. Plutonium experiments (not shown here) show a very similar behaviour, however at a considerably lower Pu concentration level.

Using the SIT and Pitzer model derived for Th(IV) [1] and assuming the same speciation scheme for Np(IV) and Pu(IV), thermodynamic constants were derived at I = 0 [3].

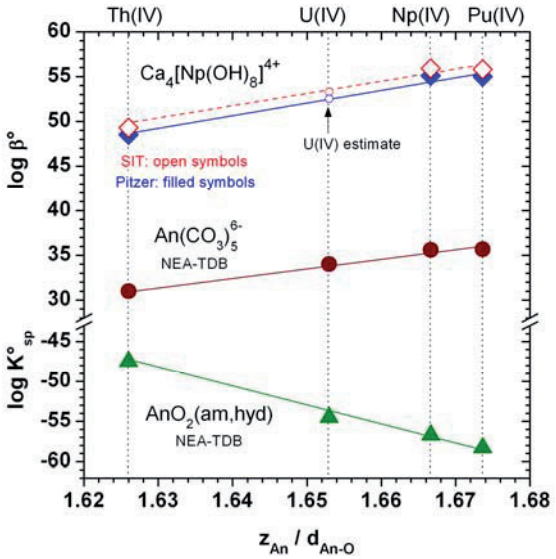

Fig. 2: *Solubility products log $K°_{sp}$ of An(IV) hydrous oxides, formation constants log $\beta°$ of $Ca_4[An(OH)_8]^{4+}$ and $An(CO_3)_5^{6-}$ (plotted for comparison) as a function of $z_{An}/d_{An\text{-}O}$. Thermodynamic data from [3].*

In Fig. 2, the formation constants of highly coordinated complexes are plotted versus the term $z_{An}/d_{An\text{-}O}$. Systematic trends in the Actinide series, e.g. known for $An(CO_3)_5^{6-}$, are evident and allow interpolation of log $\beta_{(4,1,8)}$ for the U(IV) system. As the total solubility arises from a summation of solubility products and complexation constants (log K_{sp} + log $\beta_{(4,1,8)}$), the solubility of tetravalent Uranium in concentrated alkaline $CaCl_2$ is expected to be similar the Np(IV) solubility:

$$Th(IV) > U(IV) \approx Np(IV) > Pu(IV).$$

Complexation of Cm(III) with sulphate in the temperature range of 25 to 200°C, studied by TRLFS

In order to understand the chemical behaviour of trivalent actinides under near field conditions of a nuclear waste repository, the complexation of Cm(III) with different inorganic ligands is studied at elevated temperatures. Previous work on this subject was performed with nitrate and fluoride as ligands. In the present work, the complexation of Cm(III) with sulphate was studied by TRLFS in the temperature range from 25 to 200°C. The experiments were performed in a specially designed high temperature and high pressure fluorescence cell [4]. Two sets of samples are prepared. The first set contains samples at constant ionic strength (I_m = 2.0 ($NaClO_4$)) and varying sulphate concentration ($[SO_4^{2-}]_{total}$ = $5.32 \cdot 10^{-3}$-$3.65 \cdot 10^{-1}$ mol/kg H_2O). The second set of samples is prepared at a constant sulfate concentration ($[SO_4^{2-}]_{total}$ = 0.2 mol/kg H_2O) and different ionic strengths (I_m = 1.0-4.0 ($NaClO_4$)). The proton concentration in all samples is fixed at $[H^+]_{total}$ = $8.93 \cdot 10^{-2}$ mol/kg H_2O with $HClO_4$.

The speciation of Cm(III) in sulphate solutions is derived by peak deconvolution of the emission spectra as function of ligand concentration and temperature. Some selected single component spectra which were derived for the peak deconvolution are displayed in Fig. 3.

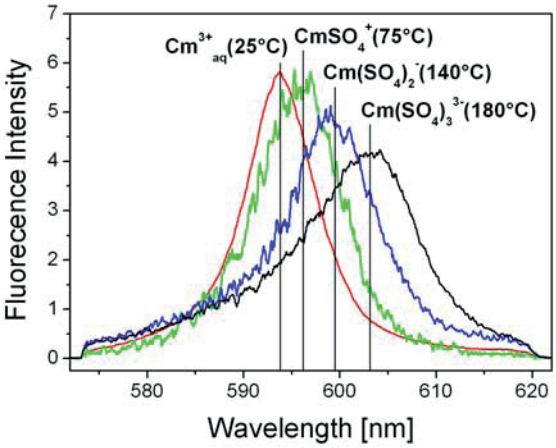

Fig. 3: *Single component spectra of the complexes $Cm(SO_4)_n^{3-(2n)}$ (n = 0, 1, 2, 3) at selected temperatures*

At T = 25°C the species distribution is governed by the molar fractions of the Cm^{3+} aqua ion and the $CmSO_4^+$ complex. The $Cm(SO_4)_2^-$ complex is formed only up to 20% and no $Cm(SO_4)_3^{3-}$ is observed under these conditions. At increased temperatures the chemical equilibrium is shifted towards the complexed species. At T = 200°C and high

sulphate concentrations molar fractions of the $Cm(SO_4)_3^{3-}$ complex of more than 90% are found.

In order to determine the conditional stepwise stability constants log $K'_n(T)$ at different temperatures, the free sulphate concentration at equilibrium conditions $[SO_4^{2-}]_{eq}$ must be known as function of temperature. The $[SO_4^{2-}]_{eq}$ is calculated using the published temperature dependent $pK_a(T)$ of SO_4^{2-} [5] and the total sulphate and total proton concentration ($[SO_4^{2-}]_{total}$ and $[H^+]_{total}$).

The log K'_n values are extrapolated to zero ionic strength using the SIT approach (specific ion interaction theory) [6]. The log $K^0_n(T)$ values are displayed in Fig. 4 as function of the reciprocal temperature. Thereby, the log $K^0_1(CmSO_4^+, 25°C)$ value is in very good agreement with literature data [7]. The comparison of log $K^0_2(Cm(SO_4)_2^-, 25°C)$ with literature data shows, that the value of log K^0_2 in this work is about 0.8 orders of magnitude higher than the corresponding value in [7]. Literature data for log K^0_3 is not available.

As shown in Fig. 4 the stepwise stability constants increase linearly with increasing temperature. Thus, constant $\Delta_r H^0_m$ of the individual, stepwise reactions are assumed and the linear Van't Hoff approach is used to model the temperature dependency of the stability constants. This approach describes the experimental data accurately over the studied temperature range, enabling the evaluation of the thermodynamic constants ($\Delta_r G^0_m$, $\Delta_r H^0_m$, $\Delta_r S^0_m$) for the stepwise formation of $CmSO_4^+$, $Cm(SO_4)_2^-$ and $Cm(SO4)_3^{3-}$ complexes (Table 1).

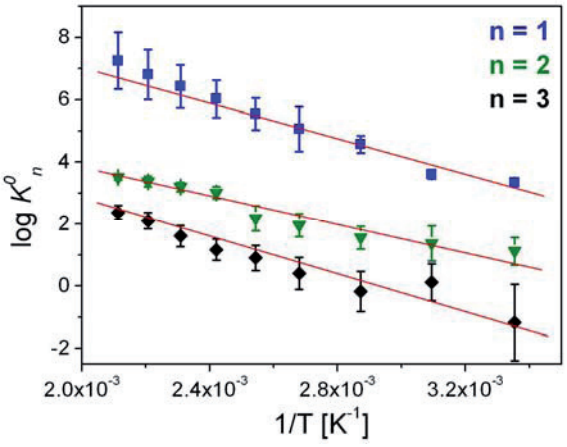

Fig. 4: *Thermodynamic stability constants of the stepwise formation of $Cm(SO4)_n^{3-2n}$ (n = 1, 2, 3) complexes.*

The results show, that the complexation of Cm(III) with SO_4^{2-} is entropy driven, yielding in an increase of the stability constants with increasing temperature.

Tab. 1: *Thermodynamic data for the stepwise formation of $Cm(SO_4)_n^{(3-2n)}$ complexes (n = 1, 2, 3)*

Reaction	n = 1	n = 2	n = 3
log K^0_n(25°C)	3.35 ± 0.13	1.12 ± 0.44	-1.17 ± 1.23
log K^0_n(200°C)	7.25 ± 0.91	3.51 ± 0.09	2.37 ± 0.23
log K^0_n (25°C) Literature [7]	3.28 ± 0.03	0.31 ± 0.03	-
$\Delta_r G^0_m$ (25°C) [kJ/mol]	-19.1 ± 0.7	-6.4 ± 2.5	6.7 ± 7.0
$\Delta_r H^0_m$ [kJ/mol]	53.5 ± 5.8	42.2 ± 4.7	55.1 ± 8.6
$\Delta_r S^0_m$ [J/mol·K]	240.4 ± 18.2	157.0 ± 10.8	160.2 ± 20.4

A series of hydrated An(III) ions (An = U-Cm, Cf): Synthesis, quantum chemistry and structural correlations

Trivalent lanthanide (Ln) and actinide (An) ions have similar coordination chemistry in solution and in the solid state. In aqueous solution, their interaction with water is electrostatic in nature and thus their hydration numbers are governed by their ionic radii. Though, with soft N-donor ligands such as BTP (2,6-bis-1,2,4-triazin-3-yl-pyridine), studies have shown that the An-N bonds are slightly shorter than the Ln-N bonds for complexes with similar An^{3+}/Ln^{3+} ionic radii, and the largest differences seem to occur near uranium [8]. This added bond contraction has been attributed to the participation of the U^{3+} 5f orbitals in the U-N bond, giving it a slight covalent character [8]. The ionic radii concept may therefore be a useful tool to assess such effects. Tabulated ionic radii are available for An^{3+} ions for six- and eight-coordination but is lacking for nine-coordination. However, values of the latter may be derived from crystal structures of isotypic compounds, e.g., $[An(H_2O)_9](CF_3SO_3)_3$ (AnTf). While the crystal structures of $[Ln(H_2O)_9](CF_3SO_3)_3$ (LnTf) were published in the 1980's [9], the first actinide triflate (PuTf) was reported more recently [10]. Since then we have reported the synthesis and crystal structures of five new actinide triflates, UTf - CmTf, and CfTf [11,12]. UTf and NpTf are extremely reactive but could nevertheless be isolated in high yields from their respective aqueous solutions using a specially designed

synthesis scheme, while CfTf required a micro-synthesis procedure owing to the scarcity and the hard gamma emission of ^{249}Cf.

The $[An(H_2O)_9]^{3+}$ and $[Ln(H_2O)_9]^{3+}$ ions in their respective triflate salts have tricapped trigonal prismatic coordination, where the six waters in the prismatic positions are tighter bound to the metal than the three in the capping positions (Fig. 5).

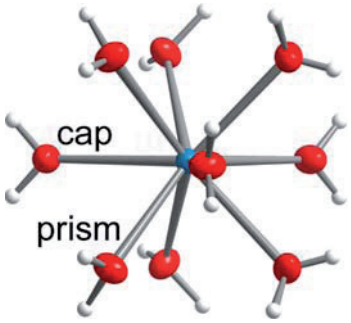

Fig. 5: *Molecular structure of the $[U(H_2O)_9]^{3+}$ ion in UTf (from X-ray single crystal data at 200 K).*

The decrease in the prismatic An-O and Ln-O distances with decreasing ionic follows roughly the An^{3+}/Ln^{3+} contraction. Also the capping distances take on this trend, but only for the lighter elements. The difference between the prismatic and capping An/Ln-O distances is ~0.1 Å in the beginning of the two series; this difference increases appreciably with decreasing ionic radii in the second half of the lanthanide series as the capping distances approach a constant value at ~2.52 Å (Fig. 6a). There are two major reasons for this effect: (*i*) the hydrogen bonding between the water ligands and the triflate ions and (*ii*) the steric crowding between the water ligands, the latter of which increases with decreasing ionic radii. The hydrogen bonding is also responsible for the special orientation of the capping waters, where the hydrogen atoms are located above and below the horizontal plane (cf. Fig. 5).

The absorption spectra of UTf, NpTf, AmTf and CmTf are rather similar to their parent aqueous solutions, suggesting likewise 9-fold coordination modes of the An^{3+} ions in aqueous solution and in the crystals. To further elucidate this point we used DFT on molecular clusters to mimic the cation structures in triflate crystals and in aqueous solution (for details, see Ch. 9.5). The An-O distances in the triflate clusters, $[La(H_2O)_9]^{3+}\cdots[An(H_2O)_9{}^{3+}\cdots Tf_9]^{6-}\cdots[La(H_2O)_9]^{3+}$, and in the aqua clusters, $[An(H_2O)_9]^{3+}\cdots(H_2O)_{18}$, are plotted in Fig. 6b. The cations in the triflate clusters mimic well those in the crystals, although the An-O bonds are ~0.06 Å longer than those derived from the X-ray data.

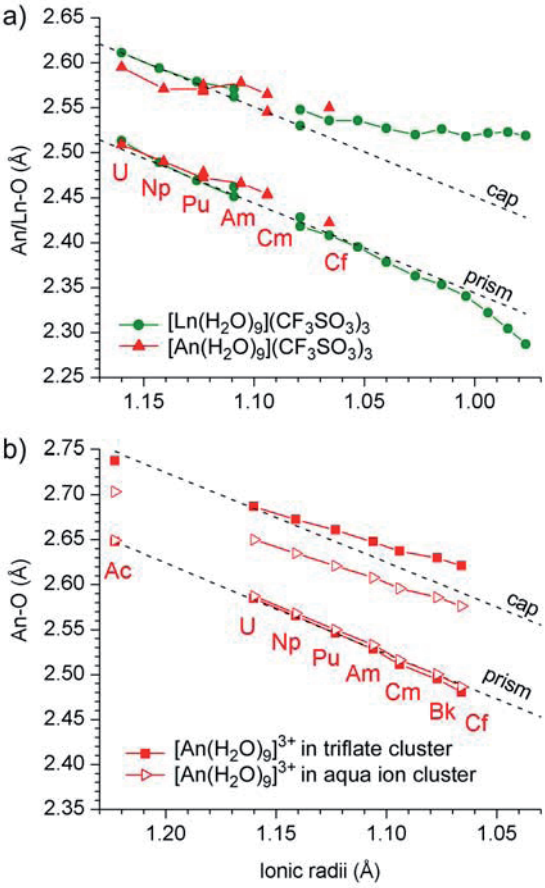

Fig. 6: *a) Comparison of the prismatic and capping An/Ln-O bond distances in the crystal structures of AnTf and LnTf. b) An-O bond distances in the triflate and aqua ion clusters (see [12] and Section 9.5 for details).*

In conclusion, we have reported the synthesis and crystal structures of AnTf (An = U-Cm, Cf) [11,12]. The structures may be used for deriving ionic radii for the An^{3+} ions in 9-coordination.

Results on the tetravalent protactinium aqueous chemistry

Whereas for the tetravalent actinides Th, U, Np and Pu an essential basic understanding of their chemistry in aquatic solution was achieved recently, this is not the case for tetravalent protactinium. Pa(IV) with the most simple $5f^1$ configuration enables speciation by optical spectroscopic and is also of large interest for quantum chemical studies. However, due to the constricted availability of Pa, the cascade of its α-emitting daughters and the low redox potential only few studies have been performed in this field. In this work, the potential of using XAFS, TRLFS, and UV-Vis spectroscopy for speciation studies of Pa(IV) is tested.

All experiments were performed with ^{231}Pa. The purification of ^{231}Pa from its daughters

^{227}Ac, ^{227}Th and ^{223}Ra was performed by ion-exchange chromatography. The activity and purity of ^{231}Pa are verified by α and γ spectrometry [13,14]. The concentration of ^{231}Pa in solution is measured by liquid scintillation counting (LSC) for all succeeding experiments. The penta- and tetravalent Pa species were characterized by absorption spectroscopy with a high-resolution UV-Vis/NIR spectrometer. To avoid oxidation by oxygen, all experiments were performed in an Ar glove box (O_2 < 5 ppm) at room temperature.

Preparation and stabilization of tetravalent Pa solutions is investigated as a prerequisite for further experimental work on aqueous Pa(IV) systems. So far, for the reduction of Pa(IV) from Pa(V) mainly liquid zinc amalgam or potentiostatic electrolysis were reported. We used here for the first time a chemical reductant, rongalite ($HOCH_2SO_2Na$) [15], for the preparation of Pa(IV). No complexation of rongalite with Pa was found under strongly acidic conditions.

It is known that Pa(IV) is easily oxidized in acids like HCl, H_2SO_4 and $HClO_4$ [13,16]. For stabilisation experiments, the rongalite concentration was fixed at 0.5 mmol/L. Three different acid solutions (HCl, $HClO_4$, H_2SO_4) at varying acidic strengths (1.0, 3.0, 6.0, 9.0 M), and with contact times between 1 h and 240 h were investigated. The Pa concentration was varied between 5 and 20 μM.

After different contact times, the oxidation states of Pa are monitored by UV-Vis and TRLFS spectroscopy. We observed that the Pa(IV) is oxidized more slowly in H_2SO_4 or HCl solution than in $HClO_4$. We found the stabilization of Pa(IV) in aqueous solution to be possible up to several days depending on the acids and increasing with their concentration.

XAFS measurements were performed at the INE-Beamline for Actinide Research at ANKA, Karlsruhe. Measurements were performed using a specially designed sample cell suitable to keep redox sensitive samples stable in an inert gas atmosphere long enough to record EXAFS data under stable redox conditions.

With this set-up we were able for the first time to record a XAFS spectrum of Pa(IV). Up to now only few Pa(V) but no Pa(IV)-XANES experiments have been reported in the literature. In Fig. 7 the Pa L3-XANES spectrum of $Pa(IV)_{aq}$ is shown in comparison to $Pa(V)_{aq}$, both in 1 M HCl. As expected, the white line maximum of the XANES of the $Pa(IV)_{aq}$ sample is clearly located at lower energy values compared to the pentavalent Pa. The corresponding energy values for the first

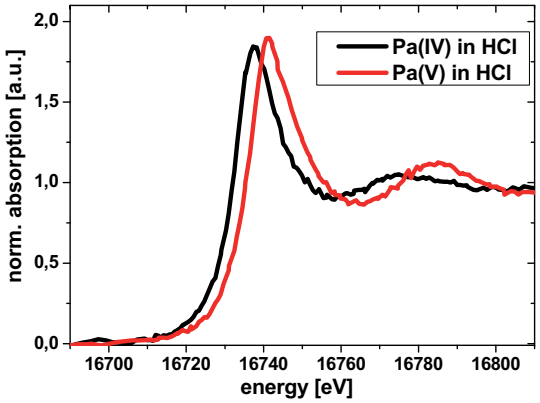

Fig. 7: *Pa L3-XANES spectra of Pa(IV) and Pa(V). The tetravalent Pa is prepared by rongalite (8.10^{-4} M) in HCl. [Pa] = $3.0 \cdot 10^{-4}$ M. The spectra have been normalized with respect to their edge jump.*

inflection points of Pa(IV) and Pa(V) are 16733.2 eV and 16735.2 eV, respectively. Energy values of the white line maxima are 16737.3 eV for Pa(IV) and 16741.5 eV for Pa(V), respectively. The white line position of the Pa(V) species in our experiments is comparable to the literature [17].

TRLFS measurements on Pa(IV) solutions were performed using a XeCl excimer laser for excitation. Emission spectra were recorded from 350 to 570 nm. Fluorescence life times of Pa(IV) species in different acid solution are comparable to literature [16]. Considerable improvement of the detection limit for Pa(IV) is possible by using TRLFS-OPO+SHG systems. Using this setup, Pa(IV) species are efficiently detected at the concentration between $1.5 \cdot 10^{-5}$ M and $5.0 \cdot 10^{-7}$ M. From the signal to noise ratio of the spectra we have derived a detection limit for Pa(IV) < $1.0 \cdot 10^{-8}$ M.

Based upon the work reported here it appears promising to further investigate the speciation and complexation of tetravalent protactinium using a combined experimental approach with TRLFS, XAFS and UV-Vis spectroscopy.

References

[1] M. Altmaier, V. Neck, T. Fanghänel, Radiochim. Acta, 96, 541-550 (2008).

[2] B. Brendebach, M. Altmaier, J. Rothe, V. Neck, M. A. Denecke, Inorg. Chem. 46, 6804 - 6810 (2007).

[3] D. Fellhauer, V. Neck, M. Altmaier, J. Lützenkirchen, T. Fanghänel, accepted for publication in Radiochim. Acta.

[4] A. Skerencak, P. J. Panak, W. Hauser, V. Neck, R. Klenze, T. Fanghänel, Radiochim. Acta, 97: 385-393, (2009).

[5] D. J. Wesolowski, D. A. Palmer, R. E. Mesmer, J. Phys. Chem. 94, 7978-7985 (1990).

[6] R. Guillaumont, T. Fanghänel J. Fuger, I. Grenthe, V. Neck, D. A. Palmer, M. H. Rand, (OECD, NEA-TDB). Chemical Thermodynamics Vol. 5. Update on the Chemical Thermodynamics of Uranium, Neptunium, Plutonium, Americium and Technetium. Elsevier, Amsterdam, (2003).

[7] P. Paviet, T. Fanghänel, R. Klenze, J. I., Kim, Radiochim.Acta 74, 99-103 (1996)

[8] J.-C Berthet, Y. Miquel, P. B. Iveson, M. Nierlich, P. Thuéry, C. Madic, M. Ephritikhine, J. Chem. Soc., Dalton Trans. 3265, (2002).

[9] J. McB Harrowfield, D. L. Kepert, J. M. Patrick, A. H. White, Aust. J. Chem., 36, 483 (1983); Chatterjee, A., Maslen, E. N., Watson, K. J., Acta Crystallogr., Sect B 44, 381 (1988).

[10] J. H. Matonic, B. L. Scott, M. P. Neu, Inorg. Chem. 40, 2638 (2001).

[11] P. Lindqvist-Reis, C. Apostolidis, J. Rebizant, A. Morgenstern, R. Klenze, C. Walter, T. Fanghänel, R. G. Haire, Angew. Chem., Int. Ed. 46, 919 (2007) c).

[12] C. Apostolidis, B. Schimmelpfennig, N. Magnani, P. Lindqvist-Reis, C. Walter, R. Sykora, A. Morgenstern, E. Colineau, R. Caciuffo, R., Klenze, R. G. Haire, J. Rebizant, F. Bruchertseifer, T. Fanghänel, (Angew. Chem., submitted).

[13] S. Suzuki et al., Bulletin of the Chemical Society of Japan, 39, 490, (1966).

[14] L. R. Morss, The chemistry of the actinides and transactinide elements, Springer, 3rd edition, Vol. 1, p.160-246.

[15] A. D. Gel'man et al., Sov.J. At. Energy., 4, 361, (1958).

[16] C. M. Marquardt et al., Radiochim. Acta, 92, 445, (2004).

[17] C. Hennig et al., Physical Review B, 77, 235102, (2008).

5.2 Sorption on mineral surfaces

E. Hartmann, N. Huittinen[*], M. Bouby, J. Lützenkirchen, T. Rabung, K. Dardenne, T. Preocanin[‡], P. Andrieux[+], J. Letho[*], T. Fanghänel[#], H. Geckeis

[*]*Laboratory of Radiochemistry, Department of Chemistry, University of Helsinki, P.O. Box 55, FIN-00014 University of Helsinki, Finland*

[‡] *Laboratory of Physical Chemistry, University of Zagreb, Horvatovac 102a, 10000 Zagreb, Croatia*

[+]*HydrASA, Université de Poitiers, 40 avenue du Recteur Pineau, 86022 Poitiers Cedex, France*

[#]*European Commission, Joint Research Center, Institute for Transuranium Elements, P.O. Box 2340, D-76125 Karlsruhe, Germany*

A Comparative batch sorption and TRLFS study on the sorption of Eu(III) and Cm(III) on synthetic and natural kaolinite

Introduction

Crystalline bedrock is considered as host rock material for the final disposal of high-level nuclear waste by a number of countries like Finland, Sweden, and Canada. Groundwater flow into the repository may mobilize radionuclides in the waste and facilitate migration in the geosphere. Fracture flow is considered as the most important transport mechanism and fracture filling minerals play a dominant role in retention and retardation for radionuclide migration. Weathering of crystalline rock results in the precipitation of a variety of alteration products like chlorites and clays finally sealing the fracture. Kaolinite is one common fracture clay mineral acting as a potential sorbent for groundwater solutes. Numerous sorption studies have been performed with natural kaolinite for elucidating the sorption mechanisms and geochemical behaviour of the investigated metal ions in the system. Natural kaolinite contains a variety of impurities like illite, micas, anatase, quartz and iron oxides. Especially, iron impurities may impede the application of ultrasensitive time-resolved laser fluorescence spectroscopy (TRLFS) due to their quenching properties.

In the present study, kaolinite was chosen to investigate trivalent actinide sorption [2]. To reduce the possible effect of quenching impurities, pure kaolinite was synthesized, characterized [2] and compared with the properties of a natural kaolinite (St. Austell, UK) up to pH 13. Cm(III) was chosen as a model substance for Pu(III) and Am(III) due to its excellent fluorescent properties suitable for investigations by means of TRLFS. The investigated pH range mimics the potential impact of alkaline solutions being generated by concrete corrosion in a repository. Batch sorption studies were also performed using Eu(III) as a homologue for trivalent actinides.

Eu(III) batch sorption study

Fig. 1 presents Eu(III) sorption diagrams for the synthetic and natural kaolinite for three Eu concentrations between $6.6 \cdot 10^{-8}$ M and $6.6 \cdot 10^{-6}$ M. At the two lowest Eu concentrations the sorption behaviour of Eu on both examined minerals is identical, typical for the so called ideal sorption range. At the highest metal ion concentration of $6.6 \cdot 10^{-6}$ M, a shift of the pH edge of approximately one pH unit is observed for both minerals due to saturation effects coupled with a surface site heterogeneity. For kaolinite two distinct mechanisms for cation sorption are possible: (i) sorption through ion exchange at the permanent negative charges dominating the sorption at low pH and low ionic strength and (ii) sorption through complex formation at the S-OH groups on the surface, occurring mainly at intermediate and high pH. For kaolinite, permanent negative charge usually arises from Si^{4+} substitution by Al^{3+} ions. The major difference in the retention of Eu(III) by synthetic and natural kaolinite can be observed for the lowest Eu(III) concentration, where sorption is only visible below pH 5 for the natural kaolinite. This difference arises from a larger Eu(III) retention through ion exchange at the permanent negative charges of the natural kaolinite mineral which is in accordance with ξ-potential data showing more negative values at pH < 5 for the natural kaolinite. This is an indication for a higher cation exchange capacity of the natural mineral.

Curium emission spectra

From peak deconvolution of the recorded emission spectra four single components in addition to the aquo ion spectrum can be resolved in the synthetic kaolinite system, with peak maxima at 598.8, 602.6, 607.4 and 610.9 nm, which are almost identical to those of the natural kaolinite (Fig. 2). From the pure spectral components the Eu(III) species distribution as a function of pH can be calculated taking into account the different fluorescence intensity (FI) factors for the individual species (Fig. 3). A very similar species distribution is obvious for the two different kaolinite minerals.

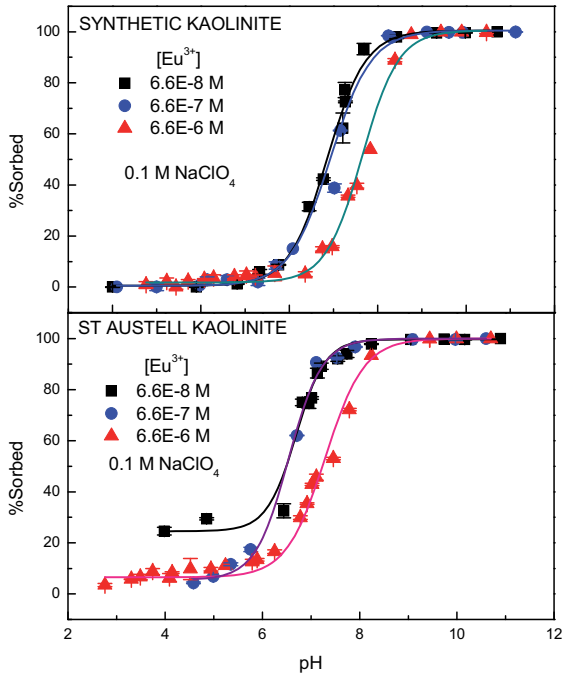

Fig. 1: *Eu(III) sorption on synthetic and natural kaolinite. c(Eu): 6.6×10^{-8}-6.6×10^{-6} M, c(solid): 0.25 g/L, I = 0.1 M $NaClO_4$*

The similarity of FI-factors for both the synthetic kaolinite without noticeable Fe-content and the natural mineral with ~1% structurally bound Fe does not support the idea discussed earlier, that Fe might partly be responsible for the decrease in fluorescence intensity which is observed for many inner-sphere surface complexes [3].

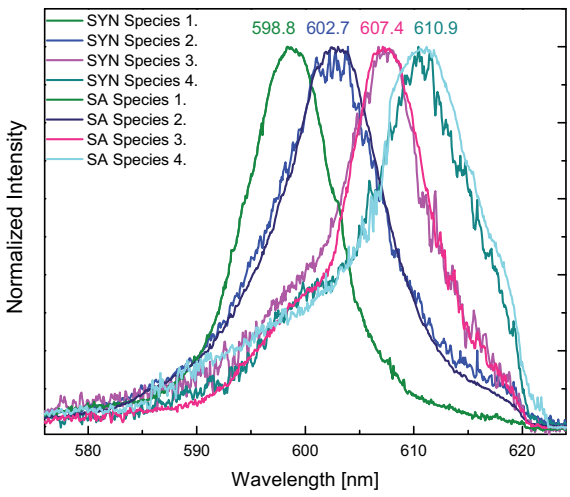

Fig. 2: *Single component spectra for synthetic (SYN) and natural (SA) kaolinite, respectively.*

Discussion

The obtained pure spectra components in our study show good agreement with Cm(III) sorption studies onto the clay minerals Ca-montmorillonite and Na-illite [3] and those for Cm(III)-kaolinite sorbed species [4]. Based on the very similar peak positions and the lifetime data extracted from our Cm(III)-kaolinite samples, yielding an average 4.3-5 H_2O/OH^- entities in the first coordination sphere of the metal ion, we can conclude that the three Cm(III) complexes on all investigated clay-minerals are very similar. However, due to the large scattering of the lifetime values obtained in the alkaline pH range, additional lifetime measurements need to be performed. The nature of the fourth species in the TRLFS study could be explained by a possible incorporation arising from the increasing solubility of both Al and Si when the pH is raised above 9. The increasing amount of these elements in solution could oversaturate the solution with respect to some other aluminosilicate phases that consequently precipitate from solution covering already surface-bound curium on the kaolinite surface. Incorporation of Cm was also found in older studies using hectorite [5] or gibbsite [6]. In the latter case dissolution and precipitation processes are assumed to be responsible for the incorporation.

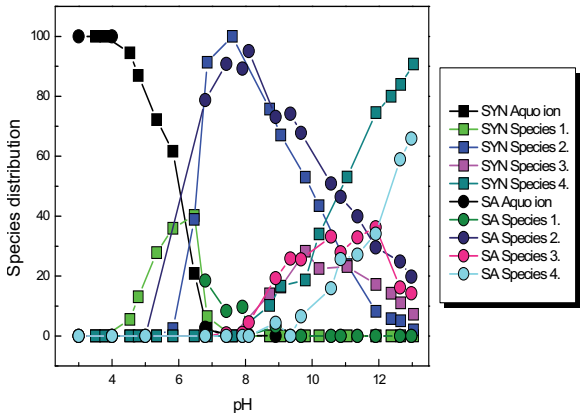

Fig. 3: *Species distribution for Cm(III) sorption onto synthetic (SYN) and natural (SA) kaolinite.*

Conclusions

The results of the present study reveal similar macroscopic sorption behaviour of Eu(III) and consequently very similar Cm(III) surface species distribution in presence of synthetic and natural kaolinite, respectively. The largest differences in macroscopic sorption behaviour occurs at the lowest Eu(III) concentration, where a significant amount of Eu(III) sorption was observed on the natural kaolinite at pH < 5, while approximately no sorption at all was found with the synthetic mineral. The occurrence of outer-sphere complexation on the natural mineral has already been reported by Stumpf et al. [4] in TRLFS studies, while no such species was evidenced in the present study for the synthetic kaolinite due to missing isomorphic substitutions. Three curium surface

species are derived from TRLFS data for both kaolinites, comparable to earlier studies on Ca-montmorillonite and Na-illite surfaces [3]. An additional possibility of Cm(III) interaction by presumably surface precipitation is proposed as a fourth pure component peak and is found for both the synthetic and natural kaolinite under alkaline conditions.

Modelling of Eu interaction with TiO_2

TiO_2 is an accessory mineral of clays as indicated in the previous section. Consequently, separate studies on this mineral do contribute to understanding uptake on the natural mineral assemblages, given that TiO_2 is a particularly strong sorbent for metal ions. Sorption of Eu(III) (and whenever more appropriate Lu(III)) onto TiO_2 (P-25, Degussa, a mixture of anatase and rutile) from aqueous solution was studied as a function of pH, ionic strength and trivalent metal ion concentration. An acid base model for the titanium dioxide surface was determined from potentiometric titrations and zeta-potential measurements. The common intersection point of potentiometric titrations coincided with the isoelectric point from electrokinetic experiments, resulting in a pristine point of zero charge of about 6.1. The experimental data were in agreement with previously published results. A previously published MUSIC-type model was used as the basis to start modelling the acid-base behaviour. Comparison of Eu(III) and Lu(III) showed no difference in the adsorption behaviour. Furthermore, no difference was observed both in uptake and spectroscopic studies whether carbonate was absent or present. The absence of a noticeable effect of the ionic strength on the adsorption behaviour was indicative of relatively strong binding. EXAFS reveals roughly conservation of the coordination with 9-8 water and surface hydroxyl groups upon sorption. A clear differentiation of surface complexation denticity was not possible based on spectroscopic data. However, EXAFS suggests the existence of various slightly different metal-oxygen distances different to what is observed for the respective aquo complexes and thus indicative for inner-sphere surface complexation. A multi site surface complexation model approach is applied by assuming monodentate and multidentate binding to describe the trivalent metal uptake data.

Model development

Model development is stepwise. The first step is to define the aqueous speciation. This is done by using thermodynamic data from the respective NEA-TDB sources [7]. The second step is to describe the acid-base properties of the sorbent. The acid-base properties were experimentally determined by surface titrations and zeta-potential measurements. The acid-base model was based on previous work by Bourikas et al. [8]. Two variants were tested. Option A included parameter values that had previously been determined by Bourikas et al. [8] for a range of titanium oxide samples. In option B these parameters were optimised. Fig. 4 shows the results for the acid-base titrations.

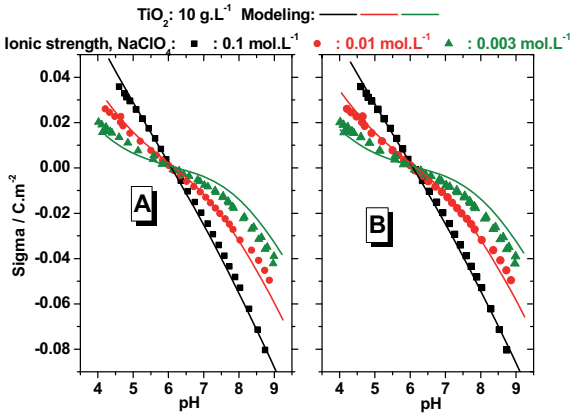

Fig. 4: *Results of the potentiometric titrations and the modelling with the acid base model; A: published parameters data by Bourikas et al. [8] were applied, B: all parameters were optimised.*

Fig. 5 shows the respective outcome for the zeta-potential measurements. The isoelectric point of the P-25 studied here was found to be close to pH 6.0, in agreement with data from the literature [8]. The fit to the data by both model options is similar and therefore the model option with fewer adjustable parameters was used for the subsequent step.

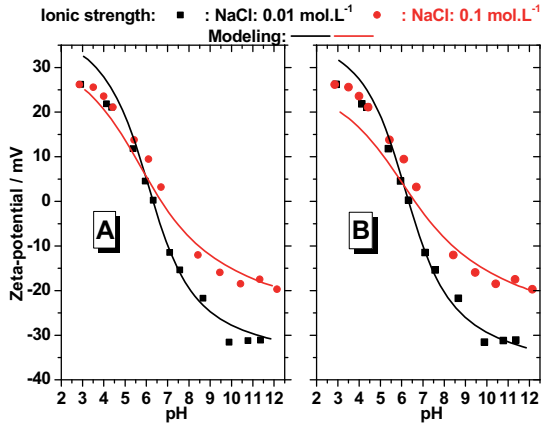

Fig. 5: *Results of the electrokinetic measurements at different ionic strengths in NaCl medium. Experimental results are fitted using the modelling with the acid base MUSIC model; A: Option A, B: Option B as described in the text and Fig.4.*

Once the acid-base model is defined the adsorption data for Eu onto the sorbent can be modelled. In the present case this is done by imposing the structures of surface complexes. The formation of monodentate complexes on TiO_2 is a possible interpretation of the EXAFS results. This defines the metal ion to surface hydroxyl ratio. The proton stoichiometry for forming such a monodentate surface complex has to be obtained from the experimental data by fitting various assumptions to the uptake data. The monodentate surface complex will be referred to as Option 1.

A second surface complex stoichiometry was tested. The structure was based on recent diffraction studies on single crystals of rutile (110) surfaces [9]. In this work it was found that trivalent cations form a tetradentate surface complex. To test whether such a structure could explain the experimental observations, the same strategy as for the monodentate structure (Option 1) was pursued and various proton stoichiometries for the tetradentate structures were tested, resulting in option 2. The Eu adsorption models were based on the acid-base model option A (with fewer adjustable parameters). Fig. 6 shows experimental results for so-called isotherms. The pH and the ionic strength are kept constant and the amount of Eu is varied. For three different pH values, the two model options describe the data equally well (Fig. 6).

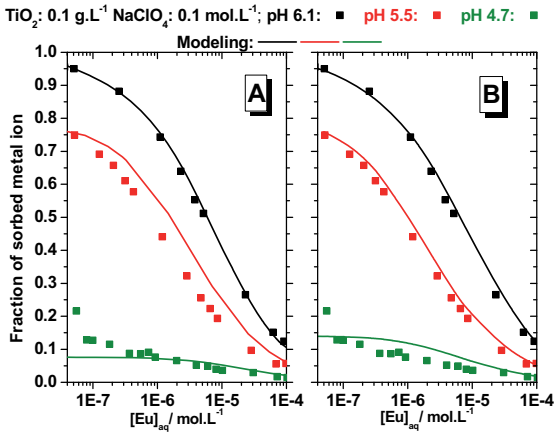

Fig. 6: *Results of adsorption experiments at constant ionic strength and variable total Europium concentration at three different pH values. A. Option 1, i.e. monodentate surface complex, based on EXAFS measurements done on the present sample. B. Option 2, i.e. tetradentate surface complex, based on surface diffraction measure-ments from the literature [9].*

The same model options also describe the effects of ionic strength on the adsorption behaviour of Eu in a similar way (data not shown).

The modelling shows that different assumptions will usually result in similar fits to the experimental data with a slight improvement for the tetradentate arrangement. EXAFS data do not provide a clear evidence for the exact surface complex structure. The assessment of a fourfold coordination of the metal ion to surface oxygen or hydroxyl groups is consistent with previous TRLFS results derived at INE, which yield five water molecules remaining in the hydration shell of trivalent metal ions on various mineral surfaces [e.g. 10, 11]. It is thus tempting to favour the tetradentate surface complex model.

Nevertheless, it is presently not possible to decide on the exact nature of the inner sphere complexes formed in this study based on spectroscopy and modelling. TRLFS as well as XAFS provide only averaged information on various different species.

Sorption of radionuclides onto natural clay rocks

Sorption onto natural mineral surfaces is regarded as a dominant retardation/retention process for radionuclides in the near and far-field of a repository for radioactive waste. Clay formations are investigated in several countries as potential host rocks for deep nuclear waste repositories. Due to their highly reactive and large surface clay minerals show a strong interaction with radionuclides.

Natural clay rocks, e.g. Opalinus clay from Switzerland and the Callovo-Oxfordian clay (COx) from the underground research laboratory near Bure in France, represent heterogeneous multiphase systems with a relatively high calcite resp. carbonate content (approx. 8 to 20 wt. %) and up to 2 wt.% natural organic matter. The clay mineral content averages 50 % whereas the rest is distributed to a multitude of different mineral phases. The aim of the present investigations is to identify the relevant mineral phases for sorption in natural clay rocks and the associated surface sorption reactions [12].

So far, batch experiments as well as spectroscopic investigations on the speciation of surface sorbed actinides and lanthanides were carried out mostly with pure mineral phases, e.g. quartz, calcite, feldspar, Fe/Al oxides/hydroxides or various purified clay minerals, e.g. smectite, kaolinite and illite. This work focuses on the sorption of Eu(III) (chemical homologue to trivalent actinides) and U(VI) onto natural clay rocks (COx and Opalinus clay) and on mixtures of purified clay, humic acid (HA) and/or calcite. Experiments

with the mixtures aim to simulating the sorption behaviour of the natural clay rocks.

Comparing the outcome of batch sorption studies with natural clay rocks and simulating mixtures with calcite as well as thermodynamic calculations suggests that U(VI) behaviour is dominated by sorption to clay minerals at pH 4-7 and formation of sorbed anionic hydroxo complexes in the high pH region (>9) under given experimental conditions. At neutral conditions the formation of aqueous U(VI) carbonate species is responsible for a strong decrease of U(VI) sorption. As an example, in Fig. 7 the results of the batch experiments and subsequent modelling are shown for U(VI) sorption onto COx. For the calculations literature data have been used [13-15] and the clay content of 42 wt% was treated as 22 wt% illite and 20 wt% montmorillonite. Possible sorption of U(VI) carbonate species has not been considered in the modelling as thermodynamic data are not available. For details see [12].

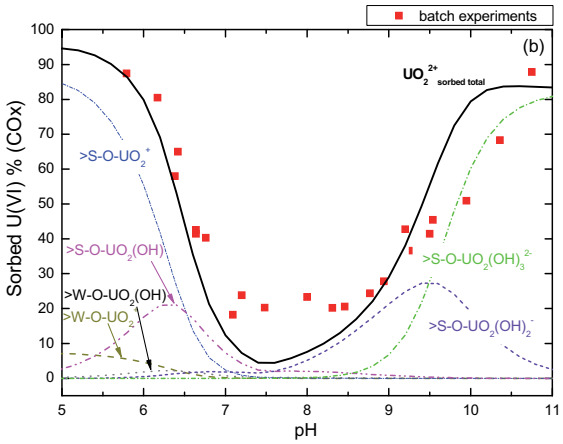

Fig. 7 *Modelled and experimental results of surface speciation of U(VI) adsorbed onto COx containing 17.3 wt.% calcite. Calculations done without consideration of aqueous complex $Ca_2UO_2(CO_3)_3$ and sorbed U(VI) carbonate species. Assumptions for calculations: see [12].*

The influence of carbonate and HA on U(VI) sorption is visualized in Fig. 8. For this experiment a purified smectite (SWy-2) in the presence and absence of calcite and/or humic acid was used.

In case of Eu(III) complete sorption to natural clay rock and a simulate containing a mixture of clay and calcite is observed at pH >7. Model calculations again point to the predominance of clay-sorbed species (Fig. 9). The small deviations between experiment and modelling at neutral pH are due to the presence of sorbed Eu(III) carbonate species not being considered in the calculations. Preliminary Time Resolved Laser Fluorescence Spectroscopy (TRLFS) studies using Cm(III) as fluorescent probe reveal the appearance of several Cm(III)-clay surface species in the pH range 5-11.

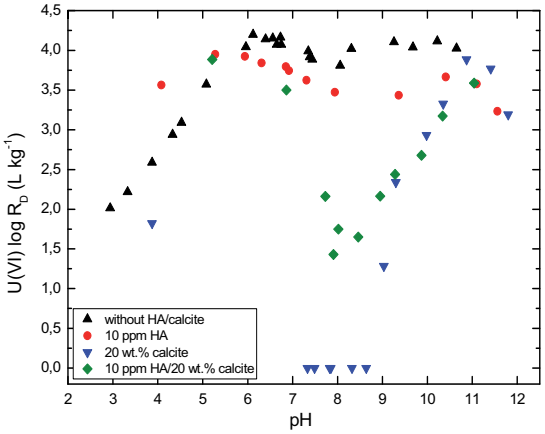

Fig. 8: *U(VI) sorption edges on SWy-2 adding humic acid (10 mg/L) and/or calcite (20 wt.%), respectively, dependent on pH. c(U(VI)) = 1 x 10^{-7} mol/L; S/L ratio = 2 g/L; background electrolyte = 0.1 mol/L $NaClO_4$.*

Based on all findings, we conclude that mainly the clay minerals in the clay rock act as sorbents for tri- and hexavalent actinides. Presence of dissolved humic matter decreases Eu(III) sorption in a pH range 7-11 showing that complexation with natural organic matter has some impact on trivalent actinide sorption in clay systems. Presence of carbonate strongly decreases the sorption of U(VI) onto clays and clay rocks.

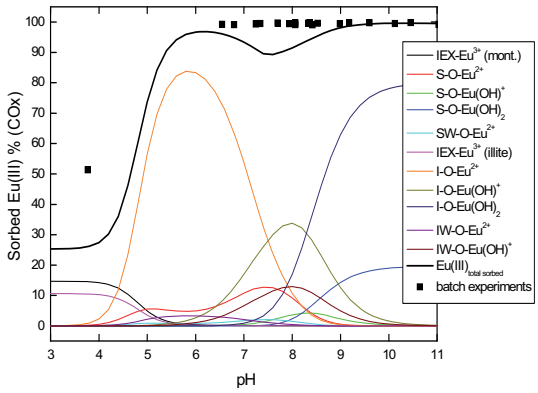

Fig. 9: *Modelled and experimental results of surface speciation of adsorbed Eu(III) in clayey system with montmorillonite and illite fraction containing 17.3 wt.% calcite. Assumptions for calculations: see [12] (IEX = ion exchange, S = smectite resp. montmorillonite, I = illite, W = weak sites)*

References

[1] A. R. Blyth, S. K. Frape, E.-L Tullborg, Appl. Geochem 24, 821-835 (2009).

[2] N. Huittinen, T. Rabung, P. Andrieux, J. Lehto, H. Geckeis, Radiochim. Acta, accepted.

[3] T. Rabung, M. C. Pierret, A. Bauer, H. Geckeis, M. H. Bradbury, B. Baeyens, Geochim. Cosmochim. Acta 69, 5393-5402 (2005).

[4] T. Stumpf, A. Bauer, F. Coppin, J. I. Kim, Environ. Sci. Technol. 35, 3691-3694 (2001).

[5] H. Brandt, D. Bosbach, P. J. Panak, T. Fanghänel, Geochim. Cosmochim. Acta 71, 145-154 (2007).

[6] N. Huittinen, T. Rabung, J. Lützenkirchen, S. C. Mitchell, B. R. Bickmore, J. Lehto, H. Geckeis, J. Colloid Interface Sci. 332, 158-164 (2009).

[7] R. Guillaumont, T. Fanghänel, J. Fuger, I. Grenthe, V. Neck, D. A. Palmer, M. H. Rand, Update on the chemical thermodynamics of uranium, neptunium, plutonium, americium and technetium, ELSEVIER B.V., Amsterdam, The Netherlands (2003).

[8] K. Bourikas, T. Hiemstra, W. H. Van Riemsdijk, Langmuir 17, 749-756 (2001).

[9] Z. Zhang. et al., Langmuir 20, 4954-4969 (2004).

[10] T. Rabung, H. Geckeis, X. K. Wang, J. Rothe, M. A. Denecke, R. Klenze, T. Fanghänel, Radiochim. Acta 94, 609-618 (2006).

[11] M. Marques Fernandes, T. Stumpf, B., Baeyens, M. H. Bradbury, Env. Sci. Technol. 44, 921–927 (2010).

[12] E. Hartmann, H. Geckeis, T. Rabung, J. Lützenkirchen, T. Fanghänel, Radiochim. Acta, 96, 699-707 (2008).

[13] M. H. Bradbury, B. Baeyens, H. Geckeis, T. Rabung, Geochim. Cosmochim Acta 69(23), 5403-5412 (2005).

[14] M. H. Bradbury, B. Baeyens, Geochim. Cosmochim. Acta, 66(13), 2325-2334 (2002).

[15] M. H. Bradbury, B. Baeyens, Geochim. Cosmochim. Acta 69(4), 875-892 (2005).

5.3 Retention of radionuclides by secondary phase formation

T. Stumpf, F. Heberling, T. Schäfer, M. Schmidt, C. Borkel, C. Walther, D. Bosbach

Carbonate minerals have turned out to contribute to the retention of highly radiotoxic actinides. In this context the actinide sorption process and the long-term retention via solid solution formation is particularly interesting. The $CaCO_3$ mineral system consists of three anhydrous polymorphs (in order of stability: calcite, aragonite and vaterite) that can all be found in nature. The thermodynamically stable polymorph under ambient conditions is calcite. In the following chapter we will focus on the interaction of Eu(III)/Cm(III) with vaterite, on the effect of Eu(III) on the calcite crystal growth and on neptunyl calcite sorption and structural incorporation into calcite.

Cm(III)/Eu(III) speciation changes during the vaterite – calcite phase transition

Eu(III) and respectively Cm(III) doped vaterite was precipitated by a method described by Turnbull [1]. Fig. 1 shows the SEM micrographs taken 2h after precipitation (a), after 24h in vacuum (b), as well as after 24h, 36h, 48h and 72h in saturated $CaCO_3$ solution (c – f, respectively). The two occurring mineral phases, vaterite and calcite, can clearly be distinguished by their characteristic morphologies. Vaterite can be recognised as framboidal spheres while calcite forms rhombohedral crystallites. With prolonged time the amount of vaterite decreases and more calcite is found. After 72h only calcite particles can be observed.

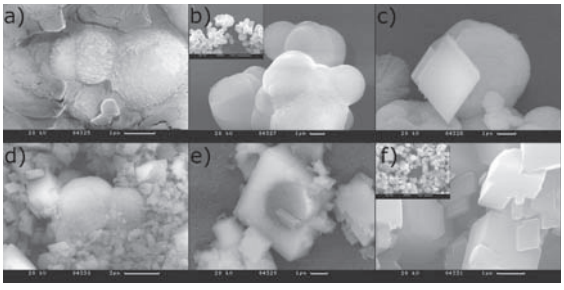

Fig. 1: *SEM micrographs of the various stages of the vaterite calcite transformation. a) 2h after precipitation, b) after 24h in vacuum, c - f) after 24h in vacuum and 24h, 36h, 48h, and 72h in saturated $CaCO_3$ solution, respectively (Inserts b: 10µm, f: 3µm scale) .*

Selective excitation of the Cm^{3+} $^8S_{7/2} \rightarrow {}^6D_{7/2}$ transition at low temperatures allows discrimination of different coordinative environments of Cm^{3+} in a sample. The sample is cooled to below 20K and subsequently excited through the spectral range of interest from 595 to 625nm. Similar applies for Eu^{3+}: here the $^7F_0 \rightarrow {}^5D_0$ transition is excited, which is most suitable as it is non-degenerate, due to the J=0 characteristics of both involved energy levels. The transition lies in between 574 and 583nm. The excitation spectrum is obtained as integral emission intensity as a function of excitation wavelength. The Cm^{3+} spectrum consists of

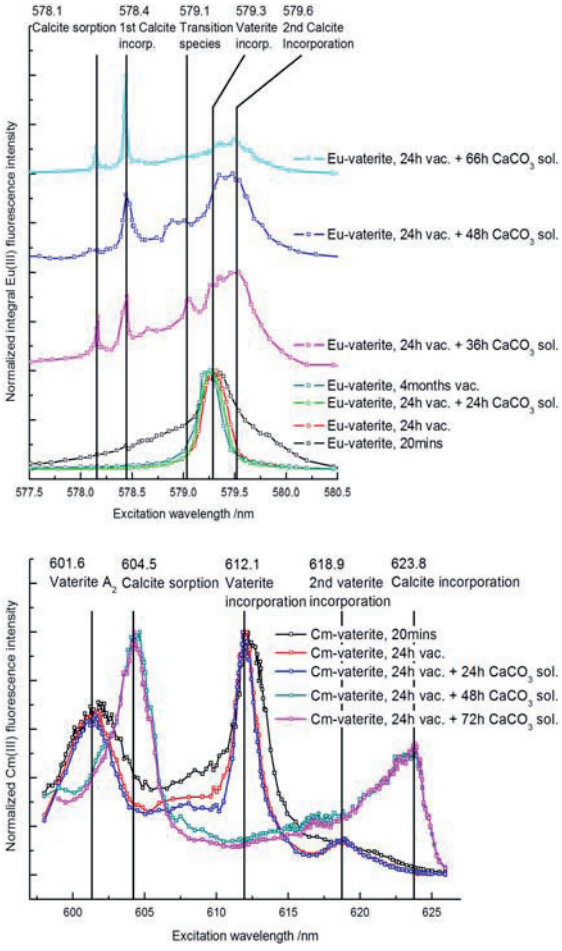

Fig. 2: *Excitation spectra of the Eu^{3+} samples (top) and Cm^{3+} samples (bottom) with the same time steps described above.*

two peaks at 612.1nm and 601.6nm, respectively, corresponding to two sublevels of the $^6D_{7/2}$ level (figure 2). Both transitions are rather broad and do not feature a recognizable splitting pattern. The Eu^{3+} excitation spectrum corroborates these observations. One broad peak centred at 579.3nm is observed, with a distinctive shoulder to the blue side of the spectrum.

After 24h in the vacuum the peak centers stay at the same wavelength for both Cm^{3+} and Eu^{3+} but the peaks become significantly sharper. Although macroscopically minor calcite traces were already detected after 24h in the $CaCO_3$ solution no significant changes are observable in the excitation spectra. Apparently no changeover to calcite takes place as long as vaterite is the dominant mineral phase.

The phase transformation becomes imminent after 36h in solution. The Eu^{3+} excitation spectrum now features a total of five different species. All three well-known Eu-calcite species are present now [2]. The surface incorporation species A is found at 578.1nm, and the asymmetrically incorporated species B at 578.4nm. The symmetrically incorporated species C, with Eu^{3+} replacing Ca^{2+} on its nearly undisturbed lattice site is centred at 579.6nm. Species C is dominant in the spectrum. However, a strong shoulder indicates the presence of the Eu-vaterite species at 579.3nm. After another 12h in solution only the known calcite species are found for both, Cm^{3+} and Eu^{3+}. All three known species are reproduced though the relative intensities varying from those obtained by direct near-equilibrium precipitation of calcite. The Cm^{3+} excitation spectrum is dominated by the surface sorption species at 604.5nm which coincides with the A_2 level of the incorporation species which is here found at 623.8nm. Its peak is extremely broad and does not show the splitting pattern known from calcite samples obtained under different conditions. The second incorporation species B at 616.9nm is strongly suppressed and thus hardly visible in the broad shoulder of species C's signal. This may be due to the very low Cm^{3+} concentration in the sample. While the Cm^{3+} excitation spectrum remains widely unchanged after another 24h in the $CaCO_3$ solution, in the Eu^{3+} spectrum another redistribution of the three species can be observed. The asymmetrically incorporated species B is becoming more pronounced, while the peaks generally appear sharper.

The results obtained earlier in near-equilibrium mixed flow reactor (MFR) experiments were finely reproduced [2]. Eu^{3+} as well as Cm^{3+} are taken up quantitatively into vaterite and consecutively are completely transferred into calcite during the phase transformation. A supplementary indication that there is thermodynamic driving force for the formation of solid solutions in the investigated systems is the fact that all species known from the near-equilibrium experiments are reproduced in the phase transformation process. It is also interesting to notice that the transition of Eu^{3+} and Cm^{3+} does not start with the first appearance of calcite, but only later when calcite has become the dominating mineral phase. This may be an indication that the eightfold carbonate coordination of trivalent f-elements in vaterite is preferred in comparison to the six fold coordination in the calcite lattice.

Effect of Eu(III) on the calcite crystal growth: A nanotopographic study

This study compares crystal growth of calcite in pure and Eu containing solutions using AFM to see the effects of foreign trace elements on nanotopography. The focus is put on growth spirals emerging on the most stable {104} crystal face because spiral growth is the dominant mechanism at low supersaturated conditions often relevant in nature.

The main result from the experiments performed in this study is that the precipitation of calcite is strongly influenced by Eu on the microscopic scale. This is consistent with macroscopic observations. The quantity of 0.1µmol/L Eu in supersaturated solutions modifies the rate of incorporation at calcite kink-sites or steps effectively. The geometrically and chemically not equivalent kink-sites on acute and obtuse steps on calcite {104} cleavage faces react differently to the foreign ion in solution what can be concluded from modifications of step velocities: The different degree of effectiveness for modification of relative step velocity is expressed by the angle φ, used as a tool to compare relative step velocities in the different sectors.

In the performed experiments dependency of φ on pump rate is not observed even though an increase in pump rate from 0.5 to 1.3mL/min is accompanied by a doubling of step velocity in the Eu^{3+} free system. That means that at least slight variation of these parameters does not cause the different angles φ, determined as roughly 115° in the pure solution and 175° when Eu^{3+} is added. This provides a reasonable indication for the significant influence of europium on calcite precipitation. Further indication for the significant influence of Eu on calcite precipitation is provided by the different solution compositions in which the spirals grow or cease to grow.

Different findings may be extracted: First, Eu^{3+} actively inhibits calcite precipitation (between pH 8.20 and 8.31) and second, Eu^{3+} is probably incorporated differentially into the not equivalent steps, suggested by the different degree of roughening and according to sectoral zoning. The results from spiral growth in pure solution together with strong inhibition of spiral growth in Eu spiked solutions demonstrate a strong inhibitory influence. This is in

good accordance with macroscopic observation by Zhong and Mucci [3] and the strong adsorption to the calcite surface. The first indication for inhibition is that growth spirals do not nucleate on the {104} surface at measured pH values of 8.31 or less and corresponding SI < 0.61 in solutions with Eu. The second point is a combined observation: Existing growth spirals do not restart growing when solution Eu-calcite at measured pH values around 8.20 is injected and grow very slow when the measured pH of the injected Eu-calcite solution is 8.31. This has to be seen in comparison to the pure system where it is observed that no obvious barrier exists for 1D nucleation at the spiral's origin or for spiral steps to restart growing after injection of new solution. Finally it is observed that in solution Eu-calcite at pH 8.39 and SI 0.69 spiral growth occurs.

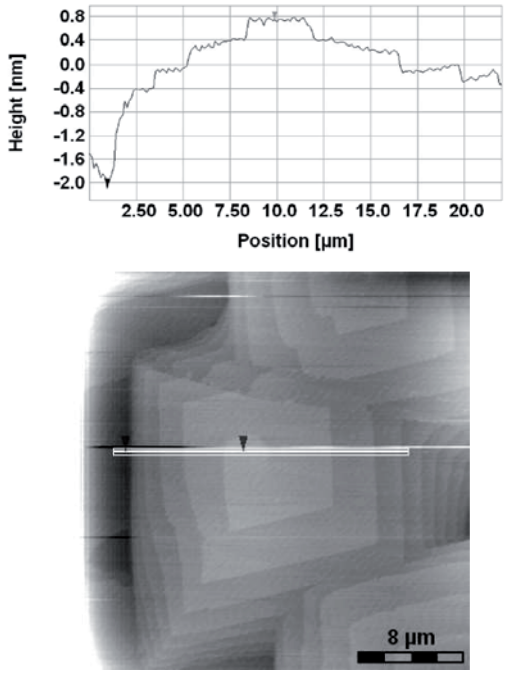

Fig. 3: *Spiral section after 25 minutes growth in calcite supersaturated solutions prepared from mixing equal amounts of Na_2CO_3 (Merck, p.a.) and $CaCl_2*2H_2O$ (Merck, p.a.) 0.1M stock solutions spiked with 0.1 µmol/L Eu^{3+} at pH_{meas} 8.39. AFM image is plane corrected with the SPIP routine to make the stepped flanks of the spiral better visible.*

crystal morphology on the nanoscale. A shortcoming of this study is that steady state conditions could not be established so that neither extrapolation to macroscopic growth rates can be drawn nor can thermodynamic data be derived from the observations (for details see [5]). However, this work probably presents the first AFM study on the nanotopography of Eu co-precipitating with calcite.

Neptunyl(V) sorption and structural incorporation into calcite

In on-going investigations to elucidate molecular processes leading to structural incorporation of neptunyl(V) into calcite, activities in 2009 focused on the determination of the structure of the Np(V)-calcite surface adsorption complex.

In last years' Annual Report [6] we reported on sorption isotherms of NpO_2^+ on calcite. To learn more about the surface adsorption and as a basis for future modelling of the adsorption data we investigate the structure and stoichiometry of the adsorption complex by EXAFS spectroscopy. The EXAFS adsorption sample is prepared at pH 8.3 and an initial NpO_2^+ concentration of 10^{-4} mol/L. Due to the low Np content of the adsorption samples (~50 ppm) the measurement of EXAFS data is difficult and time consuming. We finally succeeded to get analyzable spectra, by performing low temperature (15K) EXAFS measurements at the Rossendorf beamline (ROBL) at the ESRF in fluorescence mode in a Helium cryostat. The spectrum in k-space and the corresponding model calculation is shown in Figure 4 a). The

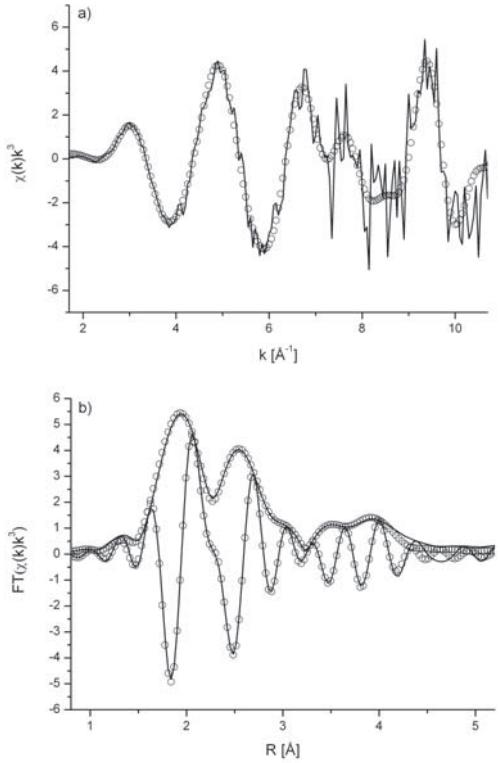

Fig. 4: *a): k^3-weighted EXAFS spectrum of the NpO_2^+ adsorption complex (line) and the corresponding model calculation (circles). b) Fourier transform of the k^3-weighted EXAFS spectrum of the NpO_2^+ adsorption complex (line) and the corresponding model calculation (circles).*

Fourier transform of spectrum and model is shown in Figure 4 b).

EXAFS data analyses is performed, using the IFEFFIT [7] software package. The results are shown in table 1. The data can be modelled using five backscattering paths.

***Tab. 1**: Coordination numbers, N, bond distances, R, and Debye-Waller factors, σ^2, obtained from the EXAFS data analysis.*

path	N	R [Å]	σ^2 [Å^2]
O(O-ax)	2.0 ±0.1	1.87 ±0.01	0.001 ±0.001
O(O-eq)	6.1 ±0.5	2.51 ±0.01	0.009 ±0.003
C(C-bi)	2.7 ±1.2	2.94 ±0.02	0.001 ±0.003
O(O-surf)	2.0 ±0.8	3.50 ±0.04	0.001 ±0.006
Ca	1.8 ±1.0	3.95 ±0.03	0.003 ±0.004

The only structural arrangement that is in agreement with both, bond distances and coordination numbers obtained from the data modelling, is when we assume that there are two bidentate and two monodentate carbonate groups coordinated in the equatorial plane around the NpO_2^+ moiety. The monodentate carbonate groups belong to the calcite surface and are located below- and at an edge on the calcite-(104)-face. The bidentate carbonate groups are located on the solution side of the neptunyl ion. A ball and stick representation of this bidentate inner-sphere biscarbonato complex, that is most likely the most abundant neptunyl adsorption complex at pH 8.3 and high surface coverage (~1.7 %), is shown in Figure 5.

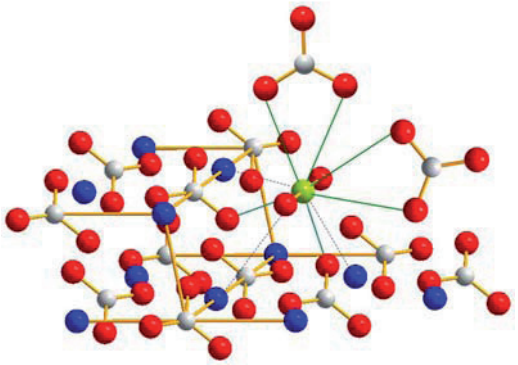

***Fig. 5:** Ball and stick representation of the most likely neptunyl adsorption species: a bidentate inner-sphere biscarbonato complex. (Np: green, O: red, Ca: blue, C: grey). Green lines indicate the bonds between Np and the six equatorial oxygen neighbours.*

Independent experimental results that support the idea of such an adsorption complex at step sites on the calcite {104} face are obtained in mixed flow reactor (MFR) coprecipitation experiments. Details about the experimental procedure of MFR experiments can be found elsewhere [8]. From MFR experiments the steady state calcite growth rate, R (mol/(m^{2}s)), can be measured at a low, constant steady state supersaturation, SI (calcite) (SI = $\log_{10}(a(Ca^{2+})a(CO_3^{2-})/K_{SP\_Calcite})$). Calcite precipitation inside the MFR occurs at slow surface controlled growth rates. A plot of MFR crystal growth rates as a function of SI(calcite) is shown in Figure 6.

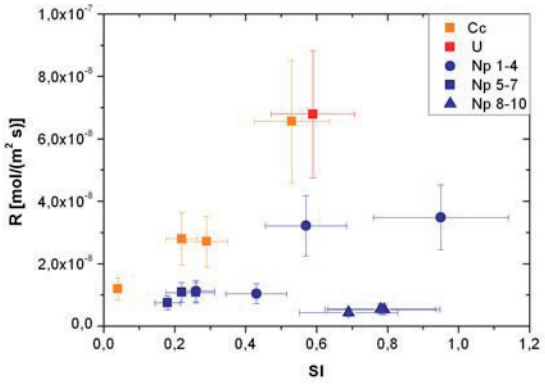

***Fig. 6:** Calcite growth rates in presence (blue) and absence (orange) of neptunyl as a function of SI(calcite). One experiment in presence of uranyl (red) suggests that this species does not have a significant effect on the calcite growth rate.*

Shown are MFR experiments with pure calcite (orange datapoints) that show the highest precipitation rates and MFR experiments in the presence of various concentrations of neptunyl(V) (blue datapoints). It is obvious that the presence of neptunyl drastically retards the calcite crystal growth rate. This is expected for a species that adsorbs at step and kink sites at the surface, and blocks these most reactive crystal growth sites. One MFR experiment carried out in the presence of uranyl(VI) (red datapoint) indicates that uranyl does not have an significant effect on the calcite growth rate. This is consistent with literature where it is reported that uranyl adsorbs at the calcite surface most likely as an outer-sphere triscarbonato complex [9, 10].

References

[1] A. G. Turnbull, Geochim. Cosmochim. Acta, 37, 1593 (1973).

[2] M. Schmidt, T. Stumpf, M. Marques Fernandes, C. Walther, T. Fanghänel, Angewandte Chemie Int. Ed., 47, 5846 (2008).

[3] S. Zhong, A. Mucci, Geochim. Cosmochim. Acta, 59, 443 (1995).

[4] A. Putnis, C. M. Pina, J. M. Astilleros, L. Fernandez- Diaz, M. Prieto, Philos. Trans. Roy. Soc. London Ser. A, 361(1804), 615 (2003).

[5] C. Borkel, Reactivity of the calcite surface during coprecipitation of Eu(III): influence of nanotopography; Master Thesis, University of Heidelberg, Geosciences Department, Heidelberg, 86 p. (2009).

[6] M. Schmidt, F. Heberling, N. Finck, T. Stumpf, M. Schlegel, K. Dardenne, D. Bosbach, Retention of radionuclides by secondary phase formation; Forschungszentrum Karlsruhe GmbH, Karlsruhe (2009).

[7] B. Ravel, M. Newville, J. Synchrotron Radiat., 12, 537 (2005).

[8] F. Heberling, M. A. Denecke, D. Bosbach, Environ. Sci. Technol. 42(2), 471 (2008).

[9] E. J. Elzinga, C. D. Tait, R. J. Reeder, K. D. Rector, R. J. Donohoe, D. E. Morris, Geochim. Cosmochim. Acta, 68(11), 2437 (2004).

[10] G. Geipel, T. Reich, V. Brendler, G. Bernhard, H. Nitsche, J. Nucl. Mater., 248, 408 (1997).

5.4 Associated graduated students investigations: Basic studies on actinides

B. Brendebach, K. Dardenne, M. A. Denecke, P. Lindqvist-Reis, M. Löble, P. J. Panak, J. Rothe, C. Ruff, T. Vitova, ,

in cooperation with

L. Aldave de las Heras[c], F. Breher[a], T. Fanghänel[c], I. Fernández[b], A. Martinez Ferri[c], N. Rausch[c],

[a]Institut für Anorganische Chemie, Karlsruher Institut für Technologie, 76131 Karlsruhe, [b]Universidad de Almería, Laboratory of Organic Chemistry, E-04120 Almería, Spain, [c]Joint Research Centre, Institute for Transuranium Elements, Karlsruhe

Interaction of Cm with human serum proteins

Introduction

In case of accidental release of radionuclides into the environment actinides represent a severe health risk to human beings after being incorporated by e.g. inhalation, ingestion or wounds. The bioavailability and toxic effects depend strongly on the speciation of the incorporated actinides.
Transferrin is one of the most abundant blood serum proteins responsible for the iron transport in blood [1]. As described in the literature the Fe(III)-transferrin complex is stabilized by an additional coordinated synergistic carbonate, acting as a bidentate bridging ligand between protein and the metal ion. Besides Fe(III) many other tri- and tetravalent metal ions have been identified to be bound to transferrin, such as Ga(III), Al(III), lanthanide(III) ions, Pu(IV), U(VI) and Th(IV) [2-4]. Therefore, TRLFS studies on the transferrin complexation of Cm(III) as a representative for the trivalent actinides are performed.

Results and discussion

Complexation at different pH

The first set of TRLFS experiments was performed at pH 7.2 corresponding to the physiological conditions in blood serum using a Cm(III) concentration of 0.5 µM and 0.05 µM to 20 µM apo-transferrin (Apo-Tf). The experimentally determined fluorescence spectra are shown in Fig. 1.

The spectrum at 0.05 µM Apo-Tf is dominated by the Cm^{3+} at 593.8 nm and the $Cm(OH)^{2+}$ species at 598.8 nm with nearly equal proportions. With increasing Apo-Tf concentration the fraction of the Cm(III)-transferrin species at 603.8 nm increases while Cm^{3+} and $Cm(OH)^{2+}$ decrease. Above 3.5 µM Apo-Tf, the Cm(III)-transferrin species is the dominating species.

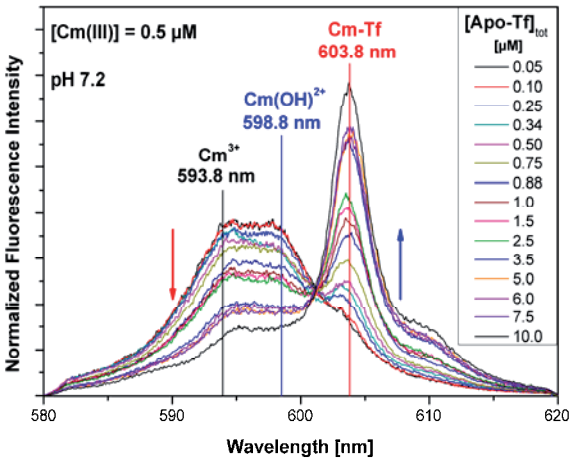

Fig. 1: *Fluorescence emission spectra of Cm(III) with increasing concentration of Apo-Tf at pH 7.2, [Cm(III)]= 0.5 µM, [Apo-Tf]= 0.05 µM to 10.0 µM*

Complexation studies at pH 6.4 and 5.7 show, that higher Apo-Tf concentrations are required to gain equal fractions of the Cm(III)-transferrin complex at lower pH values. The decreasing complexation with decreasing pH value indicates a strong pH dependency of the complexation reaction. Furthermore no Cm(III)-Tf complex is formed at pH 4.2.

Calculation of stability constants

From the experimentally determined Cm(III) species distributions at various pH values, conditional stability constants are calculated for a HEPES-buffer/NaCl medium with an molal ionic strength of I_m=0.7 m. To study the complex formation mechanism of the Cm(III)-Tf complex log([Cm(III)-Tf]/[Cm(III)]) at pH 7.2 is plotted as a function of log[Apo-Tf], yielding a slope of 1 (Fig. 2). That confirmed, that one Cm(III) ion is coordinated by one Apo-Tf molecule. Taking recourse to that, the results are fitted by two different models (with/without concomitant binding of a synergistic anion). The calculated stability constants are shown in Table 1.

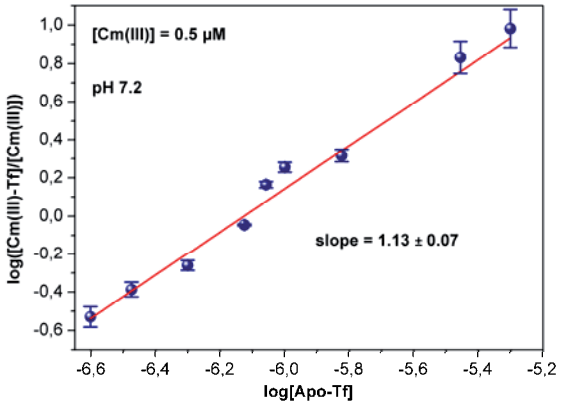

Fig. 2: *Double logarithmic plot of ([Cm(III)-Tf]/[Cm(III)]) concentration ratio versus the Apo-Tf concentration at pH 7.2*

Apparently, without synergistic anion the logK values exhibit a linear correlation with the pH-value yielding a slope of 1. Therefore, the simplest model, considering only the metal ion interaction with the protein as a global reaction is not in accordance with the experimental data and cannot be a representation of the actual Cm(III)-transferrin complexation mechanism. The logK values for Cm(III)-Tf with carbonate as an synergistic anion increase with decreasing pH, displaying a slope of -1.

Tab. 1*: Calculated stability constants for different Cm(III)-transferrin complexes at pH 5.7,6.4 and 7.2*

Cm(III)+Apo-Tf+Anion ⟶ Cm(III)-Anion-Tf				
Anion	**logK (pH 5.7)**	**logK (pH 6.4)**	**logK (pH 7.2)**	**m (logK/pH)**
without	4.80	5.08	6.24	0.99
CO_3^{2-}	13.94	12.82	12.38	-1.03
HCO_3^-	10.07	9.66	10.00	-
OH^-	12.72	12.30	12.66	-

Therefore, a model comprising carbonate as synergistic anion is inapplicable to describe the experimental data properly. In terms of hydrogen-carbonate or hydroxide the experimentally observed pH dependence is reproduced correctly and pH-independent stability constants are determined.

Fluorescence lifetimes

Besides the reaction mechanism the structure of the Cm(III)-transferrin complex is of particular interest. Valuable information on the structure of Cm(III) complexes can be obtained from fluorescence lifetime measurements. For the Cm(III)-transferrin a fluorescence lifetime of 134 µs was determined, which corresponds to five substituted water molecules in the inner coordination sphere. As known from literature [5], metal ions are coordinated by four amino acid residues of the transferrin. Therefore, a synergistic anion occupies the fifth binding site. The proposed structure of the specific metal ion binding site of the Cm(III)-Tf complex based on this model is shown in figure 3.

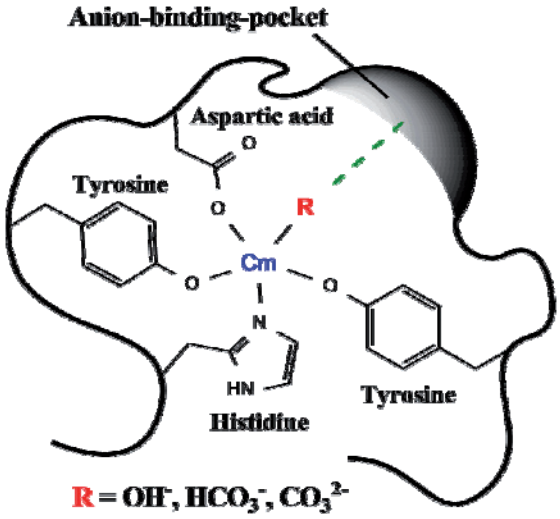

Fig. 3: *Proposed structure of the specific metal ion binding site of the Cm(III)-anion-Tf complex (four H_2O ligands are omitted)*

Structural investigation on Ln(III) and An(III) complexes with tripodal N,O-donor ligands

Introduction

The chemistry of lanthanides and actinides is basically determined by their size and ionic radii. Both favor high coordination numbers and ligands with Lewis-acidic donor atoms like oxygen and fluorine. Especially the minor actinides americium and curium show a chemical behavior very similar to the lanthanides, favoring the same valence state (+3) and possessing nearly the same ionic radii [6]. However, actinides show a different structural and electronic behavior in many coordination and organometallic compounds, which is expressed in shorter bond lengths and backbonding effects [7]. Especially the selectivity of existing *N*-donor partitioning ligands for actinide cations over their chemically similar lanthanide counterparts is yet not fully understood.

To gain further knowledge of their different chemical, structural and electronic properties, easily accessible lanthanide and actinide model compounds are necessary to develop suitable characterization methods or study methods which have not been used (on

actinides) so far. Concerning their extraction behavior, a thorough characterization in solid state and in solution is necessary to determine the influence of the interactions between

- ligand and metal cation,
- metal cation and counter anion,
- metal cation and solvent,
- metal cations with each other.

We therefore synthesized an easily accessible multidentate N-donor ligand system [8] $PS(N^{Me}Py)_3$ and several Lanthanide (La, Pr, Sm, Eu, Gd, Dy, Ho, Lu, Y) complexes thereof.

Results

Synthesis

The ligand system $PS(N^{Me}Py)_3$ is a new multidentate κ^6N-donor ligand with podand topology. Reaction with metal triflates results in coordination compounds of the form $[Ln\{PS(N^{Me}Py)_3\}(OTf)_3]$ (See Fig.4 for the ligand and the corresponding Ho-complex). All compounds crystallize isostructural. The metal cation is coordinated nonahedrally by the N-donors of the ligand and – surprisingly – by the three triflate counter anions, as the triflate anion is known to be a weakly coordinating anion [9]. We applied a combination of different methods to gain knowledge about the solution behavior of those compounds.

Characterization in solution

By combination of L3 edge EXAFS, TRLFS and especially by applying enhanced NMR methods like low temperature ^{19}F-NMR-, ^{1}H^{19}F-HOESY- (Heteronuclear Overhauser Effect) and PGSE- (Pulsed Gradient Spin Echo) spectroscopy [10] in acetonitrile solution we could show that the structure in solution is dependent on the ionic radius of the central metal cation. Complexes of the early lanthanides (La-Sm) are strong contact ion pairs with only slight differences in the diffusion coefficients of the coordinated metal-ligand species and the triflate counter anion. The complexes of the later lanthanides and Y (which was used as substitute for the paramagnetic Ho^{3+}-cation) show significant differences of their diffusion coefficients and are therefore considered as solvent separated ion pairs (see Fig.5).

Characterization of electronic properties

To study the electronic properties of these compounds, we applied several XAS-based techniques (Fig. 6). This method is uniquely capable of giving information of both, the entire

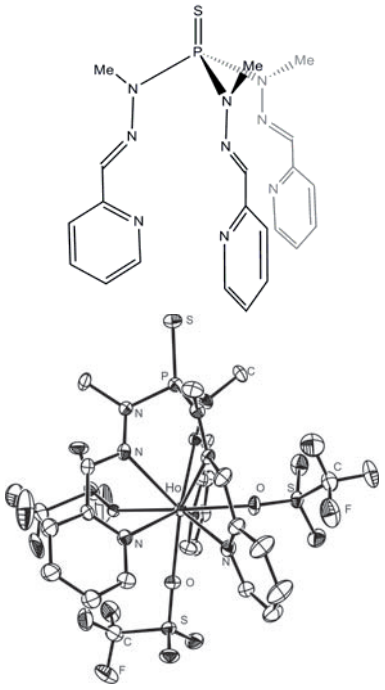

***Fig. 4**: Ligand (above) and Molecular Structure of the Ho-complex $[Ho\{PS(N^{Me}Py)_3\}(OTf)_3]$*

system and its constituent parts independently, including the electronic properties of the central metal cation (magnetism, luminescence,…) and the contribution of the ligand and the counter anions. With P K edge XANES we could show for the first time that complexation changes the electronic structure of the ligand significantly. By studying the M edges of the metal cations and high resolution X-ray emission spectroscopy (HRXES) and resonant inelastic X-ray scattering (RIXS), in combination with N K edge XANES and quantum chemical methods, we are presently studying bonding between the metal cation and the ligand directly. With the help of S K edge XANES we are also able to show the contribution of the triflate counter anions of this

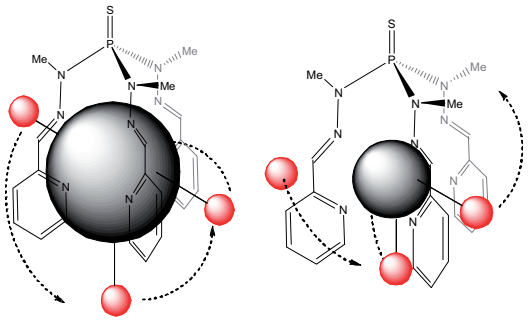

***Fig. 5:** Contact ion pair (left) and partially solvent separated ion pair (right)*

system.

Outlook

With the help of the new HRXES/RIXS spectrometer being installed by T. Vitova at the INE-beamline for Actinide research at ANKA and the new NMR-spectrometer in INE's control area we hope to successfully carry on this research with actinide compounds (e.g., the analogue Pu(III) compound) and isolate factors that contribute to the selectivity of N-donor extracting agents.

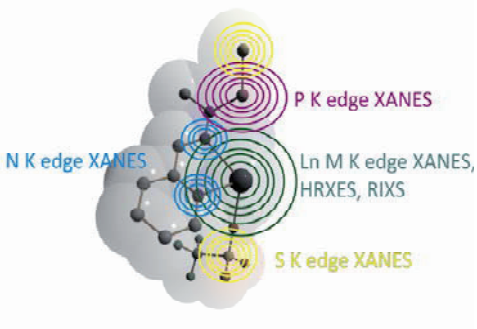

Fig. 6: *Electronic Characterization by various XAS-Methods*

References

[1] H. Sun, P. Li, J. Sadler, Chem. Rev. 99 (9), 2817-2842 (1999).

[2] W. R. Harris, L. Messori, Coord. Chem. Rev. 228 (2), 237-262 (2002).

[3] G. Montavon, C. Apostolidis, F. Bruchert-seifer, U. Repinc, A. Morgenstern, J. Inorg. Biochem. 103 (12), 1609-1616 (2009).

[4] D. M. Taylor, J. Alloys Compd. 271-273, 6-10 (1998).

[5] R. T. A. MacGillivray et al., Biochemistry 37 (22), 7919-7928 (1998).

[6] S. Cotton, Lanthanide and Actinide Chemistry, John Wiley & Sons (2006).

[7] P. L. Arnold, I. J. Casely, Chemical Reviews 109, 3599 (2009); L. Petit, C. Adamo, P. Maldivi, Inorganic Chemistry 45, 8517 (2006).

[8] I. Kuzu, I. Krummenacher, J. Meyer, F. Armbruster, F. Breher, Dalton Trans. 5836 (2008).

[9] G. A. Lawrance, Chem. Rev. 86, 17 (1986).

[10] P. S. Pregosin, P. G. A. Kumar, I. Fernández, Chem. Rev. 105, 2977 (2005).

6. Applied Studies: Radionuclide retention in the multi-barrier system

Different to the previous chapters, these studies focus on the complex systems close to “real” repository components and conditions. Most important for mobilization and retention of radionuclides is the geochemical environment. Radiolysis effects the geochemical environment and the behaviour of spent nuclear fuel (SNF). For this reason, the formation and stability of reducing and oxidizing radiolysis product needs to be understood. The mobilization and immobilization of radionuclides from SNF in the radiation field is investigated including trapping of radionuclides in canister corrosion products. For low level wastes, the long-term retention and mineralization of U(VI) in cemented waste forms is presented. Colloids may have important impacts on radionuclide migration. Depending on the geochemical environment, the kinetically controlled stability and sorption properties of colloids are analyzed by various approaches. Related to colloid facilitated radionuclide transport, the understanding of humate complexation in specific far-field conditions is indispensable. A state-of-the-art review is presented. Results of the experimental investigations are used for developing, applying and testing numerical tools to be used in safety analyses. Here, conclusions of the European Theresa project on thermo-hydro-mechanical processes are drawn. As an example, the flow and solute transport in a single fracture from the Äspö HRL is modelled on the basis of µXCT data. The development of the Thereda data base is presented which will provide an accepted, consistent thermodynamic data base to be used for all potential host rocks in Germany.

6.1 Radiolysis

E. Bohnert, C. Bube, E. Janata, M. Kelm, B. Kienzler, V. Metz, N. Müller, D. Schild, E. Soballa, J. Thomas*

** Helmholtz-Zentrum Berlin für Materialien und Energie, Solar Energy, Hahn-Meitner-Platz 1, D-14109 Berlin*

Introduction

The β- and γ-activity of the fission products in spent nuclear fuel (SNF) will decay to a large extent after several hundred years. Matrix dissolution of “old” spent fuel (> 10.000 years) in contact with groundwater will be controlled by radiolysis products formed only by α-decay. α-particles have a typical kinetic energy of 5 MeV and are stopped within ~40 µm in water. Due to the high linear energy transfer (LET) of α-radiation, reducing and oxidizing species are formed directly on the surface of SNF in contact with aqueous solution. However, matrix dissolution and the associated radionuclide release are measured in experiments with "fresh" SNF (~30 yrs. old). Corrosion of "fresh" SNF is influenced by a radiation field consisting of α-, β-, and γ-radiation. The LET, the penetration depth and the yield of reducing or oxidizing species of the α- and β- particles and of the γ-rays are different. For extrapolation of measured matrix dissolution and radionuclide release from SNF experiments to long periods of time a comprehensive understanding of the mechanisms forming the relevant radiolysis products as well as the kinetic parameters needed for modelling of the radiolytical reaction scheme are required.

Estimation of β- und γ-doses of SNF

In order to distinguish the effects of the α-, β- and γ-radiation, the β- und γ-doses of SNF were determined. A pellet of the same batch of SNF (LWR Gösgen, Pellet K7 burnup 50400 MWd/t_{HM}, mass 7.125 g, Ø 10.7 mm) was used. A sleeve was mounted over the fixed pellet holding Al absorber of thicknesses between 0.1 to 5 mm together with a thermo-luminescence detector (TLD). The sleeve was constructed in a way that the distance between the pellet surface and the detector was constant. Depending on the absorber thickness, the exposure times of the TLDs were varied. The analysis of the TLDs was performed by the local department of radiation protection (HS). The TLDs were calibrated using a ^{137}Cs source and a total dose of 10 mSv. The TLDs showed a linear dose relation between 0.1 mSv and 10 Sv.

The results are shown in Fig. 1. The figure shows the measured and calculated γ-dose rates of 4 Gy/h showing no dependence of the absorber thickness. In contrast the measured β dose rates (3 series) increased significantly with decreasing absorber thickness. Extrapolation of the dose rate to zero absorber thickness would result in a dose rate of 135 Gy/h comparable to calculated values obtained in a study on the radiation field of CANDU fuel [1].

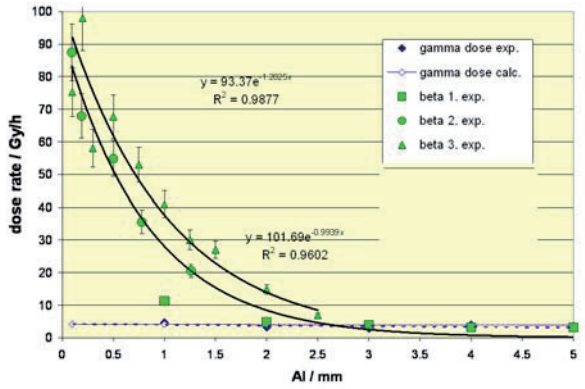

Fig. 1: *β- und γ-dose rates of SNF as function of absorber thickness*

Penetration depth of α particles (5 MeV) in SNF material is about 4 µm. The concentration of α activity in the studied SNF is ~4.7×10^{8} Bq g^{-1}. Using this activity, the α dose rate is calculated in the range of 360 Gy/h at the surface of the SNF pellet. This value corresponds to data reported for SNF of an age of ~30 years by Sunder [1].

These results show that β radiolysis cannot be neglected in experiments using 30 yrs. old SNF. For this reason, investigations of low LET irradiation effects are important to understand the complex reaction schemes.

Effects of H_2 and Br^- on γ-radiolysis of NaCl Brine

The corrosion behaviour of the fuel is influenced by a variety of factors such as radionuclide inventory, dose rates, temperature, groundwater composition, pH and redox potential. Aqueous solution in contact with spent nuclear fuel could radiolytically produce oxidants to convert the relatively stable UO_2(s) matrix of SNF into much more soluble U(VI) and thus promotes radionuclide release. Anaerobic corrosion of Fe-based waste containers will result in strongly reducing conditions (relative high Fe^{2+}/Fe^{3+} ratios) and high hydrogen concentrations. SNF leaching tests and radiolysis experiments indicated that hydrogen both considerably inhibits corrosion of the UO_2(s) matrix and impedes radiolytic decomposition of the studied groundwater simulates [2]. Recent studies on the behaviour of alpha-doped UO_2(s) under reducing alkaline conditions show a strongly inhibited UO_2(s) corrosion [3].

However, the inhibition of matrix dissolution by H_2 is influenced by competitive reactions with components of the natural groundwaters / brines: γ-radiolysis experiments in NaCl solution revealed that radiolytic formation of H_2 and O_2 depends on the concentrations of Br^- added to solution. In experiments with ≥ 10^{-4} mol l^{-1} bromide, steady state concentrations of radiolytically formed H_2 and O_2 were significantly higher compared to H_2 and O_2 produced in experiments without bromide. Measured U concentrations indicate that UO_2(s) corrosion in NaCl solution under γ-irradiation is limited by solubility of secondary U(VI) phases rather than by U(IV) phases. It was concluded that a protective hydrogen effect on γ-radiation induced UO_2(s) corrosion was considerably reduced in the presence of ≥ 10^{-3} mol l^{-1} bromide.

Since 15 years, the effects of radiolysis have been investigated extensively at INE. The investigations covered

- yield of radiolysis species in salt solutions (G values),
- approaches to distinguish between α- und β-, γ-radiolysis effects on spent fuel corrosion
- effect of hydrogen and competing components of groundwaters (e.g. bromide) on the yield of γ-radiolysis products
- pulse radiolysis studies to determine reaction rate constants, and
- kinetic modelling of radiolytic reactions.

Results from pulse radiolysis studies in NaCl solutions in combination with numerical simulations complete the reaction schemes describing the effects of the inhibitor H_2(g) [4]. A mechanistic understanding of the inhibition effects of reducing / hydrogen rich conditions on SNF corrosion is still missing, at least for groundwater containing significant contents of halogenides.

Radiolytic reaction schema

A single reaction accounts for the influence of molecular hydrogen on radiolysis of aqueous solution which converts oxidizing OH radicals into reducing H radicals

$$OH^{\bullet} + H_2 = H_2O + H^{\bullet} \qquad (1)$$

Using pulse radiolysis, the rate constant of this reaction was determined. Since molecular hydrogen interacts solely with hydroxyl radicals, a hydrogen effect on the yield of radiolytic oxidants occurs at low LET radiation, whereas in a high LET radiation field dissolved H_2 has a negligible effect on the production of radiolytic oxidants in pure water. As the rate constant k_1 of reaction (1) is relatively low, the H_2 concentration has to be sufficiently high to compete with fast reactions involving the OH

radical. Chloride ions react with hydroxyl radicals achieving equilibrium, which is in favor of free OH radicals only at low Cl^- concentrations. In NaCl solutions, hydrogen showed a decrease in the production of H_2 and O_2 but still a remarkable yield of chlorate compared to experiments conducted without hydrogen. Applying the reaction scheme of [5], it was possible to simulate experiments that had been conducted in the absence of non-radiolytic hydrogen. In contrast, radiolysis of NaCl brine in presence of hydrogen could not be simulated adequately using the database of ref [5]. In order to enable a more accurate simulation of the radiolysis in presence of hydrogen, Kelm and Bohnert (2005) [6] suggested to add an equation (2) describing an interaction of H_2 with Cl_2^-.

$$Cl_2^- + H_2 = H^\bullet + HCl + Cl^- \qquad (2)$$

Using pulse radiolysis, we investigate whether reaction (2) takes place or how otherwise it would be possible to adequately simulate radiolysis of aqueous chloride solution in presence of hydrogen.

The experimental setup was described previously [7]. The system was flushed with N_2O. Precisely timed irradiation pulses of 5, 10 and 50 ns duration are applied which generate $0.5 - 5 \cdot 10^{-6}$ mol dm^{-3} hydroxyl radicals with a yield of 5.3 molecules per 100 eV. The optical detection system consists of a lamp, lenses and mirrors, a UV band-pass filter in front of the monochromator and a photomultiplier tube. Absorption vs. time was recorded in a time range from $2 \cdot 10^{-6}$ to $2 \cdot 10^{-2}$ s. Details of the pulse radiolysis apparatus can be found elsewhere [8]. The optical signals were derived from the average of at least 10 individual experiments. The optical absorption was calculated from the optical density, the concentration of radicals generated in a pulse and by the length of the optical cell. The absorbed dose per pulse was calibrated. Optical absorbance was measured at 340 nm. At this wavelength three (oxy-) chloride species absorb, i.e. Cl_2^- with ε = 8800 dm^3 mol^{-1} cm^{-1}, $ClOH^-$ with ε = 3700 dm^3 mol^{-1} cm^{-1} and Cl_3^- with ε = 150 dm^3 mol^{-1} cm^{-1}.

Temporal evolution of the radiolysis products and the resulting absorbance of Cl_2^-, Cl_3^- and $ClOH^-$ was calculated using the Maksima Chemist code [9]. The reaction scheme of [5] consists of 82 elementary reactions for radiolysis of chloride containing solutions in presence of N_2O. 31 of the 82 reactions proof to be sufficient for simulating the radiolytic yield of Cl_2^-, Cl_3^- and $ClOH^-$ in the time interval of $2 \cdot 10^{-8}$ to $2 \cdot 10^{-2}$ s. Other reactions involving long-lived radiolysis products (e.g. ClO_3^- and ClO^-) or species in very low concentrations, were considered to be negligible under the conditions of the present study.

Evaluation of published reaction rate constants

A comparison of measured optical absorption (expressed as ε = normalized absorptivity) vs. time curves with simulated curves using the reaction scheme of Sunder and Christensen [5] showed unacceptable discrepancies with respect to the rise and decay of ε and its maximum value. To achieve a better agreement between simulations and experimental data, 31 rate constants of the scheme are checked and traced back to original data. Four rate constants for reactions of hydrogen atoms and hydroxyl radicals in H_2O and six additional rate constants for reactions of hydrogen atoms, hydroxyl radicals and chloride species in aqueous solution needed to be updated using recent publications.

The main discrepancy between the simulations based on the Sunder and Christensen reaction scheme and our experimental data concerns the ε decay which is significantly too fast in the simulations. The decay of the measured optical absorption is controlled by the disproportionation of Cl_2^- radicals. Published rate constants were compiled and simulations were calculated in order to determine rate constants showing the best agreement between simulated and measured ε evolution under the conditions of the present study.

Simulations based on the revised data-set

With the revised reaction scheme (Tab. 1) we satisfactorily simulated the change of ε over 6 decades (10^{-8} s to 10^{-2} s). Fig. 2 shows the temporal evolution of experimental and calculated values of ε in 0.1 molar NaCl without initial hydrogen for pulse lengths of 5, 10 and 50 ns. The different pulse lengths correspond to different initial concentrations of the primary radiolysis products. In the experiments, build-up of the normalized absorbed dose per pulse value ε seems to be slightly faster than the calculated rise of absorptivity. Still, simulated ε values lie all within the experimental noise of ε.

For 1 molar NaCl the deviation between experiments and simulation is larger compared to the results for 0.1 molar NaCl (Fig. 3). For instance, calculated ε peak values are in most cases significantly lower than measured ε peak values. The discrepancy between calculated and measured ε values is less than 15% and is related to the use of too low G values in the

simulations as no corrections are made for high scavenger concentrations.

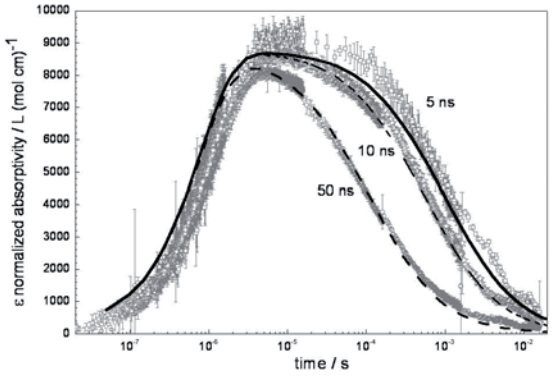

Fig. 2: *Effect of pulse length on ε in 0.1 mol dm^{-3} NaCl solution at 0 mol dm^{-3} H_2, 0.026 mol dm^{-3} N_2O and pH = 3.3. Symbols denote mean values of measured normalized absorptivity, ε, lines denote simulations of ε for the respective pulse lengths. Vertical lines denote error bars.*

Tab. 1*: Modified reaction rate constants k (mol^{-1} s^{-1}) determined by pulse radiolysis in chloride solutions equilibrated with hydrogen and N_2O*

no.	reaction	rate k I = 0 m	k given in [5]
2*	$Cl_2^- + H_2 = H + HCl + Cl^-$	disregard.	not given
5	$OH + H = H_2O$	9.7E+09	7.0E+09
7	$OH + OH^- = H_2O + O^-$	1.3E+10	1.2E+10
13	$H + H = H_2$	5.0E+09	7.8E+09
14	$H + H_2O_2 = H_2O + OH$	4.2E+07	9.0E+07
21	$H + Cl_3^- = Cl_2^- + Cl^- + H^+$	6.0E+10	1.0E+10
23	$Cl_2^- + OH^- = ClOH^- + Cl^-$	9.0E+06	7.3E+06
24	$H^+ + ClOH^- = Cl + H_2O$	6.8E+10	2.1E+10
26	$ClOH^- + Cl^- = Cl_2^- + OH^-$	2.9E+03	9.0E+04
27	$Cl^- + Cl_2 = Cl_3^-$	2.0E+04	1.0E+04
30	$Cl_2^- + Cl_2^- = Cl^- + Cl_3^-$	5.2E+08	7.0E+09
31	$Cl_3^- = Cl_2 + Cl^-$	1.1E+05	5.0E+04

In 0.1 molar NaCl solution with 0.007 (mol H_2) dm^{-3} the ε peak value yields only about one third of that in hydrogen free solution, which is in agreement with the respective simulations. In 1.0 molar NaCl solution the difference of the ε peak values in experiments with and without initial hydrogen is less pronounced compared to experiments with 0.1 molar solution (Fig. 3).

Simulations of the experimental series with varied N_2O and H^+ concentrations yielded smaller normalized absorbed dose per pulse (ε) values compared to experiments with 1 m NaCl and pulse duration between 5 and 50 ns. Calculated ε peak values of the series in presence of N_2O agreed within error range with the measured ε values.

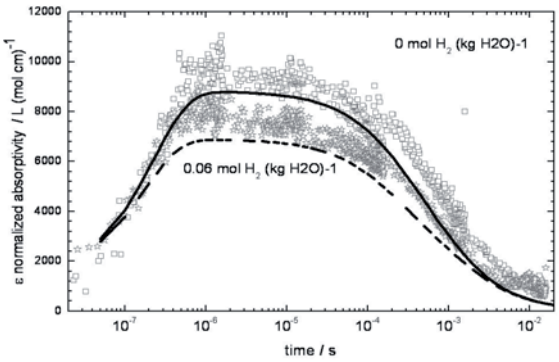

Fig. 3: *Effect of hydrogen concentration on ε in 1.0 mol dm^{-3} NaCl solution at 0.026 mol dm^{-3} N_2O, pH = 3.3 and 5 ns pulse length. Squares denote measured ε at zero H_2, stars denote measured ε at 0.06 mol dm^{-3} H_2 and lines denote simulations of ε for the respective hydrogen concentrations.*

Summary and conclusions

In pulse radiolysis experiments, production and decay of Cl_2^- radicals was investigated over a time span of $2 \cdot 10^{-2}$ s after the pulse in 0.1 and 1.0 mol dm^{-3} NaCl solutions with hydrogen dissolved under a pressure of 10 MPa. The influence of dissolved hydrogen on the Cl_2^- yield was considerably stronger pronounced in 0.1 molar than in 1.0 molar solution. Reaction constants given in the widely used scheme of Sunder and Christensen [5] are compared to the respective constants in the original publications. 11 of the reaction constants are corrected or up-dated, respectively. By the revised reaction scheme, production and decay of Cl_2^- radicals were simulated for the experimental conditions. Based on a comparison between measured and simulated ε values of Cl_2^- as a function of time, the rate constant of reaction $Cl_2^- + Cl_2^- = Cl^- + Cl_3^-$, (Tab. I, reaction 30) was determined as $k = 5.2 \cdot 10^8$ dm^3 mol^{-1} s^{-1}. This value is within the range of published rate constants. Since the effect of hydrogen on radiolysis of 0.1 and 1.0 mol dm^{-3} NaCl solutions is adequately simulated, we conclude that H_2 interacts radiation chemically solely with the OH radical. There was no evidence for reaction (2), $Cl_2^- + H_2 = H + HCl + Cl^-$, postulated by Kelm and Bohnert [6].

References

[1] S. Sunder, Nuclear Technology, 122, 211-221 (1998).

[2] J. Bruno and R. C. Ewing, Elements, 2, 343-349 (2006).

[3] T. Mennecart, C. Cachoir, and K. Lemmens, 2nd international workshop on mechanisms and modelling of waste/cement interactions, Le Croisic, 70 (2008).

[4] M. Kelm, V. Metz, E. Bohnert, E. Janata, and C. Bube, "Interaction of hydrogen with radiolysis products in 0.1 and 1.0 molar NaCl solutions – comparing pulse radiolysis experiments with simulations," in preparation (2010).

[5] S. Sunder and H. Christensen, Nuclear Technology, 104, 403-417 (1993).

[6] M. Kelm and E. Bohnert, Journal of Nuclear Materials, 346, 1-4 (2005).

[7] H. Geckeis and R. Klenze. [Editor], "Institute for nuclear waste disposal. Annual report 2007," Forschungszentrum, Karlsruhe FZKA-7444 (2008).

[8] M. S. Alam, M. Kelm, B. S. M. Rao, and E. Janata, Radiation Physics and Chemistry, 71, 1087-1093 (2004).

[9] M. B. Carver, D. V. Hanley, and K. R. Chaplin, Chalk River, Ontario: Atomic Energy of Canada Ltd., Chalk River Nuclear Laboratories, AECL-6413 (1979).

6.2 Key processes influencing corrosion of nuclear waste forms

B. Brendebach, E. Bohnert, C. Bube, N. Finck, B. Kienzler, A. Loida, V. Metz, N. Müller, M. Plaschke, Th. Rabung, J. Rothe, D. Schild, M. Schlieker, E. Soballa

Retention of U(VI) in Cemented Waste Forms under Saline Conditions

Introduction

From 1988 to 2006, U-doped and Cs-doped cemented waste simulates were corroded in NaCl- and $MgCl_2$-rich solutions. Results for compositions of the leachants and solid samples recovered from the corroded monoliths from these full-scale leaching experiments have been reported last year. This included the radioactivity and nitrate distributions, elemental and mineralogical compositions of a series of drill cores, as well as analyses of the pore water pH. The present contribution focuses on determination of the retention mechanisms for uranium in the corroded solids.

Methods

A similar U concentration (≈15 µmol g^{-1}) was measured in all drill dust samples of U-doped waste simulates. For characterization of U-bearing phases, different analytical methods were applied:

X-ray diffraction analyses: The mineralogical compositions of the powder samples were characterized by X-ray diffraction (XRD). Diffractograms were recorded from 2 to 100° with steps of 0.01° 2θ. Measured reflexes were compared to XRD patterns of relevant phases of the JCDPS database.

TRLFS: Time Resolved Laser Fluorescence Spectroscopy (TRLFS) was applied to solid samples under ambient temperature. Powdered samples were illuminated by the pulsed laser light under an angle of 40°. Perpendicular to the laser beam a circular glass fiber bundle was fixed. Measurements were conducted under following conditions: excitation wavelength λ_{ex} 400 nm, delay times 100 ns and 1 ms, gate width for fluorescence measurement 100 ns and 1 ms, respectively. In addition, a few TRLFS experiments have been performed at low temperature (3.5 K) at λ_{ex} = 266 nm.

XANES/EXAFS: The chemical environment of uranium species was investigated by X-ray absorption fine structure (XAFS) spectroscopy. U L3 XAFS spectra were recorded at the INE-Beamline. Sample pellets of 7 mm diameter were prepared after mixing the powder samples with polyethylene. Reference samples were measured in transmission mode. Corroded cement samples were investigated in fluorescence detection mode by recording the U Lα fluorescence yield. XANES spectra were also recorded for relevant reference compounds such as Ca-uranate, Na-uranate, meta-schoepite, soddyite and uranophane.

Results

XRD: Drill dust of samples of the U-free monolith #28 and and the U-doped monolith #33, both corroded in $MgCl_2$–rich brine showed following major phases: Halite, brucite, calcite, ettringite, (Mg,Ca)-Al-chlorohydroxide and $CaSO_4$. In most samples, an unambiguous identification of Mg-oxychloride was not possible, due to the weakness of the diffraction lines. Similarly, a detailed characterization of the (Mg,Ca)-Al-chlorohydroxid was prevented by superposition of diffraction lines of other minerals. In samples corroded in NaCl brine (#30 and #31) following major phases were detected: Portlandite, calcite, and halite. Phases of the hydrotalcite group, such as Friedel's Salt, as well as calcium silicate hydrate phases (CSH) could not be identified unambiguously.

The comparison of XRD patterns of U-bearing samples (#33 and #31) with those of the respective U free samples (#28 and #30) revealed the existence of at least one additional solid phase that potentially can be attributed to an uranium mineral. Most diffractograms of the U-doped samples significantly show a diffraction line at 23° (see Fig. 1). The strongest diffraction line of the U-bearing phase at 11.3° is clearly evident in one sample of the monolith #31 corroded in NaCl-rich brine. In diffractograms of samples of monolith #33 (corroded in $MgCl_2$-rich brine), strong reflexes of major constituents (gypsum and a hydrotalcite type phase) superpose the reflex of the potentially U-bearing phase at 11.3°. In addition to the 23° diffraction line, a significant reflex at 18.2° and weaker reflexes at 34.2° and 48.5° were observed in the XRD patterns of samples of monolith #33. These signals were hardly superposed by signals of major mineral phases in the $MgCl_2$ leached samples. At 34.2° and 48.5°, also portlandite and calcite (present in #31) have diffraction lines. The observed XRD reflexes of the potentially U-bearing phase were in agreement with those of (β-)uranophane ($Ca(UO_2)_2(SiO_3OH)_2 \cdot 5H_2O$), e.g. JCPDS 08-0442 or 08-0301). For comparison, a

diffractogram of a pure uranophane sample (provided by PSI) and the uranophane reflexes of the JCPDS database are plotted in Fig. 1, too. Reflexes of other U-bearing phases, such as $Na_2U_2O_7 \cdot H_2O$ or $CaU_2O_7 \cdot 3H_2O$, meta-schoepite, becquerelite or soddyite were not detected in any of the XRD patterns.

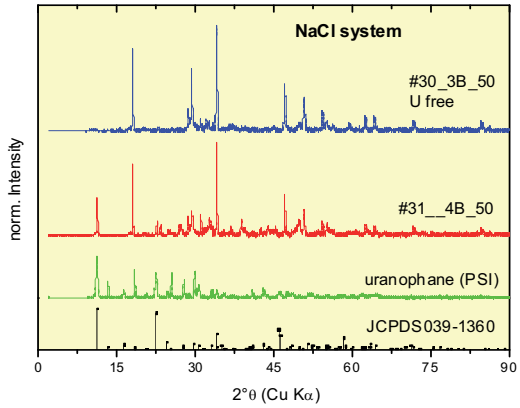

Fig. 1: *XRD patterns of cement products corroded in NaCl-rich brine and uranophane:*

U free sample (#30-3B-50), U-doped sample (#31-4B-50), uranophane (sample provided by PSI) and JCPDS uranophane pattern.

TRLFS: To identify the relevant phases, the spectra were compared to those of reference samples such as meta-schoepite, soddyite $Na_2U_2O_7 \cdot H_2O$, $CaU_2O_7 \cdot 3H_2O$ and uranophane spectra. The spectra of different drill dust and core samples taken at different positions within monoliths #31 and # 33 and measured after 1 μs delay and at a gate width of 1 ms show no significant differences and resemble closely the pattern of the long-lived fluorescence of the uranophane spectrum measured under identical conditions. The fluorescence emission spectra of uranophane and selected samples from #31 are shown in Fig. 2. Other U(VI)-bearing minerals such as soddyite, $Na_2U_2O_7 \cdot H_2O$ and $CaU_2O_7 \cdot 3H_2O$ and meta-schoepite could not be detected in the presence of an intensive uranophane fluorescence signal, even if present in comparable amounts. Fluorescence lifetimes of meta-schoepite, soddyite and uranate phases ($\tau << 1$ μs) are much shorter than those of uranophane ($\tau > 1$ μs). Selecting a shorter delay gate did not change neither the fluorescence intensities nor the shape of the spectrum significantly. For this reason we assume that the contribution of uranium phases with short-lived fluorescence to the overall spectrum is negligible.

Spectra of pure uranophane and of drill dust samples at 3.5 K and room temperature were quite similar with respect to peak positions and fluorescence lifetimes. There were no hints for additional fluorescent uranium-bearing phases under these conditions.

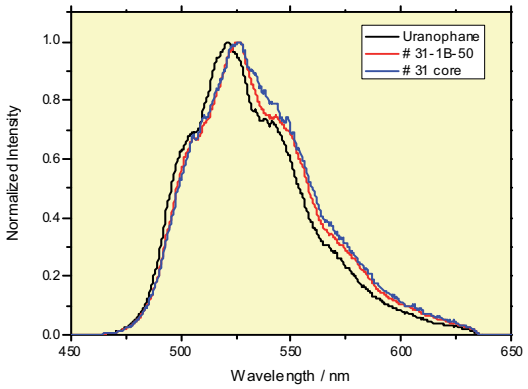

Fig. 2: *Fluorescence emission spectra of samples in comparison to an uranophane reference*

Sample #31 corroded in NaCl-rich brine

XANES and EXAFS: The U L3-edge XANES spectra of specimen taken from monolith #33 is shown in Fig. 3. Comparisons between specimen from #33 and #31 exhibited only negligible differences. The edge positions of both specimens are identical. From the white line (WL) peak position and the appearance of the characteristic multiple scattering (MS) feature (shoulder at the WL high energy flank) it is clearly confirmed that uranium in the corroded cement samples is present in the hexavalent uranyl state. In Fig. 3, XANES spectra from the U(VI) model compounds uranophane (PSI), Na- and Ca-uranate are compared to sample #33-1B-50. Considering the energy positions of the WL, uranophane corresponds well with the samples of the U-doped monoliths. However, both the WL and the MS feature are significantly broadened for these samples. Coexistence of different U(VI) coordination environments corresponding to a high structural disorder in the corroded cement samples might explain the different XANES compared to the crystalline reference compounds (Fig. 3).

EXAFS data and fits were derived, too. The bond distance of the two shorter bound axial oxygen atoms was approximately 0.08 Å longer than the respective value for meta-schoepite. It agrees well with the bond distance of 1.82 Å in α-uranophane. The coordination number of approximately 5 for the equatorial oxygen atoms matches well the known structures for a wide range of uranium oxide/hydroxide compounds. However, the bond distance of 2.23 Å is somewhat shorter than the expected averaged value of 2.35 Å for α-uranophane – corresponding to the XANES interpretation. Unfortunately, the present

EXAFS data does not contain conclusive information on further distant shells which would unambiguously support the presence of uranophane or other crystalline U(VI) phases in the corroded cement samples. Both, the apparent absence of coordination shells beyond the oxygen coordination environment and the reduced U-O_{eq} distance support the assumption of a highly distorted or asymmetric U coordination and/or the coexistence of several U(VI) phases in these samples.

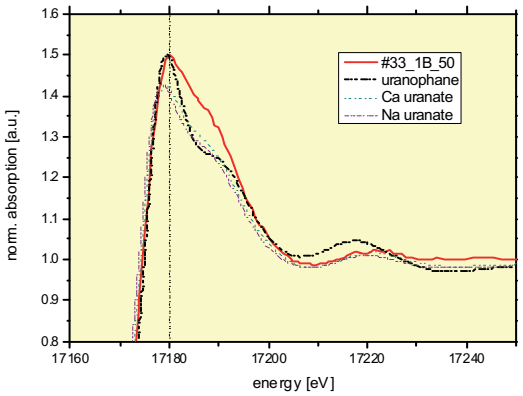

Fig. 3: *U L3-edge XANES spectra: Comparison of samples corroded in $MgCl_2$-brine with reference compounds*

Conclusions

The solid uranium phases are minor components in the corroded cement systems; therefore the evaluation required comparisons of the analytical data with reference samples and with U-free cement corroded under the same condition. Consistent results from XRD, XANES/EXAFS, and TRLFS suggest the existence of a uranophane phase like $Ca(UO_2)_2(SiO_3OH)_2 \cdot 5H_2O$ in samples corroded in $MgCl_2$-rich brine as well as samples corroded in NaCl-rich brine, respectively. The combination of the different analytical techniques shows that other solid U(VI) phases such as becquerelite, meta-schoepite or di-uranates are unlikely or may exist at low concentrations, only. Specimens taken from different vertical and radial positions of the corroded samples did not show differences in the XRD, EXAFS or TRLFS patterns.

Acknowledgement

The authors appreciate the excellent cooperation with PSI, Switzerland providing an uranophane reference sample.

Mobilization and immobilization of radionuclides from spent nuclear fuel

Introduction

The source term from spent nuclear fuel (SNF) dissolution is highly dependent on oxidative dissolution of the fuel matrix. The capacity of corroded canister iron phases to incorporate radionuclides is under investigation within the European collaborative project “ReCosy”. The stable corrosion product of steel canister material under reducing disposal conditions is magnetite. In the present study, it was intended to investigate the reductive trapping of actinides in metallic corrosion products which may provide for a driving force for SNF dissolution. About 10 years ago, an experiment (“denoted as K14Mt”) was designed investigating the effect of magnetite on the overall corrosion behaviour of SNF in NaCl solution. This experiment was terminated and the investigations of gas atmosphere, solution composition and solid material were started.

Experimental

The corrosion experiment was performed by using a pellet sized segment of high burnup SNF (50 MWd/kg U, linear power 260 W/m), 6.6 g fuel, and 10 mm in length together with commercial available magnetite (ALFA 012962, grain size ~ 5 µm). SNF sample and magnetite were immersed simultaneously in 5 mol/L NaCl solution (initial volume 200 ml, under Ar-atmosphere), using a glass vessel. During the initial phase of the experiment, the leachant was replaced entirely by fresh solution for four times until 65 days. This procedure removed the "initial release fraction (IRF)", such as Cs and fission gases in the gap and on grain boundaries. Afterwards the experiment was continued without replacing the solution (static), lasting over 3562 days. The gas phase and solution were sampled at 78, 215, 349, 771, 1895 and 3562 days after start of the static phase. The analytic procedures are described in [1]. A detailed description of the entire experimental procedure is given in [2]. After termination of the experiment, fractions of the magnetite were removed and analyzed. Various methods have been applied: SEM/EDX, XRD, Raman spectroscopy, XPS, digestion in HNO_3 and consecutive radiochemical analyses. The analyses are not yet completed.

Results and discussion

Results concerning the radionuclide release depend on the conditions kept during the 10 years of the experiment:

Gases: In the observation period, only a slight release of Xe of < 0.01 vol.% was found. Until

10 years, the H_2 concentration in the leaching vessel amounted to 18.5 vol.% and O_2 to 5.4 vol.%. After the first year, the CO_2 concentration raised from 0.1 to 0.8 vol.%, a value which cannot be explained by contact with air. The reason is still under investigation.

Solution concentrations: Fig. 4 shows the measured concentrations of the fission products Sr, Tc, Cs and the actinides U, Np, Pu, Am during the "static phase". Additionally, measured pH is also shown (right axis).

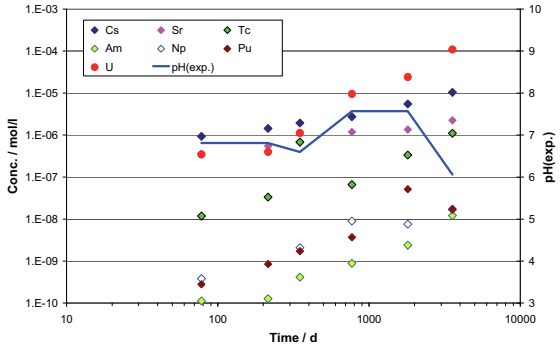

Fig. 4 *Dissolved element concentrations of the experiment K14Mt. Solid line: measured pH.*

Fig. 4 shows considerable differences in the temporal evolution of the released radionuclides. Between 215 and 3562 days, the Sr concentration increases from $6 \cdot 10^{-7}$ to $2 \cdot 10^{-6}$ mol/L. Release of Cs is slightly faster, whereas the mobilization of U is at the highest rate. The final U concentration was measured up to $1 \cdot 10^{-4}$ mol/l. The other radionuclides (Tc, Np, Pu and Am) are released at an intermediate rate. In total, fission gas release was >16%, Cs ~ 0.7%, Sr ~ 0.3%, and the actinides <0.1% of the inventory. After one year, the measured pH increased to 7.6 and dropped after 10 years to ~ 6.

Model calculations for 5 mol/L NaCl solution in contact with the measured $p(CO_2)$ revealed a decrease of the pH and the presence of dissolved carbonate. Under these conditions, solid $Na_2U_2O_7$ is dissolved forming U carbonato complexes in the range of the observed concentration of $1 \cdot 10^{-4}$ mol/l. Vice versa, at pH_{exp} ~ 7.6 in combination with the measured CO_2 partial pressure, the calculated Sr concentration is in equilibrium with solid $SrCO_3$ (strontianite). The evaluation of the radionuclide release rates in relation to the actual CO_2 partial pressures is not yet completed.

Solids: Grain agglomerations of the magnetite were recovered and investigated (Fig. 5). Measurable amounts of U were found upon the surfaces by SEM/EDS and XPS.

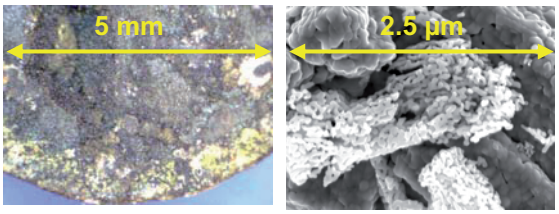

Fig. 5*: Light optical (left) and SEM (right) micrographs of magnetite on the fuel sample in an agglomeration after termination of the experiment.*

Raman spectroscopy was applied to investigate (a) if magnetite has undergone any transformation during the 10 years experiment, and (b) the redox state of U on the magnetite surfaces. The magnetite spectra of the exposed magnetite and fresh material were identical. Fig. 6 shows that U was present in the hexavalent state exclusively.

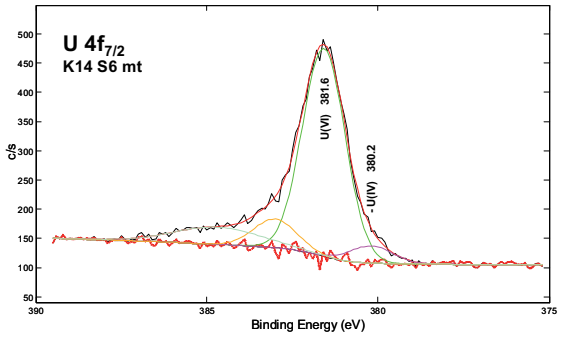

Fig. 6: *XPS spectroscopy of U onto magnetite: Narrow scan of the U 4f7/2 spectrum and result of a curve fit (red curve: sum curve of fitted functions). Analysis area: Ø 400 µm.*

Conclusions

In the glass vessel used for SNF corrosion experiments over almost 10 years the atmospheric conditions were not sustained. In particular, the origin of the high $p(CO_2)$ is not yet resolved. The presence of CO_2 and O_2 explained the observed U and Sr concentrations. Under these conditions, Sr cannot be used as indicator for SNF matrix dissolution.

Certain amounts of radionuclides are retained by the magnetite. Quantification is still pending. Due to the relatively high $p(O_2)$ the expectations with respect to the reductive trapping of actinides in corrosion products may not be achievable.

References

[1] B. Grambow, A. Loida, P. Dressler, et al. Wissenschaftliche Berichte, FZKA 5702, März 1996.

[2] A. Loida, B. Kienzler, H. Geckeis, Mat. Res. Soc. Symp. Proc., 757, 433-439 (2003).

6.3 Colloid impact on radionuclide migration

M. Bouby, A. Filby, H. Geckeis, R. Götz, W. Hauser, F. Huber, U. Noseck[1], M. Küntzel[1], M. Plaschke, T. Schäfer, H. Seher, C. Walther

[1]Gesellschaft für Anlagen- und Reaktorsicherheit (GRS), Theodor-Heuss-Str. 4, 38122 Braunschweig, Deutschland

Introduction

In the framework of the Grimsel Test Site (GTS) Phase VI the international Colloid Formation and Migration (CFM) project with partners from Japan (JAEA, AIST and CRIEPI), Switzerland (NAGRA), Sweden (SKB), Finland (POSIVA), South Korea (KAERI) and Germany (KIT-INE, GRS) processes related to the erosion of the compacted bentonite buffer and the possible formation of colloids are investigated. In the case of granite as host rock formation the bentonite will seal the wastes from water conduction features (fractures). Consecutively, it will be water saturated forming a gel layer. The recently in Sweden discussed scenario of glacial water intrusion estimates a high erosion of bentonite buffer due to the contact with glacial water of high pH and low salinity favoring the release of bentonite/ smectite colloids/ particles [1].

Once, bentonite colloids are released from the bentonite they might transport associated radionuclides along shear zone as demonstrated in studies within the CRR/CFM project [2]. Work performed in the framework of the BMWi project KOLLORADO and its successor KOLLORADO-2 (project duration 2009-2012) is closely related to the in situ experiments of the CFM project. The aim of the project goes beyond the pure investigation of colloid behavior in the geological barrier of a nuclear waste repository in crystalline rock. The goal is to obtain reliable experimental data

- on colloid/nanoparticle behavior in the geosphere,
- to gain deeper insight into fundamental processes,
- to implement these data into reactive transport codes as well as in PA relevant modeling codes, and
- to provide significant progress in the assessment of the colloid relevance for various repository concepts.

In this chapter, we report on the progress concerning (a) bentonite colloid stability, (b) studies on radionuclide bentonite sorption reversibility, and (c) colloid mineral surface interaction forces probed by AFM colloid probe technique.

Bentonite colloid stability

The critical coagulation concentration (CCC) of Febex bentonite colloids is determined by coagulation studies under variation of pH, electrolyte concentration and fulvic acid (GoHy-573FA) content and compared to groundwater geochemistry found in different potential repository sites. For $CaCl_2$ electrolyte solution a pH independent Ca-CCC of 1 $mmol \cdot L^{-1}$ was found (see Fig. 1). In the case of NaCl background electrolyte a pH dependent Na-CCC could be determined with 15 ± 5 $mmol \cdot L^{-1}$ at pH 6, 20 ± 5 $mmol \cdot L^{-1}$ at pH 7, 200

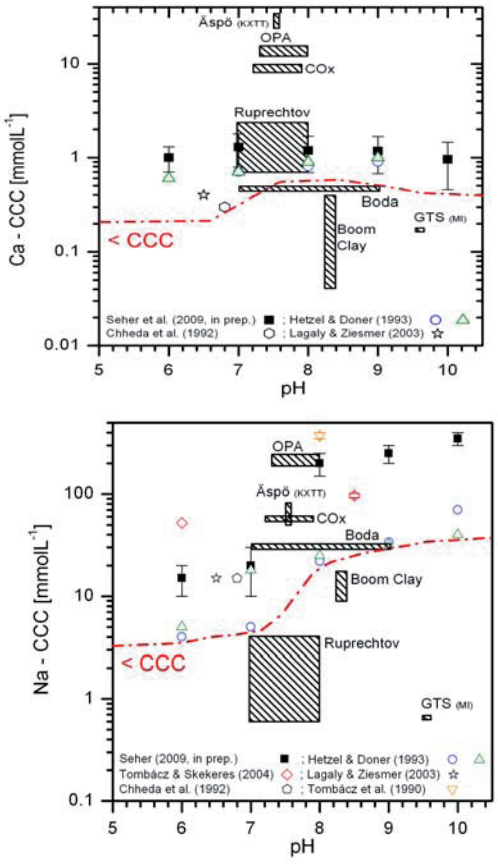

Fig. 1: *Critical coagulation concentration (CCC) as a function of the pH value determined for the calcium (Ca-CCC) and the sodium (Na-CCC) system for different montmorillonites. The red dash-dotted line indicates the onset of purely diffusion controlled coagulation. The pH - cation concentration regions for the different host rocks are indicated.*

± 50 mmol·L^{-1} at pH 8, 250 ± 50 mmol·L^{-1} at pH 9 and 350 ± 100 mmol·L^{-1} at pH 10, respectively. The addition of 1 mg·L^{-1} DOC FA increases the Ca/FA-CCC to 2 mmol·L^{-1} (not shown). An FA association with Febex bentonite colloids as surface coating and specific hot spots could clearly be identified by Scanning Transmission X-Ray Microscopy (STXM).

In Fig. 1 the experimentally determined Ca-CCC and Na-CCC values for bentonite derived montmorillonite nanoparticles and the water chemistry of the fractured rocks (Grimsel Test Site, Migration shearzone; Äspö Hard rock Laboratory, water KXTT), indurated and plastic clay formations (Boom Clay, Callovo- Oxfordian argillite, Opalinus Clay and Boda Claystone), and the Ruprechtov Natural Analogue Site are compiled. Based on this comparison montmorillonite nanoparticle stability is not expected for the COx, OPA, Boda claystones and the Äspö system both from the Ca and Na porewater concentrations under the current groundwater geochemistry. Furthermore, based on the Ca concentration montmorillonite nanoparticles should coagulate at the Ruprechtov site. However, for the Boom Clay system, based on the Ca and Na concentrations and also considering the elevated dissolved organic carbon concentrations additionally stabilizing clay colloids nanoparticle stability can be expected. The strongest colloid/nanoparticle stabilizing geochemical conditions are clearly found in the Grimsel granite groundwater, as expected.

The experimental bentonite stability results were described by means of a DLVO approach summing up hydration forces, short-range Born repulsion, van der Waals attraction and electrical double layer repulsion. The measured zeta (ζ) -potential of the bentonite colloids is used as platelet face charge and the edge charge is estimated by the combination of silica and alumina ζ-potential data in the ratio given by the Febex bentonite structural formula. Adjusting the montmorillonite face charge by a maximum of $\pm$ 12 mV was sufficient to successfully reproduce the measured stability ratios. However, the Na- CCC values could only be reasonably predicted using solely the edge-face interaction energy calculated. The strong deviations of the model predictions and the experimental determined Na-CCC values found at low electrolyte concentrations are explained by the model assumption of a "spill-over" of the platelet face electrical double layer (EDL) shielding the positive platelet edge charge.

Bentonite radionuclide sorption reversibility

Desorption kinetics of radionuclides from bentonite colloids and a possible subsequent sorption onto fracture filling material (FFM) can influence colloid-facilitated radionuclide migration in groundwater. To shed light on the significance of this issue batch-type experiments in presence of fracture filling material with different grain sizes spanning a range from 0.25 to 2 mm from Grimsel using a cocktail of strong and weak sorbing radionuclides spiked to natural groundwater from Grimsel have been conducted. Results show that tri- and tetravalent radionuclides, ^{232}Th(IV), ^{242}Pu(IV) and ^{243}Am(III) are clearly colloidal associated in contrast to ^{233}U(VI), ^{237}Np(V) and ^{99}Tc(VII). Concentrations of ^{232}Th(IV), ^{242}Pu(IV) and ^{243}Am(III) decrease after ~ 100h while ^{233}U(VI) and ^{99}Tc(VII) concentrations remain constant over the whole experimental duration of up to 7500h showing both no interaction with the fracture filling material due to sorption effects and no reduction to sparingly soluble phases.

Taking the batch sorption data derived partitioning coefficients of the binary systems "bentonite colloids – radionuclide" ($R_{d,coll}$) and "FFM – radionuclide" ($R_{d,FFM}$) published in [3] the resulting $R_{d,tot}$ of the ternary system can be calculated. The stable aluminium concentration measured throughout the experimental period infers that the interaction of colloids with the fracture filling material can be neglected ($R_{d,coll-FFM}$=0) and therefore the following equation can be applied:

$$R_{d,tot} = \frac{R_{d,FFM}}{1 + C_C \cdot R_{d,coll}}$$

whereas C_c is the bentonite colloid concentration in solution. The time dependent radionuclide concentrations variation of the ternary system (black symbols) in Fig. 2 is within the first approx. 500h below the calculated equilibrium concentration (red symbols) expected based on the binary system data. This observation can be interpreted as an effect of slow radionuclide bentonite colloid dissociation kinetics. However, after approx. 500h contact time the established radionuclide solution concentrations in the ternary system is within the concentration range expected from the binary systems and equilibrium conditions can be assumed. Results for ^{232}Th(IV) do not significantly differ from the ^{242}Pu(IV) data (not shown) in terms of the reversibility kinetics. In the case of ^{237}Np(V), a decrease in concentration after ~300h is observed (Fig. 3) which can be explained by either a slow reduction kinetic to Np(IV) in accordance with the experimental

pe/pH conditions reached and/or with a slow sorption kinetic on the FFM. No influence of the different Grimsel FFM size fractions (0.25-0.5mm, 0.5-1mm and 1-2mm) can be observed through comparison of surface normalized R_d values (not shown) implying an independence of the kinetic processes under the given volume to mass ratio used throughout this study.

The driving force of the observed reversibility is the excess of FFM surface compared to the available surface area of introduced FEBEX bentonite colloids (76 to 1). Overall, the results show that the desorption kinetics from bentonite colloids are rather independent from (i) the grain size of the investigated material, at least in the size fraction range 0.25-2 mm and (ii) the concentration of ^{237}Np(V), ^{242}Pu(IV) and ^{243}Am(III).

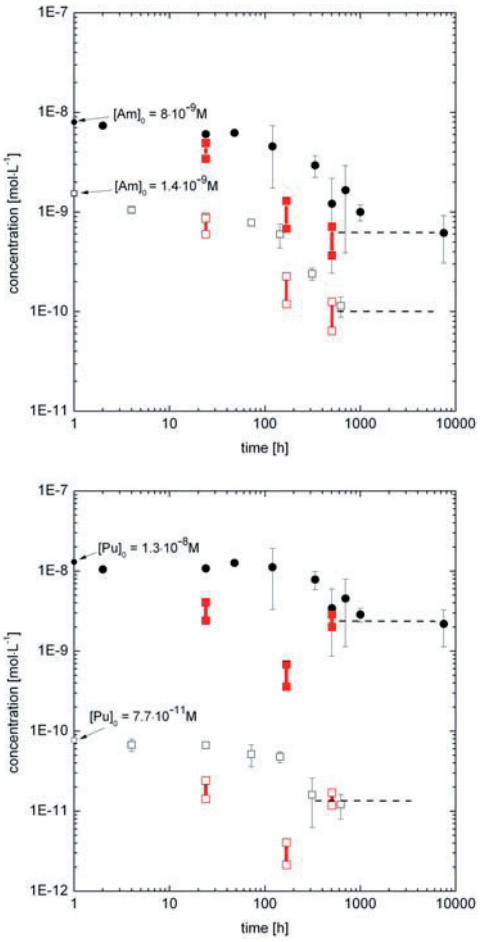

Fig. 2: *Time dependent variation of ^{242}Pu(IV) (lower graph) and ^{243}Am(III) (upper graph) solution concentration monitored in the ternary system bentonite colloids (C_c=20mg·L^{-1}), Grimsel FFM (1-2 mm) (V/m=4mL·g^{-1}; N_2-BET surface area 0.15 m^2·g^{-1})and radionuclide (low concentration open symbols, high concentration filled symbols). Additionally inserted are calculated concentration ranges based on batch experiments in binary systems published in [2] for the two initial concentrations used. Dashed lines visualize the proposed equilibrium solution concentration.*

Overall it has to be stated that the experimental duration of approx. 1000h seems to be sufficient to establish equilibrium conditions for tri- and tetravalent radionuclides (Am, Pu(IV), Th(IV)) under the experimental conditions used. However, further experimental studies on the binary systems and the ternary system are in progress to reduce uncertainties especially towards longer time scales.

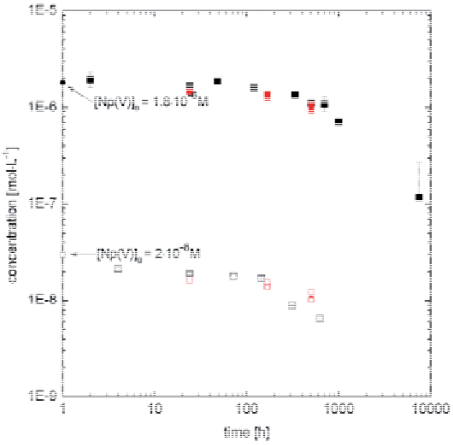

Fig. 3: *Time dependent variation of ^{237}Np(V) solution concentration monitored in the ternary system bentonite colloids, Grimsel FFM and radionuclide (low concentration open symbols, high concentration filled symbols). Additionally inserted are calculated concentration ranges based on batch experiments in binary systems published in [2] for the two initial concentrations used.*

AFM force spectroscopy application to study colloid mineral surface interaction

The aim of this work was to gain insight into the interaction of negatively charged model colloids with natural mineral and rock surfaces. This was accomplished using different surface sensitive methods: sorption experiments were carried out with fluorescing carboxylated latex model colloids and Grimsel granodiorite and its main component minerals (quartz, biotite, muscovite, feldspar, apatite, and titanite. Sapphire was used as model for clay minerals and analogous iron phases). Sorption of the colloids was made visible by fluorescence microscopy. By using Scanning Electron Microscope (SEM) and energy-dispersive X-ray analysis (EDX) those mineral phases were identified on which predominant colloid adsorption took place. The latex colloids were chosen as model for natural bentonite colloids since both are negatively charged over a wide pH

range and the difference of surface potentials is not too high. However, one has to make a distinction regarding the comparability between natural and synthetic colloids: the spherical latex colloids do not exhibit the heterogeneous charge distribution typical of a natural clay colloid with its differing charges on edges and planes. Furthermore, it has to be noted, that colloid attachment and agglomeration are kinetically controlled phenomena. The short-term experiments with a contact time of 15 min carried out in this work are thus not

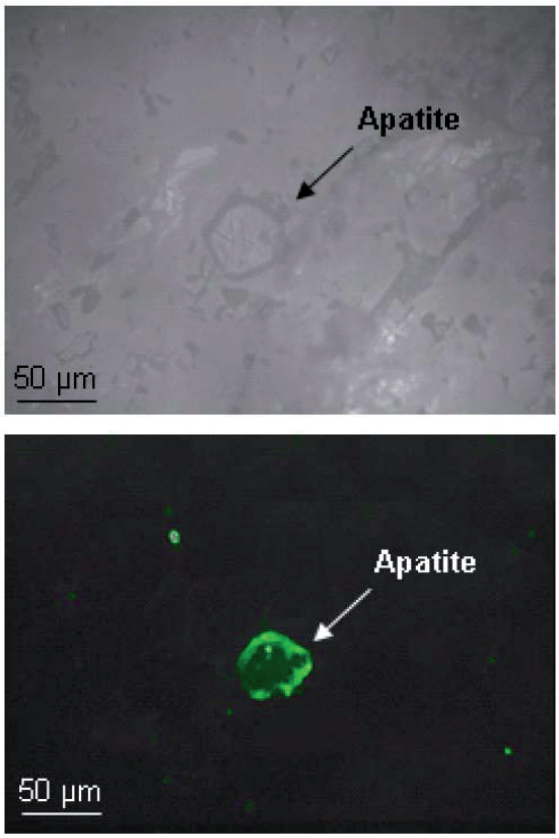

Fig. 4: *(upper image) Light-optical image and (lower image) fluorescence-optical image of a granodiorite surface; fluorescence as indication for colloid attachment was detected on the entire apatite surface (pH 6, I = 10^{-2} M NaCl, C_c = 0.05 g/l)*

transferable to long time scales without further confirmation. In the colloid adsorption experiments attractive interaction in the alkaline regime could only be observed on apatite (see Fig. 4). On all other mineral phases no colloid adsorption could be detected in alkaline conditions.

For colloid desorption tests carboxylated latex colloids were initially adsorbed onto the Grimsel granodiorite rock surface at acidic pH. The desorption of the colloids was observed in alkaline conditions. The fluorescence intensity measured on albite and biotite minerals decreased rapidly in the first 10 days and after 25 days desorption time, no fluorescence could be detected on the whole rock surface. The measurements clearly show that the carboxylate latex colloid adsorption/attachment is reversible.

Complementary Atomic Force Microscopy (AFM) force spectroscopy experiments were undertaken with the "colloid probe technique" to gain insight into colloid-mineral surface binding mechanisms. With this method it was possible to identify and quantify attractive and repulsive forces resulting from the colloid-mineral sur-face interaction with high sensitivity. Both ex-perimental approaches were conducted in a wide pH range and showed strong adsorption or attractive forces, respectively, at pH values close to or below the points of zero charge (pH_{pzc}) of the mineral surfaces. The influence of metal cations such as Eu(III) (used as chemical homologue for trivalent actinides), UO_2^{2+}, Ca(II) (as main divalent cation in Grimsel groundwater) and natural Grimsel groundwater on colloid-mineral interaction was investigated. Depending on mineral phase and pH, a significant increase of colloid adsorption and attractive forces was observed in the presence of the cations due to their adsorption on the mineral and colloid surfaces. The experiments indicated that the adsorbed cations may reduce the overall repulsive interaction at pH values higher than the individual mineral pH_{pzc}. No colloid adsorption on most of the minerals investigated (quartz, biotite, muscovite, feldspar, titanite, sapphire) was observed in the alkaline regime. In correspondence to the sorption experiments an attractive interaction in alkaline conditions could only be observed in the experiments with apatite and Grimsel groundwater or 10^{-4} M Ca(II). Adhesion forces were significantly enhanced (and the magnitude of repulsive forces decreased) at alkaline pH in presence of 10^{-4} M Ca(II) ions and in Grimsel groundwater (see Fig. 5).

The shear forces due to groundwater flow were estimated and found to be not high enough to overcome the measured colloid adhesion under all observed conditions. Detachment of

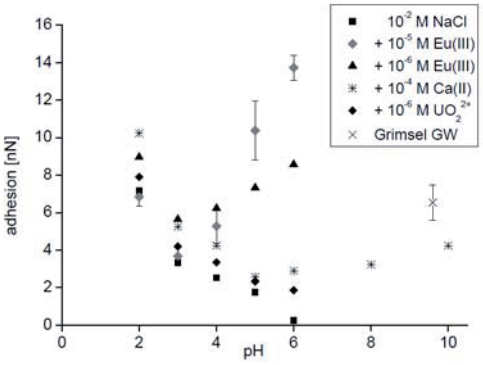

Fig. 5: *Experimental adhesion forces on muscovite.*

adsorbed colloids due to ground water flow can thus be assumed as negligible.

To support the experimental results, the AFM measurements were compared to theoretical DLVO calculations. These calculations showed that the experiments can be well predicted by theory but that the calculations do not regard possibly present hydration forces which may prevent a possible colloid adsorption. Results of this study prove that the interaction of colloids with mineral surfaces is determined by electrostatic interactions. According to the results, colloid adsorption in the alkaline regime is critically dependent on the divalent cation composition in the contact water.

References

[1] J. Liu, I. Neretnieks SKB Report R-06-103, Svensk Kärnbränsle-hantering AB (2006).

[2] M. Bouby, A. Filby, H. Geckeis, F. Geyer, R. Götz, W. Hauser, F. Huber, B. Kienzler, P. Kunze, M. Küntzel, J. Lützenkirchen, U. Noseck, M. Plaschke, A. Pudewills, T. Schäfer, H. Seher, C. Walther, Colloid/ Nanoparticle formation and mobility in the context of deep geological nuclear waste disposal (Project KOLLORADO; Final report). In: T. Schäfer, U. Noseck, (Eds.), FZKA report 7515. Forschungszentrum Karlsruhe, Karlsruhe, 210 (2010).

[3] Nagra Technical Report NTB 03-02, Nagra, Wettingen (2006).

6.4 Actinides in the far-field: Influence of natural organics

G. Buckau, C.M. Marquardt, Th. Schäfer

Expert views on the state-of-the-art on humate complexation processes with recommendations for future studies.

Background

The impact of humic substances on the migration of radionuclides in the geosphere has been an issue for safety of nuclear waste disposal since the mid 80's. At that time the European Commission (EC) launched the project MIRAGE (Migration of radionuclides in the geosphere) within the EURATOM program. The issue of humic substances was one out of three key topics in that project (the other ones were thermodynamics and colloids). Since then the potential impact of humic substances has been studied within the different EC framework programs and in various national programs. Examples of very recent activities are a number of research, training and mobility projects conducted within the EURATOM FP6 Network of Excellence ACTINET [1]. At the end of these activities, the partners concluded that the field on metal ion complexation with humic substances is still suffering under very diverse and partly contradicting findings, conclusions and views. It was agreed that an assessment of the present state of knowledge together with topics of key importance would be beneficial for future activities and progress in this field. Based on this aim a report was established, and published [2].

The Report

The partners of the recent set of ACTINET projects got together at a workshop in Larnaca, Cyprus, 27-31 October 2008. A number of additional persons were invited to contribute to the report. The organizations who have contributed to the report are Commissariat à l'Energie Atomique (France), Research Centre Dresden-Rossendorf, Institut für Radiochemie (Germany), Karlsruhe Institute of Technology, Institut für Nukleare Entsorgung (Germany), Laboratoire de Physique Subatomique et des Technologies Associees, Ecole des Mines de Nantes (France), Moscow State University (Russia), University of Cyprus (Cyprus), University of Manchester (United Kingdom) and University of Potsdam, Physical Chemistry (Germany).

The different topics treated in the report consider the characterization, spectroscopic, redox, and complexation properties. The topic on complexation properties include mass distribution, ternary complex formation, functional group response and kinetics. Also, model substances in the form of simple organic molecules, polyelectrolytes and designed reference substances are treated. The comprehensive main report (48 pages) is supported by 12 annex papers on specific issues.

The main report has no literature references, but documents the state-of-the-art, including the views of the authors, with recommendations for future investigations. The report thus reflects the consensus of the contributors without the intension to cover the entire spectrum of knowledge or views in the literature.

State-of-the-art and remaining questions

The report addresses two categories, namely (i) developments during the past two decades, and (ii) remaining questions for future studies.

The most important developments in the past decades are absolutely essential with respect to basic assumptions concerning the overall behavior of humic substances, and especially the metal ion complexation. The present report documents the state-of-the-art and overcome past misinterpretations and misunderstandings. Documentation of the consensus will help avoiding future dead-end investigations.

The report documents a large number of remaining questions for future studies. Some of these are of more generic character and some of them more specific and fundamental with respect to issues where key information is lacking.

Molecular mass and size distribution

In the eighties, Gel-pPermeation Chromatography, or Size Exclusion Chromatography (GPC or SEC) was introduced for determination of the humic acid mass distribution. Both methods do not measure the mass, but the size distribution. Misinterpretation in comparison with compact globular protein standards lead to the incorrect assumption that humic acid mass distribution maxima are found at 10.000 and up to 100.000 or more mass units. Introduction of mass spectroscopy and correct interpretation of size distribution measurement (including flow field flow fractionation; FFF) has lead to a complete

revision of this issue. It is agreed that the number weighted molecular average mass distribution is in the range of 450 to 550. This includes the impact of protonation and metal ion complexation induced association and flocculation leading to a progressively diminishing number of humic acid entities in solution.

Humate ligand function

A new approach is used for analysis of the complexation behaviour of humic acid. The humate ligand function, i.e. the quantity and physico-chemical behaviour of humic acid with respect to metal ion complexation, is found to be based on the number concentration of humic acid in solution. This is different than previous approaches where the concentration of functional groups has been postulated to represent the humate ligand function. The new analysis is based on comparison of basic analytical data. This includes mass distribution, the proton exchange function (the response of humic acid to protonation of relevant functional groups), and the measured complexation capacities (the amount of complex formed per amount of humic acid under specific physico-chemical conditions). The humate ligand concentration is decreasing with decreasing pH. An example is given in Fig. 1, with the complexation capacity (mmol complex per g humic acid), for An^{3+} with Gohy-573(HA) at I=0.1 mol/L $NaClO_4$.

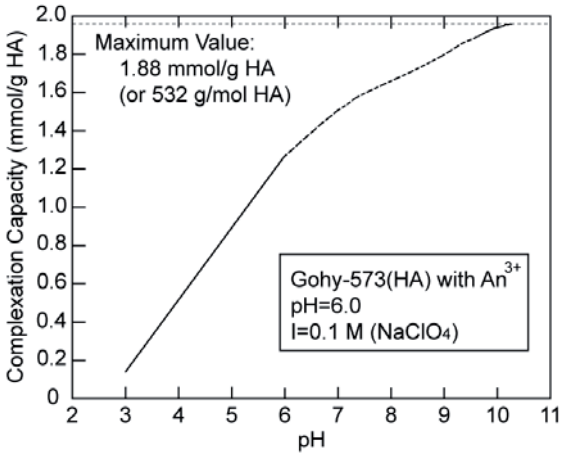

Fig. 1: *Gorleben humic acid (Gohy-573) An^{3+} complexation capacity as a function of pH*

Complexation constants and kinetics

With this new approach, the stability constant is defined as ß = [ML] / ([M] · [L]), where M is the metal ion and L the humate ligand. The free humate ligand concentration [L], is written $[L] = [L_{max}] \cdot \alpha - [ML]$, with $[L_{max}]$ = total number concentration of humic acid molecules. The latter is given by the number weighted average mass distribution of the humic acid (in g/mol) and its concentration (in g/L). The impact of pH is described through α, being the degree of ionization of humic acid proton exchange groups. $[L_{max}] \cdot \alpha$ can also be directly measured as the Complexation Capacity under given physico-chemical conditions. This is done by metal ion titration of humic acid solution, determining the saturation value for the complex formation. It should be noted that the average mass distribution and the protonation behaviour vary from one humic acid to the other. Therefore, generic information about a specific humic acid is required, preferentially in combination with direct determination of the complexation capacity under at least some physico-chemical conditions.

This new interpretation gives the humic acid complexation a simple and physico-chemically sound basis.

UV-Vis absorption and fluorescence properties

One of the most frequently used properties is the light absorption and the resulting fluorescence/phosphorescence emission. This refers amongst others to absorption and emission energies, the fluorescence decay time function, the fluorescence quenching between different bound metal ions and the anisotropy of emission as a function of molecular rotation. It is noted that the underlying processes are still not well understood and thus the use of this tool is hampered. It is recommended to gather available information, conduct specific experiments and try to achieve consensus on what the actual energy absorption, transition and emission processes are.

Redox properties

There is no accepted definition of the redox capacity. Numbers presented in the literature are normally redox buffer response from an undefined starting point to an undefined end-point with a given redox agent. For this reason the published numbers reach from much less than one redox functional group per molecule to almost four such groups per molecule. The very low numbers may reflect that only a part of redox inventory is observed by the empirical

approaches used. The higher numbers probably reflects the irreversible oxidation of the organic material. Several published numbers give an average around one redox group per humic acid molecule.

It is desired to determine the inventory of redox buffering groups, including its dependency of the Eh. Thereby, it should be distinguished if an inventory is reversible, or associated with irreversible changes in the humic acid. Spectroscopic methods should be used in order to characterize the changes of humic acid with the redox state. For this purpose, laser fluorescence spectroscopy in the nano second time resolution range appears to be promising. Such spectroscopic characterization is important in order to gain information on functional groups involved, but also for identification of reversible versus irreversible changes.

Summary and conclusions

A large number of experts with long experience in the field of humic substances have jointly formulated and documented the present state-of-the-art, with emphasis on metal ion complexation properties. The report includes a large number of recommendations for future studies. Remaining open questions address inter alia the following issues:

i The metal ion complexation and protonation processes lead to flocculation of humic acid. An open question is to which extent the association of humic acid molecules is initiated with the first complexation/protonation, or if the flocculation starts after achieving a critical complexation/protonation driven charge neutralization.

ii Increasing concentration of electrolyte medium cations leads to a decrease in the effective humate ligand concentration. The dependency is much lower than that observed for complexation/protonation. A question concerns the mechanism driving this decrease in effective ligand concentration, especially if it is a distinct localization of counter-ions at the humic acid functional groups (weak complexes) or if it is rather a medium effect acting on the overall physico-chemical properties of humic acid.

   The question is not trivial as it is not clear how to define parameters for the ionic strength dependency of humic acid. Furthermore, presently the experimental basis is insufficient. Consequently, a broader set of experimental data would be required prior to determining the physico-chemically correct way to proceed.

iii The formation of ternary complexes is reported by several authors. Other authors question the formation of distinct ternary complexes. It is open, if such ternary complexes are formed. If they exist, their stoichiometry, stability and reversibility (via different routes) are required.

These and the many other questions formulated in the report may be used as an important source of reference when initiating future studies and projects.

References

[1] http://www.actinet-network.org/

[2] “Expert views on the state-of-the-art on humate complexation processes with recommendations for future studies”, Ed. G. Buckau, Report: FZKA 7465, Karlsruhe Institute of Technology (2010).

6.5 Development and Application of Numerical Tools for Safety Analyses

For long-term safety analysis of nuclear waste disposal, numerical models and associated databases are indispensable. KIT-INE contributes to the whole set of required modelling tools with

- *Geochemical models and thermodynamic databases,*
- *Thermo-Hydro-Mechanical-Chemical (THMC) modelling,*
- *Thermodynamic Sorption Models,*
- *Coupled reactive modelling*
- *NEA-Thermodynamic Data Base Project and*
- *NEA Sorption Board.*

In the present report, examples of modelling exercises and participation in database projects are presented. The examples cover

- *Evaluation and Improvement of the THM Modelling Capabilities for Rock Salt Repositories in the Frame of THERESA Project (Author: A. Pudewills)*
- *CFD modelling of flow and solute transport in a µXCT scanned single fracture from the Äspö HRL, Sweden (Authors: F. Huber, A. Pudewills, Th. Schäfer, F. Enzmann, University of Mainz, Institute for Geoscience, D-55099 Mainz)*
- *THEREDA – A German Thermodynamic Reference Database (Authors: M. Altmaier, C.M. Marquardt, V. Neck, B. Kienzler, C. Bube)*

Evaluation and Improvement of the THM Modelling Capabilities for Rock Salt Repositories in the Frame of THERESA Project

Introduction

The objectives of the THERESA project [1, 2] are to develop, verify and improve the modelling capabilities of constitutive models and computer codes for analysis of coupled processes in geological and engineered barriers for use in performance assessment of the long-term safety of nuclear waste repositories. The Work Package 3 (WP3) of this project addresses the evaluation and improvement of numerical modelling capabilities for assessing the performance and safety of nuclear waste repositories in rock salt, with particular regard to the long-term evolution of the excavation damaged zone, considering the thermal-hydraulic-mechanical (THM) processes.
In the final step of the WP3 a triaxial compressive test (TC2B) and the large-scale benchmark test (BMT) on a thick-walled hollow cylinder both conducted on Asse rock salt were considered for the benchmark analyzes [3]. The main objectives of the benchmark calculations are the validation of the actual capabilities of the constitutive model and to identify further improvements of the model. The numerical analysis focused on the simulation of strains and permeability development in the rock salt samples. The calculation results were compared posterior to experimental data.

Modelling of the Laboratory Benchmark Test TC2B with ADINA code

As the first tests with a large hollow cylinder failed due to apparative problems and because no new large sample could be made available, two normal-scale samples of 100 mm diameter and 190 mm length were used for new tests. The second of these experiments (TC2B) was chosen for the benchmark simulation, because a distinct permeability increase under deviatoric load could be detected. The test procedure was similar to the one for the hollow cylinder.

Figure 1 illustrates the test loading history of the test TC2B performed at GRS. The confining pressure was raised after 7 days from 1MPa to 8MPa. The axial stress was increased and decreased in several steps which are also depicted in Fig.1. The temperature was 30° C up to 7.8 days and then raised to 70° C.

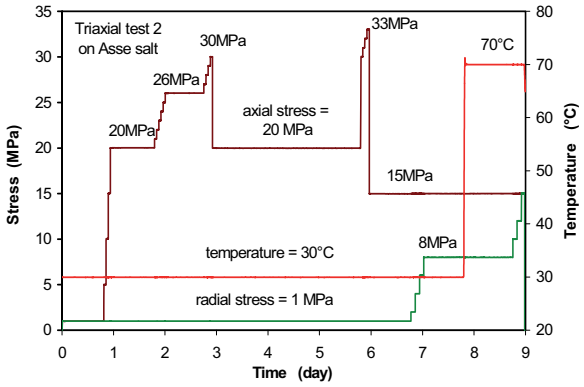

Fig. 1: *Loading conditions applied to the sample*

The evolution of the THM processes occurring during this test was calculated using the finite element code ADINA [4]. The initial and boundary conditions are assumed as follows:

- Thermal: The whole sample was kept at room temperature of 30°C for about 8 days after this period the temperature was rapidly increased to 70°C and kept constant until the test ends.
- Hydraulic: Boundaries are impervious except for the both top boundaries to permit gas in- and outflow, where gas pressure at the bottom of 0.5 MPa and the atmosphere pressure at top were imposed.
- Mechanical: At the top boundary a time dependent vertical stress and at the outer cylinder surface a radial stress was applied. The bottom surface of the model was fixed in the normal and horizontal directions.

The complete material model and the parameters adopted in the simulation coincide with those assumed in the previous model calibration report [5].

The comparison of the calculated strains with the strains measured in the laboratory test is shown in Fig. 2 on which the dots are the experimental data and the continuous line is the response of the model. There are same differences during the second creeping stage due to the fast increase of the vertical stress from one to 20 MPa. During the next moderate increase and decrease of the loading stages there is a better agreement between the experimental and predicted strains.

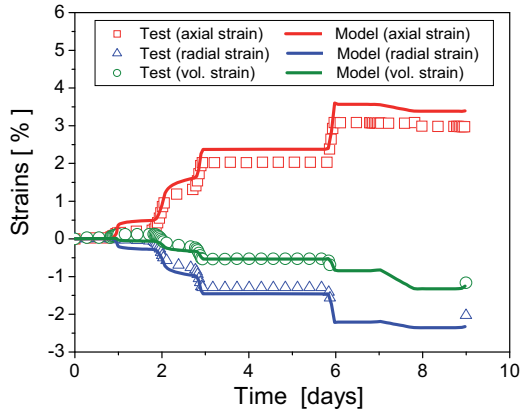

Fig. 2: *Comparison of measured and predicted axial, radial and volumetric strains.*

The calculated salt permeability using two available relations [6, 7] shows differences in the first loading stages (Fig. 3) because of the assumed initial porosity of the salt sample as near zero (η_0=0.0002).

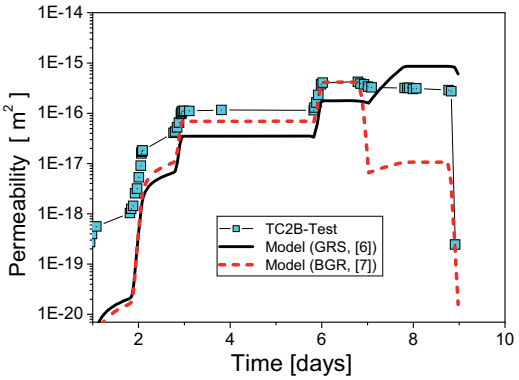

Fig. 3: *Permeability of the sample during the creep test and the calculated evolution of the permeability with two different relations between permeability, volumetric strain and confining pressure.*

Taking into account that the initial porosity of the sample was about 0.2% and the corresponding permeability of about 10^{-19} m^2, a new simulation will match quite well with the measured behaviour. The increasing temperature and also the confining pressure have different influences on the actual results. Unfortunately, it must be mentioned that at the moment there are too few experimental results available to be sure that our assumptions are correct.

Conclusions

The predictive capabilities of the constitutive model for rock salt developed originally for crushed salt have been increased to describe the dilatancy deformations. The mathematical formulation of the model is relatively simple and can be easily implemented in different numerical codes. The numerical simulation results of the laboratory benchmark tests have shown a quite good agreement with experimental data. The model is able to describe the main hydro-mechanical behaviour of the rock salt such as transient creep, dilatancy and material damage. In case of the sealing (re-consolidation) of the damaged salt, there is still a considerable difference between the model and experimental data. A future improvement of the purposed model is required.

CFD modelling of flow and solute transport in a µXCT scanned single fracture from the Äspö HRL (Sweden)

Introduction

Fluid flow as well as solute transport through fractured rock plays an important role in safety analysis of a geologic repository. In contrast to porous media, fluid flow through fractured rock is bound to discrete roughly shaped planes,

which act as main flow paths. As a consequence this issue has been extensively studied in the past by several authors [8-11]. Both experimental and theoretical approaches have been applied to shed light on the processes governing flow and solute transport in single fractures as well as in fracture networks. In most cases, fractures were treated with the parallel plate model or the streaming tube approach, where real natural fracture morphologies are replaced by simplified and abstracted geometries. The governing equations describing fluid flow are the Navier-Stokes equations, a nonlinear system of partial differential equations, only to be solved numerically in 3D [12].

Modern laboratory techniques, like e.g. computer tomography (μXCT) can serve as a non-destructive tool for characterisation of natural fractures in drill cores providing geometrical information which can be used directly in numerical codes to conduct flow and mass transport simulations on the measured scale. This more realistic approach has been applied in our study.

Core characterization

The core used in this study stems from the hard rock laboratory (HRL) in Äspö (Sweden) from the drill hole KOV 01 774.7-775.2 (later referred to as core#8). From a petrologic point of view, it would be classified as a diorite. For further geological, petrologic and geochemical details of the site, see [13]. Prior to characterisation, the core was placed in an acryl column and the periphery sealed. To gain information both about geometrical features of the fracture and porosity as well as aperture distribution, it was scanned using a μXCT. For further details about the applied experimental techniques it is referred to [14]. The size of the core is 13.528 cm in length and 5.048 cm in diameter. With the μXCT setup a resolution of 80 μm was achieved. Figure 4 shows the fracture as rendered from the pre-processed data set. As expected for a real fracture, it reveals a complex 3D spatial geometry and fracture surface morphology. The fracture is wedge shaped. The border of the fracture shows a smooth shape towards the larger side of the wedge, while the border is irregularly shaped towards the narrow side. The complex geometric feature is assumed to have a strong impact on the flow field and in consequence a strong influence for solute transport. Here, the occurrence of so called trapping zones is likely which can retard tracers and colloids when entering these zones [15].

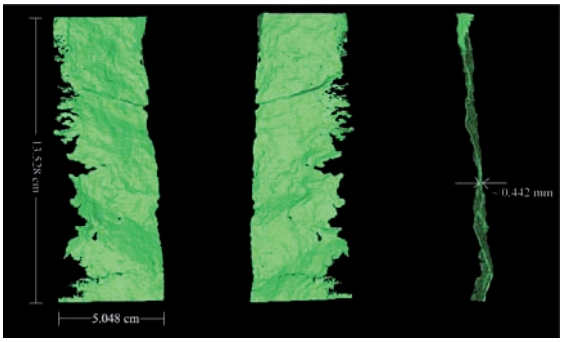

Fig. 4: *Rendered 3D image of the fracture in core#8 on the basis of the μXCT data set which shows the complex overall geometry and surface morphology. Notice the very irregular boundary on the narrow side of the wedge shaped fracture.*

Finite Element Models

The commercial finite element code ADINA-F [4, 16] was applied to model fluid and solute transport through the fracture. To study the effect of the fracture geometry 4 different models concerning the geometrical complexity have been generated, both in 2D and 3D.

1. The first model in 2D is a simple parallel plate model (thereafter referred to as 2D-PPM) which uses a mean aperture of 0.00044 m as determined by the μXCT dataset and the core length of 0.1353 m.
2. A slightly more complex model called "mean aperture model" in 2D (thereafter referred to as 2D-APM) is based on the mean aperture of every μXCT slices (1691 slices), thus incorporating more geometrical information as the 2D-PPM.
3. The third model in 2D completely ignores the aperture. By projecting the midplane of the fracture onto a 2D plane a model with no aperture is obtained which incorporates the full geometrical information of the side boundaries (referred to as 2D-MPM).
4. The last model is a 3D representation of the fracture applying the full resolution of the model containing all geometrical information available by the μXCT data (referred to as 3D-FM). Number of elements are 3.7 million.

Meshes of the 2D-PPM and the 2D-APM were produced using the ADINA-F build-in mesh generator. The 2D-MPM and the 3D-FM volume mesh were generated out of the μXCT data set by means of the commercial software Mimics® and 3-matic® (both Materialise Inc., Belgium). In Figure 5 both 2D meshes used in the study are depicted together with the corresponding calculated velocity distributions. Regarding all models, all surfaces except the inlet at the bottom and the outlet at the top of the

fracture are assigned no-slip (no-flow) boundary conditions. At the inlet of all models velocity and mass (= solute) boundary conditions on basis of the exact tracer input function from the experiments have been applied.

A possible existence of matrix porosity in the vicinity of the fracture boundary and especially on narrow side of the fracture are completely ignored, to exclusively study the influence of geometrical information on the velocity flow field and thus on the mechanisms governing solute transport. Due to the same reason, calculations are conducted without regarding any chemical processes like e.g. sorption or sorptive reduction. The flow is laminar and water as fluid is incompressible with a density of 998.2 kg/m^3 and a viscosity of 0.001 kg/ms. A diffusion coefficient of $2.5 \cdot 10^{-9}$ m/s^2 for HTO has been used. All four models are used to calculate the same HTO breakthrough curves (BTC) obtained by migration experiments in core#8 with a flux of 0.05ml/min.

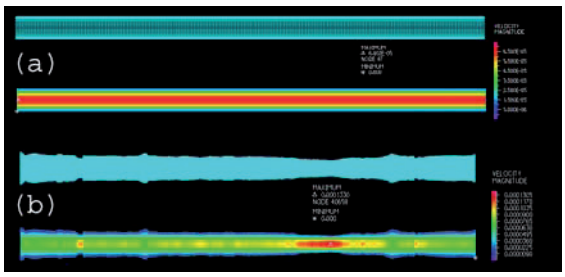

Fig. 5: *View of the finite element meshes and velocity distributions of (a) the 2D-PPM and (b) the 2D-APM model. Note that the aperture for both models is shown as 30 times exaggerated for visualizing reasons.*

Results

Calculated velocity distributions of all models are shown in Figure 5 and Figure 6. Generally speaking, calculated parabolic velocity profiles have evolved and maximal fluid flow velocities correlate with zones of smaller aperture and vice versa. In case of the 2D-MPM maximum flow velocities match areas where the model cross section is smaller. The pressure distribution (not shown) yields continuous gradients representing steady state flow conditions in all 4 models. Figure 7 shows experimentally obtained breakthrough curves from two migration experiments on core#8 (volumetric flux = 50µl/min) in comparison with breakthrough curves calculated using the above described finite element models.

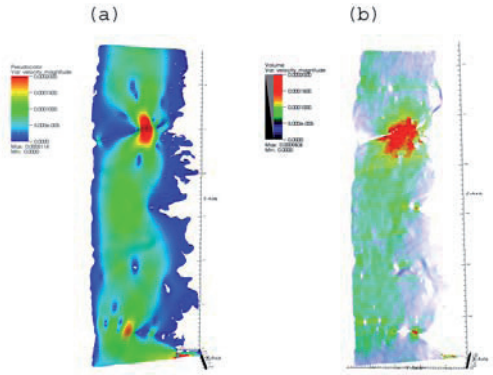

Fig. 6: *Velocity distribution of the (a) 2D-MPM and (b) of the 3D-FM. Both models show preferential flow paths due to the complex fracture geometry.*

Regarding the 2D-PPM, the calculated peak position correlates satisfactorily with the experimental peak position. A clear deviation in the tailing of the BTC is observed which can be explained by the averaging step of the geometrical information. The tailing is mainly produced by Taylor dispersion and by molecular diffusion. It is obvious that the application of a mean aperture results in an averaging of the tailing in the calculated BTC. The 2D-APM possesses a higher average velocity than the 2D-PPM due to the variability in the aperture distribution resulting in a faster arrival of the peak maximum. An even higher average velocity is observed for the 2D-MPM leading to a faster peak arrival compared to the experimental breakthrough curve. In contrast to the 2D-PPM and 2D-APM, the 2D-MPM exhibits a strong tailing caused by the very irregular narrow boundary of the fracture. Here the

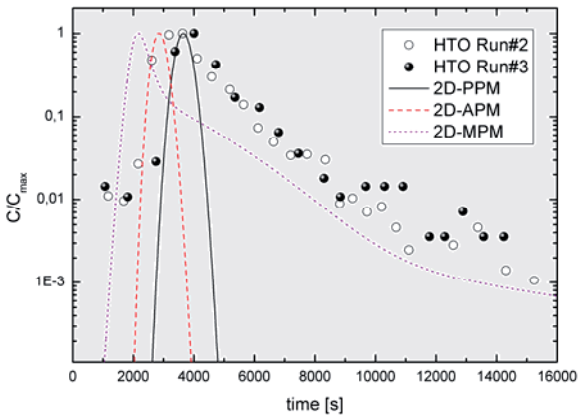

Fig. 7: *Normalized experimental HTO (open symbols) and calculated (line) BTC as function of time.*

occurrence of so called recirculation zones is observed which causes a retardation and dispersion of the solute.

The 3D-FM velocity distribution in Figure 6 shows the impact of the full 3D fracture ge-

ometry on the flow field. In general, the velocity field is similar to the flow field of the 2D-MPM, thus it is likely that the solute will exhibit a comparable strong tailing. First calculations using the 3D model are conducted at the moment.

Summary and conclusions

Fluid flow and mass transport were simulated using the CFD approach on basis of datasets from a µXCT (resolution 80µm) of a single fracture in a diorite drill core. Goal of this study is to investigate the influence of real fracture geometry on the flow and transport behaviour. Two of the three 2D models, 2D-PPM and 2D-APM, only use the mean aperture of the fracture and the average aperture for every µXCT slice, respectively. Due to the over-simplification of the real fracture geometry both models fail in reproducing the experimentally observed breakthrough curve. The third 2D model (2D-MPM) represents a projection of the fracture midplane to the Y-Z plane in-corporating the side walls of the fracture and completely excluding the fracture aperture. On the one hand, the effect of the fracture side walls leads to a distinct tailing in the breakthrough curve in good agreement to the experimental findings but on the other hand the model overestimates the experimental peak position due to a higher average velocity compared to the both aforementioned 2D models. The 3D model (3D-FM) using the full resolution of the µXCT dataset shows a very heterogeneous flow distribution which leads to a channelling of the flow and solute. Solute transport calculations are underway at the moment. Despite the greater computational and technical effort in creating a 3D model on a basis of µXCT data, this approach will be a step towards a more fundamental understanding of the processes governing flow and mass transport in real single fractures.

THEREDA – A German Thermodynamic Reference Database

Introduction

Safety analysis for a geological radioactive waste repository relies on geochemical model calculations. The thermodynamic description of the processes between the aqueous and the solid components is a key step in assessing the amount of radionuclides that can potentially be released from a repository. A reference database which meets high quality standards and is used in a standard and binding manner is a basic precondition for comparable and traceable results from geochemical modelling in all geological settings.

In order to establish such a thermodynamic reference database in Germany, the THEREDA project (Participating institutions (funded by BMBF, BMWi and BMU): 1) Karlsruhe Institute of Technology, Institut für Nukleare Entsorgung 2) Institute of Radiochemistry, Forschungszentrum Dresden-Rossendorf, 3) Gesellschaft für Anlagen- und Reaktorsicherheit mbH, Braunschweig, 4) Institute of Inorganic Chemistry, TU Bergakademie Freiberg, 5) AF-Colenco Ltd, Baden-Dättwil, Switzerland) started in 2006 with the goal of providing consistent and reliable thermodynamic data for all repository host rock formations (salt, clay, granite) discussed in Germany.

Existing databases

THEREDA relies on numerous thermodynamic data taken from the NEA-TDB (Thermochemical Database of the Nuclear Energy Agency). NEA-TDB covers mainly the actinides Th, U, Np, Pu and Am as well as Tc. Furthermore the NEA-TDB provides data for the elements Ni, Se and Zr. Presently, the database for tin and iron are under preparation. The selection of consistent thermodynamic data by NEA-TDB ("Selected Values") is based on an extensive review process, on "CODATA Auxiliary Data" and on the specific ion-interaction theory (SIT). Due to the strict concept of "selected values", the NEA database is incomplete and cannot be applied directly to specific field of applications to be covered by THEREDA. Therefore, in THEREDA additional data are included which do not fulfil the NEA-TDB quality criteria.

The existing databases which are used for modelling speciation and solubility are of limited reliability because of lack of data for some major and trace elements, inconsistencies between the considered species and the corresponding formation constants, restricted ranges of intensive parameters, e.g. temperature, density, and pressure, and restrictions with respect to ionic strengths.

THEREDA contains verified thermodynamic parameters. It aims to fill data gaps wherever possible, provides estimated values where no data are available and indicates the quality of each value together with its validity limits. The handbook for THEREDA and the corresponding quality guidelines are available and are used for the data selection. THEREDA is a centrally administered and maintained database.

Elements

The thermodynamic data included comprises mainly the elements needed for geochemical

calculations of the behaviour of chemotoxic and radioactive substances in a deep geological repository.

The THEREDA database project will provide evaluated thermodynamic data for the following elements:

- Na, K, Mg, Ca, Cl, sulfates (for temperatures up to 393 K);
- analogue system with carbonate at 298.15 K; (to be expanded to higher temperatures);
- Radionuclides (actinides, fission products): Th, Pa, Np, U, Pu, Am, Cm, Tc, Cs, Sm, I, Se, Sr, Ni, Ra;
- Toxic elements: Zn, Cr, Co, Cu, Cd, Hg, Pb, As;
- Zircaloy and container material: Fe, Zr and alloying elements (Sn, Ni, Nb);
- Matrix elements: Si, Al (including a thermodynamic model for the cement system).

In order to describe the chemical behavior of contaminants, actinides and long-lived fission products in aqueous solution by means of geochemical modeling some parameters are fundamental:

- Solubility products of the solubility-dominating solid phases relevant to the system under consideration;
- Equilibrium constants that describe the different complexation processes in solution;
- Activity coefficients (at higher ionic strength it is indispensable to account for the influence of ion-ion interactions).

The Pitzer equations for activity calculations factor in ion-ion interactions between ions of equal as well as of opposite charge and thus yield realistic results from low up to very high ionic strengths. Therefore, in addition to the solubility products and equilibrium constants, the THEREDA database includes both SIT- and Pitzer- parameters for the calculation of activity coefficients. The database is also organized in a way to allow for managing compatibility restrictions (e.g. from data which are exclusively SIT- or Pitzer- compatible).

Quality assessment/management

The guidelines that form the basis of the data compilation, selection and evaluation processes within the THEREDA project are based largely on the guidelines, which were constituted by the NEA for its Thermochemical Database Project.

Furthermore, THEREDA assigns clearly defined and documented quality labels to each data according to three general categories with regard to the type, source and quality of the data. Supplementary remarks contain additional information, e.g. literature references, validity limits or information on underlying analogues or approximation methodologies. This information allows for the traceability of each entry and raises the awareness of the quality of each data set.

In a later project stage, the THEREDA partners will provide transparently documented estimate values for the thermodynamic data that are still unavailable by then.

Data sets

THEREDA will offer two possibilities of accessing the thermodynamic data: a) there will be several predefined and application-oriented data sets that contain only data needed for a certain application; in a first stage, repository scenarios in clay, salt and crystalline shall be covered by these tailored databases; b) the user can subscribe on the THEREDA webpage to access the complete database in order to perform interactive single queries and to derive individual data sets.

A manual is compiled at present in order to explain not only the technical aspects but rather to illustrate the meaning of the data quality features, details of data traceability and to point out possible limitations in the applicability of the database.

The database can be accessed via the THEREDA web page (www.thereda.de). Additionally supplied software tools will enable to translate the requested data compilations into database files for commonly used geochemical codes (e.g. EQ3/6, PHREEQC, Geochemist`s Workbench, or CHEMAPP).

References

[1] Theresa project: “Description of Work”, Annex 1 to the project contract FP6-036458 (2007)

[2] K. Wieczorek, T. Rothfuchs, C. -L. Zhang, Th. Spies, U. Heemann, Chr. Lerch, S. Keesmann, A. Pudewills, P. Kamlot, J. Grupa, K. Herchen, S. Olivella, Chr. Spiers, EURADWASTE, Luxembourg, (2008).

[3] C.-L. Zhang, K. Wieczorek, T. Rothfuchs, Theresa Project, Work Package 3, Deliverable D7, Braunschweig, Germany, (2009).

[4] Adina R&D Inc.: ADINA, Report ARD-01-9, Watertown, MA, US, (2008).

[5] K. Wieczorek, U. Heemann, S. Keesmann, A. Pudewills, S. Olivella, P. Kamlot, C. Spiers and K. Herchen, THERESA project, Work Package 3, Deliverable D8,

Braunschweig, Germany, (2008).

[6] W. Bechthold et al. [eds.], BAMBUS II: Final Report, EUR-20621-EN (2004).

[7] U. Heemann, Heusermann, S. DisTec-2004, Int. Conf. on Radioactive Waste Disposal, April 26-28, Berlin (2004).

[8] L. Moreno et al., Water Resources Research, 24(12), 2033-2048 (1988).

[9] Y. W. Tsang et al., Water Resources Research, 24(12), 2049-2060 (1988).

[10] P. M. Meier, A. Medina, J. Carrera, Ground Water, 39(1), 10-17 (2001).

[11] Carrera, J., Journal of Contaminant Hydrology, 13(1-4), 23-48 (1993).

[12] G. K. Batchelor "An introduction to fluid dynamics", Cambridge Univ. Press, 615pp (2000).

[13] M. Laaksoharju, et al., Applied Geochemistry, 14(7): p. 835-859 (1999).

[14] F. Enzmann, and M. Kersten, in 1st Annual workshop Proceedings of IP FUNMIG, report CEA R-6122, P. Reiller, et al., Editors. Commissariat a l'energie atomique (CEA): Gif sur Yvette (France). p. 211-215 (2006),

[15] D.F Boutt, et al., Geophysical Research Letters, 33 (21) (2006).

[16] K. J. Bathe, H. Zhang, M. H. Wang, Computers & Structures, 56 (2-3): p. 193-213 (1995).

7. Separation of long-lived minor actinides

A. Geist, U. Müllich, P.J. Panak, S. Trumm

Background

Plutonium and the minor actinides (neptunium, americium, and curium) are the major contributors to the long term radiotoxicity of used nuclear fuels. Alternatively to their direct final disposal in a deep geological repository, actinides could be separated from spent nuclear fuels and be recycled in advanced nuclear reactors – the Partitioning & Transmutation strategy [1]. Partitioning involves chemical separations processes based on pyrometallurgy or hydrometallurgy.

Work at INE regards hydrometallurgical (i.e., based on chemical liquid-liquid extraction) actinide separation, with a focus on the separation of trivalent americium and curium from the chemically similar lanthanides.

Alkylated bis-triazinyl-pyridines (BTP, Figure 1 left) were the first N-donor extracting agents

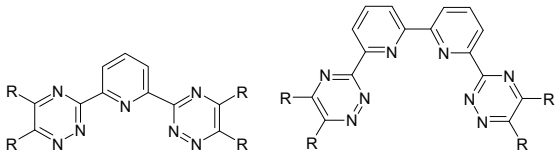

Fig. 1: *BTP (left) and BTBP (right).*

able to extract Am(III) and Cm(III) from acidic solutions with good selectivity over the lanthanides [2]. Alkylated bis-triazinyl-bipyridines (BTBP, Figure 2 right) [3] were later developed from the BTP; with $CyMe_4$-BTBP (6,6'-bis(5,5,8,8-tetramethyl-5,6,7,8-tetrahydro-benzo-1,2,4-triazin-3-yl)-2,2'bipyridine) [4] being the current European reference molecule for actinides(III)-lanthanides separation. $CyMe_4$-BTBP has successfully been employed in a hot lab-scale demonstration test [5]. Nevertheless, its solubility and kinetics are not fully satisfactory. Hence, there is still a need for improved extracting agents.

To support this development, we continue our fundamental studies [6, 7] aimed at understanding selectivity. Also, we investigate kinetics and synthesize new extracting agents.

Complexation of Cm(III) and Eu(III) with BTP and BTBP in aqueous solution

Introduction

We compare the complexation of Cm(III) and Eu(III) with BTP [8] or BTBP [9] ligands in aqueous solution: Cm(III) or Eu(III) solutions are titrated with the ligand solution, and the fluorescence emission spectra are recorded. Speciation, stability constants, and thermodynamic data are derived.

Complexation with BTBP

The complexation of Cm(III) and Eu(III) with BTBP (here, 4-*t*-butyl-6,6'-bis-(5,6-diethyl-1,2,4-triazin-3-yl)-2,2'-bipyridine) in water/ 2-propanol 1:1 solution is studied using time-resolved laser fluorescence spectroscopy (TRLFS). A mixed solvent is used due to the low aqueous solubility of the ligands.

Fluorescence spectra of Cm(III) or Eu(III) at increasing BTBP concentration are show in Figure 2. With increasing ligand concentration, complexes form from the solvated metal ions. Slope analysis and fluorescence lifetime identify these as 1:2 $[M(BTBP)_2(H_2O)]^{3+}$ complexes.

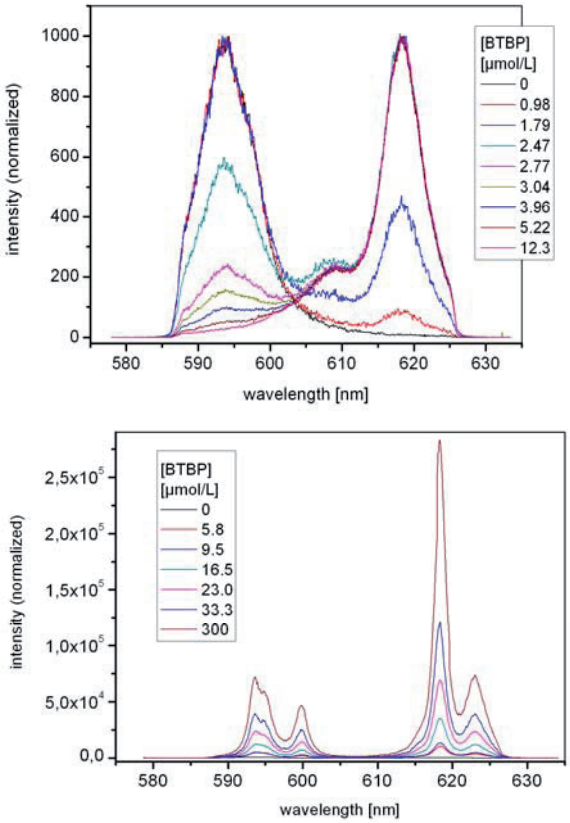

Fig. 2: *Fluorescence spectra of Cm(III) (top) and Eu(III) (bottom) in water/2-propanol 1:1 as a function of the BTBP concentration.*

The Cm(III) complex forms at a much lower BTBP concentration than the corresponding Eu(III) complex (see Figure 3); the respective stability constants are log $K_{Cm(III)}$ = 11.1 and

log $K_{Eu(III)}$ = 9.0, corresponding to $\Delta\Delta G$(20 °C) = $-RT\ \ln(K_{Cm(III)}/K_{Eu(III)})$ = −11.8 kJ/mol in favour of Cm(III).

Thermodynamic data of the complex formation reaction are determined from the temperature dependencies of stability constants, see Table 1. For both Cm(III) and Eu(III), the complexation reaction is both enthalpy and entropy driven. $\Delta H_{Cm(III)}$ is 11.7 kJ/mol more negative than $\Delta H_{Eu(III)}$, whereas the entropy difference is negligible. The difference in ΔG(20 °C) of −10.1 kJ/mol in favour of Cm(III) agrees well with that of −11.8 kJ/mol from the titration experiments.

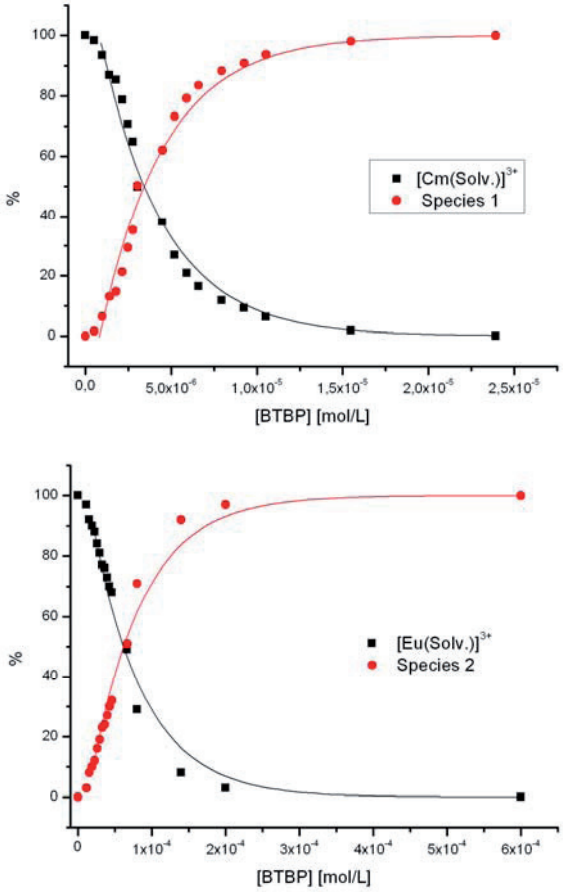

Fig. 3: *Species distribution of Cm(III) (top) and Eu(III) (bottom) in water/2-propanol 1:1 as a function of the BTBP concentration Lines are calculated with log* $K_{Cm(III)}$ *= 11.1 and log* $K_{Eu(III)}$ *= 9.0.*

Complexation with BTP

A similar complexation study is also performed with BTP (here, bis(5,6-dipropyl-1,2,4-triazin-3-yl)-2,6-pyridine) in water/methanol 1:1. Again, Cm(III) or Eu(III) complexes form upon addition of BTP, with the Cm(III) complex forming at lower BTP concentration than the Eu(III) complex. Slope analysis confirms the formation of 1:3 complexes, and lifetime measurements show the absence of water in the first coordination sphere; the complexes thus are $[M(BTP)_3]^{3+}$.

Tab. 1: *Thermodynamic data for the complexation of Cm(III) and Eu(III) with BTBP in water/2-propanol 1:1.*

	Δ*H* [kJ/mol]	Δ*S* [J/(mol·K)]	Δ*G* (20 °C) [kJ/mol]
Cm(III)	−34.7 ± 1.6	93.4 ± 5.5	−62.1 ± 2.6
Eu(III)	−23.0 ± 3.8	99.2 ± 12.3	−52.0 ± 5.2
Δ	−11.7	−5.8	−10.1

The respective stability constants are log $K_{Cm(III)}$ = 14.4 and log $K_{Eu(III)}$ = 11.9, corresponding to a difference in ΔG(20 °C) of −14.0 kJ/mol in favour of Cm(III).

Tab. 2: *Thermodynamic data for the complexation of Cm(III) and Eu(III) with BTP in water/methanol 1:1.*

	Δ*H* [kJ/mol]	Δ*S* [J/(mol·K)]	Δ*G* (20 °C) [kJ/mol]
Cm(III)	−36.5 ± 4.7	148 ± 17	−79.9 ± 7.5
Eu(III)	−26.4 ± 1.8	138 ± 7	−66.8 ± 2.8
Δ	−10.1	−10	−13.1

Thermodynamic data are summarised in Table 2. As with BTBP, complexation is driven by entropy and enthalpy. $\Delta H_{Cm(III)}$ is 10.1 kJ/mol more negative than $\Delta H_{Eu(III)}$; the entropy difference again is negligible. The difference in ΔG(20 °C) of −13.1 kJ/mol in favour of Cm(III) agrees well with that of −14.0 kJ/mol from the titration experiments.

Conclusion

The complexation of Cm(III) with BTBP or BTP in aqueous solution is compared to that of Eu(III). Complexation is favoured both by enthalpy and entropy. However, significant differences in Δ*H* cause the complexation of Cm(III) to occur at much lower BTBP or BTP concentrations. These studies demonstrate the thermodynamic driving force for BTBPs' and BTPs' selectivity. It explicitly points out significant differences in the complexing and thermodynamic behaviour towards An(III) and Ln(III) under comparable conditions, which are relevant to the actual extraction chemistry. These differences are the driving force for the selectivity observed in liquid-liquid extraction.

The results are of importance for a clear-cut understanding of the selectivity on a molecular level. The present study confirms that BTBP and BTP maintain their selectivity in both organic and aqueous monophasic conditions. Also, the complexes that form in aqueous solution are identical to those found in organic solution. This is a very important aspect concerning the development of innovative SANEX processes.

$CyMe_4$-BTBP mass transfer kinetics

Introduction

Extraction of Am(III) into $CyMe_4$-BTBP dissolved in 1-octanol is rather slow but can be accelerated by addition of DMDOHEMA or TODGA (extractants used in the DIAMEX process), as shown in qualitative kinetic tests [4]. DMDOHEMA or TODGA are assumed to act as phase transfer catalyst. Besides, their addition results in the formation of smaller droplets, which also accelerates mass transfer kinetics. To identify a possible phase transfer catalytic action, we perform kinetic investigations in a constant-interfacial stirred cell [10, 11] which allows to clearly discriminate hydrodynamic and kinetic contributions.

We measure Am(III) extraction rates as a function of $CyMe_4$-BTBP, TODGA, and NO_3^- concentrations, and interfacial area.

Results

Extraction rates are determined from the slope of $\log[Am(III)]_{aq}$ vs. t (see Figure 4). The low extraction rates (< 10^{-6} m/s) mean that mass transfer is controlled by the chemical reaction; diffusive resistance is negligible. Hence, all experiments are performed at a constant stirring speed (300/min).

With an organic phase consisting of $CyMe_4$-BTBP in 1-octanol, Am(III) extraction rate increases first order both with $CyMe_4$-BTBP concentration (see Figure 5) and with the interfacial area. Nitrate concentration has a small effect.

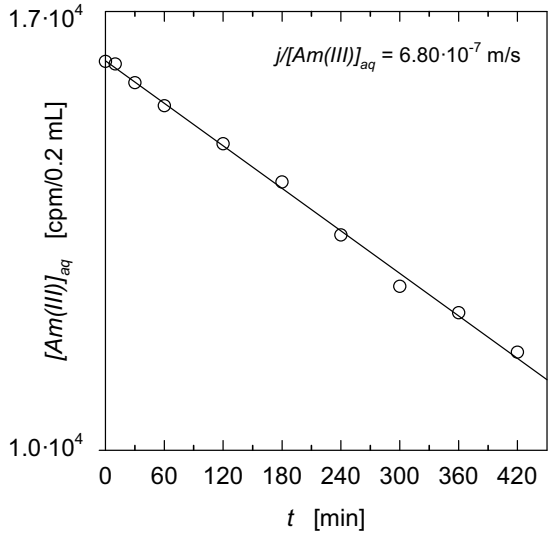

Fig. 4: *Typical result from a stirred cell experiment. 20 mmol/L $CyMe_4$-BTBP + 10 mmol/L TODGA in 1-octanol; Am(III) in 1 mol/L HNO_3; 300/min; 20 °C.*

TODGA has a positive effect on kinetics; e.g., Am(III) extraction rate increases by approx. one order of magnitude when 5 mM TODGA is added to the organic phase. With an organic phase consisting of $CyMe_4$-BTBP + TODGA in 1-octanol, Am(III) extraction rate is practically independent of $CyMe_4$-BTBP concentration. However, Am(III) extraction rate increases first order both with TODGA concentration (see Figure 6) and with the interfacial area.

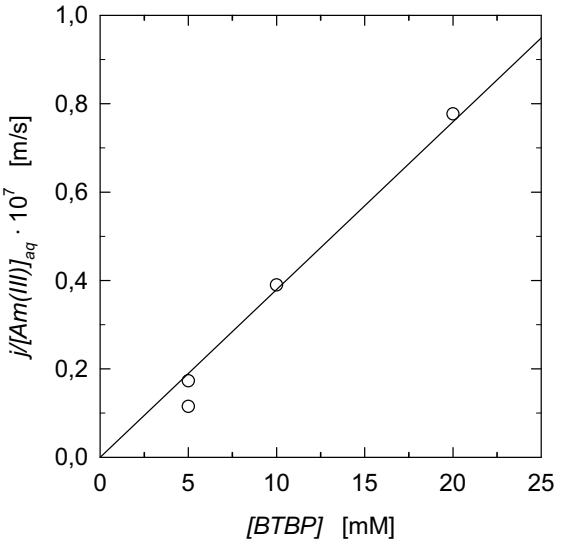

Fig. 5: *Am(III) extraction rate as a function of $CyMe_4$-BTBP concentration. $CyMe_4$-BTBP in 1-octanol; Am(III) in 1 mol/L HNO_3; 300/min; 20 °C.*

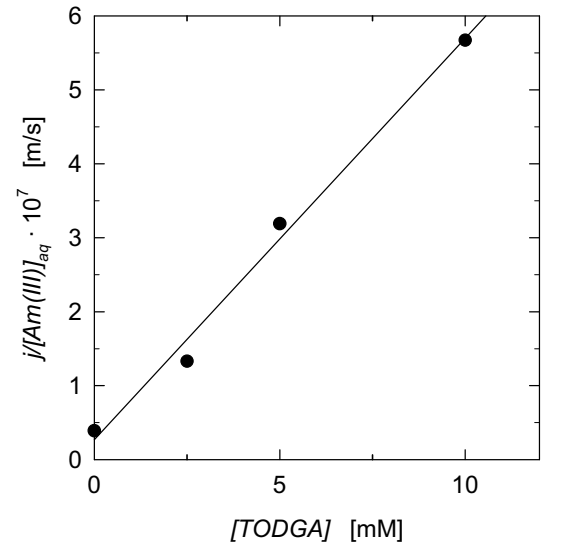

Fig. 6: *Am(III) extraction rate as a function of TODGA concentration. 10 mmol/L $CyMe_4$-BTBP + TODGA in 1-octanol; Am(III) in 1 mol/L HNO_3; 300/min; 20 °C.*

Conclusions

From the results it is concluded that mass transfer in the system Am(III) – NO_3^- / $CyMe_4$-BTBP (– TODGA) – 1-octanol is controlled by the rate of the chemical reaction; this reaction is located at the liquid-liquid interface. Extraction rate increases first order with BTBP

concentration in the absence of TODGA. With TODGA, extraction rate is practically independent of BTBP concentration but increases first order with TODGA concentration. This means that TODGA participates in the rate determining step and actually acts as a phase transfer catalyst (the small concentrations used do not influence the extraction equilibrium).

Further studies on the kinetics of back extraction and on the influence of the diluent on extraction rate are in progress.

Improved BTP

Introduction

A new BTP extracting agent was synthesized and tested. This compound, CA-BTP [12] (Fig. 6), has improved properties compared to $CyMe_4$-BTBP, the current SANEX reference extracting agent [4].

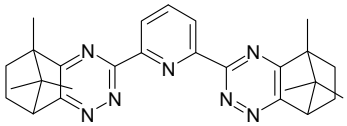

Fig. 6: *CA-BTP (bis-2,6-(5,6,7,8-tetrahydro-5,9,9-trimethyl-5,8-methano-1,2,4-benzotriazin-3-yl)-pyridine).*

Results

CA-BTP dissolved in 1-octanol extracts Am(III) from HNO_3 with a separation factor over Eu(III) of approx. 70; back extraction is possible at low HNO_3 concentration (see Fig. 7). Similar to $CyMe_4$-BTBP, CA-BTP is stable versus nitric acid. However, CA-BTP has better properties than $CyMe_4$-BTBP with respect to solubility and kinetics: Whereas in 1-octanol $CyMe_4$-BTBP has a solubility of only 10 mmol/L, CA-BTP's solubility is higher than 0.2 mol/L. Also, CA-BTP has substantially faster extraction kinetics, requiring no phase transfer catalyst as does $CyMe_4$-BTBP (see "$CyMe_4$-BTBP mass transfer kinetics").

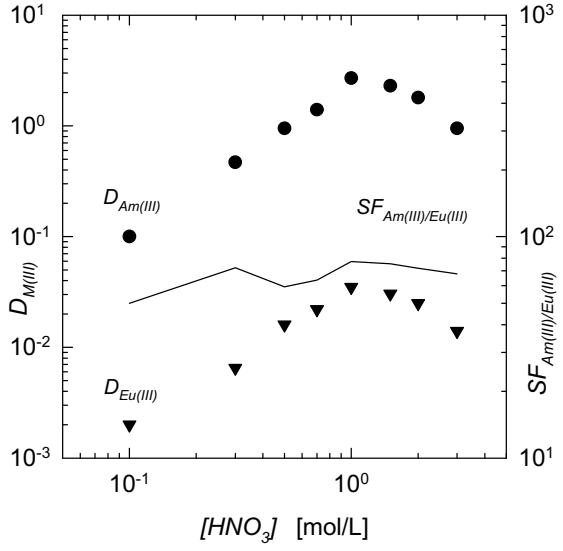

Fig. 7: *Extraction of Am(III) and Eu(III) from HNO_3 into 50 mmol/L CA-BTP in 1-octanol. Distribution ratios and separation factor as a function of initial HNO_3 concentration. T = 20 °C.*

Conclusion

CA-BTP has good stability, high solubility, and reasonably fast extraction kinetics, making it a promising candidate for SANEX process development.

References

[1] J. Magill, V. Berthou, D. Haas, J. Galy, R. Schenkel, H.-W. Wiese, G. Heusener, J. Thommasi, G. Youinou, Nucl. Energy 42 (5), 263–277 (2003).

[2] Z. Kolarik, U. Müllich, F. Gassner, Solvent Extr. Ion Exch. 17, 1150–1170 (1999).

[3] M. R. S. Foreman, M. J. Hudson, A. Geist, C. Madic, M. Weigl, Solvent Extr. Ion Exch 23, 645–662 (2005).

[4] A. Geist, C. Hill, G. Modolo, M. R. S. Foreman, M. Weigl, K. Gompper, M. J. Hudson, C. Madic, Solvent Extr. Ion Exch. 24, 463–483 (2006).

[5] D. Magnusson, B. Christiansen, M. R. S. Foreman, A. Geist, J.-P. Glatz, R. Malmbeck, G. Modolo, D. Serrano-Purroy, C. Sorel, Solvent Extr. Ion Exch. 27, 97–106 (2009).

[6] M. A. Denecke, A. Rossberg, P. J. Panak, M. Weigl, B. Schimmelpfennig, A. Geist, Inorg. Chem. 44, 8418–8425 (2005).

[7] M. A. Denecke, P. J. Panak, F. Burdet, M. Weigl, A. Geist, R. Klenze, M. Mazzanti, K. Gompper., C. R. Chimie 10, 872–882 (2007).

[8] S. Trumm, P. J. Panak, A. Geist, T. Fanghänel, Eur. J. Inorg. Chem. (submitted).

[9] S. Trumm, G. Lieser, M. R. S. Foreman, P. J. Panak, A. Geist, T. Fanghänel, Dalton Trans. 39, 923–929 (2010).

[10] M. Weigl, A. Geist, K. Gompper, J. I. Kim, Solvent Extr. Ion Exch. 19, 215–229 (2001).

[11] M. Weigl, A. Geist, U. Müllich, K. Gompper, Solvent Extr. Ion Exch. 24, 845–860 (2006).

[12] S. Trumm, A. Geist, P. J. Panak, T. Fanghänel, Verbesserte alkylierte Bis-triazinylpyridine und -bipyridine zur Actiniden-abtrennung. Eur. Pat. Application 10157567.8 (24.3.2010)

8. Vitrification of High-Level Radioactive Liquid Waste

H. Braun, W. Grünewald, K. Hardock, J. Knobloch, K. Meyer, G. Roth, A. Salimi, W. Tobie, S. Weisenburger, U. Weiler, K.-H. Weiß, M. Böttle, F. Geyer, A. Görtzen, K. Gompper, S. Heck, A. Kaufmann, T. Kisely, M. Lagos, M. Plaschke, A. Seither, C. Walschburger

8.1 VEK Project

In February 2009 the second operational license was granted clearing the way for start-up of hot vitrification operation. Whereas the first license was restricted to nonradioactive activities the second operational license is attributed to the management of radioactive materials inside the plant. It covers administrative measures dealing with the organisation and management of the plant operation as well as technical measures including the preparation of the plant for radioactive use, performance of a final cold test, its hot commissioning and finally the radioactive vitrification operation. The steps of execution of the second operation license have been accompanied and supervised by the licensing authorities and their experts.

Preparation of VEK for radioactive operation

As an essential step after release of the radioactive operational license, a second nonradioactive vitrification test was performed from April to May 2009. It served as final training of the operators prior to processing of radioactive material in the plant. Goal of this second nonradioactive test operation using HLLW simulate has been the performance of the integral plant operation within the scope of the radioactive operational license, i. e. under the conditions and in compliance with the rules of the regulatory body by application of the operational manuals established for radioactive operation. That also included that eventually necessary maintenance steps had to be carried out by consequently using the available remote handling installations of the radioactive process cells. During the test operation of about 4 weeks 5 m^3 of HLLW simulate were converted to almost 4 metric tons of waste glass poured into 10 canisters of the European standard type (capacity 400 kg). As already applied in the first cold test operation in 2007 the HLLW simulate used did not contain any noble metals constituents to avoid any problems arising during the idling phase between end of the test run and start-up of radioactive operation.

The complete operation had passed successfully without even minor problems. Table 1 contains some main production data of the test. For completeness of the cold testing of VEK the data of the first cold test operation are also indicated. Parallel to the performance of the second nonradioactive test, all steps were taken to prepare the plant for final start-up of radioactive vitrification. This included administrative measures like the installation of control and safety areas and the establishment of the operational organization and plant management. Technical measures included the removal of several provisions that had been installed to allow the nonradioactive testing of the plant operation. Piping connection of the plant exhaust line to the central stack as well as of the transfer lines to the storage tanks were set up. Other pipe connections to be made concerned the sampling delivery line to the hot lab and the chemicals and steam supply. Subsequently transfer checks between VEK and the storage area were performed in both directions to check the transfer systems.

Tab. 1: *Main production data of the cold test operation of VEK*

Parameter	Cold test II	Cold test I
Time	April / May 2009	April – July 2007
Simulate	5 m^3	16,9 m^3
Glass product	3,8 tons	12,7 tons
Glass pourings	38	127
Canisters	10	32
Operation time	23 days	78 days

Hot test operation

Preceding the start-up of the routine vitrification operation a one week test operation with a reduced level of radioactivity was conducted in September 2009. For this test a mix of HLLW simulate and a small portion of genuine HLLW was prepared. The activity of this diluted waste solution was in the range of 1.5E11 Bq/l. During this operation period three glass canisters were produced. The production data are given in Table 2. Main purpose of the radioactive test was to check the radiometric measurement equipment, to obtain information about the radioactive status of the plant during and after the test and to perform steps of a dose rate measurement program based on the radioactive inventory of the glass canisters. Fig. 1 shows the calculated radioactive inventory of the canisters produced during the

Tab. 2: *Main Data of hot test operation*

Parameter	Hot test
Period	Sept. 4-12, 2009
Simulate/HLLW	1,7 m^3
Spec. Radioactivity	Approx.1.5•10^{11} Bq/l
Glass product	1,2 tons
Glass pourings	12
Number of canisters	3
Operation time	8 days

hot test.

All systems were found to work well. The positive results obtained from this test enabled entering the routine HLLW vitrification operation without further measures.

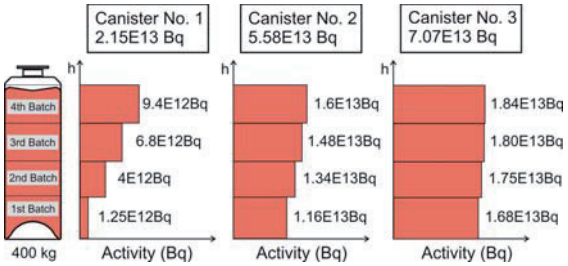

Fig. 1: *Radioactive inventory of the glass canisters from hot test*

Vitrification Operation

Start-up of processing of the stored HLLW immediately followed the radioactive test by mid of September. Alternating from one of the two storage tanks the HLLW has been transferred to VEK in batches of about 1.5 m^3, which corresponds to a weekly production. The sequence of batches is illustrated in Fig. 2 as a cumulative curve. It indicates that up to end of December 2009, 17 batches were transferred. The figure also contains the cumulative mass of waste oxides fed to the melter and the cumulative quantity of glass poured into the canisters. Corresponding to the increase of the activity in the canister of the hot test as shown in Fig. 1, Fig. 3 contains the calculated inventory of the first three canisters (numbered canister 4-6) produced with genuine HLLW during routine vitrification operation. It shows a strong increase for canister No. 4 with a distinct vertical radioactivity profile. Canister No. 6 already contains about 80 % of the inventory of a nominal canister. The nominal content of radioactivity is expected for canister 8.

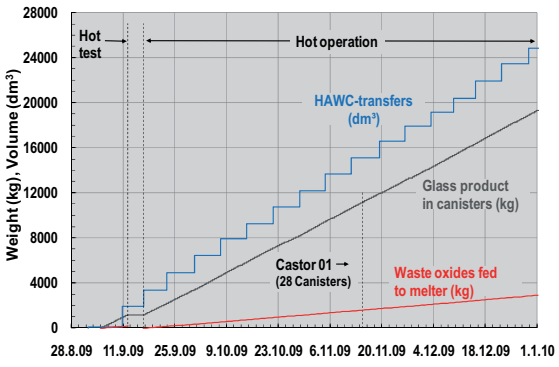

Fig. 2: *Cumulative data of HLLW batches transferred to VEK as well as of quantities of vitrified waste oxides and glass poured into canisters.*

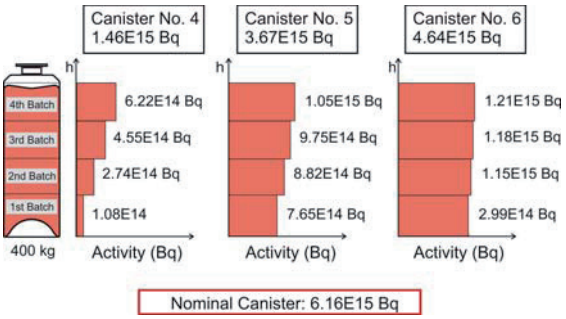

Fig. 3: *Radioactive inventory of the glass canisters No.4-6 produced with genuine HLLW*

The actual production status of VEK is compiled in Table 3 and compared with the expected total production data. During an overall operation time of maximum 18 months (net operation time 10 months) about 125 canisters with a capacity of 400 kg of waste glass each are expected be produced. As of December 31, 2009, 24 m^3 of HLLW were processed. The processed waste solution was immobilized in 19.2 metric tons of glass. The glass was poured into 48 canisters.

Tab. 3: *Actual Production Data Compared with Total Production Data*

Parameter	Actual production data*	Total production data
Production time	3.5 month	18 (10**) months
HLLW volume	24 m^3	60 m^3
Glass production	19,2 tons	50 tons
Number of canisters (400 kg)	48	125
Number of pourings	193	500
Waste glass loading	16.0 – 16.2 wt.%	16 wt.% (target)

* Reference date December 31, 2009; start-up September 16, 2009
** net processing time based on design throughput and continuous operation

Melter performance

The small-scale ceramic-lined Joule-heated melter proved to work very reliable and steady. The processing of the HLLW showed similar

behavior as the simulate. In both cases the design liquid throughput of 10 l/h could be met. The diagram shown in Fig. 4 contains information about waste loading with oxides calculated on the basis of the melter feed streams over a balance period of approximately 25 hours. The range of tolerable waste oxide loading of the glass is 13-19 wt.% with a target loading of 16 wt.%. The operational range has been set to 16±1.5 wt.%. The average loading of all produced canisters is very close to the target. The lower diagram of Fig. 4 shows the pouring batches into the canisters. Each canister requires filling by 4 batches due to the relatively small inventory of the VEK melter. Production of one canister lasts about 57 hours. All pouring operations could be well controlled with respect to pouring rate as well as to the quantity of glass poured.

A main focus of the vitrification operation concerns the behavior of the noble metals in the melting process, as the HLLW is characterized by high concentration of these elements. In total approximately 460 kg of noble metals (in terms of oxides) are contained in the HLLW solution. Noble metals cannot be incorporated in the borosilicate glass structure and form separate phases which tend to accumulate on the melter floor forming highly electrically conductive and highly viscous sediment layers. Their presence can have a strong impact on the operation of Joule-heated melters. The melter type applied by VEK has been equipped with a noble-metals design, which should avoid noble metals problems. Up to the actual status described here no indication of accumulation of noble metals in the melter could be observed. Fig. 5 shows the electrical data recorded for the power electrodes in the glass pool. It contains the electrical current, the voltage, the power and the electrical resistance calculated as ration of voltage and current. The data did not show any significant change in the electrical resistance of the glass pool which would appear in case of severe accumulation in the lower part of the melter. Also the performance of the pouring operation which is sensitive to the presence of the viscous noble metals sediments did not show any irregularities.

Problems that were encountered during vitrification operation concerned the retention of cesium in the melter and the cleaning of the off-gas pipe connecting the melter with the dust scrubber as first off-gas component. Compared to experiences from the PAMELA plant and from the long-term test runs with INE's prototype test facility PVA the retention of cesium in the melter proved to be distinctly reduced. Up to now no clear explanation can be given.

The periodic cleaning of the off-gas pipe using the air blasters showed a decreasing efficiency with increasing operation time. An inspection

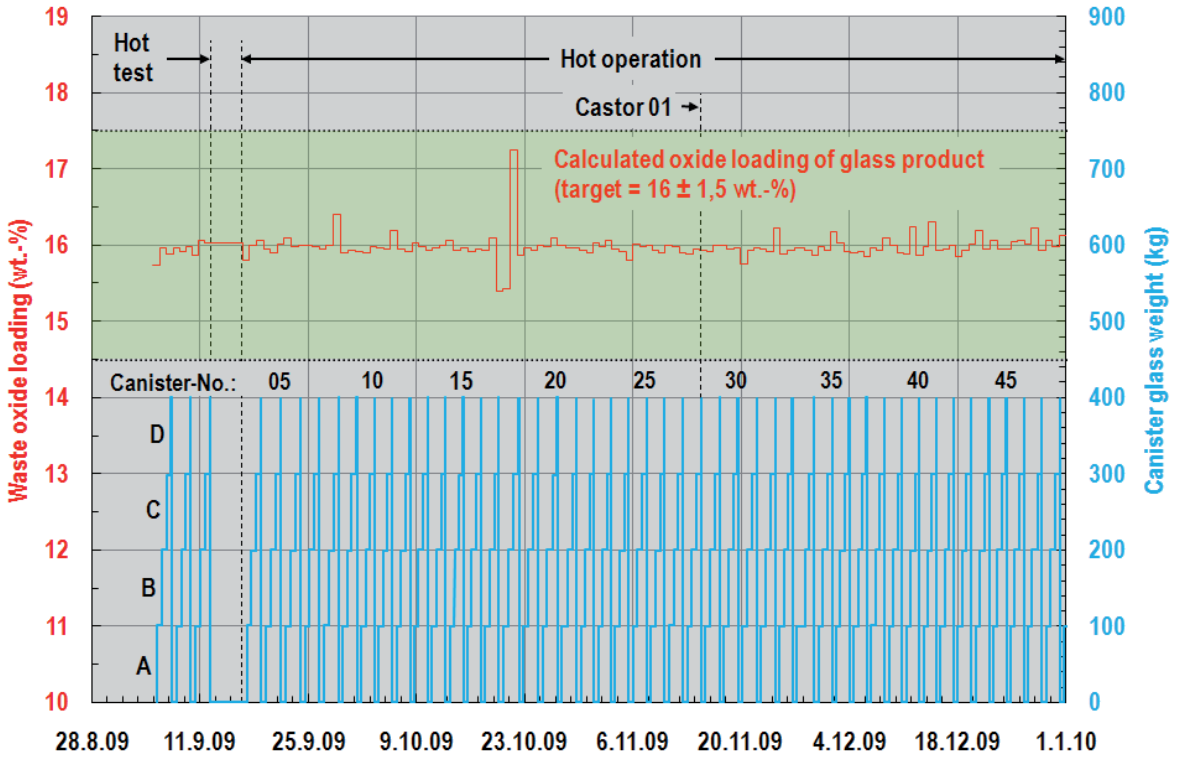

Fig. 4: *Weekly operational diagram. Upper diagram: melter feed rate. Middle diagram: calculated waste oxide loading of the glass. Lower diagram: Quantity of glass contained in canister.*

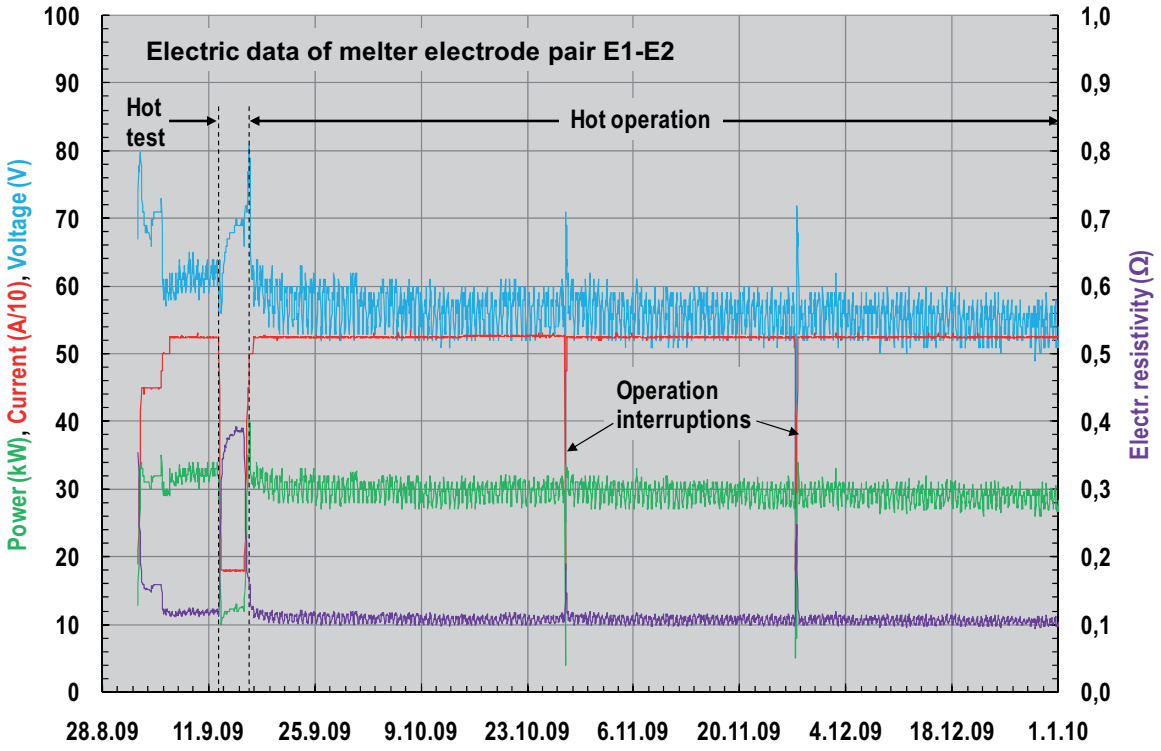

Fig. 5: *Power data and electrical resistivity of the glass melter*

inside the pipe arrangement indicated material deposit caused by melter emissions. Their properties proved to be of hard nature what makes their removal difficult. Samples were taken during inspection, but not yet analysed. It can be assumed that cesium and also technetium is present in the material. Technetium belongs to the radioactive species and is highly volatile under melting conditions.

The melter off-gas pipe assembly is designed for remote exchange. If it tends to be completely clogged it has to be replaced. However, the experiences made so far by VEK operation requires a modification of this essential component for other applications.

Canister specification

From 48 canisters already produced, each of them met well the required specification defined by a set of quality parameters established as acceptance criteria of the waste container for final disposal. The guaranteed values of some of these parameters are compiled in Table 4 and compared to those of a typical canister produced by VEK. After approval by the experts of federal office for radiation protection (BfS) the first 28 canisters were loaded into a CASTOR transport cask and shipped out of the plant, awaiting their transportation to the Interim Storage North (ZLN) near Greifswald in the northern part of Germany. In total five CASTOR casks are already on site to take the complete number of canisters produced by VEK. Fig. 6 shows the loading of a canister into the CASTOR. Fig. 7 illustrates the handling of the cask after leaving the plant.

Tab. 4: *Typical Canister Data Compared with Guaranteed Values.*

PARAMETER	GUARANTEED VALUE	CANISTER No.27
Waste oxide loading	≤ 19 wt.%	15.9 wt.%
Canister weight	< 550 kg	497 kg
Activity Sr-90/Y-90	< 4.5 E15 Bq	3.52 E15 Bq
Activity Cs-137/Ba-137	< 5.1 E15 Bq	4.33 E15 Bq
α activity	< 8.6 E13 Bq	6.07 E13 Bq
β/γ activity	< 9.6 E15 Bq	8.46 E13 Bq
Mass of U	< 7200 g	4424 g
Mass of Pu	< 210 g	135.9 g
Dose rate:		
β/γ (on surface)	< 440 Gy/h	198 Gy/h
β/γ (1m distance)	< 35 Gy/h	15.4 Gy/h
Decay heat	< 734 W	669 W

Analytical work

In the beginning of 2009 the whole procedure of sampling, sample preparation, transportation and chemical analysis of HAWC was trained under the guidelines of the VEK analysis handbook. Sampling and sample preparation

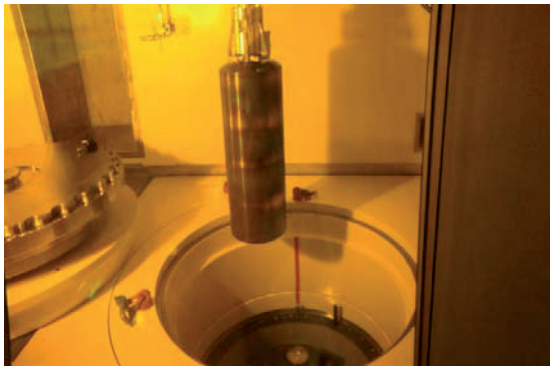

Fig. 6: *Loading of the CASTOR cask with glass canisters*

Fig. 7: *Handling of the CASTOR cask outside VEK*

(i.e., filtration and dilution) is accomplished by WAK-VEK hot laboratory and sample transport is organized by WAK-HDB. Further sample preparation, multi-element and isotope analysis and data evaluation is performed at KIT-INE. Analysis results of HAWC test samples conducted at INE were in good agreement with reference data and time schedules could always be kept. After the second part of the official approval of operation was given in February a second test operation of the VEK followed in April/May where inactive HAWC stimulant was vitrified. During this operation analytical work was carried out as scheduled for the nuclear operation. Samples from receipt tanks, wet off-gas treatment and secondary liquid waste treatment components were analyzed as specified. It turned out that the outer surfaces of sample tubes originating from VEK hot laboratory exhibited elevated radioactive contamination. Therefore, samples had to be repacked inside a glove box which was provided and equipped at INE.

Early in September the first transfer of HAWC from storage tank to receipt tank took place followed by a two-week nuclear test operation with diluted HAWC. The successful operation including analytical work gave way to the nuclear operation which is still ongoing. Until now an efficient analytical procedure including a safe sample handling and disposal could be assured.

In this regard intensive communication between the organizations involved, clear responsibilities, detailed work plans, quality control of chemical analysis and accurate documentation are indispensable.

Element and isotope analysis of HAWC is performed by inductively coupled plasma optical emission spectrometry (ICP-OES, Perkin Elmer Optima 4300) and inductively coupled plasma mass spectrometry (ICP-MS, Perkin Elmer Elan 6100). Special measuring procedures were developed for both methods. Fig. 8 for example summarizes the analysis data of receipt tank samples having a high priority with respect to data availability. As expected, the elemental composition is constant during nuclear operation.

Outlook

Based on the current results the mission of VEK can be expected to be finished according to the time schedule in mid of 2010. After processing of the HLLW solution and subsequent flushing of the components and piping network, the produced canisters will be subject to transportation to ZLN by train by five CASTOR casks for interim storage. Subsequently steps will be taken to deregulate the VEK plant and to start the decommissioning and dismantling procedure of the cells and the technical equipment. The removal of the HLLW represents another important milestone towards conversion of the WAK site to green field will be reached.

8.2 VPC Project

By end of July 2009 the contract of the VPC (Vitrification Project China) project between the Chinese organizations involved (SEPEC, CNEIC, CNNC) and the German consortium was signed. This signature was celebrated in the scope of an official ceremony in Beijing on August 14 under participation of Chinese government representatives and representatives of the German embassy. After a three months period the contract became effective on October 30, 2009.

As laid down in the contract, shortly after signing the final composition of the Chinese HLLW was delivered. There was no severe deviation from the composition that has been provided from China for the glass formulation development program. Based on this composition the glass for high sulphur incor-

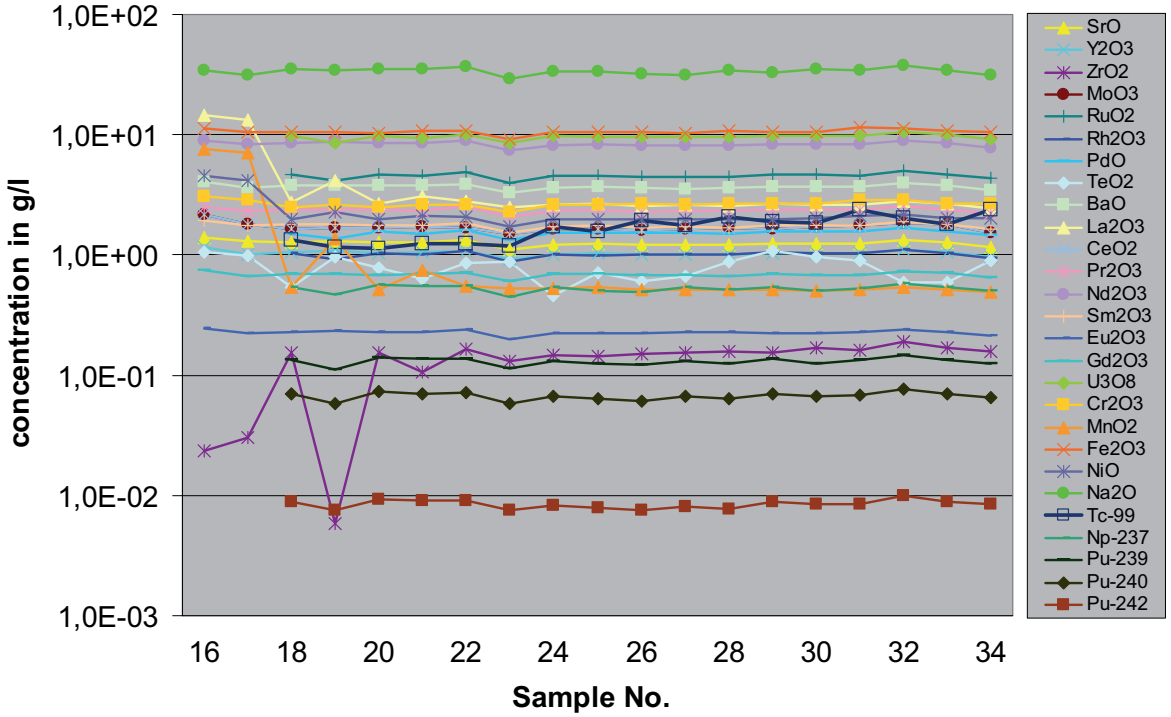

Fig. 8: *Elemental analysis of receipt tank samples (status December 2009)*

poration has been developed by INE and the required technical demonstration of the applicability had been performed in the scope of glass formulation test using INE's PVA prototype test facility.

Before start of the effectiveness German experts from all institutions participating in the project visited the location at Guang Yuan/Sichuan province for inspection of the site of the future VPC plant. This visit has been required from the German side to clarify the local conditions and constraints.

The vitrification technology of the Chinese vitrification plant will be based on the technology of KIT-INE. The application of the technology in this project by the German consortium is regulated in the scope of a licence agreement. The delivery of the licence documentation according to this agreement took place in November 2009.

References

[1] G. Roth, S. Weisenburger, J. Fleisch, M. Weishaupt, „Process technique and safety features of the German VEK vitrification plant currently under commissioning", proceeding of GLOBAL 2005, Tsukuba, Japan, Oct. 9-13, Paper No. 296 (2005).

[2] W. Grünewald, G. Roth, W. Tobie, K.H. Weiß, S. Weisenburger, "The role of the platinum group elements ruthenium, rhodium and palladium in the vitrification of radioactive high level liquid waste using Joule-heated ceramic-lined waste glass melters", Glass Tech.: Eur. J. Glass Sci. Technol. A, December 49 (6), 266-278 (2008).

[3] J. Fleisch, W. Grünewald, G. Roth, E. Schwaab, W. Tobie, M. Weishaupt, „Cold Test operation of the German VEK Vitrification Plant", Proc. WM2008 Conference, February 24-28, Phoenix, AZ, Paper No. 8326 (2008).

9. Development of actinide speciation methods

INE has continued to invest substantial effort in the development of speciation techniques for actinide speciation at a molecular scale and at low concentrations. The symbiosis of theoretical efforts with advanced spectroscopy at INE has continued to bring forth new insights, in 2009 one noteworthy result being elucidation of the quenching mechanism of fluorescence for hydrated CmF^{2+}. Other notable results presented in the following include increased selectivity and sensitivity for Cm speciation with TRLFS by using resonant excitation to obtain fluorescence emission lines with inherently small widths (fluorescence line narrowing, FLN), surface diffraction crystal truncation rod measurements of mineral surfaces to provide input parameters to surface complexation models, TEM characterization of radioactive material only recently possible at INE and application of theoretically calculated orbital energies to support peak assignment in interpretation of XPS data spectra.

9.1. Instrumental Development at the INE-Beamline for Actinide Research

K. Dardenne, M. A. Denecke, F. Heberling, J. Rothe, T. Vitova, B. Brendebach

Introduction

Synchrotron radiation techniques contribute to a large number of projects within INE's R&D program on basic and applied actinide research. The major part of these studies is carried out at the INE-Beamline for actinide research [1] at the synchrotron source ANKA (KIT North Campus). Access to INE-Beamline instrumentation is provided for INE internal use and within the framework of ANKA's peer review proposal system [2]. Besides supporting users at planning, conducting and evaluating experiments, INE-Beamline staff strives at continually improving and extending the instrumental capabilities at the beamline. Improvements are mainly driven by internal and external users' needs. In addition to experiments at ANKA, INE researchers conduct various projects at external synchrotron radiation sources in Germany, Europe and the USA. Examples are given below.

Beamline user operation in 2009

The high demand for actinide speciation studies with synchrotron radiation based techniques is reflected by a total of 23 internal and external projects hosted at the INE-Beamline in 2009. INE in-house research (~30% of all available shifts) covers a broad range of topics related to safe high level radioactive waste (HAW) disposal and the reduction of HAW radiotoxicity. Studies include, e.g., the characterization of liquid-liquid extraction ligands - both from the actinide/ lanthanide (An/Ln L3-edges) and the ligand (P/S K-edges) point of view [3], sorption of actinide and lanthanide cations onto mineral phases or their interaction with humic and fulvic acids [4], Np/Pu redox speciation in the presence of Fe phases or U characterisation in corroded cement [5]. Many of these studies are presented in more detail elsewhere in this report.

External projects scheduled via the SMIS proposal system at ANKA and the cooperation between INE and Bonn University are carried out by 11 groups in 2009 (representing nearly 50% of the total available user operation time). Researchers from the following institutions conduct experiments at the INE-Beamline in 2009:

- Departament d'Enginyeria Química, ETSEIB-UPC, Barcelona, Spain
- Lomonosov Moscow State University, Chemistry Dept., Radiochemistry Div., Russia
- School of Earth & Environment, University of Leeds, England
- JRC Institute for Transuranium Elements, EU
- Institut für Kernchemie, Universität Mainz
- Natural History Museum, Department of Mineralogy and Petrology, Prague, Czech Republic
- FZD-Rossendorf, Institut für Radiochemie, Dresden
- Institut für Interdisziplinäre Isotopen-forschung, Leipzig
- Institut für Nanotechnolgie, KIT Campus Nord
- Universität Bonn, Physikalisches Institut
- Fachhochschule Niederrhein, FB Öko-trophologie

As in the past years, a significant percentage of in-house and external beamtime (~30%) is used by PhD and diploma students as part of their theses work. The long-term contractual

cooperation with Bonn University Institute of Physics (PI-Bonn) has been extended in 2009 for two years. This cooperation is not limited to students scientific investigations, it also focuses on instrumental development at the beamline (e.g., development of HRXE spectroscopy [6], cf. section below).

Beamline upgrades in 2009

Instrumental improvements at the INE-Beamline in 2009 can be classified into three major areas: 1. extension of the available energy range, 2. reduction of the beam spot size at the sample position, and 3. increase of the energy resolution. All developments adhere to the modular concept adopted for the INE-Beamline since its inauguration in 2005.

Spatially resolved measurements with a µ-focused beam

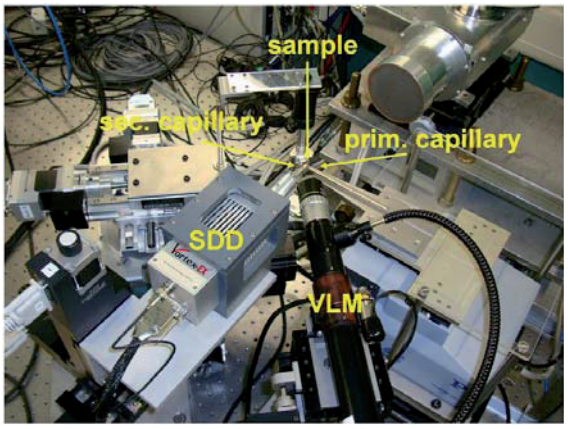

Fig. 1: *Setup for confocal measurements with a µ-focused beam.*

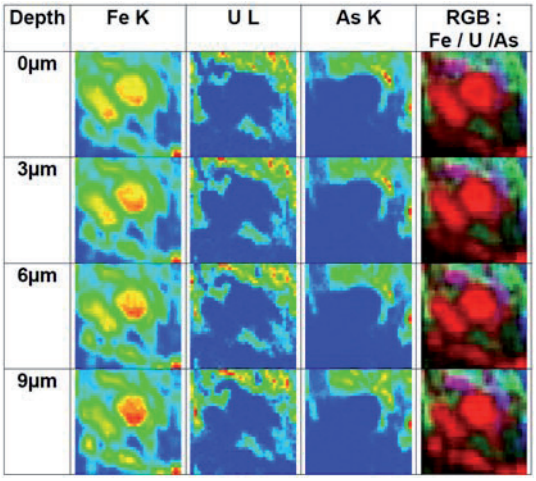

Fig. 2: *Elemental distributions for Fe, U and As from confocal µ-XRF measurements at different depths below the surface of a U-rich sediment and corresponding red-green-blue (RGB) overlay image.*

To increase horizontal beam stability as a prerequisite for spectroscopy with a micro-focused beam, a new actuator driven and computer controlled alignment system for the second crystal of the PI-Bonn built double crystal monochromator (DCM) is designed and successfully tested. This upgrade also requires a major modification of the DCM vacuum vessel in 2009. The setup for confocal µ-XAFS and µ-XRF measurements based on polycapillary half-lenses is completed by integrating a new x/y/z-stage, which allows precise positioning of the silicon drift fluorescence detector (SDD) relative to the primary focus. All components (primary capillary hexapod positioning system, sample stage, detector stage, visible light microscope) are integrated and tested (Fig. 1). First measurements on a uranium rich sediment are shown in Fig. 2. This setup will be available for general user operation with the beginning of ANKA Call 16 (Oct. 2010 – Mar. 2011).

The microfocus option at the INE-Beamline is requested for external use for the first time in 2009. JRC-ITU (S. Heathman, G. Lander) conducts experiments to investigate Am-243

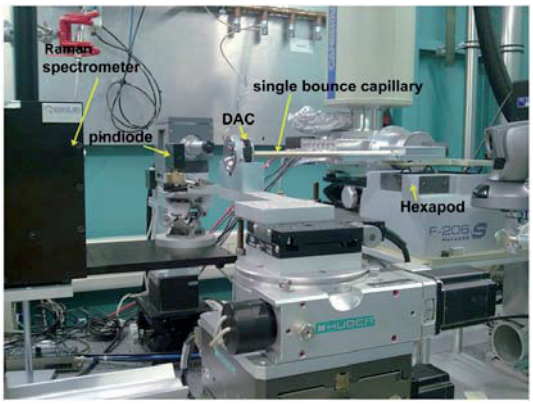

Fig. 3: *Setup for in situ studies on Am-243 metal phase transitions by µ-XAFS and µ-diffraction. The autoradiography film for detection of the XRD pattern (not shown) is positioned between the DAC and the Raman spectrometer.*

metal high pressure phase transitions in a diamond anvil cell (DAC). Structural and electronic changes are followed by combining Am L3 µ-XAFS and µ-diffraction in transmission geometry (Fig. 3). The incident beam is focused by a single bounce capillary (IfG, Berlin) into the DAC aperture of ~175 µm diameter. The cell pressure is measured by a Raman spectrometer via the pressure-dependent luminescence shift of a ruby crystal.

Low energy measurements

One major advantage of the modular concept at the INE-Beamline is the possibility to easily switch between setups for different energy ranges. The low energy limit is extended to routinely allow XAFS measurements down to the phosphor K edge (~2150 eV). In this energy range, X-ray attenuation in air or by windows in the beam path has to be minimized. A new set of ionization chambers (OKEN Ltd., Japan) is directly attached to the beamline exit flange and integrated with the sample chamber to form a windowless volume. Operated with He at ambient or N_2 at reduced pressure, this setup is successfully applied for S or P K-XAFS measurements in transmission

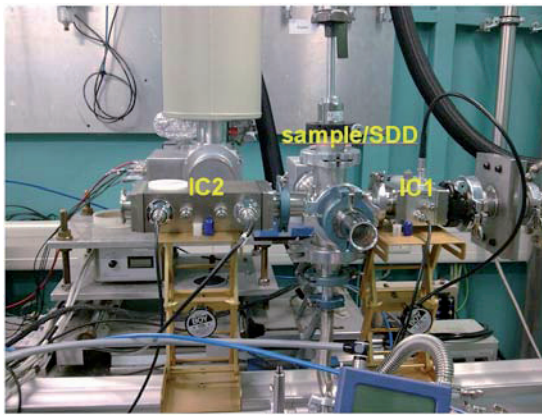

Fig. 4: *Setup for low energy measurements.*

mode (Fig. 4). Vacuum tight insertion of the SDD into the sample chamber also allows to record high quality spectra in fluorescence detection mode. Initial studies in 2009 focus on sulfur speciation in humic acids (IIF, Leipzig), interaction of bacterial phosphate proteins with uranyl (FZD, Dresden) and metal complexation effects in N-donor ligands (KIT South Campus). The low energy setup will be completed by computer controlled sample change and positioning motors, available in ANKA Call 15 (Apr.-Sept. 2010).

High-resolution X-ray emission (HRXE) spectroscopy

The most ambitious ongoing project at the INE-Beamline is the adaption and installation of a high-resolution X-ray emission (HRXE) spectrometer, offering a variety of methods based on wavelength dispersive fluorescence yield detection (cf. INE Annual Report 2008 [7]). Activities in this field in 2009 include commissioning of the spectrometer and investigations at other synchrotron sources.

The basic HRXE instrumentation for the INE-Beamline is completed in 2009. A precise heavy load hexapod positioning system for the spectrometer and a motorized sample positioning stage are integrated into the system, followed by first commissioning steps of the Andor CCD detection system. Measurements at the In Lα emission lines yield count rates increased by one order of magnitude compared to initial experiments in 2008. A demonstration of one of the spectrometer's possible applications is shown in Fig. 5 a). The spectrometer resolves the Lα and Lβ emission lines of a Z / Z+1 element mixture (Sb_2O_5 / $SnCl_2$), whereas these lines completely merge to a broad peak in the spectrum measured with a conventional solid state fluorescence detector (Fig. 5 b)). This improved energy resolution is sufficient for EXAFS measurements of element mixtures, where the presence of the Z+1 absorption edge normally limits the available k-space for measurements of the Z element. A similar spectral overlap problem circumvented by HRXE detection also exists for lanthanide / 3d transition metal mixtures (e.g., Eu / Fe).

In addition to the ongoing spectrometer development at ANKA, the potential of the new HXRE technique for studying the electronic and geometric structure of actinide (An) compounds is explored by performing experiments at external synchrotron facilities (ESRF, HASYLAB). As an example for these

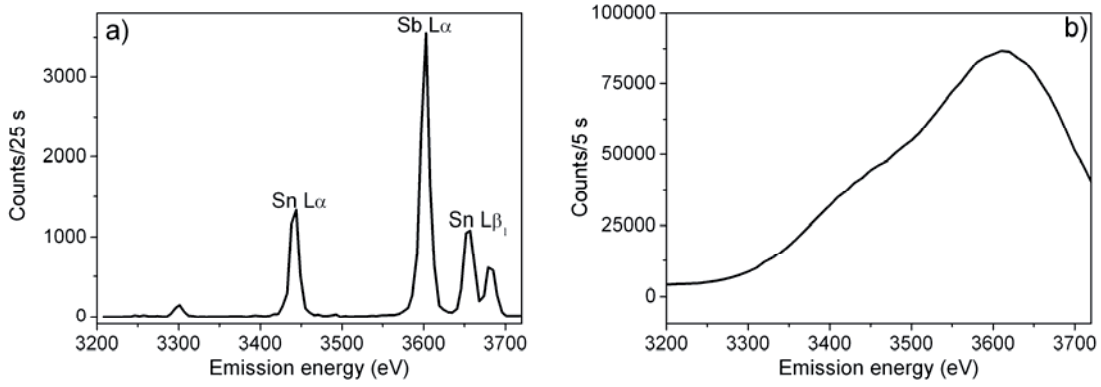

Fig. 5: *HRXE a) and conventional b) Sn and Sb emission spectra of a mixed Sb_2O_5 / $SnCl_2$ sample.*

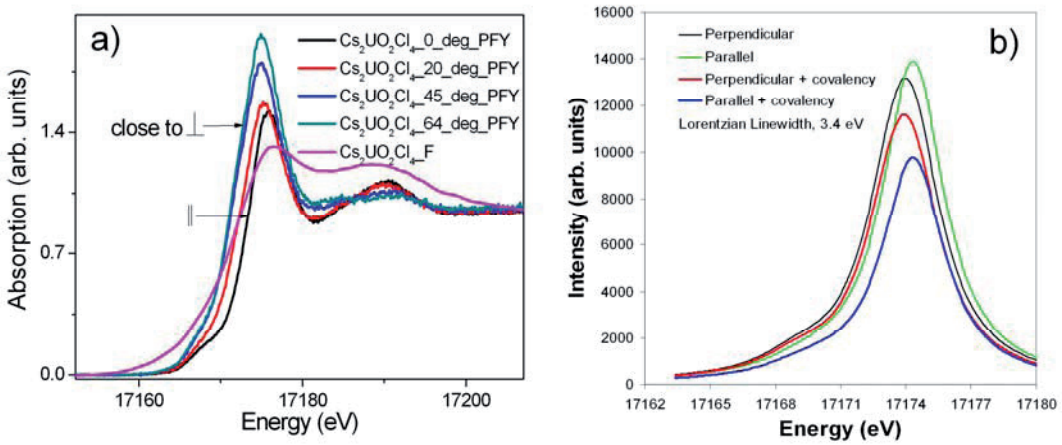

Fig. 6: *Experimental a) and theoretical b) $Cs_2UO_2Cl_4$ single crystal PD-PFY/F U L3- XANES spectra.*

external studies, polarisation dependent partial fluorescence yield (PD-PFY) U L3-XANES spectra of a $Cs_2UO_2Cl_4$ single crystal, measured at ESRF beamline ID26, are shown in Fig. 6a). All spectral features in the PD-PFY XANES are sharper and better resolved compared to the simultaneously measured conventional fluorescence XANES spectrum (labelled "$Cs_2UO_2Cl_4$_F" in Fig. 6a)). As a result, changes in the local atomic environment of the U absorbing atoms are readily detectable in the PFY-XANES spectra. Moreover, a pre-edge feature is clearly visible in all these spectra. This resonance originates from 2p transitions to U 5f states and is observed here for the first time ever in actinide L3 edge XANES spectra. The orientation between the polarisation vector (ε) of the beam and the uranyl ($[UO_2]^{2+}$) axis is varied during PD-XANES measurements, thereby enhancing transitions to certain molecular orbital states. Transitions to the U $6d_\pi$ or $6d_\delta$ orbitals dominate in the spectrum's main resonance or 'white line' (WL), when ε is parallel or perpendicular to the $[UO_2]^{2+}$ axis, respectively (Fig. 6a)). The experimental spectra are well reproduced by ADF DFT calculations performed by R. G. Denning (Oxford University), cf. Fig. 6b). Experimental and theoretical efforts lead to the following results:

1. Theory reproduces the general shape of the experimental spectra;
2. U $6d_\pi$ orbitals strongly interact with O and Cl π-orbitals and U $6d_\sigma$ orbitals with O π-orbitals;
3. The theoretical difference of 0.5 eV between absorption maxima in parallel and perpendicular orientation is comparable to the experimental value of 0.8 eV;
4. Quadropole 5f transition intensity relative to the 6d dipole transition is well reproduced;
5. Theoretical separation between 5f and 6d absorption peaks (5.2 eV) differs slightly from the experimental separation (7 eV);

HRXE spectroscopy provides well-resolved data, which can be used to refine theory for calculating transition intensities to An 5f and 6d orbitals and their energies. This experimental technique can unambiguously help us to gain new general insight into An electronic structures.

CTR measurements on the calcite(104)-water interface structure at the APS

Surface diffraction measurements are performed at the GeoSoilEnviroCARS undulator beamline, 13IDC, at the Advanced Photon Source (APS) in Argonne, USA, to characterize the 3D interface structure between the calcite(104)-face and solutions of various composition.

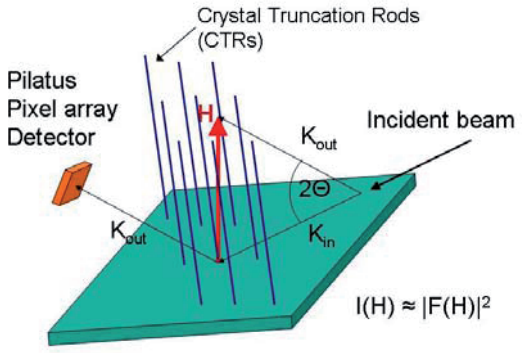

Fig. 7: *Sketch showing the principle of x-ray surface diffraction measurements.*

The basic principle of surface diffraction measurements is illustrated in the sketch in Fig. 7. The orientation of the sample (green cuboid) and the position of the detector define the scattering geometry. Momentum transfer,

H, is the difference between the outgoing and the incoming wavevector, $\mathbf{H} = \mathbf{K}_{out} - \mathbf{K}_{in}$.

Rods of intensity perpendicular to the crystal surface (indicated by blue lines in Fig. 7), so called Crystal Truncation Rods (CTRs) carry the information about the atomic structure of the interface between crystal surface and solution. The Intensity measured at each point, **H**, is proportional to the square modulus of the Structure Factor, F(**H**). F(**H**) is the sum of the Structure Factor of the semi infinite bulk crystal, $F_{bulk}(\mathbf{H})$, and the surface Structure Factor, $F_{surf}(\mathbf{H})$:

$F(\mathbf{H}) = F_{bulk}(\mathbf{H}) + F_{surf}(\mathbf{H})$.

A least square fitting routine is used to refine structural parameters: x,y,z-coordinates, Debye-Waller factors, and site occupancy of all surface atoms from the measured intensities.

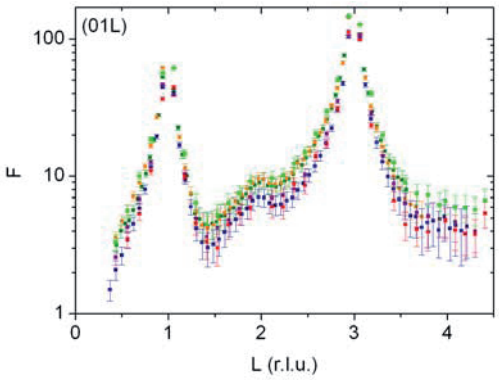

Fig. 8: *Data measured on the (01L) CTR at all six solution conditions (1 ■ , 2 ■ , 3 ■ , 4 ■ , 5 ■ , 6 ■).*

The composition of the contact solution is chosen according to the results of zetapotential measurements presented in the Annual Report 2008 [8]. The idea behind this investigation is to ascertain if changes in the solution composition that cause changes in the zetapotential are accompanied by changes in the interface structure. Six solution compositions are investigated - four equilibrium and two non-equilibrium solutions:

1. equilibrium, air-water-calcite-NaOH 0.002 mol/L, expected pH: 8.6, expected zetapotential: ~0 mV.
2. equilibrium, air-water-calcite-NaOH 0.003 mol/L - NaCl 0.097 mol/L, expected pH: 8.6, expected zetapotential: ~0 mV.
3. equilibrium, air-water-calcite-NaCl 0.03 mol/L - HCl 0.07 mol/L, expected pH: 7.5, expected zetapotential: ~9 mV.
4. equilibrium, CO_2-water-calcite-NaCl 0.03 mol/L - HCl 0.07 mol/L, expected pH: 5.8, expected zetapotential: ~12 mV.
5. non-equilibrium, NaOH 0.001 mol/L – $CaCl_2$ 0.01 mol/L – NaCl 0.01 mol/L , expected pH: 10.9, expected zetapotential: ~8 mV.
6. non-equilibrium, NaOH 0.0005 mol/L – Na_2CO_3 0.01 mol/L – NaCl 0.01 mol/L , expected pH: 11.1, expected zetapotential: ~ -25 mV.

Equilibrium solutions are pre-equilibrated by percolating a calcite suspension of desired composition with the corresponding gas phase until the expected pH, calculated with PhreeqC [9] and the Nagra/PSI thermodynamic database [10], is reached.

At each solution condition a set of nine CTRs is measured. Measurements are performed in situ through a thin film of solution covered by a Kapton membrane. A pseudo orthogonal unit cell is used, defined in a way such that the vector perpendicular to the calcite(104)-face becomes the (001) vector. The 00L CTR (the specular rod) is measured in a specular geometry. For the measurement of the non-specular CTRs the angle between the incident X-rays and the surface is fixed at 2°.

An example for surface diffraction data measured on the (01L) CTR at the six contact solution compositions described above is shown in Fig. 8. Plotted is the modulus of the Structure Factor, F, versus L, the component of the momentum transfer perpendicular to the crystal surface (in reciprocal length units (r.l.u.)). It is remarkable that hardly any difference is observable between the six datasets. The same is true for the other CTRs measured. The interface structure is refined for all datasets separately. Fig. 9 shows exemplarily the (21L) rod measured in contact with solution 1 and the corresponding model calculation.

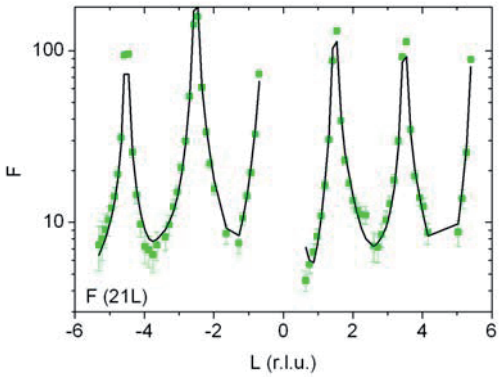

Fig. 9: *Exemplary CTR fit for the (21L) rod measured under solution 1. (data: ■, model: —).*

From the data analyses we obtain the 3D atomic structure of the mineral solution interface at all six solution compositions. The analysis of the data yields a number of important results. In the depth range of the

calcite(104)–water interface, where surface diffraction measurements are mainly sensitive, structures do not change significantly, even upon the investigated extreme changes in the composition of the contact solutions. In addition, we observe no indication for calcium or carbonate inner-sphere complexes at the flat calcite(104)-face. The water above the calcite surface is well ordered, arranged in layers. Water molecules of the first layer, 2.35 ± 0.05 Á above the surface, are associated with the surface calcium ions. Those of the second layer, 3.24 ± 0.06 Á above the surface, are located above the surface carbonate ions. The surface ions are found to relax only slightly from their bulk positions. The most significant relaxation, observed throughout all datasets, is a ~4° tilt of the surface carbonate ions towards the surface.

Outlook for 2010

The following list the major portion of instrumental developments and scientific projects at the INE-Beamline planned for 2010:

- Replacement of the beamline control and safety system ('RST-System') by a Siemens-SPS based system - necessary to maintain compatibility with the new ANKA standard (cooperation with ISS-IT).
- Completion of commissioning of all optimized HRXE spectrometer components including the analyzer crystal bender unit (cooperation with PI-Bonn).
- First external HRXE user project to study the PuO_2 / water interaction (cooperation with S. Butorin, Uppsala University).
- Combination of Pu L3-XAFS and UV-Vis spectroscopy for the in situ investigation of Pu polymer formation (cooperation with C. Walther et al.).
- Am L3 XAFS investigation of the aqueous Am-243 speciation at elevated temperatures using an optimized high-T sample cell (cooperation with A. Skerencak et al.)

Acknowledgement

Cooperation with KIT-ISS, especially S. Mangold (ANKA-XAS) and T. Spangenberg (ISS-IT group) for hardware and software implementation at the INE-Beamline, is gratefully acknowledged. Part of the INE-Beamline development is a contractual cooperation between KIT-INE and PI-Bonn. Many thanks to H. Blank (PI-Bonn), A. Neumann and V. Krepper (INE) for technical support.

References

[1] K. Dardenne, B. Brendebach, M. A. Denecke, J. Rothe, T. Vitova, Journal of Physics, Conference Series, 190, 012037 (2009).

[2] http://ankaweb.fzk.de/

[3] M. Löble, T. Vitova, M. A. Denecke, F. Breher, ANKA Annual Report 2009, 147 (2009).

[4] M. Freyer, C. Walther, T. Stumpf, G. Buckau, B. Brendebach, J. Rothe, R.G. Haire, ANKA Annual Report 2009, 171 (2009).

[5] B. Kienzler, V. Metz, B. Brendebach, N. Finck, J. Lützenkirchen, M. Plaschke, T. Rabung, D. Schild, Radiochimica Acta, submitted.

[6] T. Vitova, K. Dardenne, M. A. Denecke, A. Lebid, M. Löble, J. Rothe, O.N. Batuk, J. Hormes, D. Liu, F. Breher, H. Geckeis, IOP Conference Series: Materials Science and Engineering, accepted (2010).

[7] B. Brendebach, K. Dardenne, M. A. Denecke, X. Liu, J. Rothe, T. Vitova, FZK-INE Annual Report 2008, 58 (2009).

[8] M. Schmidt, F. Heberling, N. Finck, T. Stumpf, M. Schlegel, K. Dardenne, D. Bosbach, FZK-INE Annual Report 2008, 21 (2009).

[9] D. L. Parkhurst, C. A. J. Appelo, User's guide to PhreeqC (Version 2), US Geological Survey: 326 (1999).

[10] W. Hummel, U. Berner, E. Curti, F. J. Pearson, T. Thoenen, Radiochimica Acta, 90(9-11), 805 (2002).

9.2 Laser spectroscopy

S. Büchner, R. Götz, W. Hauser, R. Klenze, P. Lindqvist-Reis, P.J. Panak, B. Schimmelpfennig, O. Schwindt, A. Skerencak, T. Stumpf, M. Trumm, C. Walther, Th. Fanghänel [1], B. Baeyens[2], M. H. Bradbury[2], M. Marques Fernandes[2]

[1] *Universität Heidelberg, Physikalisch-Chemisches Institut, Im Neuenheimer Feld 253, D-69120 Heidelberg*
[2] *Paul Scherrer Institute, Laboratory for Waste Management, 5232 Vissingen PSI, Switzerland*

New insights on the quenching mechanism of the fluorescence of the hydrated CmF^{2+} complex, studied by Density Functional Theory (DFT)

TRLFS-studies of aqueous CmF_n^{3-n} complexes have shown that all Cm(III) fluoride complexes have the same fluorescence lifetime (~ 65 µs) [1]. This is quite peculiar, since it is well known from the literature, that the fluorescence lifetime of Cm(III) is linearly correlated with the number of H_2O ligands in the first coordination sphere [2].

To investigate this phenomenon quantum chemical calculations on DFT level are performed on $[CmX(H_2O)_8]^{2+}(H_2O)_{18}$ (X = F, Cl) complexes, employing the B3-LYP functional as implemented in the TURBOMOLE program package. The structures are optimized using basis sets of TZVP quality on the water and fluoride as well as an f-in-core ECP and associated basis set on Cm(III). To assure numerical precision, the optimized structures and vibrational frequencies are obtained by employing the m5 grid in all DFT calculations. The chloro complexes are chosen for comparison as their lifetimes do not show deviant behaviour and increases linearly with the number of exchanged first shell water molecules [3]. The resulting structure, the $[CmF(H_2O)_8]^{2+}(H_2O)_{18}$ complex, is displayed in Fig. 1.

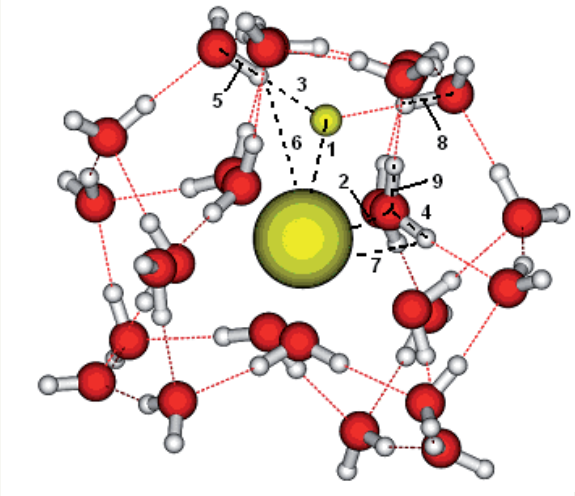

Fig. 1: *Structure of $[CmF(H_2O)_8]^{2+}(H_2O)_{18}$, optimized by Density Functional Theory (DFT).*

The bond lengths and vibrational frequencies of the two calculated complexes, according to the indices of Fig. 1, are summarized in Tab. 1. The results show, that the fluoride ion is coordinated closely to the metal centre (234 pm, Ind. 1). Because of this short distance second shell protons, which build a hydrogen bridge to the fluoride ion, also show an exceptionally short distance to the central metal cation (333 pm, Ind. 6). This matches the distance of the protons of a first-shell water molecule to Cm(III) fairly well (320 pm, Index 7).

Tab. 1: *Distances and vibrational frequencies between atom pairs of DFT optimized $[CmX(H_2O)_8]^{2+}(H_2O)_{18}$ (X = F, Cl) complexes*

		$[CmF(H_2O)_8]^{2+}(H_2O)_{18}$		$[CmCl(H_2O)_8]^{2+}(H_2O)_{18}$	
	Index[a]	*d*/pm	ν/cm^{-1}	*d*/pm	ν/cm^{-1}
M-X	1	234	374	293	168
M-OH_2	2	257	178[b]/ 181[c]	254	155[b]/ 147[c]
H···X	3	162		215	-
H-O	4 / 9	98	3564[b]/ 3558[c]	98	3475[b]/ 3467[c]
H-O	5 / 8	99	3409[b]/ 3337[c]	99	3435[b]/ 3359[c]
M···H	6	333		392	-
M-H	7	320		317	-

[a] Index acc. to Fig. 1; [b] Sym. stretch; [c] Asym. stretch

Furthermore, comparing the OH vibrational modes of OH-groups of first shell H_2O ligands and the OH-groups of second shell H_2O, which are coordinated to the fluoride ion, only little differences are observed. These results suggests, that the energy of the excited Cm(III) can be transferred to vibrational modes of two OH-bonds from second shell waters which are connected via hydrogen bonds to the fluoride ion. These modes are then capable to efficiently quench the excited state of Cm(III), similar to OH vibrational modes of first-shell water. Therefore, the fluorescence lifetime of the first excited state of Cm(III) remains unchanged upon complexation with fluoride ions. Due to the elongated bond lengths of the Cm(III)-chloride complex (see table S1) an energy transfer to second shell waters is not possible. This is in good agreement with experimental data.

Influence of laser beam characteristics and focusing optics on optical laser-induced breakdown detection

Laser-induced breakdown detection (LIBD) is a well established technique for measuring size and concentration of inorganic colloids in liquids [4]. However, most applications of LIBD are restricted to the measurement of mean sizes which is problematic in cases of wide colloid size distributions (PSD) as typically is the case in natural systems. Evaluation of PSDs from LIBD is possible but requires detailed control of the power density within the laser focus as described in [5]. Using spatial beam profile and focusing conditions as input parameters allows one to calculate the power density in the laser focus [6]. Fig. 2 shows spatial beam profiles of a single transversal mode laser, BMI soliton DIVA (left), a laser with a less well defined profile, approximated by a flat top, Continuum, Minilite, (middle) and a high power laser with slightly lower intensity in the central region, i.e. a donut-like shape, Continuum Surelite (right).

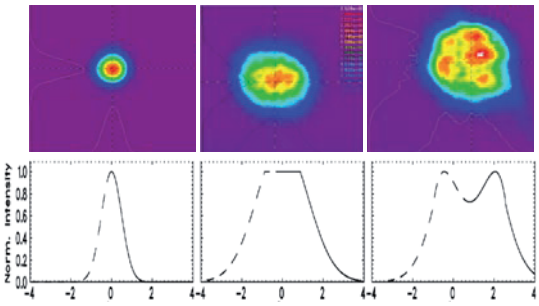

Fig. 2: *Beam profiles of a BMI Soliton DIVA (left), a Continuum Minilite, (center) and a Continuum Surelite (right). The profiles used for the simulation are depicted below.*

The approximated profiles (Fig.2 bottom) are used to calculate the power density distribution of the three laser setups. In the following, the simulations are compared to measured distributions of breakdown events obtained as described in [7].

In the case of the TEM_{00} profile (DIVA laser), the right wing of the distribution, `down stream' along the laser beam, resembles closely an aberration free focused ideal Gaussian profile (Fig.3), whereas the intensity distribution is strongly altered at the left wing, closer to the focusing optics (Airy rings). The lower part of Fig. 3 depicts the breakdown distributions for four different samples. While the breakdown

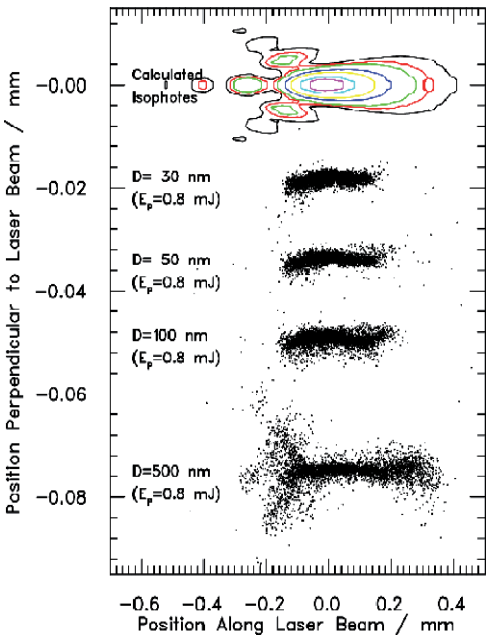

Fig. 3: *Regions of equal power density for the typical beam profile of a Diva (Gaussian) focused by a plano-convex spherical lens (f=+60mm, diameter 25mm) and measured BD distributions for various sizes of polystyrene particles at constant pulse energy.*

events initiated by 30 nm sized colloids populate the central region, 50 nm, 100 nm and 500 nm colloids ignite breakdown events at systematically decreasing intensity and mimic the contour plot very well (bottom).

An analogous comparison is shown in Fig. 4 for the mobile LIBD system [8] comprising a Continuum Minilite laser. The breakdown distributions for 400 nm and 800 nm colloids, respectively, agree well with the modeled contour plot (e.g. red line), including even minor asymmetries such as visible in the case of the 400 nm sample. That the two left hand wings of the calculated intensity distribution are not resolved in the experimental breakdown distribution is due to the fact that a 2-dimensional perspective view through the focal region is recorded by the CCD camera, whereas the distribution must be imagined as a 3-dimensional object, given by rotating the intensity contour plot along the laser beam axis.

A Gaussian fit to the data (uppermost part of Fig. 4) must nevertheless be interpreted carefully, since in the outer focal region the profile (solid line) exceeds the Gaussian fit (dashed line) which might erroneously be attributed to the presence of a small fraction of large particles with bigger ignition length.

Summarizing, both setups are very well suited for optical particle size measurements. The Minilite system combines a high degree of

robustness with a large effective focal volume and an intensity distribution which can be fitted

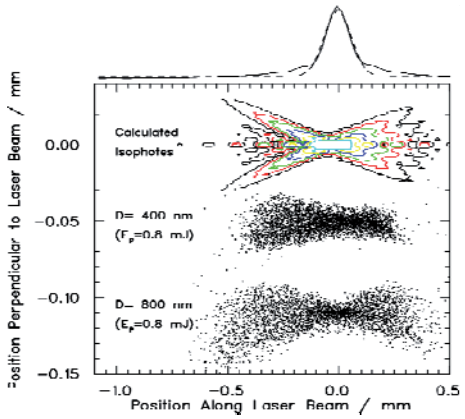

Fig. 4: *Regions of equal power density for the typical beam profile of a Continuum Minilite focused by a bi-convex lens (f=+8 mm, diameter 6 mm). and measured BD distribution for 400 nm and 800 nm polystyrene particles at constant pulse energy.*

empirically by use of simple analytical expressions. The Diva system, due to its TEM_{00} mode of operation and very low pulse to pulse fluctuations is well suited for precise PSD measurements but must be operated in an air conditionned laboratory. Modeling of the third setup used for LIBD (Continuum Surelite, not shown) confirmed the observed very strong deviations from the optimum profile and – along with the strong pulse to pulse fluctuations – rendered this system unsuited for PSD measurements.

Fluorescence line narrowing of ternary Cm(III) carbonate surface complexes

Introduction

Aqueous complexes of trivalent actinide ions such as Cm(III) have been studied recently at INE as molecular species, adsorbed onto mineral surfaces or incorporated into dielectric hosts [9]. The favourable luminescence properties of Cm(III)) enables ultrasensitive and selective speciation, as well as the characterization of the first hydration shell and of the vibrations of the coordinated ligands and solvent. Resonant excitation of the lowest emitting state ($^6D_{7/2}$ <- $^8S_{7/2}$) at cryogenic temperatures provides often highly resolved excitation and emission spectra showing the groundstate splitting on the order of several wavenumbers. However, for some systems such as calcite [10] and CSH-phases [11] only broad Cm(III) spectra were observed. The method of fluorescence line narrowing (FLN) has been applied for Cm(III) and Cm(IV) on inhomogeneous matrices such as glasses [12] or radiation damaged samples [13] to resolve the broad bands generated by UV excitation or at high temperatures. Recently we studied the adsorption of Cm(III) onto γ-Al_2O_3, kaolinite and smectite, in the presence and absence of carbonate, at neutral pH [14]. We observed FLN in all the systems studied at extremely low Cm(III) concentration of ~10^{-7} M in solution. As the spectroscopic results are rather similar for the mineral phases, the discussion is restricted to γ-Al_2O_3. Chemical and spectroscopic details are found elsewhere [14].

Results and discussion

TRLFS measurements were carried out at 17K on a γ-Al_2O_3 wet paste (BET 119 m^2/g) loaded with $1.25 \cdot 10^{-7}$ M Cm(III) and 20 mM $NaHCO_3$ at pH~8.4. Excitation and emission spectra, as well as lifetimes, were recorded by broadband (396.6 nm) and resonant excitation (596-622 nm). Using resonant excitation of the lowest crystal-field level (A_1) of the first excited multiplet $^6D_{7/2}$, the Cm-species exhibit sharp emission peak on a broad background. Correlated with the excitation wavelength, this peak moves and the broadband emission changes in a way characteristic for fluorescence line narrowing [15]. In Fig. 5 the resonant emission is shown, scanning the laser frequency in 1 nm steps from 596 to 622 nm. The resonant emission peaks in these experiments are usually homogenously broadened resulting in extreme sharp bands [15]. However, due to the low Cm concentration,

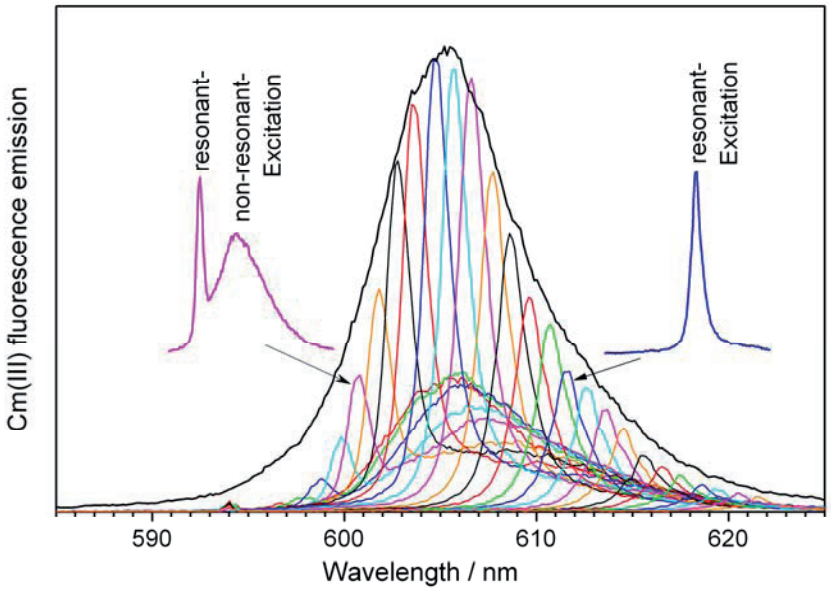

Fig. 5: *Fluorescent line narrowed emission spectra of the ternary Cm(III) complex at the γ-Al_2O_3 surface with carbonate. The laser is scanned in 1 nm steps from 596 to 622 nm. The line-width of 1 nm is given by the instrumentation settings. Characteristic for FLN are the (relatively) sharp resonant emission peaks correlated with the excitation wavelength and the non-resonant broad background at the low energy side. The insets show typical low and high energy spectra. The shown envelope curve corresponds to the non-resonant broadband excitation.*

we had to increase the polychromator slit-width to about 1 nm bandwidth. The envelope of integrated individual emission spectra compares largely with the non-resonant/ broadband emission.

In the absence of carbonate the luminescence decay using resonant excitation shows a mono-exponential decay with a lifetime of 107±2 µs (see Fig. 6). This corresponds to five water molecules in the first Cm coordination shell, which is in good agreement with literature data at room temperature. In the presence of carbonate, however, a multi-exponential decay is observed. This can be fit by two decay rates with 138±3 and 418±10 µs corresponding to four and one water, respectively. This may be assigned to the additional formation of ternary Cm-Al_2O_3-CO_3^{2-} surface complexes. As to be expected, the ternary complex should have nearly lost its complete first hydration shell.

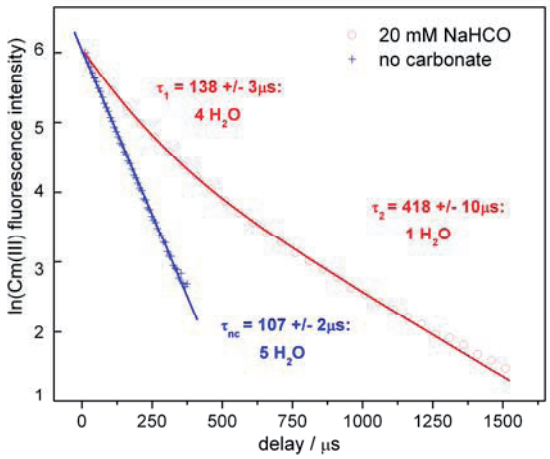

Fig. 6: *Emission decay of the Cm(III) sorbed onto γ-Al_2O_3 in the absence and presence of carbonate.*

The bi-exponential decay is in agreement with the presence of a mixture of ternary Cm species. However the bi-exponential decay can be ascribed as well by spectral diffusion, which is frequently found in FLN systems. The fast process is caused by resonant energy transfer between equal subsites (exciton hopping) until the exciton is trapped by an appropriate defect. Other excitons may release stepwise energy by a phonon assisted process and contribute to non-resonant population of low energy sites. The spectroscopic differences in the absence and presence of carbonate are explained by the faster decay rate for the former complex species.

Conclusions

We observe FLN at extreme low Cm concentrations (in solution 1.25×10^{-7} M), whereas the usual concentrations in FLN experiments are in the mM range. The average Cm-Cm distance for the given concentration is about 200 nm, which is far beyond the critical Förster radius. By Cm sorption on colloidal γ-Al_2O_3 pre-concentration will reduce the Cm-Cm distance to about 50 nm, which is still too large and indicates cluster formation of Cm(III) at the surface. Interesting further applications of FLN will be Cm(III)-doped Ca-carbonates and Ln-hydrates.

References

[1] W. Aas, E. Steinle, T. Fanghänel, J. I. Kim, Radiochim. Acta, 84, 85 (1999).

[2] T. Kimura, G. R. Choppin, J. Alloys Compd., 213/214, 313, (1994).

[3] M. Arisaka, T. Kimura, R. Nagaishi, Z. Yoshida, J. Alloys Compd, 408-412, 1307 (2006).

[4] L. J. Radziemski, D. A. Cremers, *Laser induced Plasmas and Applications*. Optical Engineering, ed. B.J. Thompson. 1989, Rochester: Marcel Dekker.

[5] J. I. Kim, C. Walther, *Laser-induced breakdown detection*, in *Environmental colloids and particles: Behaviour, separation and characterisation*, J. Lead and K. Wilkinson, Editors. 2007, John Wiley & Sons: West Sussex. p. 555.

[6] C. Walther, W. Hauser, Appl. Phys. B, 97, 877 (2009).

[7] T. Bundschuh, W. Hauser, J. I. Kim, R. Knopp, F. J. Scherbaum, Coll. Surf. A, 180, 285 (2001).

[8] W. Hauser, H. Geckeis, J. I. Kim, T. Fierz, Coll. Surf. A, 203, 37 (2002).

[9] N. M. Edelstein, R. Klenze, T. Fanghänel, S. Hubert, Coord. Chem. Rev., 250, 948-973 (2006).

[10] M. Marques Fernandes, T. Stumpf, T. Rabung, D. Bosbach, T. Fanghänel, Geochim. Cosmochim. Acta, 72, 464-474 (2008).

[11] T. Stumpf, J. Tits, C. Walther, E. Wieland, T. Fanghänel, J. Coll. Interf. Sci., 276, 118-124 (2004).

[12] R. T. Brundage, R. L. Powell, J. V. Beitz, G. K. Liu, J. Lum., 69, 121-129 (1996).

[13] G. K. Liu, V. V. Zhorin, S. T. Li, J. V. Beitz, J. Chem. Phys., 112, 373-382 (1999).

[14] M. Marques Fernandes, T. Stumpf, B. Baeyens, C. Walther, M. Bradbury, Envir. Sci. Technol., 44, 921-927 (2010).

[15] A. A. Kaplyanskii, R. M. Macfarlane, (Eds) Optical Properties of Excited States in Solids, Plenum Press, New York (1992).

9.3 Mass spectrometry methods

N.L. Banik, S. Büchner, R. Burakham, M. Fuss, F. Geyer, H. Geckeis, M. Lagos, C.M. Marquardt, ,C. Walther, B. Kuczewski[1], J. Aupiais[2] N. Baglan[2], S. Topin[2], A.G. Maslennikov[3]

[1]Department of Nuclear Chemistry, University of Cologne, Germany; [2]Centre de Bruyères-le-Châtel, DAM/DIF/DASE, CEA; [3]Frumkin Institute of Physical and Electrochemistry, RAS, Moscow, Russia France

In the frame of research on safety assessment of final disposal the INE develops and applies sophisticated methods to investigate radionuclides in various environmental systems. Inductively-coupled-plasma mass-spectrometry (ICP-MS) allows detecting radionuclides at tracer concentrations and combined with capillary electrophoresis (CE), radionuclides can be characterised sensitively in various aquatic solutions. On the other side mass spectrometry (MS) can separate species by their masses and hence, allows to detect oligomers and polymer species of radionuclides. This can be achieved by combination of MS with a soft injection method, the electro-spray ionisation method (ESI). In the following sections the power of ESI-MS and CE-ICP-MS are demonstrated in four examples.

$(MoO_3)_n$ polymers in strongly acidic solution measured by electrospray mass-spectrometry

Molybdenum polymerization is of concern in reprocessing of spent nuclear fuel, in particular the speciation of Mo(VI) in the presence of Zr(IV) in 0.5-0.6M HNO_3. Within the framework of the Helmholtz Joint Research Group in collaboration with MSU we performed first test experiments to the applicability of ESI TOF MS to this question.

Using mild declustering conditions[1], a solvent

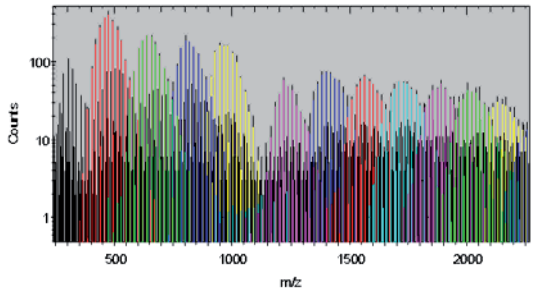

Fig. 1: *Time-of-Flight Mass Spectrum of a sample with [^{98}Mo] = 40mM, [HNO_3] = 3M.*

shell surrounding the polymers is preserved. In contrast to Zr, Th and Pu polymers, the Mo(VI) polymers we find here, carry a charge due to an additional H^+ ion. We cannot tell from ESI alone whether this H^+ ion is part of the aqueous complex or whether the proton is transferred to the polymer during the spray process. An example of an ESI TOF mass-over-charge spectrum in logarithmic representation is shown in Fig.1: Each color corresponds to one polymer size Mo_xO_y with various numbers of water molecules in the droplet causing clusters of peaks.

$MoNa_2O_4$*$2H_2O$ was dissolved in appropriate acid ([HNO_3] = 3M, 1M, 0.5M) to give the [Mo] =5mM to [Mo]=30mM samples. While dimers, trimers and tetramers dominate the [Mo]=5mM solution (Fig.2, black) the higher concentrated solutions show a broad size distribution (blue).

In a second set of measurements, Mo metal powder was dissolved in conc. nitric acid and after 1d diluted with distilled water to give the

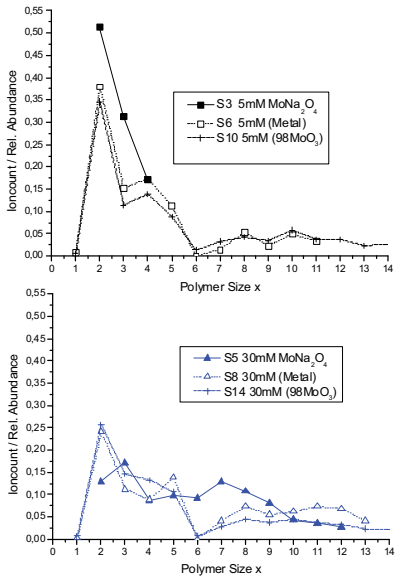

Fig. 2: *Comparison of species distributions for $MoNa_2O_4$ (■) Mo metal (□) and $^{98}MoO_3$ (+). Top [Mo]=5mM, Bottom: [Mo]=30mM.*

stock solution ([HNO_3]=3M, [Mo]=60mM, aged for 13 d). Prior to each measurement the actual samples were prepared by dilution with 3M nitric acid to achieve the appropriate concentration. In spite of some scatter, the species distribution shifts to higher polymerization with increasing [Mo] concentration (Fig.2).

In order to achieve better statistics, additional measurements were performed with isotopically enriched ^{98}Mo oxide. Use of isotopically

pure ^{98}Mo avoids the distribution of the polymer signal over many peaks due to the 7 stable isotopes of Mo. $^{98}MoO_3$ was dissolved in appropriate acid ([HNO_3] = 0.5M – 3 M) to give the [Mo] = 1mM to 40mM samples. The polymerization increases, with increasing [Mo] concentration (Fig.2).

In summary, we confirm that nano ESI is well suited for quantifying the species distribution of Mo in highly acidic media. Spectra were unambiguously evaluable and measurements were well reproducible. Depending on concentration more or less pronounced ageing of solutions was observed over a time span up to ~45d, leading in all cases to formation of larger polymers. After sufficient equilibration time the polymerization seems to be independent of the chemical form, the molybdenum was introduced into the acid. Monomers do not play a significant role in any of the solutions and the dimer is most frequently the most abundant species. In many solutions the hexamer is almost absent and the pentamers and heptamers are suppressed. The reason of this behavior is not yet clear. It might originate in a geometrical destabilization of the hexamer.

According to [2] approximately 50% dimers are expected for ([H^+]=3M, [Mo]=30mM), for [Mo]=5mM approximately 30%, the rest should be monomers. Given the fact that the applied technique in [2] (UV absorbance) cannot distinguish polymers of different size, the results must be interpreted, that 50% or 70%, respectively, are monomers, whereas 50%, and 30% are polymers of size x≥2. In all measured samples the fraction of polymers is higher and the abundance of monomers of the order of only a few percent. However, the measurements of [2] were performed in perchloric acid. It is known for other metal ions like the tetravalent actinides that polymerization in nitric media is much stronger than in the case of a weakly complexing anion such as ClO_4^-.

Pu(IV) hydrolysis at low concentrations studied with CE-ICP-MS – first results

The understanding of the formation of Pu(IV) colloids and their behaviour in ground water is an important aspect of the migration of plutonium in aquifers. Up to now, the formation and characterisation of Pu(IV) colloids were mainly studied at high Pu concentration [3,4]. But for migration studies, speciation is required at low plutonium concentrations up to 10^{-9} M. Online-coupled capillary electrophoresis (CE) with inductively coupled plasma mass spectrometry (ICP-MS) has been successfully applied for the speciation of actinide ions at low concentration [5-7], recently. We have used the CE-ICP-MS to demonstrate the feasibility of CE-ICP-MS for characterisation of Pu(IV) hydrolysis species at low concentrations. This study was in collaboration with CEA in the frame of the ACTINET, and the experiments were performed at DAM/DIF/DASE-CEA in Bruyères-le-Châtel, France.

We investigated Pu(IV) at pH 2 and 5 with a concentration of $1.0x10^{-8}$ M and ionic strength of 0.5 M NaCl. The CE experiments were

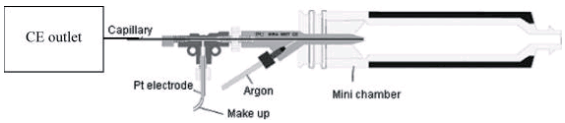

Fig. 3: *Setup for the coupling of CE to ICP-MS [5].*

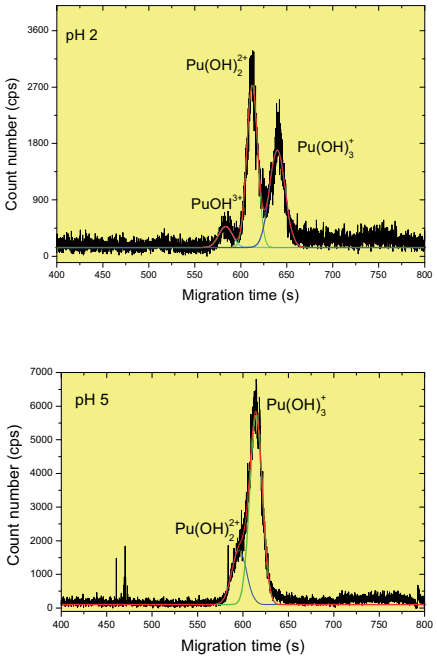

Fig. 4: *Electropherograms of plutonium(IV) hydroxo species characterized by CE-ICP-MS (a) pH 2 (b) pH 5. [Pu(IV)]=1.0x10^{-8} M, [NaCl]= 0.1 M.*

performed on a Beckmann P/ACETM MDQ capillary electrophoresis instrument (Fullerton, USA). CE separations were carried out using an uncoated fused silica capillary (60 cm x 50 µm i.d., 360 µm o.d.). For detection an Axiom (VG Elemental, Winsford, Cheshire, U.K.) inductively coupled plasma sector field mass spectrometer (ICP-SFMS) was coupled with the CE. As interface between CE and ICP-MS MiraMist nebuliser was used. Fig. 3 shows the setup for the coupled CE to ICP-MS [5]. The separations have been performed with a voltage of 5000 V.

Fig. 4(a) shows the electropherogram of Pu(IV) species at pH 2. Three peaks emerge at

different migration time of 580, 610, and 640 sec, respectively. Consistent with the electrophoretic mobility and ionic conductivity we propose that the three peaks are attributed to $Pu(OH)^{3+}$, $Pu(OH)^{2+}_2$ and $Pu(OH)^{+}_3$, respectively (Fig. 4(a)). In contrast to pH 2, the electropherogram at pH 5 shows only one main peak with a small shoulder at shorter times (Fig. 4(b)) It is not clear, if the main peak is attributed to $Pu(OH)^{+}_3$ or to polymeric species of Pu(IV). However, this preliminary study shows that CE-ICP-MS is suitable to investigate Pu(IV) hydrolysis at low concentrations and encourage us to perform more detailed investigations in future.

Redox speciation of arsenic and selenium by CE-ICP-MS

Arsenic and selenium play an important role in the environment as toxicant, non-radioactive or radioactive, for human health. Inorganic arsenic species, arsenite (As(III)) and arsenate (As(V)), and tetravalent (Se(IV)) and hexavalent (Se(VI)) selenium are mainly found under aerobic conditions. The aim of the present study was to develop and optimize the coupling of the CE with the ICP-MS for simultaneous speciation of arsenic and selenium.

The CE experiments were performed on a Beckmann P/ACE^{TM} MDQ capillary electrophoresis instrument (Fullerton, USA). CE separations were carried out using an uncoated fused silica capillary (60 cm length, 50 µm i.d.). The ICP-MS instrument used was a Perkin-Elmer ELAN6000. The background electrolyte (BGE) was prepared from sodium dihydrogen phosphate monohydrate ($NaH_2PO_4 \cdot H_2O$). Two different nebulisers were used in this work: an Apex inlet system equipped with MicroFlow PFA nebulizer and a MicroMist nebuliser (AF Analysentechnik, Germany). The analytical performance of the two nebulization interfaces for speciation of arsenic and selenium species were investigated and compared. Electropherogram obtained by using the APEX system for the separation of As(III)/(V) and Se(IV)/(VI) is shown in Fig. 5(a).

A sheath flow interface was used to introduce the CE eluent to the MicroMist nebuliser followed by ICP-MS detection. Fig. 5(b) shows the electropherogram. Compared with the elctropherogram obtained with APEX nebuliser, better peak shape and shorter analysis time were achieved with MicroMist nebuliser. Under the selected experimental conditions, the linear range, precision and limit of detection (LOD) was examined. The sensitivity of As(III) was found to be 15 times better with the MicroMist based interface than using the Apex system. Data for repeatability in migration times and peak areas in term of the relative standard deviation (%RSD) were evaluated by eleven successive injections of the mixed standard solution of 0.1 to 1.5 mg L^{-1} of As(III), As(V), Se(IV) and Se(VI), respectively. It was found that better analytical performance was obtained with the MicroMist nebuliser. The CE-ICP-MS system with MicroMist nebulizer was applied on synthetic and real samples where we assumed that they might be contaminated with arsenic and selenium. For that sediment samples collected in the Nam Phong river basin, Khon Kaen,

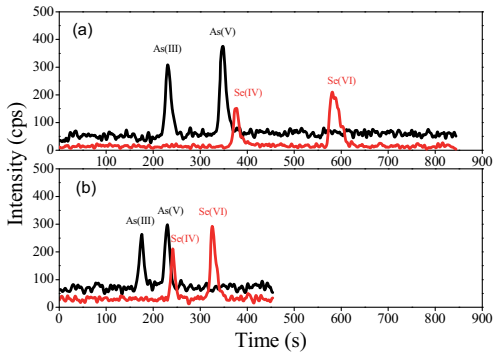

Fig. 5: *Electropherograms of standard mixture of arsenic and selenium by CE-ICP-MS using (a) APEX and (b) MicroMist nebulizer.*

Thailand, were leached with MilliQ water and the solution was analysed by CE-ICP-MS. It was not surprising that some metal species were not detectable in these samples (see Fig.6). Therefore, the accuracy of the procedure was checked by spiking 0.1 mg L^{-1} of As(III), As(V) and 1.0 mg L^{-1} of Se(IV), Se(VI) to the samples. Recoveries of spiked As(III), As(V), Se(IV) and Se(VI) in all samples were satisfactory (87 to 105 %). Typical electropherograms are shown in Fig. 6.

This work presented the hyphenation of CE and ICP-MS for speciation analysis of arsenic and selenium by comparative study of two different sample introduction systems. The best analytical features were obtained using MicroMist nebulizer. The studied species were separated by CE within 7 min using phosphate buffer at pH 11 as background electrolyte. Applications have been demonstrated to natural and synthetic samples. Finally, it should be noted that the sensitivity of the method could be potentially enhanced by coupling the proposed system to an on-line sample pre-concentration unit.

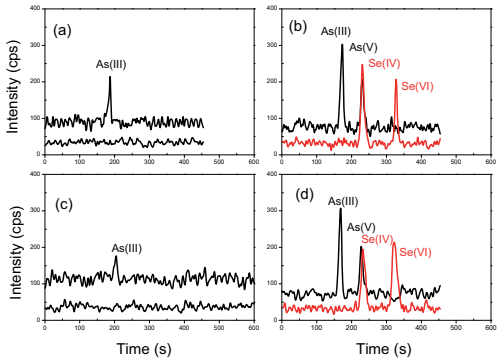

Fig. 6: *Typical electropherograms of arsenic and selenium in synthetic and real samples (a) SRM 1, (b) spiked SRM 1 (c) sediment 3 and (d) spiked sediment 3.*

Separation of Uranium Species by CE-ICP-MS

The speciation of actinides in solution is necessary to elucidate their environmental behaviour. To characterise trace amounts in solution a reliable technique is needed that does not influence the redox species ratio during the measurement. For plutonium and neptunium, use of CE-ICP-MS is a well established technique [7]. However, the separation of U(IV) and U(VI) under similar conditions is not possible. Therefore we developed suitable separation conditions by varying the electrolyte buffer.

The U(IV) solution was prepared by electrochemical reduction of uranyl nitrate dissolved in hydrochloric acid (~0.8M). After preparation the stock solution was stored under oxygen free argon atmosphere.

By using 1 M acetic acid as separation buffer, the U(VI) and U(IV) was not separated and found in only on fraction. UV/Vis spectra of comparable samples with higher U concentrations showed that the uranium was still U(IV). Knowing from the separation of the plutonium and neptunium species the complexation is important for the conservation of the redox species ratio. The addition of complexing agents like α-hydroxy-iso-butyric, β-alanine acid or similar buffers were also not successful. Therefore we used EDTA to form a strong complex with U(IV) in solution. As electrolyte 100mM acetic acid with 10mM Na_2EDTA turned out as suitable buffer system. The pH value of the electrolyte was ~3.5.

The successful separation of a mixture of 83% U(IV) and 17% U(VI) is shown in Fig. 7. Cs was added to the sample as an internal standard for the EOF-mobility of the ions. Several samples with various ratios of U(VI) and U(IV) were probed to ensure the reliability of the separation. Although the samples were stored under air for 80 min a change of the U(IV)/(VI) ratios of only 1% was observed and this is within the error of the method (~± 5%).

The method has now to be applied at environmental relevant conditions with lower metal concentrations and in presence of NOM and other possible interfering substances.

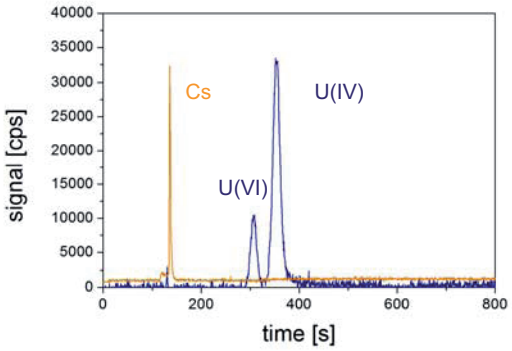

Fig. 7: *Separation of U(IV) and U(VI) in 100 mM AcOH / 10 mM Na_2EDTA by use of CE-ICP-MS, c(U) 2400µg/l.*

References

[1] C. Walther, J. Rothe, M. Fuss, S. Büchner, S. Koltsov, T. Bergmann, Anal. Bioanal. Chem., 388, 409 (2007).

[2] E. Esbelin, P. Gareil, M. Masson, J. L. Emin, Analytica Chimica Acta, 433, 299 (2001).

[3] V. Neck, J. I. Kim, Radiochim. Acta, 89, 1-16, (2001).

[4] J. Rothe, C. Walther, M. A. Denecke, T. Fanghänel, Inorganic Chemistry, 43, 4708-4718, (2004).

[5] S. Topin, J. Aupiais, N. Baglan, T. Vercouter, P. Vitorge, P. Moisy, Analytical Chemistry, 81, 354–5363, (2009).

[6] C. Ambard, A. Delorme, N. Baglan, J. Aupiais, F. Pointurier, C. Madic, Radiochimica Acta, 93, 665-673 (2005).

[7] B. Kuczewski, C. M. Marquardt, A. Seibert, H. Geckeis, J. V. Kratz, N. Trautmann, Analytical Chemistry, 75, 6769-6774 (2003).

9.4 Transmission electron microscopy (TEM) to the nanoscale analysis of radioactive materials

D. Bach, D. Schild, E. Soballa

Introduction

The transmission electron microscopy (TEM) applied to radioactive materials will give further insight into nanoscopic structures and chemical processes relevant for safety assessment of a nuclear repository. TEM is a versatile materials characterization technique that is unique in terms of spatial resolution. It comprises a broad range of methods that make use of the interactions between an electron beam and matter to generate different kinds of images, diffraction patterns, and spectra revealing chemical and structural information at a resolution down to the atomic scale (see, e.g., [1]). Some of the principles and possibilities of TEM are briefly presented as well as the experimental equipment to which we have currently access to analyze radioactive specimens. Some of the first results obtained from the investigation of green rust interacted with neptunyl are developed as example.

Transmission electron microscopy

In a transmission electron microscope (TEM, the same acronym is used to denote the method and the instrument), a beam of fast electrons (primary energy of typically some 100 keV) is projected on a thin specimen. If the specimen is thin enough, most of the electrons can pass through the material without scattering. The incident electrons have also a certain probability of undergoing different elastic and/or inelastic scattering processes which are the source of contrast in images and allow structural and composition analyses. An exhaustive listing of all the TEM methods is far beyond the scope of this paragraph. Only some of the most important TEM techniques are presented here.

The contrast in a TEM image consists of a combination of mass-thickness contrast, diffraction contrast, and at higher magnification phase contrast. The last-mentioned contrast type is caused by the interference between unscattered and scattered electrons and allows high-resolution (HR) - atomically-resolved – TEM. It results in so-called lattice fringe patterns yielding information on lattice spacing and orientation.

TEM also enables the obtainment of electron-diffraction patterns. Each point in the pattern is related to a specific scattering angle, thus allowing crystal-structure characterization (the interaction of the incident electrons with regularly spaced atomic planes results in constructive interference of elastically scattered electrons in well-defined directions given by *Bragg*'s law).

In the scanning TEM mode (STEM), a nanometer-sized electron probe is focused on the specimen and scanned in the specimen plane. At each point the transmitted signal can be measured by different types of detectors and contributes to a corresponding point in an image. For instance, a high-angle annular dark-field (HAADF) detector collects electrons scattered through high angles. Since high-angle elastic scattering strongly depends on the atomic number *Z* (*Rutherford* scattering) the contrast in a HAADF image is dominated by the chemical composition (*Z*-contrast).

Electron energy-loss spectroscopy (EELS) in a TEM tends to elemental identification and speciation. It reveals the distribution of the inelastically scattered electrons as a function of their energy loss. Hence, it results in a spectrum showing features such as ionization edges (stemming from the excitation of inner-shell atomic electrons to unoccupied states above the *Fermi* level) that are characteristic for the elements present in the specimen. A specific edge may present some fine structure which can serve as "fingerprint" of changes of the oxidation state, chemical bonding, and atomic environment. In addition, the intensities under appropriate edges enable elemental quantification.

Elemental identification and quantification can also be performed in a TEM by means of energy-dispersive x-ray spectroscopy (EDXS).

Experimental

For analysis of radioactive specimens we have access to a 200 keV FEI Tecnai G^2 F20 TEM located in a radioactive control area at the *Institute for Materials Research* (IMF II) of the *Karlsruhe Institute of Technology*. It allows HRTEM, can be operated in STEM mode, and is equipped with a HAADF detector, an EDX system, and with a *Gatan imaging filter* (GIF) *Tridiem* allowing EELS.

A double-tilt vacuum-transfer specimen holder allows safe transport of the TEM specimen between the control area of INE and that of IMF II. A glove-box adapter for the specimen

holder is under construction. It will enable to load a redox-sensitive specimen on the holder in an inert-gas glove box and then to transfer this specimen into the vacuum of the TEM without exposure to air.

One main limitation of TEM is the specimen preparation. Indeed, TEM requires extremely thin "electron-transparent" specimens (typically some 10 nm thick) making their preparation a challenge. The preparation from a bulk sample requires a variety of dedicated tools. However, to prepare a specimen from a solution containing particles that are small enough in at least one dimension, the easiest method that can be tried is the deposition of a small drop of solution on a copper TEM grid covered by a carbon film. If necessary, the electrolyte of the solution can be removed by rinsing the specimen with one drop of water. This method was employed to prepare the green-rust specimens whose investigation is briefly presented in the following.

First results on green rust interacted with neptunyl

Green rust (GR) belongs to a family of Fe(II)-Fe(III) layered double hydroxides with anions (e.g. SO_4^{2-}), cations (e.g. Na^+), and water structurally arranged in the interlayers and it crystallizes in thin hexagonal platelets [2]. It may form in anoxic groundwater and is likely to evolve during corrosion of steel canisters in a nuclear-waste repository. Hence, owing to its redox properties, it is a potential candidate for attenuating the migration of radionuclides in the environment.

^{237}Np is a long-lived actinide present in nuclear waste. When water has access to the waste it may exist as pentavalent species like the mobile neptunyl-ion $Np(V)O_2^+$ [3].

B.C. Christiansen and coworkers investigated the interaction of NpO_2^+ with green rust sodium-sulphate ($GR_{Na,SO4}$) [3]. They showed that Np(V) is immobilized via reduction and formation of less soluble Np(IV)-species. However, details of the immobilization mechanisms are not yet clear. There is still a lack of direct evidence concerning the exact location where Np(IV) is immobilized on the GR particles.

In the present study, two types of specimens were analyzed by TEM: $GR_{Na,SO4}$ alone (synthesized at *Nano-Science Center, Department of chemistry, University of Copenhagen, [2]*) and after interaction with a NpO_2^+ solution (Np-GR, [3]).

A bright rim (~ 3-5 nm thick) was observed at the edge of the Np-GR platelets by means of STEM-HAADF (Fig. 1a), suggesting the presence of a high-*Z* element. Such a rim was not observed for GR alone. To correlate the high HAADF signal with Np, an EDX-linescan was performed across the rim with 16 spectra recorded on a 32 nm path by means of an electron probe of about 1-2 nm in diameter (Fig. 1b). Two representative spectra are shown in Fig. 1c. A strong Np signal dominates the spectrum recorded at the rim (spectrum 1) whereas Np cannot be identified inside the GR particle (spectrum 2). Hence, Np is clearly localized at the edge of the GR platelets, suggesting that NpO_2^+ did not enter the GR interlayer.

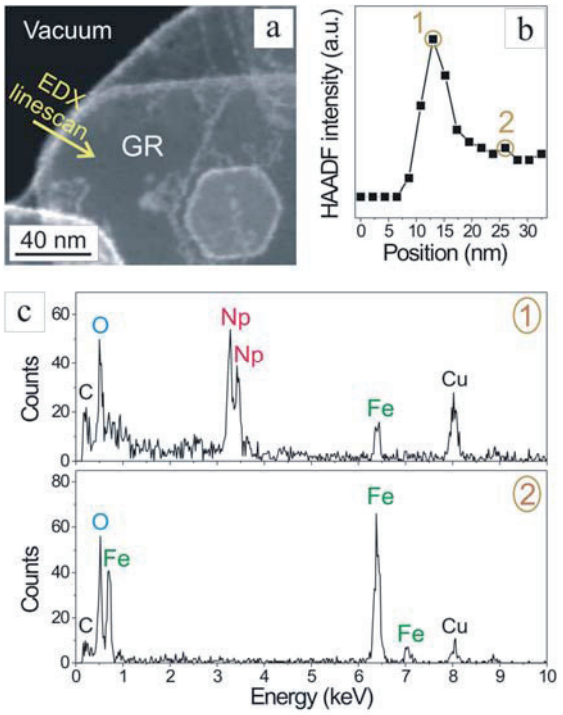

Fig. 1: *EDX linescan across the edge of Np-GR. a) STEM-HAADF image; b) HAADF signal as a function of the position of the electron probe; c) representative EDX spectra. The Cu signal results from the TEM grid.*

References

[1] D. B. Williams, C. B. Carter, *Transmission Electron Microscopy*. New York: Springer (2009).

[2] B. C. Christiansen, T. Balic-Zunic, P. O. Petit, C. Frandsen, S. Morup, H. Geckeis, A. Katerinopoulou, S. L. S. Stipp, Geochim. Cosmochim. Acta, 73(12), 3579-3592 (2009).

[3] B. C. Christiansen, H. Geckeis, C. M. Marquardt, A. Bauer, J. Römer, D. Schild, S. L. S. Stipp, Geochim. Cosmochim. Acta, in preparation.

9.5 Computational Chemistry

B. Schimmelpfennig, R. Polly, M. Trumm, M. Flörsheimer, Th. Rabung, P. Linqvist-Reis, D. Schild, N. Banik

Introduction

Computational Chemistry at INE has been established as a predicting and supporting tool in various research fields, such as extraction chemistry, chemical and physical properties of mineral surfaces, oxo-hydroxo systems from small size in solution to nano-particles or actinides in solution. Quantum chemically calculated properties range from structure parameters to spectroscopic data such as, e.g., vibrational spectra, XPS or NEXAFS data.

Whereas structures and vibrational modes of actinide complexes are predicted with sufficient accuracy, the relative binding energies of actinide ions in water with respect to the coordination number is still a major challenge. Within an international collaboration we have developed state-of-the-art force fields for present calculations on small Th(IV)- and Cm(III)-water complexes.

Interaction of the corundum surface with water and formation of trivalent f-element interface complexes studied by cluster and plane-wave DFT calculations

As a model for the hydroxylated corundum (110) surface we used the $Al_{27}O_{75}H_{67}$ cluster. In our earlier studies we showed that Density functional theory (DFT) with the BP86 functional and the cc-pVDZ basis set is an appropriate theoretical tool for this task [1].

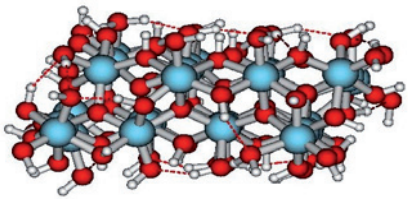

Fig. 1: *$Al_{27}O_{75}H_{67}$ clusters as a model for the corundum (110) surface*

In a first step we determined the structure of the $Al_{27}O_{75}H_{67}$ clusters. Based on the optimised structures we calculated the vibrational frequencies of the surface OH groups (Fig.1). This in turn can directly be compared to the experimental Sum Frequency Spectra of the respective corundum surface. We found that the vibrational frequencies extent over a wider range as found in the case of the (001) surface (3100-3750 cm^{-1}). Another interesting result of this calculations shows that the vibrational frequencies are determined by the tilt angle of the OH species.

Additionally we used the cluster to extent the study of the sorption of solvated trivalent metal ions, such as La^{3+}, Eu^{3+} and Cm^{3+} from the corundum (001) surface (Fig. 2) [2] to the corundum (110) surface. The inner sphere complexes formed by the metal ions, the remaining water molecules and the surface are theoretically characterized and studied. This study is currently in progress.

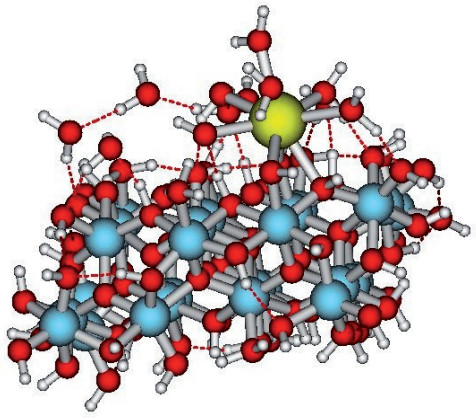

Fig. 2: *Sorption of solvated trivalent metal ions on the corundum (110) surface*

Another model used to study the sorption on the corundum (0001) surface are Keggin Clusters $Al_{13}O_4(OH)_{24}(H_2O)_{12}{}^{7+}$. These clusters are highly symmetric and have t_d symmetry (Fig.3).

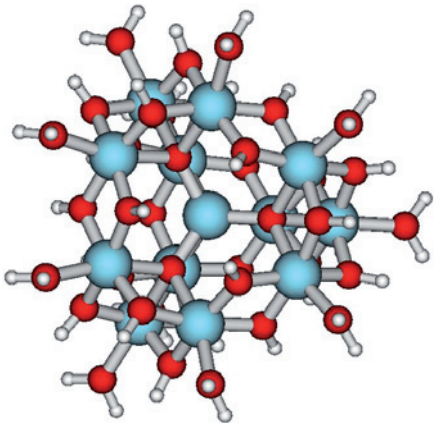

Fig. 3: *The $Al_{13}O_4(OH)_{24}(H_2O)_{12}{}^{7+}$ Keggin Cluster*

We studied the stability and reaction energies of these clusters depending on the charge, varying from +7, +6, … down to a neutral cluster by removing protons from the cluster and determining the optimal structure of the new species. Based on these results we studied inner and outer sphere complexes of trivalent lanthanide and actinide ions on these clusters (Fig.4). We found, in good agreement with experimental results, the formation of inner or outer sphere complexes for charges smaller or equal than four.

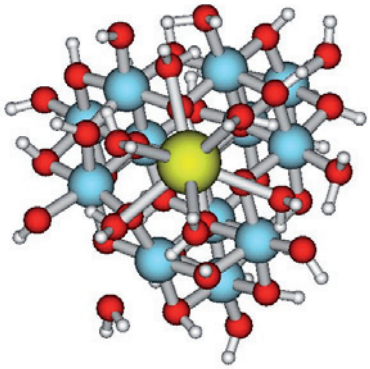

Fig. 4: *Sorption onto the Keggin Cluster*

In order to extent our theoretical studies we started to complement the cluster models with another approach describing surfaces. For this we use the plane wave Density functional methods using periodic boundary conditions with the Projector Augmented Wave (PAW) ansatz, as implemented in Vienna Ab initio Simulation Package (VASP) (Fig.5). First results with this alternative theoretical approach to describe the corundum (001) surface provides results for the orientation and vibrational frequencies of the surface aluminol species very similar as obtained with the cluster approach.

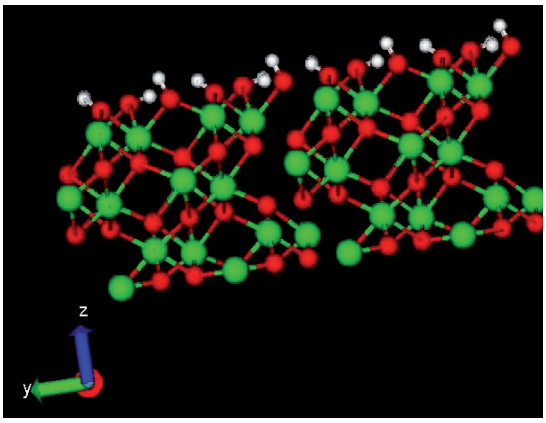

Fig. 5: *2x2 Supercell as a model for the corundum (001) surface in plane wave DFT calculations*

Development of force fields for actinide ions and complexes in aqueous solution

With the help of quantum-chemical methods we are able to calculate binding energies of complexes of about 30 water molecules around a given central ion in acceptable CPU-time.

Despite this being helpful when determining, for example, the coordination numbers in gas phase, for a proper description of the solvation effects about 1000 water molecules are needed to reach bulk behavior [3]. Hence we need an alternative way of computing such big structures. Therefore we started to employ the force-field TCPEp developed by Masella and Cuniasse [4]. The results will also deliver starting points for quantum-chemical calculations.

To achieve a high accuracy, the parameters of the force field are fitted to quantum-mechanical data obtained using large state-of-the-art basis sets and electron-correlation approaches like MP2 or CCSD(T) (Fig. 6).

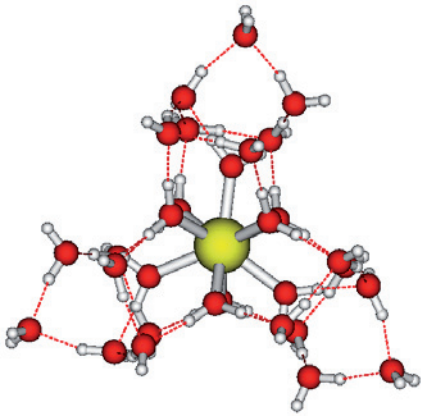

Fig. 6: *MP2-geometry-optimized structure of a 9-fold coordinated Th(IV) with second shell and parts of a third shell*

With such a structure a molecular dynamic is started and carried out on the nanosecond scale (Fig.7). Recording the trajectory of the central Th(IV) cation leads to a statistical coordination number. The aim of these calculations in addition to finding coordination numbers for solvated actinides is to achieve i.e. dipole-moments, structure analysis, transition mechanisms, exchange rates or thermodynamic data. The investigations will be continued with large-scale simulations of the Th(IV) and Cm(III)- system, further studies of many-body effects and their parameterization as well as transferring the developed

techniques to other tri- and tetravalent actinides in solution and counterions.

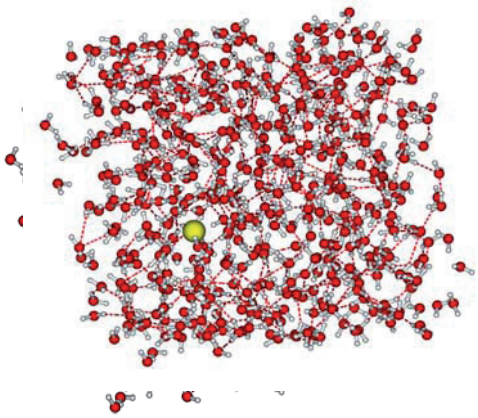

Fig. 7: *Th(IV) ion embedded in 512 water molecules*

This project was initiated as a collaboration within the ACTINET network and involves apart from the computational chemistry group at INE, V. Vallet, F. Real (ACTINET-fellow) and J.P. Flament from Lille and M. Masella from CEA / Saclay.

DFT calculations on an isotypic series of $[An^{III}(H_2O)_9]$ triflates

An^{III} triflates, $[An(H_2O)_9](CF_3SO_3)_3$ (An = U-Cm, Cf) have recently been synthesized and their crystal structures determined (see Sec. 5.1 for details). From a theoretical point of view, it is a challenge to find a model system suitable to compare to XRD data and to understand the An^{III} – water distances along the series as well as similarities or differences compared to the trivalent lanthanides. Such a model system could be constructed in the form $[La(H_2O)_9]^{3+} \cdot [An(H_2O)_9^{3+} \cdot (CF_3SO_3)_9]^{6-} \cdot [La(H_2O)_9]^{3+}$ (Fig. 8), where the central unit is described in a way including the inner-complex hydrogen bonds between the prismatic and capping waters to the triflate anions. DFT calculations in the Resolution-of-the-Identity (RI) approximation were carried out with the BP86 functional using the TURBO-MOLE software package. F-in-core pseudopotentials for trivalent actinides and lanthanides were used and all basis sets were of TZVP quality. The C_{3h} point group was assumed in all the calculations as suggested by experiment. It should be noted that using the approach outlined above, geometry optimizations for such comparably large complexes can be carried out efficiently in single-processor mode on a standard Linux PC.

Apart from a systematic shift of 6-7 pm to longer An^{III}/Ln^{III}–water distances, which is not atypical for DFT calculations, the trends for the An^{III}/Ln^{III}–prismatic water distances are nicely reproduced, whereas the deviations between XRD and calculations are larger for capping waters and the lighter An^{III} ions. As the deviations between theory and experiment are much smaller for the Ln^{III} complexes, we consider this not to be due to limitations of the chosen cluster model but more likely to be some lacking description of covalency for the prismatic waters which should enhance the deviation for the capping waters. First results have been obtained for the vibrational modes of such clusters and compared to experiment.

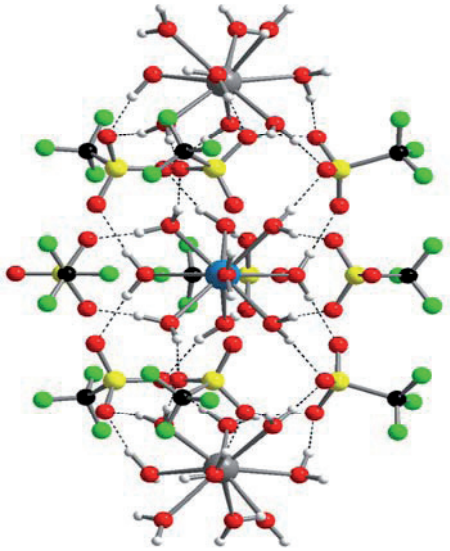

Fig. 8: *Cluster model for An^{III} triflates*

Theoretical analysis of EXAFS results on An^{III}–N distances in 1:3 BTP complexes and of combined theoretical and experimental N 1s-XPS on $Eu^{III}BTP_3$ nitrate

The An(III) bond to BTP ligands and its difference to the Ln(III) case has been studied extensively over the last years (see Sec. 7). EXAFS analysis gives An(III)-N distances 256 to 257 pm along the series An=U-Cm which is in contrast to the ionic radii, thus suggesting a shortening by 5 pm along the series and thus a covalency effect in the An(III)-BTP bond [5]. We attempted to clarify this discrepancy by carrying out geometry optimizations at the DFT and MP2-level using the f-in-core approximation for An(III) ions as well as DFT calculations employing small-core pseudopotentials for the actinides. Surprisingly, the f-in-core approximation led, apart from some systematic shift, to bond-distances in agree-

ment with the ionic radii. Only when using DFT in combination with the small-core approximation we were able to reproduce the experimental result of Am(III)-N distances to be the same for all complexes investigated. Population analysis indicates no significant contribution by the 5f orbitals to the bond. The reasons for this drastic difference between the f-in-core and the small-core approximation are still to be revealed in future studies. Nevertheless, the results we obtained strongly suggest to use at least the small-core approximation when dealing with An(III) soft-donor ligand complexes.

In the presence of nitrate, 1:3 complexes of trivalent actinides with BTP may also form ten-coordinated complexes with one nitrate binding monodentate to the metal centre. For the case of Am(III) we carried out structure optimization calculations at the DFT-level with the f-in-core approximation, which is sufficient for the present purpose. Starting with three nitrates for charge compensation, we always found one nitrate to bind to the metal centre whereas the other two are weakly coordinated to the BTP ligands (Fig. 9).

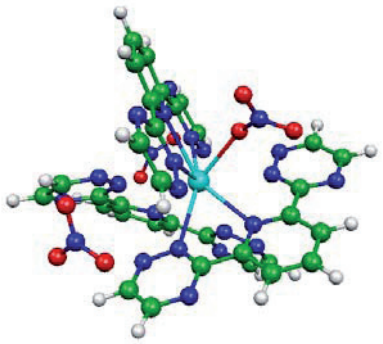

Fig. 9: *DFT-optimized Am(III)$BTP_3(NO_3)_3$*

For such a optimized structure at the B3LYP-level we carried out a single-point Hartree-Fock calculation and identified the N(1s) orbitals and their corresponding orbital energies as an estimate of the binding energy. XPS analyses were performed on samples prepared from solution onto aluminum foil. XP spectra were recorded by use of monochromatic Al K_α x-ray excitation. Spectra are charge referenced to C 1s (C_xH_y) at 284.8 eV (propyl chains of nPr-BTP).

Apart from a systematic shift of 25.9 eV, the orbital energies turn out to give a reasonable estimate for the interpretation of XP spectra. The experimental peaks can thus be assigned to nitrogen atom of either BTP or nitrate and it is even possible to mutually confirm one nitrate to be coordinated to the metal centre and two nitrate anions to be weakly coordinated to the BTP ligands (Fig. 10).

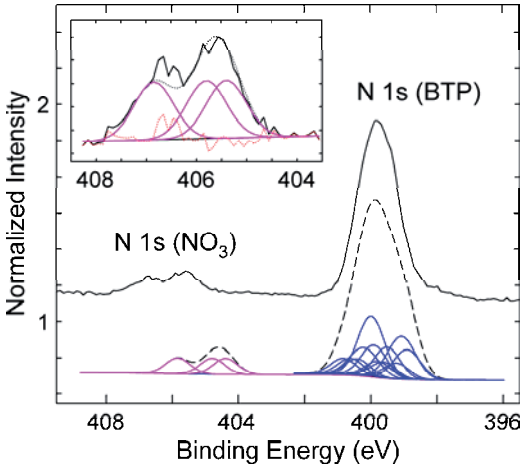

Fig. 10: *Narrow scan of N 1s XP spectrum of Eu(III)$BTP_3(NO_3)_3$ compared to the result of a Hartree-Fock calculation. The insert shows a curve fit to N 1s (NO_3) with 3 Gaussian functions with fixed relative distances as calculated.*

References

[1] R. Polly, B. Schimmelpfennig, M. Flörsheimer, K. Kruse, A. AbdElMonem, R. Klenze, G. Rauhut, Th. Fanghänel, J. Chem. Phys., 130, 064702, (2009).

[2] R. Polly, B. Schimmelpfennig, T. Rabung, M. Flörsheimer, R. Klenze, H. Geckeis, accepted for publication in Radiochimica Acta.

[3] D. Hagberg, E. Bednarz, N. M. Edelstein, L. Gagliardi, J. Am. Chem. Soc., 129, 14136 (2007).

[4] M. Masella, Ph. Cuinasse, J. Chem. Phys., 119, 1866, (2003).

[5] See INE Anual Report 2008 for details.

10 Publications

Papers in Books and Peer Reviewed Journals

ALTMAIER, M.; NECK, V.; LÜTZENKIRCHEN, J.; FANGHÄNEL, TH.

Solubility of plutonium in $MgCl_2$ and $CaCl_2$ solutions in contact with metallic iron

Radiochim. Acta 97 (2009) 187–192.

ARMBRUSTER, M.; SCHIMMELPFENNIG, B.; PLASCHKE, M.; ROTHE, J.; DENECKE, M. A.; KLENZE, R.

Metal-ion complexation effects in C 1s-NEXAFS spectra of carboxylic acids -Evidence by quantum chemical calculations

Journal of Electron Spectroscopy and Related Phenomena 169 (2009) 51-56.

BOSBACH, D.; LUCKSCHEITER, B.; BRENDEBACH, B.; DENECKE, M. A.; FINCK, N.

High-level nuclear waste glass corrosion in synthetic clay pore solution and retention of actinides in secondary phases

J. Nucl. Mater. 385 (2) (2009) 456-460.

BRENDEBACH, B.; BANIK, N. L.; MARQUARDT, C. M.; ROTHE, J.; DENECKE, M. A.; GECKEIS, H.

X-ray absorption spectroscopic study of trivalent and tetravalent actinides in solution at varying pH values

Radiochimica Acta 97 (2009) 701-708.

CHRISTIANSEN, B. C.; BALIC-ZUNIC, T.; PETIT, P. O.; FRANDSEN, C.; MORUP, S.; GECKEIS, H.; KATERINOPOULOU, A.; STIPP, S. L. S.

Composition and structure of an iron-bearing, layered double hydroxide (LDH) - Green rust sodium sulphate

Geochim. Cosmochim. Acta 73 (12) (2009), 3579-3592.

CURTIUS, H.; UFER, K.; DARDENNE, K.

Preparation and characterization of Zr-IV-containing Mg-Al-Cl layered double hydroxide

Radiochim. Acta 97 (2009) 423–428.

DARDENNE, K.; SEIBERT, A.; DENECKE, M. A.; MARQUARDT, C. M.

Plutonium(III,IV,VI) speciation in Gorleben groundwater using XAFS

Radiochimica Acta 97 (2009) 91-97.

DENECKE, M. A.; BRENDEBACH, B.; DE NOLF, W.; FALKENBERG, G.; JANSSENS, K.; SIMON,R.

Spatially resolved μ-XRF and μ-XAFS study of a fractured granite bore core following a radiotracer experiment

Spectrochimica Acta B 64 (2009) 791-795.

FINCK, N.; SCHLEGEL, M. L.; BOSBACH, D.

Sites of Lu(III) sorbed to and coprecipitated with hectorite

Environ. Sci. Technol. 43 (2009) 8807-8812.

FISCHER, C.; SCHMIDT, C.; BAUER, A.; GAUPP, R.; HEIDE, K.

Mineralogical and geochemical alteration of low grade metamorphic black slates due to oxidative weathering

Chemie der Erde 69 (2009) 127–142.

FREYER, M.; WALTHER, C.; STUMPF, T.; BUCKAU, G.; FANGHÄNEL, T.

Formation of Cm Humate Complexes in aqueous solution at pHC 3 to 5.5: The role of fast interchange

Radiochim Acta 97 (2009) 547-558.

GORSCHINSKI, A.; KHELASHVILI, G.; SCHILD, D.; HABICHT, W.; BRAND, R.; GHAFARI, M.; BÖNNEMANN, H.; DINJUS, E.; BEHRENS, S.

A simple amonoalkyl siloxane-mediated route to functional magnetic metal nanoparticles and magnetic nanocomposites

Journal of Materials Chemistry 19 (2009) 8829-8838.

GRÜNEWALD, W.; ROTH, G.; TOBIE, W.; WEIß, K.; WEISENBURGER, S.

The role of the platinum group elements ruthenium, rhodium and palladium in the vitrification of radioactive high level liquid waste using joule heated ceramic lined waste glass melters

Glass Technology - European Journal of Glass Science and Technology A 49 (2008) 266-278.

HUBER, F.; LÜTZENKIRCHEN, J.

Uranyl Retention on Quartz-New Experimental Data and Blind Prediction Using an Existing Surface Complexation Model

Aquatic Geochemistry 15 (3) (2009) 443-456.

HUITTINEN, N.; RABUNG, T; LÜTZENKIRCHEN, J.; MITCHELL, S. C.; BICKMORE, B.; LEHTO, J.; GECKEIS, H.

Sorption of Cm(III) and Gd(III) onto gibbsite, alpha-$Al(OH)_3$: A batch and TRLFS study

J. Coll. Interface Sci. 332(1) (2009) 158-164.

KIENZLER,B.; VEJMELKA,P.; RÖMER, J.; SCHILD, D.

Actinide migration in fractures of granite host rock: Laboratory and in situ investigations

Nuclear Technology 165 (2009) 223 -240.

KOLOKASSIDOU, K.; SZYMCZAK, W.; WOLF, M.; OBERMEIER, C.; BUCKAU, G.; PASHALIDIS, I.

Hydrophilic Olive Cake Extracts: Characterization by Physicochemical Properties and Cu(II) Complexation

Journal of Hazardous Materials 164 (2009) 442–447.

LEON, A.; ROTHE, J.; CHLOPEK, C.; ZABARA, O.; FICHTNER, M.

Fluorescence XAFS study of $NaAlH_4$ doped with a Ce-based precursor

Phys. Chem. Chem. Phys. 11 (2009) 8829–8834.

LINDQVIST-REIS, P.; WALTHER, C.; KLENZE, R.; EDELSTEIN, N. M.

Optical spectra and crystal-field levels of $[Cm(H_2O)_9]^{3+}$ ions with C_{3h} symmetry in isotypic rare-earth triflate and ethyl sulfate salts

Journal of Physical Chemistry 113 (2009) 449-458.

MAGNUSSON, D.; CHRISTIANSEN, B.; FOREMAN, M. R. S.; GEIST, A.; GLATZ, J.-P.; MALMBECK, R.; MODOLO, G.; SERRANO-PURROY, D.; SOREL, C.

Demonstration of a SANEX Process in Centrifugal Contactors using the $CyMe_4$ BTBP Molecule on a Genuine Fuel Solution

Solvent Extr. Ion Exch. 27 (2009) 97–106.

NÄSTREN, C.; JARDIN, R.; SOMERS, J.; WALTER, M.; BRENDEBACH, B.

Actinide incorporation in a zirconia based pyrochlore $(Nd_{1.8}An_{0.2})Zr_2O_7^+$ x (An = Th, U, Np, Pu, Am)

Journal of Solid State Chemistry 182 (2009) 1–7.

MONTAVON, G.; GUO, Z.; LÜTZENKIRCHEN, J.; ALHAJJII, E.; KEDZIOREK, M. A. M.; BOURG, A. C. M.; GRAMBOW, B.

Interaction of selenite with MX-80 bentonite: Effect of minor phases, pH, selenite loading, solution composition and compaction

Colloids Surfaces A 332(2-3) (2009) 71-77.

NECK, V.; ALTMAIER, M.; RABUNG, T.; LÜTZENKIRCHEN, J.; FANGHÄNEL, T.

Thermodynamics of trivalent actinides and neodymium in NaCl, $MgCl_2$, and $CaCl_2$ solutions: Solubility, hydrolysis, and ternary Ca-M(III)-OH complexes

Pure Appl. Chem. 81(9) (2009) 1555-1568.

RABUNG, T; GECKEIS, H.

Influence of pH and metal ion loading on the Cm(III) humate complexation: a time resolved laser fluorescence spectroscopy study

Radiochim. Acta 97 (2009) 265-271.

POLLY, R.; SCHIMMELPFENNIG, B.; FLÖRSHEIMER, M.; KRUSE, K.; ABDELMONEM, A.; KLENZE, R.; RAUHUT, G.; FANGHÄNEL, TH.

Theoretical investigation of the water/corundum(0001) interface

J. Chem. Phys. 130 (2009) 064702.

REGENSPURG, S.; SCHILD, D.; SCHÄFER, T.; HUBER, F.; MALMSTRÖM, M. E.

Removal of uranium(VI) from the aqueous phase by iron(II) minerals in presence of bicarbonate

Appl. Geochem. 24 (2009) 1617-1625.

RISBERG, E. D.; MINK, J.; ABBASI, A.; SKRIPKIN, M. Y.; HAJBA, L.; LINDQVIST-REIS, P.; BENCZ, E.; SANDSTRÖM, M.

Ambidentate coordination in hydrogen bonded dimethyl sulfoxide, $(CH_3)_2SO…H_3O^+$, and in dichlorobis(dimethyl sulfoxide) palladium(II) and platinum(II) solid solvates, by vibrational and sulfur K-edge X-ray absorption spectroscopy

Dalton Trans. (2009) 1328–1338.

SCHÄFER, T.; MICHEL, P.; CLARET, F.; BEETZ, T.; WIRICK, S.; JACOBSEN, C.

Radiation sensitivity of natural organic matter: Clay mineral association effects in the Callovo-Oxfordian argillite

Journal of Electron Spectroscopy and Related Phenomena 170 (2009) 49-56.

SCHMIDT, M.; STUMPF, T.; WALTHER, C.; GECKEIS, H.; FANGHÄNEL, T.

Incorporation versus adsorption: Substitution of Ca^{2+} by Eu^{3+} and Cm^{3+} in aragonite and gypsum

Dalton. Trans. (2009) 6645-6650.

SKERENCAK, A.; PANAK, P. J.; HAUSER, W.; NECK, V.; KLENZE, R.; LINDQVIST-REIS, P. FANGHÄNEL, T.

TRLFS study on the complexation of Cm(III) with nitrate in the temperature range from 5 to 200 °C

Radiochim. Acta 97 (2009) 385-393.

STEPPERT, M.; WALTHER, C.; GEIST, A.; FANGHÄNEL, T.

Direct nano ESI time-of-flight mass spectrometric investigations on lanthanide BTP complexes in the extraction-relevant diluent 1-octanol

New J. Chem. 33 (2009) 2437–2442.

STUMPF, S.; SEIBERT, A.; GOUDER, T.; HUBER, F.; WISS, T.; RÖMER, J.

Development of fuel-model interfaces: Investigations by XPS, TEM, SEM and AFM

J. Nucl. Mater. 385 (2009) 208-211.

WÅHLIN, P.; SCHIMMELPFENNIG, B.; WAHLGREN, U; GRENTHE, I.; VALLET, V.

On the combined use of discrete solvent models and continuum descriptions of solvent effects in ligand exchange reactions: a case study of the uranyl(VI) aquo ion

Theor. Chem. Acc. 124 (2009) 377–384.

WALTHER, C.; FUSS, M.; BÜCHNER, S.; GECKEIS, H.

Stability of Th(IV) polymers measured by electrospray mass spectrometry and laser-induced breakdown detection

J. Radioanal. Nucl. Chem. 282 (2009) 1003-1008.

WALTHER, C.; HAUSER, W.

Influence of laser beam characteristics and focusing optics on optical laser-induced breakdown detection

Appl. Phys. B 97 (2009) 877-886.

WALTHER, C.; ROTHE, J.; BRENDEBACH, B.; FUSS, M.; ALTMAIER, M.; MARQUARDT, C. M.; BÜCHNER, S.; CHO, H.-R.; YUN, J.-I.

New insights in the formation processes of Pu(IV) colloids

Radiochim. Acta 97 (2009) 199-207.

WALTHER, C.; ROTHE, J.; FUSS, M.; BÜCHNER, S.

A link between the oxidation states? Colloids and mixed-valence polymers of plutonium in aqueous solution

Actinide Research Quarterly 17 (2009) 19-22.

WALTER, M.; SOMERS, J.; BOUEXIERE, D.; GACZYNSKI, P.; BRENDEBACH, B.

Oxidation behaviour of uranium and neptunium in stabilised zirconia

Journal of Solid State Chemistry 182 (2009) 3305–3311.

Proceedings of Workshops and Conferences

ALTMAIER, M.

Intercomparison exercise on redox determination methods: a key activity within the EURATOM FP7 “RECOSY” project

Proceedings of the Workshop TRePro II, Karlsruhe, March 18-19 (2009) 7-8.

BRENDEBACH, B.; DARDENNE, K.; DENECKE, M. A.; GÖTTLICHER, J.; LANG, R.; MANGOLD, S.; ROTHE, J.; STEININGER, R.; SIMON, R.; VITOVA, T.; ZÖLLER, H.

X-ray Spectroscopy Beamlines

ANKA Annual Report (2009) 43–49.

BRENDEBACH, B; DARDENNE, K.; DENECKE, M. A.; LIU, X.; ROTHE, J.; VITOVA, T.

The INE-Beamline for actinide research at ANKA

Proceedings of Actinide-XAS-2008 : Speciation, Techniques, and Facilities for Radioactive Materials at Synchrotron Light Sources. July 15-17, 2008, St Aubin, France, OECD – NEA, NEA/NSC/DOC (2009) 131-137.

BRENDEBACH, B.; DENECKE, M. A.; ROTH, G.; WEISENBURGER, S.

Sulfur incorporation in high level nuclear waste glasses: a S K-edge XAFS investigation

Journal of Physics: Conference Series 190, Proceedings of XAFS14, July 26-31, 2009, Camerino, Italy, 012186.

BUCKAU, G.; DURO, L.; KIENZLER, B.

EURATOM FP7 collaborative project “REDOX PHENOMENA CONTROLLING SYSTEMS” (CP RECOSY)

Proceedings of the Workshop TRePro II, Karlsruhe, March 18–19, 2009, 14.

DARDENNE, K.; BRENDEBACH, B.; DENECKE; LIU, X.; ROTHE, J.; VITOVA, T.

New developments at the INE-Beamline for actinide research at ANKA

Journal of Physics: Conference Series 190, Proceedings of XAFS14, July 26-31, 2009, Camerino, Italy, 012037.

DENECKE, M. A.; MICHEL, P.; SCHAEFER, T.; HUBER, F.; RICKERS, K.; ROTHE, J.; DARDENNE, K.; BRENDEBACH, B.; VITOVA, T.; ELIE, M.

Spatially resolved XRF, XAFS, XRD, STXM and IR investigation of a natural U-rich clay

Journal of Physics: Conference Series 190, Proceedings of XAFS14, July 26-31, 2009, Camerino, Italy, 012187.

FINCK, N.; SCHLEGEL, M. L.; BOSBACH, D.

Lu(III) co-precipitation with hectorite: a polarized EXAFS approach

Geochimica et Cosmochimica Acta, 73 (13) (2009) A376.

FINCK, N.; SCHLEGEL, M. L.; BOSBACH, D.

XAFS investigations of the Ln(III) co-precipitation with clay minerals

ESRF experimental report No 39117 (2009).

FREYER, M.; WALTHER, C.; STUMPF, T.; BUCKAU, G.; BRENDEBACH, B.; ROTHE, J.; HAIRE, R. G.

XAFS Investigation of Cm Humate Complexation in Aqueous Solution

In ANKA Annual Report 2009, Karlsruhe Institute of Technology, October 2009.

GEIST, A.; MODOLO, G.

TODGA process development: an improved solvent formulation

Proc. Internat. Conf. GLOBAL 2009 (The Nuclear Fuel Cycle: Sustainable Options & Industrial Perspectives), Paris, September 6–11, 2009, paper 9193, 1022–1026.

HUBER, F.; KIENZLER, B.; LÜTZENKIRCHEN, J.; PFINGSTEN, W.; TIFFREAU, C.

Karlsruher Geochemical Workshop TRePro II 2009: Workshop on Modelling of Coupled Transport Reaction Processes

atw 54 (7) (2009) 478–479.

HUBER, F.; LÜTZENKIRCHEN, J.

Interaction of uranyl with quartz – experiments and modelling

Proceedings of the Workshop TRePro II, Karlsruhe, March 18-19 (2009) 52-53.

KHELASHVILI, G.; BÖNNEMANN, H.; SCHULENBURG, H.; SCHERER, G. G.; SCHILD, D.

Aluminium alkyl preparation of cobalt-rich Co3Pt@C fuel cell electrocatalyst for ORR

The International Conference on Nanotechnology: Science and Applications, Nanotech Insight ´09, Barcelona, Spain, March 29 – April 2, 2009, Book of Abstracts, 285-286.

KIENZLER, B.; SCHILD, D.; RÖMER, J.; JANSSON, M.

Retention of Tc-99 onto fractures of crystalline rock

Workshop “Mobile Fission and Activation Products in Nuclear Waste Disposal” La Baule (F), Jan 16-19, 2007, OECD 2009, NEA No 6310, 77-86.

KUPCIK, T.; BRENDEBACH, B.; ROTHE, J.; HUITTINEN, N.; RABUNG, T.; LÜTZENKIRCHEN, J.; GECKEIS, H.; FANGHÄNEL, T.

Trivalent Metal Ion Interaction with Aluminum Oxides/Hydroxides

ANKA Annual Report 2009, 160–161.

KUPCIK, T.; HUITTINEN, N.; RABUNG, T.; LÜTZENKIRCHEN, J.; GECKEIS, H.; FANGHÄNEL, T.

Interaction of trivalent ions with various aluminium minerals

Proceedings of the Workshop TRePro II, Karlsruhe, March 18–19 (2009) 57-58.

KUPCIK, T.; HUITTINEN, N.; RABUNG, T.; LÜTZENKIRCHEN, J.; GECKEIS, H.; FANGHÄNEL, T.

Wechselwirkung von trivalenten Metallionen Aluminiumoxiden/hydroxiden

GDCh-Wissenschaftsforum Chemie 2009, Frankfurt am Main, Deutschland, August 30 -September 2, 2009, Book of Abstracts, 211.

KUPCIK, T.; HUITTINEN, N.; RABUNG, T.; LÜTZENKIRCHEN, J.; GECKEIS, H.

Interaction of trivalent ions with various Aluminium minerals

Eighth Keele Meeting on Aluminium, Czech Republic, Trest, 21-25 February 2009 Book of Abstracts, 4.

KUPCIK, T.; HUITTINEN, N.; RABUNG, T.; LÜTZENKIRCHEN, J.; GECKEIS, H.; FANGHÄNEL, T.

Trivalent metal ion interaction with aluminium oxides/hydroxides

Migration '09, 12th International Conference on the Chemistry and Migration Behaviour of Actinides and Fission Products in the Geosphere, Kennewick, Washington, USA, September 20-25, 2009, Book of Abstracts, 168.

LAW, G. T. W.; GEISSLER, A.; LLOYD, J. R.; BURKE, I. T.; LIVENS, F. R.; DENECKE, M. A.; DARDENNE, K.; MORRIS, K.

Uranium and neptunium interactions with biogenic iron minerals

Geochim. Cosmochim. Acta 73 (2009) A729.

LINDQVIST-REIS, P.; APOSTOLIDIS, C.; KLENZE, R.; BRENDEBACH, B.

EXAFS studies on isotypic $[An(H_2O)_9](CF_3SO_3)_3$ hydrates

In ANKA Annual Report 2009, Karlsruhe Institute of Technology, October 2009.

LIU, X.; FIEHN, B.; BRENDEBACH, B; DARDENNE, K.; MARQUARDT, C. M.; ROTHE, J.; DENECKE, M. A.

Design of a spectro-electrochemical cell for in-situ XAFS studies of actinides

Proceedings of Actinide-XAS-2008 : Speciation, Techniques, and Facilities for Radioactive Materials at Synchrotron Light Sources. 15-17 July 2008, St Aubin, France: OECD – NEA, NEA/NSC/DOC (2009)15 171-177.

LIU, X.; BANIK, N. L.; BRENDEBACH, B.; DARDENNE, K.; ROTHE, J.; MARQUARTD, C.; DENECKE, M. A.

Neptunium redox speciation in perchloric acid by in situ XANES/EXAFS using a newly developed spectro-electrochemical cell

In ANKA Annual Report 2009, Karlsruhe Institute of Technology, October 2009.

LIU, X.; FIEHN, B.; BRENDEBACH, B.; DARDENNE, K.; MARQUARDT, C.; ROTHE, J.; DENECKE, M. A.

Design of a Spectro-Electrochemical Cell for in situ XAFS Studies

In ANKA Annual Report 2009, Karlsruhe Institute of Technology, October 2009.

LÖBLE, M.; VITOVA T.; DENECKE, M. A.; BREHER, F.

Ln-L3 edge XANES/EXAFS investigations of lanthanide complexes consisting of a κ^6*N*-donor ligand with podand topology

ANKA Annual Report 2009, Karlsruhe Institute for Technology, October 2009.

LOIDA, A.; GENS, R.; METZ, V.; LEMMENS, K.; CACHOIR, C.; MENNECART, T.; KIENZLER,B.

Corrosion Behavior of High Burnup Spent Fuel in High Alkaline Solutions MRS 09

Scientific Basis for Nuclear Waste Management XXXIII, St. Petersburg (RUS), May 23-30, 2009, Mat. Res. Soc. Symp. Proc. XXXIII, (2009) 597-604.

LÜTZENKIRCHEN, J.; WELLS, J. D.; VAN MAALE, J.; LEERMAAKERS, F.; SJÖBERG, S.

Interaction of polyacrylic acid with dissolved aluminium – preliminary modelling of polyacrylic acid titrations

Proceedings of the Workshop TRePro II, Karlsruhe, March 18-19 (2009) 66-67.

LÜTZENKIRCHEN, J.; RABUNG, T.; HUITTINEN, N.; KUPCIK, T.; SCHILD, D.; FILBY, A.; WALTHER, C.; FUSS, M.; PLASCHKE, M.; GECKEIS, H.; ZIMMERMANN, R.; KÜTTNER, D.; WERNER, C.; PREOCANIN, T.; LEFEVRE, G.; FEDOROFF, M.

Interfacial behaviour of sapphire basal planes –effects of adding Al-polymers and their relation to the gibbsite basal plane

Seventh international Symposium on Surface Heterogeneity Effects in Adsorption and Catalysis on Solids, ISSHAC-7, Poland, Kazimierz Dolny, July 6-10, 2009 Proccedings, 255-256.

LÜTZENKIRCHEN, J.; WELLS, J. D.; SJÖBERG, S.

Interaction of polyacrylic acid with dissolved Aluminium and boehmite

Eighth Keele Meeting on Aluminium, Czech Republic, Trest, February 21-25, 2009, Book of Abstracts, 40.

LÜTZENKIRCHEN, J.; RABUNG, T.; SCHILD, D.; FILBY, A.; PLASCHKE, M.; GECKEIS, H.; ZIMMERMANN, R.; KÜTTNER, D.; WERNER, C.; PREOCANIN, T.

Interfacial behaviour of sapphire basal planes

Eighth Keele Meeting on Aluminium, Czech Republic, Trest, February 21-25, 2009, Book of Abstracts, 1.

MICHEL, P.; SCHÄFER, T.; DENECKE, M. A.; BRENDEBACH, B.; DARDENNE, K.; HUBER, F.; ROTHE, J.

Multi method (STXM, µFT-IR, µXAFS) approach to identify uranium speciation in argillites from the Lodève Basin (France)

9th International Conference on X-Ray Microscopy, 21–25 July 2008, Zürich, Switzerland, Journal of Physics: Conference Series 186 (2009) 012090.

MICHEL, P.; DENECKE, M. A.; SCHÄFER, T.; BRENDEBACH, B; DARDENNE, K.; ROTHE, J.; VITOVA T.; HUBER, F.; RICKERS, K.; ELIE, M.; BUCKAU, G.

A combined µ-XRF, µ-XAS, STXM and µFTIR investigation on the uranium speciation of samples from Autonian shales of the Permian Lodève Basin (France)

Proceedings of Actinide-XAS-2008 : Speciation, Techniques, and Facilities for Radioactive Materials at Synchrotron Light Sources. July 15-17, 2008, St Aubin, France: OECD – NEA, NEA/NSC/DOC(2009)15, 179-189.

MODOLO, G.; KLUXEN, P.; GEIST, A.

Selective separation of americium(III) from curium(III), californium(III), and lanthanides(III) by the LUCA process

Proc. Internat. Conf. GLOBAL 2009 (The Nuclear Fuel Cycle: Sustainable Options & Industrial Perspectives), Paris, September 6–11, 2009, paper 9336, 1046–1050.

MODOLO, G.; SYPULA, M.; GEIST, A.; HILL, C.; SOREL, C.; MALMBECK, R.; MAGNUSSON, D.; FOREMAN, M. R. S.

Development and demonstration of a new SANEX process for actinide(III)/lanthanide(III) separation using a mixture of CyMe4-BTBP and TODGA as a selective extractant.

In: Actinide and Fission Product Partitioning and Transmutation, 10th Information Exchange Meeting, Mito, Japan, October 6–10, 2009. NEA No. 6420, OECD-NEA (2010), 235–241.

MORRIS, K.; LAW, G. T. W.; BEGG, J. D., BURKE, I. T., LLOYD, J. R.; LIVENS, F. R., GEISSLER, A.; DENECKE, M. A.

Neptunium geomicrobiology in reducing sediments

ANKA Annual Report 2009, Karlsruhe Institute for Technology, October 2009, 155-156.

PAUL-BONCOUR, V.; THIÉBAUT, S.; DARDENNE, K.; ROTHE, J.

X ray diffraction study of Pd aged under tritium

ANKA Annual Report 2009, Karlsruhe Institute for Technology, October 2009, 74-75.

PLASCHKE, M.; ROTHE, J.; KLENZE, R.; WISSLER, J.; NABER, A.

STXM and LSLM investigation of Eu(III) induced humic acid colloid aggregation

Journal of Physics: Conference Series, 186 (2009) 012094.

PUDEWILLS, A.; HUBER, F.; SCHÄFER, T.

Numerical modelling of tracer tests and estimation of hydro-geological properties of a shear zone at the Grimsel test site

Proceedings of the Workshop TRePro II, Karlsruhe, March 18-19, 2009, 87-88.

ROTH, G.; GRÜNEWALD, W.; FLEISCH, J.; KUTTRUF, H.; WEISHAUPT, M.

Verglasungsanlage VEK - Nukleare Inbetriebsetzung und Heißer Verglasungsbetrieb

Jahrestagung Kerntechnik 2009, Dresden, May 12-14, 2009.

ROTHE, J.; WALTHER, C.; BRENDEBACH, B.; BÜCHNER, S.; FUSS; M.; DENECKE, M. A.; GECKEIS, H.

A combined XAFS, ESI TOF-MS and LIBD study on the formation of polynuclear Zr(IV), Th(IV) and Pu(IV) species

Journal of Physics: Conference Series, 190 (2009) 012188.

SHARRAD, C. A.; GOFF, G. S.; MAY, I.; RUNDE, W. H.; BANIK, N. L.; BRENDEBACH, B.; DARDENNE, K.; DENECKE, M. A.; MARQUARDT, C. M.

Pu L3 edge XAFS investigation on Pu(IV) peroxy-carbonate species

ANKA Annual Report 2009, Karlsruhe Institute for Technology, October 2009, 152-154.

SHARRAD, C. A.; GOFF, G. S.; MAY, I.; RUNDE, W. H.; BANIK, N. L.; BRENDEBACH, B.; DARDENNE, K.; DENECKE, M. A.; MARQUARDT, C. M.

U L3 edge XAFS investigation on U(VI) peroxy-carbonate species

ANKA Annual Report 2009, Karlsruhe Institute for Technology, October 2009, 154.

STUMPF, S.; SEIBERT, A.; PETERSMANN, T.; BATUK, O.

EXAFS investigation of UO_2 thin films doped with Pd and Mos

ANKA Annual Report 2009, Karlsruhe Institute for Technology, October 2009, 157-158.

VITOVA, T., LEBID, A., LIU, D., DARDENNE, K., BRENDEBACH, B., ROTHE, J., HORMES, J., DENECKE, M. A.

The high resolution X-ray fluorescence spectrometer (HRXF): An advanced tool for actinide research

Proceedings of Actinide-XAS-2008, July 15-17, 2008, St Aubin, France: OECD–NEA, NEA/NSC/DOC, 2009, 205-208.

VITOVA, T., DENECKE, M. A.

High-resolution polarisation dependent x-ray absorption fine structure (HR-P-XAFS) study of uranyl complexes

ESRF Annual Report 2009.

VITOVA, T., DENECKE, M.A., BATUK, O., CALIEBE, W.

High-resolution X-ray emission oxidation state investigation of CeO2 nano-particles", HASYLAB user report

HASYLAB Annual Report 2009.

VITOVA, T.; BREHER, F.; CALIEBE, W.; DARDENNE, K.; DENECKE, M. A.; LÖBLE, M.; ROTHE, J.

Resonant X-ray emission feasibility study of Eu compounds

HASYLAB Annual Report 2009.

VITOVA, T.; BRENDEBACH, B.; DARDENNE, K.; DENECKE, M. A.; LEBID, A.; LÖBLE, M.; ROTHE, J.; HORMES, J.; LIU, D.; BREHER, F.; GECKEIS, H.

The high-resolution X-ray emission (HRXE) spectrometer at the INE-Beamline: an advanced tool for actinide research

ANKA Annual Report 2009, Karlsruhe Institute of Technology, October 2009, 168-169.

VITOVA, T.; MANGOLD, S.; GOSPODINOV, M.; MIHAILOVA B.

X-ray absorption spectroscopy of Ru- and Rh-doped relaxor ferroelectrics with a perovskite-type structure

ANKA Annual Report 2009, Karlsruhe Institute for Technology, October 2009, 67-68.

WALTHER, C.; ROTHE, J.; FUSS, M.; BÜCHNER, S.; GECKEIS, H.

Actinide Metal Complexes Speciation by nano-Electrospray Mass-Spectrometry.

Proceedings Volume of ISMAS 09. 2009, 238-247.

WIECZOREK, K.; ROTHFUCHS, T.; ZHANG, C. L.; SPIES, TH.; HEEMANN, U.; LERCH, C. H. R.; KEESMANN, S.; PUDEWILLS, A.; KAMLOT, P.; GRUPA, J.; HERCHEN, K.; OLIVELLA, S.; SPIERS, C. H. R.

THERESA - Evaluation and improvement of numerical THM modelling capabilities for rock salt repositories (THERESA project). Davies, C. [Hrsg.] Euradwaste '08: 7th European Commission Conf. on the Management and Disposal of Radioactive Waste, Luxembourg, October 20-22, 2008 Luxembourg: Publications Office of the European Union, 2009, 489-494.

WIECZOREK, K.; ROTHFUCHS, T.; ZHANG, C. L.; SPIES, TH.; HEEMANN, U.; OLIVELLA, S. ; LERCH, C. H. R.; KEESMANN, S.; PUDEWILLS, A.; KAMLOT, P.; GRUPA, J.; HERCHEN, K.; SPIERS, C. H. R.

Data compilation and lab testing for calibration and improvement of numerical THM models for rock salt repositories in the frame of THERESA. EC-TIMODAZ-THERESA THMC Conf., Luxembourg, September 29 - October 1, 2009.

Reports

BRUNO, J.; MERINO, J.; TAMAYO, A.; FERRY, C.; QUINONES, J.; IGLESIAS, E.; RODRIGUEZ VILLAGRA, N.; NIETO, J. M.; MARTÍNEZ-ESPARZA, A.; LOIDA, A.; METZ, V.; JONSSON, M.; EKEROTH, E.

Model uncertainty for the mechanism of dissolution of spent fuel in nuclear waste repository. Application of models to selected datasets

MICADO project, Deliverable 3.1., European Commission, Brussels (2009).

BRUNO, J.; MERINO, J.; TAMAYO, A.; POINSSOT, C.; FERRY, C.; QUINONES, J.; IGLESIAS, E.; RODRIGUEZ VILLAGRA, N.; NIETO, J. M.; MARTÍNEZ-ESPARZA, A.; FARIAS, J., LOIDA, A.; METZ, V.; JONSSON, M.; VAN ISEGHEM, P.; MARIVOET, J.; LUNDSTRÖM, T.; GRAMBOW, B.

Model uncertainty for the mechanism of dissolution of spent fuel in nuclear waste repository. Comparison of fitting strategies and uncertainty analyses

MICADO project, Deliverable 3.2. European Commission, Brussels (2009).

BUCKAU, G.; DURO, L.; KIENZLER, B.; MONTOYA, V.; DELOS, A.

Proceedings of the Integrated Project „Fundamental Processes of Radionuclide Migration" (FUNMIG)

Wissenschaftliche Berichte, FZKA-7461 (2009).

BUCKAU, G.; KIENZLER, B.; DURO, L.; GRIVÉ, M.; MONTOYA, V.

1st Annual Workshop Proceedings of the Collaborative Project "Redox Phenomena Controlling Systems" (7th EC FP CP RECOSY)

Wissenschaftliche Berichte, FZKA-7466 (2009).

GECKEIS, H.; KLENZE, R.

Institute for nuclear waste disposal. Annual report 2008

Wissenschaftliche Berichte, FZKA-7510 (2009).

GRAMBOW, B.; BRUNO, J.; DURO, L.; MERINO, J.; TAMAYO, A.; MARTIN, C.; PEPIN, G.; SCHUMACHER, S.; SMIDT, O.; FERRY, C.; JEGOU, C.; QUIÑONES, J.; IGLESIAS, E.;

RODRIGUEZ VILLAGRA, N.; NIETO, J. M.; MARTÍNEZ-ESPARZA A.; LOIDA, A.; METZ, V.; KIENZLER, B.; BRACKE, G.; PELLEGRINI, D.; MATHIEU, G.; WASSELIN-TRUPIN, V.; SERRES, C.; WEGEN, D.; JONSSON, M.; JOHNSON, L.; LEMMENS, K.; LIU, J.; SPAHIU, K.; EKEROTH, E.; CASAS, I.; DE PABLO, J.; WATSON, C.; ROBINSON, P.; HODGKINSON, D.

MICADO - Model Uncertainty for the Mechanism of Dissolution of Spent Fuel in Nuclear Waste Repository - EURATOM Final Project Report

Specific Programme for Research and Training on Nuclear Energy.

HUBER, F.; LÜTZENKIRCHEN, J.; PFINGSTEN, W.; TIFFREAU, C.

TRePro II 2009: Workshop on Modelling of Coupled Transport Reaction Processes

Wissenschaftliche Berichte, FZKA-7482 (2009).

PUDEWILLS, A.

Modelling of the laboratory benchmark tests on salt rock. THERESA project

Deliverable D8: Model Application on Laboratory, Benchmark Test, Brussels: European Commission, (2009).

SCHÄFER, T.

Molecular geochemistry in hydrogeology: a pathway to reactive transport process understanding in natural systems

Wissenschaftliche Berichte, FZKA-7452 (2009).

Habilitationsschrift, Freie Universität Berlin (2009).

SEIBERT, A.; STUMPF, S.; SCHILD, D.; GOUDER, T.; BOSBACH, D.

Surface science investigations on spent nuclear fuel model systems

Wissenschaftliche Berichte, FZKA-7489 (2009).

Internal Reports

EKBERG, C.; GEIST, A.

Optimisation of the formulation of a set of SANEX extraction systems: An(III) selective extraction

ACSEPT (EC Contract № FP7-CP-2007-211 267): Deliverable report D1.3.1 (2009).

GEIST, A.

Design, Synthesis and assessment of novel ligands – 1st year report

ACSEPT (EC Contract № FP7-CP-2007-211 267): Deliverable report D1.2.1 (2009).

KIENZLER, B.; BAUER, A.; METZ, V.; PLASCHKE, M.; RÖMER, R.; BENDER, K.; HILPP, S.; NESOVIC, M.; SCHLIEKER, M.; SOBALLA, E.; SCHILD, D.; FACHINGER, J.; ENGE, R.

Analyse der Eigenschaften von simulierten, zementierten, 1:1 Gebinden und ihres Phasenbestands nach 20 Jahren Auslaugung in Salzlösungen

BfS Bestellnr 8566-5, February 2009. FZK-INE 001/09.

LOIDA, A.; MÜLLER, N.; SOBALLA, E.; SCHILD, D.; KIENZLER, B.

Investigation of the Corrosion Behaviour of Irradiated Spent Fuel in High pH Solutions

Draft Final Report, Working Period 2007 – 2008, Contract No 350 150 65 with ONDRAF/NIRAS, February 2009. FZK-INE 002/09.

Presentations

Invited oral presentations

ALTMAIER, M.

Aqueous redox chemistry of Np and Pu: solubility, thermodynamics, colloids and kinetics

Institutsseminar PSI-LES, Villigen, Switzerland, December 2009.

BUCKAU, G.

Radionuclide complexation with humic acid

South-West Research Institute (SWRI), USA, September 2009.

BUCKAU, G.

EURATOM Program on Nuclear Waste Disposal

South-West Research Institute (SWRI), USA, September 2009.

BUCKAU, G.

Grundwasserbeschaffenheit und Rückschlüsse auf die Hydrostratigraphie

Workshop „Grundsatzfragen Hydrogeologie - Reduzierung von Inkonsistenzen in der Interpretation von Ergebnissen“, GRS Braunschweig, Germany, November 2009.

DENECKE, M. A.

Spatially resolved synchrotron-based investigations with micrometer resolution on actinide containing heterogeneous, natural geological media

Geochimica Actie Spring 2009 seminar series, Utrecht University, Utrecht, Netherlands, March 2009.

DENECKE, M. A.

Using focus hard X-rays for investigations of nuclear waste repository analogs

European Geosciences Union General Assembly Conference Vienna, Austria, April 2009.

DENECKE, M. A.

Actinide spectroscopy at synchrotrons

Scientific inaugural colloquium of the “l’Institut de Chimie Séparative de Marcoule, France, June 2009.

DENECKE, M. A.

Actinide speciation using synchrotron techniques

14th International Clay Conference, Castellaneta Marina, Italy, July 2009.

DENECKE, M. A.

Synchrotron-based X-ray spectroscopy in partitioning research

ACSEPT Meeting, Bologna, Italy, September 2009.

GECKEIS, H.

Partitioning and Transmutation (P+T): Eine Alternative zur Endlagerung?

18. Diskussionstagung, Anorganisch-Technische Chemie, DECHEMA, Frankfurt, Germany, February 2009.

GECKEIS, H.

Partitioning und Transmutation (P+T): zukünftige Lösungswege für die Entsorgung hochradioaktiver Abfälle?

Festveranstaltung „Betriebsbeginn der VEK“, Karlsruhe, Germany, April 2009.

GECKEIS, H.

Colloid-borne radionuclide migration – relevant interaction mechanisms

Russian-German Symposium on Actinide nano-Particles, Moscow, Russia, May 2009.

GECKEIS, H.

Nukleare Endlagerung: Technisch gelöstes Problem - oder Herausforderung für die Wissenschaft ?

Karlsruher Chemische Gesellschaft, Ortsverband der GDCH, Universität Karlsruhe (TH), Karlsruhe, Germany, June 2009.

GECKEIS, H.

Nuclear waste disposal: Facts and perspectives

The 5th Summer School on Actinide Science and Applications, Karlsruhe, Germany, June 2009.

GECKEIS, H.

Actinide reactions at solid/liquid interfaces

42nd IUPAC Congress, Glasgow, UK, August 2009.

GECKEIS, H.

Geochemische Grundlagenforschung: wichtiger Baustein für eine sichere Endlagerung?

20. Sitzung des Kompetenzverbunds Kerntechnik, Peine, Germany, November 2009.

LOIDA, A.

Experimental study of the corrosion behavior of irradiated spent fuel in high pH solutions

Seminar at ONDRAF-NIRAS, Bruxelles, Belgium, March 2009.

LÜTZENKIRCHEN, J.

Aluminium in aqueous solutions – formation of macroions and some of their properties

University of Zagreb, Croatia, December 2009.

PANAK, P. J.

Spektroskopische Speziation von Actiniden und ihre Anwendung im Bereich der Langzeitsicherheitsforschung zur nuklearen Endlagerung, der Abtrennung von Actiniden ("Partitioning") und der Toxikologie

Institut für Radiochemie, Forschungszentrum Dresden, Germany, March 2009.

PANAK, P. J.

Speciation of Actinides by Time-resolved Laser Fluorescence Spectroscopy

Actinides 2009, San Francisco, USA, July 2009.

STUMPF, T.

Erfolgreich eine Nachwuchsgruppe beantragen und leiten

GAIN Jahrestagung „Wissenstransfer“, San Francisco, USA, September 2009.

STUMPF, T.

TRLFS: Process understanding on a molecular level

Jahresseminar des Graduiertenkollegs 826/3, Bad Münster an der Nahe, Germany, October 2009.

WALTHER, C.

Polymerisation of An(IV) in aqueous solution – the first step of nano-particle formation

Russian-German Symposium On Actinide nano-Particles, Moscow, Russia, May 2009.

WALTHER, C.

Poly-nuklear

Festvortrag zum 65. Geburtstag von Prof. J.V. Kratz, MPI für Polymerforschung, Mainz, Germany, May 2009.

WALTHER, C.

Speziation von Actinidionen in aquatischen Systemen

Symposium Moderne Trends in der Radiochemie, TU München, Germany, June 2009.

WALTHER, C.

Von der Hydrolyse zur Kolloidbildung - Polymerisierung vierwertiger Actinidionen

GDCh-Wissenschaftsforum Chemie, Frankfurt, Germany, September 2009.

WALTHER, C.

ESI-MS for nuclear safety assessment: Polymerization of actinides

11th ISMAS-TRICON-2009, Ramoji Film City Hyderabad, India, November 2009.

Presentations at Workshops and Conferences

ALTMAIER, M.

Critical evaluation of the Questionnaire on Redox measurement techniques

ReCosy 1st Annual Workshop, Barcelona, Spain, 9-12 February 2009.

ALTMAIER, M.; BRENDLER, V.; GESTER, S.; HAGEMANN, S.; HERBERT, H.-J.; MARQUARDT, C. M.; MOOG, H. C.; NECK, V.; RICHTER, A.; VOIGT, W.; WILHELM, S.; WILLMS, T.; WOLLMANN, G.

THEREDA – eine thermodynamische Referenzdatenbasis zur Modellierung endlagerrelevanter aquatischer Systeme

GDCh Wissenschaftsforum Chemie, Frankfurt, Germany, August 29 - September 02, 2009.

ALTMAIER, M.; BRENDLER, V.; GESTER, S.; HAGEMANN, S.; HERBERT, H.-J.; MARQUARDT, C. M.; MOOG, H. C.; NECK, V.; RICHTER, SCHARGE, T.; A.; VOIGT, W.; WILHELM, S.; WOLLMANN, G.

THEREDA – a joint German project towards a thermodynamic reference database

Migration '09, 12th International Conference on the Chemistry and Migration Behaviour of Actinides and Fission Products in the Geosphere, Kennewick, Washington, USA, September 20-25, 2009.

ALTMAIER, M.; BUCKAU, G.; KIENZLER, B.

Intercomparison exercise on redox determination methods: a key activity within the EURATOM FP7 “ReCosy” project

TRePro II 2009 – Workshop on Modeling of Coupled Reactive Transport Processes, Karlsruhe, Germany, March18-19, 2009.

ALTMAIER, M.; BUCKAU, G.; KIENZLER, B.

Intercomparison exercise on redox determination methods: a key activity within the EURATOM FP7 “ReCosy” project

Migration '09, 12th International Conference on the Chemistry and Migration Behaviour of Actinides and Fission Products in the Geosphere, Kennewick, Washington, USA, September 20-25, 2009.

ALTMAIER, M.; METZ, V.; LÜTZENKIRCHEN, J.; NECK, V.; KIENZLER, B.

Abschätzung der Radionuklidlöslichkeit in hochsalinaren aquatischen Systemen für Endlager schwach- und mittelaktiver Abfälle in Salzformationen

GDCh Wissenschaftsforum Chemie, Frankfurt, Germany, August 29 - September 02, 2009.

ALTMAIER, M.; NECK, V.

Solubility of An(III) and An(IV) in carbonate free NaCl, $MgCl_2$ and $CaCl_2$ brines

Technical Exchange Workshop “German Salt Repository Project and WIPP”, New Mexico State University / Los Alamos National Lab., Carlsbad, USA, September 18, 2009.

ALTMAIER, M.; NECK, V.; LÜTZENKIRCHEN, J.

SIT and Pitzer model for the UO_2^{2+} ion in NaCl, $MgCl_2$ and $CaCl_2$ solutions applied to trace activity coefficients determined by solvent extraction with TBP

Migration '09, 12th International Conference on the Chemistry and Migration Behaviour of Actinides and Fission Products in the Geosphere, Kennewick, Washington, USA, September 20-25, 2009.

ALTMAIER, M.; NECK, V.; RUNKE, J.; FELLHAUER, D.; FANGHÄNEL, TH.

Quantification of the redox potential for the reduction of Np (V) in non-complexing aqueous solutions at pH 5-10

ReCosy 1st Annual Workshop, Barcelona, Spain, February 9-12, 2009.

APOSTOLIDIS, C.; LINDQVIST-REIS, P.; WALTER, O.; SYKORA, R.; MORGENSTERN, A.; MAGNANI, N.; COLINEAU, E.; CACIUFFO, R.; KLENZE, R.; HAIRE, R.G.; REBIZANT, J. FANGHÄNEL, TH.

Synthesis, crystal structure, vibrational spectra and magnetic behavior of isotypic $[An(H_2O)_9](CF_3SO_3)_3$ (An = U-Cm, Cf) salts

Actinides 2009, San Francisco, USA, July 12–17, 2009.

BANIK, N.L.; DENECKE, M.A.; FANGHÄNEL, T.; GEIST, A.; MODOLO, G.; PANAK, P.J.; TRUMM, S.

Speciation and structural studies on the An(III)/Ln(III) selectivity of N-donor extractants on the example of BTP

Actinides 2009, San Francisco, USA, July 12–17, 2009.

BATUK, O.; VINGA SZABO, D.; VITOVA, T.; SCHILD, D.; DENECKE, M.A.; KALMYKOV, S.

Synthesis and electronic structure of cerium and actinide dioxide clusters

Russian-German Symposium on Actinide nano-Particles, Moscow, Russia, May 21-22, 2009.

BRENDEBACH, B.; DENECKE, M. A.; ROTH, G.; WEISENBURGER, S.

Sulfur incorporation in high level nuclear waste glasses: a S K-edge XAFS investigation

14th International Conference on X-ray Absorption Fine Structure (XAFS14), Camerino, Italy, July 26-31, 2009.

CHRISTIANSEN, B.C.; GECKEIS, H.; MARQUARDT, C.; SCHILD, D.; PLASCHKE, M.; STIPP, S.L.S.

Reduction of Neptunyl (NpO_2^+) by Green Rust Sodium Sulfate

Migration '09, 12th International Conference on the Chemistry and Migration Behaviour of Actinides and Fission Products in the Geosphere, Kennewick, Washington, USA, September 20-25, 2009.

DARDENNE, K.; BRENDEBACH, B.; DENECKE; LIU, X.; ROTHE, J.; VITOVA, T.

New developments at the INE-Beamline for actinide research at ANKA

14TH INTERNATIONAL CONFERENCE ON X-RAY ABSORPTION FINE STRUCTURE (XAFS14), Camerino, Italy, July 26–31, 2009.

DENECKE, M. A.

Recent developments at the INE-Beamline for actinide research at ANKA

CEA-Centre Saclay, France, March 31, 2009.

DENECKE, M. A.

Confocal µ-XRF and µ-XANES and nano-tomographic mapping of radiotracer Np in a fractured granite bore core

3D Microscopy, Interlaken, Switzerland, July 13-16, 2009.

DENECKE, M. A.; MICHEL, P.; SCHAEFER, T.; HUBER, F.; RICKERS, K.; ROTHE, J.; DARDENNE, K.; BRENDEBACH, B.; VITOVA, T.; ELIE, M.

Spatially resolved XRF, XAFS, XRD, STXM and IR investigation of a natural U-rich clay

14TH INTERNATIONAL CONFERENCE ON X-RAY ABSORPTION FINE STRUCTURE (XAFS14), Camerino, Italy, July 26–31, 2009.

FELLHAUER, D.; NECK, V.; ALTMAIER, M.; RUNKE, J.; FANGHÄNEL, TH.

Quantification of the redox potential for the reduction of Np(V) in non-complexing aqueous solutions at pH 5 – 10

GDCh Wissenschaftsforum Chemie, Frankfurt, Germany, August 29 - September 02, 2009.

FELLHAUER, D.; NECK, V.; ALTMAIER, M; LÜTZENKIRCHEN, J.; FANGHÄNEL, TH.

Solubility of tetravalent actinides in alkaline $CaCl_2$ solutions and formation of $Ca_4[An(OH)_8]^{4+}$ complexes: Np(IV) and Pu(IV) under reducing conditions

Migration '09, 12th International Conference on the Chemistry and Migration Behaviour of Actinides and Fission Products in the Geosphere, Kennewick, Washington, USA, September 20-25, 2009.

FILBY, A.; PLASCHKE, M.; GECKEIS, H.; BOSBACH, D.

Interaction of carboxylated latex colloids with mineral surfaces studied by AFM force spectroscopy

19th Annual V.M. Goldschmidt Conference, Davos, June 21-26, 2009.

FINCK, N.; ALEKSEENKO, E.; BOSBACH, D.

Investigations in the Fe – S – Se system

Anka User's Meeting, Karlsruhe, Germany, October 8-9, 2009.

FINCK, N.; SCHLEGEL, M.L.; BOSBACH, D.

Lu(III) co-precipitation with hectorite: a polarized EXAFS approach

19th Annual V.M. Goldschmidt Conference, Davos, June 21-26, 2009.

FINCK, N.; SCHLEGEL, M.L.; DARDENNE, K.; BOSBACH, D.

Mechanisms of Lu(III) and Eu(III) uptake by the clay mineral hectorite: a polarized EXAFS approach

12th International Conference of the Chemistry and Migration behaviour of Actinides and Fission Products in the Geosphere, Kennewick, USA, September 20-25, 2009.

GECKEIS, H.

Role of colloids in actinide speciation and migration

Technical Exchange Workshop, German Salt Repository Project and WIPP, Carlsbad, New Mexico, USA, September 17-18, 2009.

GEIST, A., MODOLO, G.

TODGA process development: an improved solvent formulation

Internat. Conf. GLOBAL 2009 (The Nuclear Fuel Cycle: Sustainable Options & Industrial Perspectives), Paris, France, September 6–11, 2009.

GEIST, A.; MODOLO, G.; MALMBECK, R.

Actinidenabtrennung – vom Schüttelgläschen zum kontinuierlichen Test im Labormaßstab

Jahrestreffen der ProcessNet-Fachausschüsse Computational Fluid Dynamics, Mischvorgänge und Extraktion, Fulda, Germany, March 30–31, 2009.

GEIST, A.; MODOLO, G.; MALMBECK, R.

Actinides(III)/Lanthanides(III) Separation Using $CyMe_4$-BTBP — Lab-scale Tests

ACHEMA-Kongress, ACHEMA 2009, Frankfurt/M., Germany. May 11–15, 2009.

HEBERLING, F.; DENECKE, M.A.; BOSBACH, D.

Neptunyl(V) coprecipitation with calcite – interfacial reactions studied with synchrotron x-ray radiation

EGU General assembly, Wien, Austria, April 19-24, 2009.

HEBERLING, F.; DENECKE, M.A.; LÜTZENKIRCHEN, J.; BOSBACH, D.

Structural incorporation of Neptunyl(V) into calcite – interfacial reactions

Goldschmidt Conference, Davos, Switzerland, Juni 21-26, 2009.

HEBERLING, F.; DENECKE, M.A.; LÜTZENKIRCHEN, J.; BOSBACH, D.

Neptunyl(V) coprecipitation with calcite – interfacial reactions

GDCh Wissenschaftsforum Chemie, Frankfurt, Germany, August 29 - September 02, 2009.

HEBERLING, F.; DENECKE, M.A.; LÜTZENKIRCHEN, J.; BOSBACH, D.

Structural incorporation of Neptunyl(V) into Calcite – Interfacial reactions studied with Syncrotron X-ray Methods

Migration '09, 12th International Conference on the Chemistry and Migration Behaviour of Actinides and Fission Products in the Geosphere, Kennewick, Washington, USA, September 20-25, 2009.

HUITTINEN, N.; RABUNG, Th.; ANDRIEUX, P.; LEHTO, J.; GECKEIS, H.

A comparative batch and TRLFS study on the sorption of Eu(III) and Cm(III) on synthetic and natural kaolinite

Migration '09, 12th International Conference on the Chemistry and Migration Behaviour of Actinides and Fission Products in the Geosphere, Kennewick, Washington, USA, September 20-25, 2009.

KHELASHVILI, G.; BÖNNEMANN, H.; SCHULENBURG, H.; SCHERER, G. G.; SCHILD, D.

Aluminium alkyl preparation of cobalt-rich Co3Pt@C fuel cell electrocatalyst for ORR. The International Conference on Nanotechnology: Science and Applications

Nanotech Insight ´09, Barcelona, Spain, March 29 - April 2, 2009.

KIENZLER, B.; BUCKAU, G.

The collaborative EC project ReCosy.

12th Internat.Conf.on Environmental Remediation and Radioactive Waste

Management (ICEM '09), Liverpool, GB, October 11-15, 2009.

KIENZLER, B.; METZ, V.

Modelling long-term corrosion of cemented waste forms in salt brines

12th Internat.Conf.on Environmental Remediation and Radioactive Waste Management (ICEM '09), Liverpool, GB, October 11-15, 2009.

KUPCIK, T.; HUITTINEN, N.; RABUNG, T.; LÜTZENKIRCHEN, J.; GECKEIS, H.; FANGHÄNEL, T.

Interaction of trivalent ions with various Aluminium minerals

Eighth Keele Meeting on Aluminium, Trest, Czech Republic, February 21-25, 2009.

KUPCIK, T.; HUITTINEN, N.; RABUNG, T.; LÜTZENKIRCHEN, J.; GECKEIS, H.; FANGHÄNEL, T.

Interaction of trivalent ions with various Aluminium minerals

Proceedings of the Workshop TRePro II, Karlsruhe, Germany, March 18-19, 2009.

KUPCIK, T.; HUITTINEN, N.; RABUNG, T.; LÜTZENKIRCHEN, J.; GECKEIS, H.; FANGHÄNEL, T.

Wechselwirkung von trivalenten Metallionen Aluminiumoxiden/hydroxiden

GDCh Wissenschaftsforum Chemie, Frankfurt, Germany, August 29 - September 02, 2009.

KUPCIK, T.; HUITTINEN, N.; RABUNG, T.; LÜTZENKIRCHEN, J.; GECKEIS, H.; FANGHÄNEL, T.

Trivalent metal ion interaction with aluminium oxides/hydroxides

Migration '09, 12th International Conference on the Chemistry and Migration Behaviour of Actinides and Fission Products in the Geosphere, Kennewick, Washington, USA, September 20-25, 2009.

LINDQVIST-REIS, P.; EDELSTEIN, N. M.; KLENZE, R.; WALTHER, C.; GECKEIS, H.

Crystal-field levels and vibronic spectra of Cm^{3+} aqua complexes

Very Heavy Metals 2009, Canet-Plage, France, May 27 - June 1, 2009.

LOIDA, A.; METZ, V.; KIENZLER,B.

Retention of radionuclides during alteration of high burnup spent fuel in high alkaline solution

International Spent Fuel Workshop, University of Western Ontario, Toronto, Canada, May 7-8, 2009.

LOIDA, A.; GENS, R.; METZ, V.; LEMMENS, K.; CACHOIR, C.; MENNECART, T.; KIENZLER,B.

Corrosion Behavior of High Burnup Spent Fuel in High Alkaline Solutions

MRS 09, Scientific Basis for Nuclear Waste Management XXXIII, St. Petersburg, Russia, May 23-30, 2009.

LÜTZENKIRCHEN, J.; RABUNG, T.; SCHILD, D.; FILBY, A.; PLASCHKE, M.; GECKEIS, H.; ZIMMERMANN, R.; KÜTTNER, D.; WERNER, C.; PREOCANIN, T.

Interfacial behaviour of sapphire basal planes

Eighth Keele Meeting on Aluminium, Czech Republic, Trest, February 21-25, 2009.

LÜTZENKIRCHEN, J.; RABUNG, T.; HUITTINEN, N.; KUPCIK, T.; SCHILD, D.; FILBY, A.; WALTHER, C.; FUSS, M.; PLASCHKE, M.; GECKEIS, H.; ZIMMERMANN, R.; KÜTTNER, D.; WERNER, C.; PREOCANIN, T.; LEFEVRE, G.; FEDOROFF, M.

Interfacial behaviour of sapphire basal planes –effects of adding Al-polymers and their relation to the gibbsite basal plane

Seventh international Symposium on Surface Heterogeneity Effects in Adsorption and Catalysis on Solids, ISSHAC-7, Kazimierz Dolny, Poland, July 6-10, 2009.

MACE, N.; WIELAND, E.; DAHN, R.; TITS, J.; SCHEINOST, A.; STUMPF, T.; WALTHER, C.

Determination of the local coordination environment of U(VI) sorption species on cementitious materials under alkaline conditions

MRS 09, Scientific Basis for Nuclear Waste Management XXXIII, St. Petersburg Russia, May 23-30, 2009.

MODOLO, G.; KLUXEN, P.; GEIST, A.

Selective separation of americium(III) from curium(III), californium(III), and lanthanides(III) by the LUCA process

Internat. Conf. GLOBAL 2009 (The Nuclear Fuel Cycle: Sustainable Options & Industrial Perspectives), Paris, France, September 6–11, 2009.

NECK, V.; ALTMAIER, M.; FANGHÄNEL, T.

Th(IV) and Pu(IV) oxyhydroxide colloids / polymers in aqueous solid-liquid equilibrium systems

Russian-German Symposium on Actinide nano-particles, Moscow, Russia, May 21–22, 2009.

NECK, V.; ALTMAIER, M.; FELLHAUER, D.; RUNKE, J.; FANGHÄNEL, T.

Reduction of Np(V) in non-complexing aqueous systems (pH 5 - 10): general aspects on thermodynamics, kinetics and mechanism

Migration '09, 12th International Conference on the Chemistry and Migration Behaviour of Actinides and Fission Products in the Geosphere, Kennewick, Washington, USA, September 20-25, 2009.

PLASCHKE, M.; ROTHE, J.; DENECKE, M.A.; GECKEIS, H.

STXM/NEXAFS investigation of humic acid metal cation interaction

EGU General Assemly 2009, Wien, Austria, April 20-24, 2009.

PLASCHKE, M.; ROTHE, J.; GECKEIS, H.

STXM/NEXAFS study of Eu(III) and Uranyl bound humic acid aggregates

ICXOM20, 20th International Congress on X-ray Optics and Microanalysis, Karlsruhe, Germany, September 14-18, 2009.

PUDEWILLS, A.; SCHÄFER, T.; HUBER, F.

Modeling of fluid flow and solute transport in a shear zone at the Grimsel test site

5th M.I.T. Conf. on Computational Fluid and Solid Mechanics, Cambridge, USA, June 17-19, 2009.

ROTH, G.; GRÜNEWALD, W.; FLEISCH, J.; KUTTRUF, H.; WEISHAUPT, M.

Verglasungsanlage VEK - Nukleare Inbetriebsetzung und Heißer Verglasungsbetrieb

Jahrestagung Kerntechnik 2009, Dresden, Germany, May 12-14, 2009.

ROTHE, J.; WALTHER, C.; BRENDEBACH, B.; BÜCHNER, S.; FUSS, M.; SCHIMMELPFENNIG, B.; DENECKE, M. A.; GECKEIS, H.

A combined XAFS, LIBD and ESI TOF-MS study on the formation of polynuclear An(IV) complexes and colloids

14th International Conference on X-ray Absorption Fine Structure (XAFS14), Camerino, Italy, July 26-31, 2009.

RUFF, C.; MARTINEZ-FERRI, A.; RAUSCH, N.; ALDAVE DE LAS HERAS, L.; PANAK, P. J.; FANGHÄNEL, T.

Interaction of Cm(III) with blood serum proteins studied by time-resolved laser fluorescence spectroscopy (TRLFS)

Actinides 2009, San Francisco, USA, July, 12-17, 2009.

RUFF, C.; MARTINEZ-FERRI, A.; RAUSCH, N.; ALDAVE DE LAS HERAS, L.; PANAK, P. J.; FANGHÄNEL, T.

Interaction of Cm(III) with blood serum proteins studied by time-resolved laser fluorescence spectroscopy (TRLFS)

GDCh Wissenschaftsforum Chemie, Frankfurt, Germany, August 29 - September 02, 2009.

SEIBERT, A.; GOUDER, T.; HUBER, F.; PETERSMANN, T.; STUMPF, S.; WEGEN, D.; WISS, T.; BATUK, O.; DENECKE, M.A.; SCHILD, D.; SOBALLA. S.

Spectroscopic, structural and electrochemical investigations at actinide system interfaces

Russian-German Symposium on Actinide nano-Particles, Moscow, Russia, May 21-22, 2009.

SKERENCAK, A.; PANAK, P. J.; NECK, V.; TRUMM, S.; SCHIMMELPFENNIG, B.; LINDQVIST-REIS, P.; KLENZE, R.; FANGHÄNEL, T.

Die Komplexierung von Cm(III) mit Fluorid im Temperaturbereich von T=20-90°C; eine kombinierte spektroskopische, thermodynamische und quantenchemische Studie

GDCh Wissenschaftsforum Chemie, Frankfurt, Germany, August 29 - September 02, 2009.

SKERENCAK, A.; PANAK, P. J.; NECK, V.; HAUSER, W.; LINDQVIST-REIS, P.; KLENZE, R.; FANGHÄNEL, T.

Complexation and thermodynamics of Cm(III) with fluoride and nitrate at elevated temperatures studied by time-resolved laser fluorescence spectroscopy

12th International Conference on the Chemistry and Migration Behaviour of Actinides and Fission Products in the Geosphere, Kennewick, USA, September 20– 25, 2009.

STEPPERT, M.; WALTHER, C.; GEIST, A.; FANGHÄNEL, T.

Determination of the stoichiometry of lanthanide-BTP-complexes with nano-ESI-TOF MS

Actinides 2009, San Francisco, USA, July 12–17, 2009.

STEPPERT, M.; WALTHER, C.; GEIST, A.; FANGHÄNEL, T.

Bestimmung der Stöchiometrie von Lanthanid-BTP-Komplexen mittels nano-Electrospray Flugzeit Massenspektrometrie

GDCh Wissenschaftsforum Chemie, Frankfurt, Germany, August 29 - September 02, 2009.

STUMPF, S.; PETERSMANN, D.; SEIBERT, A.; HUBER, F.; DENECKE, M.A.; GOUDER, T.

Vergleichende Untersuchungen zum Einfluss von Edelmetalleinschlüssen auf die Struktur und das elektrochemische Verhalten von UO_2

GDCh Wissenschaftsforum Chemie, Frankfurt, Germany, August 29 - September 02, 2009.

STUMPF, T.; HARTMANN, E.; BAEYENS, B.; BRADBURY, M.; GECKEIS H.

Spectroscopic Characterization and Quantification of M(III)/Clay Mineral Outer-Sphere Complexes

GDCh Wissenschaftsforum Chemie, Frankfurt, Germany, August 29 - September 02, 2009.

STUMPF, T.; SCHMIDT, M.; WALTHER, C.; GECKEIS, H.; FANGHÄNEL, T.

Structural incorporation of Eu(III) into calcite, Aragonite and Vaterite: a comperative TRLFS study

Goldschmidt Conference, Davos, Switzerland, Juni 21-26, 2009.

STUMPF, T.; SCHMIDT, M.; WALTHER, C.; GECKEIS, H.; FANGHÄNEL, T.

Interaction of trivalent actinides with $CaCO_3$: Process understanding on a molecular level

Actinides 2009, San Francisco, USA, July 12-17, 2009.

TRUMM, S.; DENECKE, M. A.; PANAK, P. J.; FANGHÄNEL, T.; GEIST, A.

Structural investigation on actinide(III)-BTBP and lanthanide(III)-BTBP 1:2 complexes in organic solution

Actinides 2009, San Francisco, USA, July 12-17, 2009.

TRUMM, S.; PANAK, P. J.; GEIST, A.; DENECKE, M. A.; FANGHÄNEL, T.

Synthese und spektroskopische Untersuchungen elektronisch derivatisierter BTP-Liganden für die selektive Extraktion dreiwertiger Actiniden

GDCh Wissenschaftsforum Chemie, Frankfurt, Germany, August 29 - September 02, 2009.

VITOVA, T.; BREHER, F.; BRENDEBACH, B.; DARDENNE, K.; DENECKE; M. A.; LEBID, A.; LÖBLE, M.; ROTHE J.

High Resolution X-ray Emission Spectroscopy (HRXES): an Advanced Tool for Actinide Research

ACTINIDES 09, San Francisco, USA, July 12-17, 2009.

VITOVA, T.; BRENDEBACH, B.; DARDENNE, K.; DENECKE; M. A.; LEBID, A.; LÖBLE, M.; ROTHE J.

High Resolution X-ray Emission Spectroscopy (HRXES): an Advanced Tool for Actinide Research

GDCh Wissenschaftsforum Chemie, Frankfurt, Germany, August 29 - September 02, 2009.

VITOVA, T.; BREHER, F.; BRENDEBACH, B.; DARDENNE, K.; DENECKE; M. A.; LEBID, A.; LÖBLE, M.; ROTHE J.

High Resolution X-ray Emission Spectroscopy: an Advanced Tool for Actinide Research

14th International Conference on X-ray Absorption Fine Structure (XAFS14), Camerino, Italy, July 26-31, 2009.

VITOVA, T.; BREHER, F.; BRENDEBACH, B.; DENECKE; M. A.; LÖBLE, M.; ROTHE J.

Application of IXS in actinide science

Workshop on Electronic Excitations studied by Non-Resonant Inelastic X-Ray Scattering at PETRA III (P01), Hamburg, Germany, May 7–8, 2009.

WALTHER, C.; ROTHE, J.; ALTMAIER, M.; GECKEIS,H.

Speciation of polynuclear An(IV) complexes by electrospray mass-spectrometry, methods and applications of radioanalytical chemistry

MARC 8, Keauhou Hawaii, USA, April 6-10, 2009.

WALTHER, C.; ROTHE, J.; ALTMAIER, M.; GECKEIS, H.

Formation of polynuclear actinide complexes

MRS 09, Scientific Basis for Nuclear Waste Management XXXIII, St. Petersburg Russia, May 23-30, 2009.

WALTHER, C.; ROTHE, J.; ALTMAIER, M.; GECKEIS, H.

Formation of polynuclear plutonium complexes and their role in Pu redox chemistry

ACTINIDES 09, San Francisco, USA, July 12-17, 2009.

WALTHER, C.; ROTHE, J.; ALTMAIER, M.; SCHÄFER, T.; SEHER, H.; GECKEIS,H.

The Role of polymerization and (Pseudo)colloid formation for understanding the behavior of an ions in aqueous solution

APSORC `09 Napa, USA, November 29 – December 4, 2009.

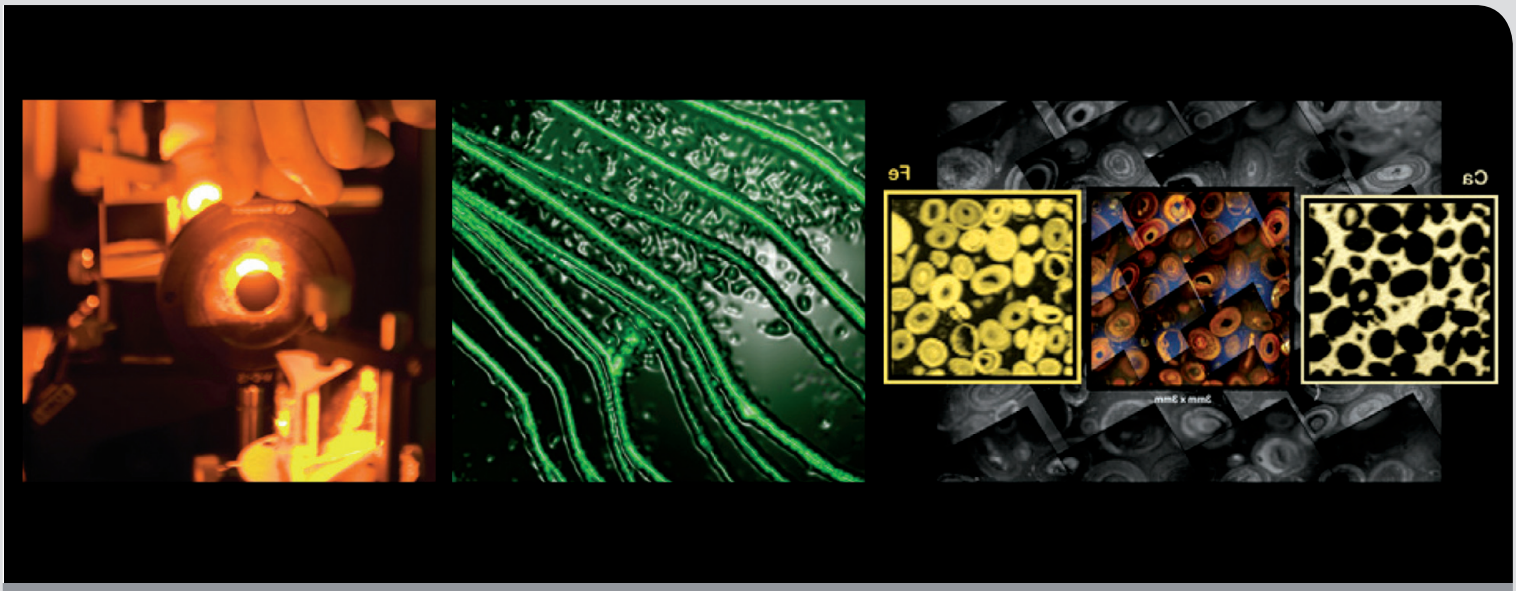

On October 01, 2009, the Karlsruhe Institute of Technology (KIT) was founded by a merger of Forschungszentrum Karlsruhe and Universität Karlsruhe (TH). KIT bundles the missions of both precursory institutions: a university of the state of Baden-Wuerttemberg with teaching and research tasks and a large-scale research institution of the Helmholtz Association conducting program-oriented provident research on behalf of the Federal Republic of Germany. Within these missions, KIT is operating along the three strategic fields of action, research, teaching, and innovation.

With about 8000 employees and an annual budget of about EUR 700 million, KIT is one of the largest research and teaching institutions worldwide. It has the potential to assume a top position worldwide in selected fields of research. The objective: KIT will become an institution of excellent research and scientific education, as well as a prominent location of academic life, life-long learning, comprehensive advanced training, unrestricted exchange of know-how and sustainable innovation culture.

The largest organizational units of KIT are the KIT Centers. They focus on problems of fundamental importance to the existence and further development of our society or on key issues of basic science. KIT Centers are characterized by the uniqueness of their scientific approach, their strategic objective and mission and by a long-term perspective.

The Institut für Nukleare Entsorgung, INE, (Institute for Nuclear Waste Disposal) belongs to the KIT Energy Center. The KIT Energy Center comprises some 40 institutes of the Universität Karlsruhe (TH) and 18 large institutes of the Forschungszentrum Karlsruhe with, at present, a total of approx. 1100 staff members. The participating institutes and research groups are the operating research units. An interdisciplinary KIT School of Energy establishes ideal framework conditions for teaching. For external partners from industry, the KIT Center develops solutions in energy technology from a single source. Moreover, it acts as a highly valuable consultancy institution for politics, business and society in all questions of energy.

ISSN 1869-9669